Voltage-sensitive Dye Recording from Networks of Cultured Neurons

Thesis by

Chi-Bin Chien

In Partial Fulfillment of the Requirements

for the Degree of

Doctor of Philosophy

California Institute of Technology,

Pasadena, California

1990

(Submitted April 16, 1990)

DEDICATED TO MY PARENTS

who brought us up better than we knew

Acknowledgments

First, I must thank my thesis advisor, Jerry Pine, whose support and constant insistence that life is one long freshman physics experiment helped to turn me into an experimental scientist. I would like to thank Helen Rayburn for the initial dye screening, Andrew Hsu for building the fiber-optic camera, Becky Tanamachi for her near-indispensable help with cell culture, and John Gilbert, Wade Regehr, and Tina Kramer Garyantes for general assistance through the years. Thanks to Amiram Grinvald for helping us to start dye-recording, and to Amiram and Leslie Loew for supplying dyes. Many thanks to Henry Lester for providing our lab with space and a place to eat lunch.

One benefit of a rather lengthy graduate career has been the large number of excellent humans with whom I have had the pleasure to work, live, and play. Utpal Banerjee, John Bowman, Bay-Wei Chang, Chi-An Chien, Chi-Kai Chien, Paul Garrity, Tina Garyantes, John Gilbert, Eric Grove, Jim Knierim, Bette Korber, Michael Kovari, Mary Sara McPeek, Mark Muldoon, Mani Ramaswami, Wade Regehr, Pat Renfranz, Paul Stolorz, Becky Tanamachi, Mark Tanouye, Sean Tavtigian, James Theiler, Becky Truman, Al Walter, Dave Wark, and Scott Welsch—just to name a few.

Thanks to Tina Garyantes, John Gilbert, David Kleinfeld, Tom Parsons, Jerry Pine, and Wade Regehr for their helpful comments on early versions of this thesis. Any remaining errors or poor phrasings are of course my fault, not theirs.

Finally, I would like to thank Drs. David Van Essen, Steven Frautschi, and Thomas Soifer for serving on my thesis committee and endeavouring to read such an interdisciplinary thesis.

Abstract

This thesis describes the development and testing of a sensitive apparatus for recording electrical activity from microcultures of rat superior cervical ganglion (SCG) neurons by using voltage-sensitive fluorescent dyes.

The apparatus comprises a feedback-regulated mercury arc light source, an inverted epifluorescence microscope, a novel fiber-optic camera with discrete photodiode detectors, and low-noise preamplifiers. Using an NA 0.75 objective and illuminating at 10 W/cm^2 with the 546 nm mercury line, a typical SCG neuron stained with the styryl dye RH423 gives a detected photocurrent of 1 nA; the light source and optical detectors are quiet enough that the shot noise in this photocurrent—about .03% rms—dominates. The design, theory, and performance of this dye-recording apparatus are discussed in detail.

Styryl dyes such as RH423 typically give signals of 1%/100 mV on these cells; the signals are linear in membrane potential, but do not appear to arise from a purely electrochromic mechanism. Given this voltage sensitivity and the noise level of the apparatus, it should be possible to detect both action potentials and subthreshold synaptic potentials from SCG cell bodies. In practice, dye recording can easily detect action potentials from every neuron in an SCG microculture, but small synaptic potentials are obscured by dye signals from the dense network of axons.

In another microculture system that does not have such long and complex axons, this dye-recording apparatus should be able to detect synaptic potentials, making it possible to noninvasively map the synaptic connections in a microculture, and thus to study long-term synaptic plasticity.

Table of Contents

Chapter 1
Introduction

The main reason neurobiology is both so interesting and so challenging is that nervous systems are very, very complicated. The human brain has about a trillion neurons, each of which makes on average about a thousand connections to other neurons. It is known to have scores of different neuronal cell types and scores of different neurotransmitters. This extraordinary mechanism allows people to perform complex behaviors such as reading Shakespeare, inventing general relativity, and understanding the infield-fly rule. Confronted with this complexity, the optimistic young neurobiologist foresees a rich and fruitful career full of new scientific questions, while the pessimist is daunted and goes back to easier pursuits.

In order to understand information processing in the brain, one would ideally record electrical activity simultaneously from every neuron. Sheer numbers make this impossible. Conventional glass or metal electrodes can record from at most a few neurons at any one time; using these electrodes to understand the entire brain is a bit like analyzing a million-transistor microprocessor, one transistor at a time . The main strategy for coping with nervous system complexity has been reductionistic: starting first by analyzing a simple nervous system, or a simple part of a nervous system, and working up from there. For example, much has been learned by studying invertebrates such as the lobster or the leech, whose nervous systems are relatively simple and stereotyped; for vertebrate brains, much has been learned by studying specific subsystems such as the visual system that have well-defined sensory inputs. The vast majority of these studies have used conventional electrodes to record from or stimulate a few cells at a time. Though these systems are

simple compared to the complete vertebrate brain, they are still tremendously complicated; and conventional electrodes can sample only a tiny fraction of their neurons.

Another more recent strategy, which may be very loosely called holistic, is to develop methods for recording from many neurons at once. Techniques such as positron-emission tomography (Heiss and Phelps, 1983; Phelps *et al.*, 1986), voltage-sensitive dye recording (Cohen and Lesher, 1986; Grinvald *et al.*, 1988) and optical recording of intrinsic signals (Grinvald *et al.*, 1988) can simultaneously record from many groups of neurons in intact vertebrate brains, while voltage-sensitive dyes (Cohen *et al.*, 1989; Parsons *et al.*, 1989) and multielectrode arrays (Pine *et al.*, 1980; Meister *et al.*, 1989) can simultaneously record from many individual neurons in intact invertebrate ganglia, isolated vertebrate retinas, or neuronal cell cultures.

1.1 DYE RECORDING FROM MICROCULTURES

This thesis describes the development of an experimental approach that combines both of these strategies. It uses a multicell recording technique—voltage-sensitive dye recording—with a drastically reduced preparation—microcultures of rat SCG neurons. Each microculture is an isolated island of one to ten SCG neurons, grown in cell culture on a petri dish. Microcultures are far simpler than an entire brain: each island has only a few cells, only a few possible synapses per cell, a single relatively homogeneous cell type, and a single functional neurotransmitter (acetylcholine). Further, any given pair of neurons is quite likely to be synaptically connected, so the microcultures have interesting electrical activity. This high connectivity seems to be due to the microculture conditions: it is as though each cell needs to make a certain number of synapses, and only having a few cells to choose from, connects to most of them. For optical recording with voltage-sensitive fluorescent dyes, the microcultures are stained with an appropriate dye, then their electrical activity is detected as small changes in fluorescence. A spatially-resolved optical detector can separately record the fluorescence of each cell, and so simultaneously monitor the

activity of all of the cells. By using dye-recording in this highly simplified system, it is possible to achieve what is impossible in the entire brain: complete knowledge of the firing patterns of every neuron.

This approach ties together two strands of previous research. First, Furshpan and Potter's group developed a microculture system (Furshpan *et al.*, 1976) for neurons from the rat superior cervical ganglion (SCG). Each microculture had only a few neurons, which often made synapses on one another (Furshpan *et al.*, 1986; Higgins *et al.*, 1984). Second, Grinvald's group had found voltage-sensitive fluorescent dyes that gave very large signals from neuroblastoma cells grown in cell culture (Grinvald *et al.*, 1983). Salzberg's group has pursued a very similar strategy, using dye recording on microcultures of *Aplysia* neurons (Parsons *et al.*, 1989).

1.2 GOALS FOR MICROCULTURE EXPERIMENTS

This thesis work represents an exploration of the capabilities of the voltage-sensitive dye recording technique. The work has three main parts. First, the design, construction, and testing of an apparatus for dye-recording. Second, experiments that optimized the conditions for dye recording. Third, experiments that used the apparatus and optimized conditions to record from SCG microcultures, with the aim of understanding the capabilities of the technique.

There are two sorts of experiments on neuronal microcultures that dye recording might make possible: *acute* experiments that map the synaptic connections of a microculture at a particular time, and *chronic* experiments that follow changes in these connections over time. For such experiments, dye recording provides two main advantages that conventional recording with intracellular electrodes does not have: *multicell recording* (already mentioned) and *noninvasive recording*. By using separate photodetectors for each cell, one can dye-record from many cells at once (two or three cells is the practical limit for intracellular electrodes). Since dye recording does not require

penetrating the cell with a large glass electrode, it is less damaging than intracellular recording, as long as dye phototoxicity is avoided by limiting the illumination. For synaptic mapping, dye recording must be combined with an intracellular or extracellular stimulation technique: in order to measure the strength of a synapse, it is necessary to stimulate the presynaptic cell as well as record from the postsynaptic cell. Acute and chronic experiments place different requirements on the stimulation technique and on the sensitivity of dye recordings.

The dye-recording experiments in this thesis were all acute. The goal of an acute experiment is to completely map the synaptic connections in a microculture, *i.e.*, to determine which neurons synapse on which others, and to measure the strength of each synapse (the size of its synaptic potential). This mapping is done by stimulating each cell in turn, then recording the responses from the other cells. In a culture with suprathreshold connections, the responses can become very complicated indeed, and it is essential to know the firing patterns of each cell in order to sort out the connections; this information is provided by multicell dye recording. For stimulation, acute experiments can use (invasive) intracellular electrodes, since the cells need not survive the experiment. For dye recording, acute experiments *require* the detection of action potentials; detection of subthreshold synaptic potentials is not necessary, but makes the experiments much easier. (Synaptic potentials can be measured intracellularly, but this requires tedious pairwise penetrations.)

Our hope was that once acute experiments were perfected, they could be extended to chronic experiments. The goal of a chronic experiment is to synaptically map a microculture, just as for an acute experiment, but to do this mapping noninvasively, so that the culture can be mapped several times over the course of days or weeks. Such experiments could look for long-term synaptic plasticity (changes in synaptic connections) in microcultures; synaptic plasticity is extremely interesting because it is widely thought to be the cellular substrate of learning and memory. Chronic experiments are technically very demanding: they require noninvasive stimulation and noninvasive multicell recording. For

stimulation, they must use extracellular electrodes; for dye recording, they require the detection of both action potentials and subthreshold synaptic potentials. (An extracellular electrode would stimulate individual cells while action potentials and synaptic potentials were dye-recorded.)

In summary, the technical goals for dye recording from microcultures are first, to detect action potentials, and second, to detect subthreshold synaptic potentials. For acute experiments, the former goal is necessary and the latter desirable; for chronic experiments, both are necessary. Chronic experiments also require some form of reliable extracellular stimulation.

1.3 SUMMARY OF RESULTS

For a typically-stained SCG neuron, the dye recording apparatus has sufficient sensitivity to detect potential changes of 10 mV without signal-averaging, and smaller changes with averaging (see Chapter 3). Based on this technical limit, it should be possible to detect action potentials easily, and large synaptic potentials with a little work. Experiments on SCG microcultures (Chapter 7), found that action potentials were indeed routinely detectable, but synaptic potentials were not. The problem is the complex anatomy of these microcultures: SCG neurons have long branching axons that form very dense mats in culture. The axons often curve back over the cell bodies, and action potentials that propagate through the axons often give rise to dye signals that superpose on the signals from the cell bodies proper. Though the system's sensitivity is sufficient to detect synaptic potentials from isolated cell bodies, in practice the dye signals from synaptic potentials are obscured by signals from the dense net of axons. SCG microcultures can be synaptically mapped in acute experiments, using dye recording in conjunction with dual intracellular penetrations, but since synaptic potentials cannot be detected noninvasively, these cultures are not suited for chronic experiments.

There is another reason that SCG microcultures cannot be used for chronic experiments: they cannot be stimulated extracellularly in a satisfactory way. While I was developing a dye-recording system, John Gilbert and then Wade Regehr in the Pine laboratory developed multielectrode dishes (Pine, 1980; Regehr *et al.*, 1989). These are petri dishes with an array of 61 metal extracellular electrodes built into the bottom, which can be used for extracellular stimulation. In preliminary experiments, I tried to stimulate neurons in SCG microcultures using these dishes. A full explanation of the results would be quite long and is beyond the scope of this thesis, but the main problem was again the complex anatomy of these cells: since the axons run everywhere, it was not possible to pick electrodes that would reliably stimulate a neuron's cell body without sometimes stimulating axons that passed nearby. Preliminary experiments at stimulation with glass extracellular experiments ran into a similar problem.

In summary, the signal-to-noise ratio of the apparatus developed here is theoretically sufficient to detect both action potentials and synaptic potentials from isolated SCG cell bodies, and indeed action potentials are detected routinely. However, SCG microcultures have a very complex anatomy, with axons running everywhere, and dye signals from the axons make it impossible to detect synaptic potentials reliably. Since the problem is with the culture system and not the apparatus, it is very tempting to try microcultures of a different neuronal type. In a microculture system with more restrained axons, it might well be possible to reliably detect synaptic potentials; further, it might well be possible to extracellularly stimulate the cells of such microcultures in a reliable way. This combination of optical detection of synaptic potentials with reliable extracellular stimulation would make it possible to study long-term synaptic plasticity in chronic synaptic mapping experiments.

1.4 THESIS OUTLINE

Voltage-sensitive dye recording is not popular enough that its principles are widely known, and so Chapter 2 begins with a basic description of the technique. It then briefly reviews the history of dye recording, with particular attention to recordings of synaptic potentials and recordings from neurons in cell culture. Appendix A discusses the biophysical mechanisms by which the dyes are thought to work.

Chapters 3 through 5 describe the dye-recording apparatus. This comprises a stabilized light source, an inverted fluorescence microscope, a very low-noise 256-pixel optical detector, and a data acquisition system. Some care was taken to ensure that the signal-to-noise ratio for dye recording is limited by the shot noise (statistical fluctuations due to the quantum nature of light) in the detected fluorescence, rather than by light source noise or detector noise. Chapter 3 starts by discussing the overall design of the system and the theory of noise in optical detection, then summarizes the overall performance of the apparatus. Less interested readers may want to skip Chapters 4 and 5, which describe the apparatus in detail. Chapter 4 describes the light source and microscope; Chapter 5, the optical detector and data acquisition system.

Throughout the discussion of the dye-recording apparatus, I have tried to point out the fundamental tradeoffs involved in the design. One decision that must be made early on is whether to use fluorescence or absorption for optical recording; Appendix B provides the theoretical basis for making this decision, and applies this theory to the particular case of cultured SCG neurons. Appendix C discusses the optical theory of illumination efficiency and collection efficiency, which is important when choosing an objective lens for the microscope. Finally, Appendix D discusses the detailed design of the 256 preamplifiers for the optical detector.

Chapter 6 describes experiments that optimized the conditions for dye recording. Many dyes were screened to find the ones that worked best on SCG neurons, different

staining conditions were tried, and different sets of optical filters were tested. The latter tests, besides finding the best filters to use, also have some bearing on the biophysical mechanism of the dyes. Other experiments show that the dye signal is in fact linear with membrane potential, and explore dye bleaching and phototoxicity.

Chapter 7 describes microculture experiments. A reliable method for growing microcultures was developed, and preliminary experiments used intracellular electrodes to characterize their synaptic physiology. Acute dye-recording experiments were carried out with 24 microcultures; this chapter presents examples of recordings made from two of these, and summarizes the results from the others. It then discusses the usefulness of dye recording for synaptic mapping in light of these results.

Chapter 8 summarizes the thesis and discusses possible directions for future work.

Throughout, I have followed J. Pine's rule that a thesis is meant for the next graduate student. Because of its large technical component, dye recording is a very interdisciplinary technique: it requires knowledge of conventional electrophysiology, photochemistry, optics, and electronics. Barring the resurrection of Leonardo da Vinci, a single person is unlikely to be fully conversant with all of these fields, and so I have tried to start from first principles whenever possible, and have usually opted for length and completeness rather than concision and possible confusion.

CHAPTER 1 REFERENCES

L. B. Cohen and S. Lesher (1986) Optical monitoring of membrane potential: Methods of multisite optical measurement. In *Optical Methods in Cell Physiology,* eds. P. DeWeer and B. M. Salzberg. Wiley (Interscience), New York, NY. pp.71-99.

L. B. Cohen, H.-P. Hopp, J.-Y. Wu, C. Xiao, J. London, and D. Zecevic (1989) Optical measurement of action potential activity in invertebrate ganglia. *Ann. Rev. Physiol.* **51**:527-541.

E. J. Furshpan, P. R. MacLeish, P. H. O'Lague, and D. D. Potter (1976) Chemical transmission between rat sympathetic neurons and cardiac myocytes developing in microcultures: Evidence for cholinergic, adrenergic, and dual-function neurons. *Proc. Natl. Acad. Sci. U. S. A.* **73**:4225-4229.

E. J. Furshpan, S. C. Landis, S. G. Matsumoto, and D. D. Potter (1986) Synaptic functions in rat sympathetic neurons in microcultures. I. Secretion of norepinephrine and acetylcholine. *J. Neurosci.* **6**:1061-1079.

A. Grinvald, A. Fine, I. C. Farber, and R. Hildesheim (1983) Fluorescence monitoring of electrical responses from small neurons and their processes. *Biophys. J.* **42**:195-198.

A. Grinvald, R. D. Frostig, E. Lieke, R. Hildesheim (1988) Optical imaging of neuronal activity. *Physiol. Rev.* **68**:1285-1366.

W.-D. Heiss and M. E. Phelps, eds. (1983) *Positron Emission Tomography of the Brain,* Springer-Verlag, New York.

D. Higgins, L. Iacovitti, and H. Burton (1984) Fetal rat sympathetic neurons maintained in a serum-free medium retain induced cholinergic characteristics. *Dev. Brain Res.* **14**:71-82.

M. Meister, J. Pine, and D. A. Baylor (1989) Multielectrode recording from the vertebrate retina. *Invest. Ophthalmol. Vis. Sci.* **30** (Suppl.):68.

T. D. Parsons, D. Kleinfeld, F. Raccuia-Behling, and B. M. Salzberg (1989) Optical recording of the electrical activity of synaptically interacting *Aplysia* neurons in culture using potentiometric probes. *Biophys. J.* **56**:213-221.

M. Phelps, J. Mazziotta, and H. Schelbert, eds. (1986) *Positron Emission Tomography and Autoradiography: Principles and Applications for the Brain and Heart,* Raven Press, New York.

J. Pine (1980) Recording action potentials from cultured neurons with extracellular microcircuit electrodes. *J. Neurosci. Meth.* **2**:19-31.

W. G. Regehr, J. Pine, C. S. Cohan, M. D. Mischke, and D. W. Tank (1989) Sealing cultured neurons to embedded dish electrodes facilitates long-term stimulation and recording. *J. Neurosci. Meth.* **30**:91-106.

Chapter 2
A review of dye recording

2.1 INTRODUCTION

Optical methods—in particular, the use of voltage-sensitive dyes—promise to be powerful tools for neurobiology, since they can measure electrical activity in places where electrodes cannot reach. For recording from small cells and processes, for recording from tens or hundreds of sites at once, and for recording in situations when penetration with a glass electrode would be undesirably invasive, dye-recording methods can provide information that is otherwise unobtainable.

This chapter describes the technique of voltage-sensitive dye recording. Dyes have been used in many disparate ways, and there is much about them that is not understood. I have tried to provide a broad outline that emphasizes their most important aspects and limitations. Section 2.2 sets the stage with an illustration of the technique and explanation of common terminology. This section briefly describes fluorescence and absorption dye recording, and mentions other optical techniques. It also describes the procedure, apparatus, and analysis used for measuring dye signals. Finally, this section summarizes what is known about the biophysical mechanisms underlying dye signals; a more detailed discussion may be found in Appendix A. Section 2.3 is a brief history of the development of optical recording: the discovery of voltage-sensitive dyes, the development of new dyes, the biological systems on which they have been used, and in particular, previous dye recording in culture and of synaptic potentials.

Since there have been many recent reviews on dye recording, I've only tried to cover the more basic aspects in this chapter. In particular, the reader is referred to the

review by Amiram Grinvald's group (Grinvald *et al.*, 1988), which has an an excellent discussion of all the technical aspects of dye-recording, from dye synthesis through design of photodetectors and amplifiers, as well as a good review of the preparations on which dyes have been used. Also see the recent books edited by De Weer and Salzberg (DeWeer and Salzberg, 1986) and Leslie Loew (Loew, 1988). For more detailed discussions of recent biological uses of dyes, see the set of reviews in the most recent Annual Review of Physiology (Cohen, 1989; Cohen *et al.*, 1989; Salzberg, 1989; Lieke *et al.*, 1989; Blasdel, 1989). For reviews on related optical methods, see Tsien, 1989 (Ca^{++}-sensitive dyes and other ion-sensitive dyes), and Lieke *et al.*, 1989 (intrinsic activity-dependent signals).

2.2 A DYE-RECORDING PRIMER

2.2.1 *Optical recording*

The basic principle of optical recording is that the electrical activity of neurons modulates certain of their optical properties. By measuring changes in these optical properties, one may indirectly measure electrical activity. Usually, the optical signals intrinsic to the preparation are quite small, and so it is stained with an extrinsic probe—a voltage-sensitive dye—in order to get bigger signals.

For dye recording, the cells of interest are first stained with a suitable dye, and are then illuminated at an appropriate wavelength during a period when electrical activity is occurring. The optical signal is usually measured either in absorption (observation wavelength equal to illumination wavelength) or in fluorescence (observation wavelength longer than illumination wavelength). Dye molecules bind to the plasma membrane of the neurons, and thus are in a position to respond to changes in the electric field across the membrane. When the neuron is electrically active, the change in membrane potential alters the absorption and/or fluorescence of the dye molecules. These changes are usually quite small (between 1 part in 10^5 and 1 part in 10), and the light levels can be very low

(especially when recording fluorescence from single cells), calling for quite sophisticated optical detectors.

A note on terminology: absorption measurements are interchangeably called transmission measurements, since the light actually detected is the transmitted light that has passed through the specimen without being absorbed. Transmission measurements are always along the direction of illumination, whereas fluorescence can be recorded at 0°, 90°, or 180°, whichever is most convenient.

2.2.2 Dye staining

Fig 2.1 shows three neurons that have been stained with the voltage-sensitive dye RH423, a styryl dye used for fluorescence measurements. The cells shown are part of a

100 µm
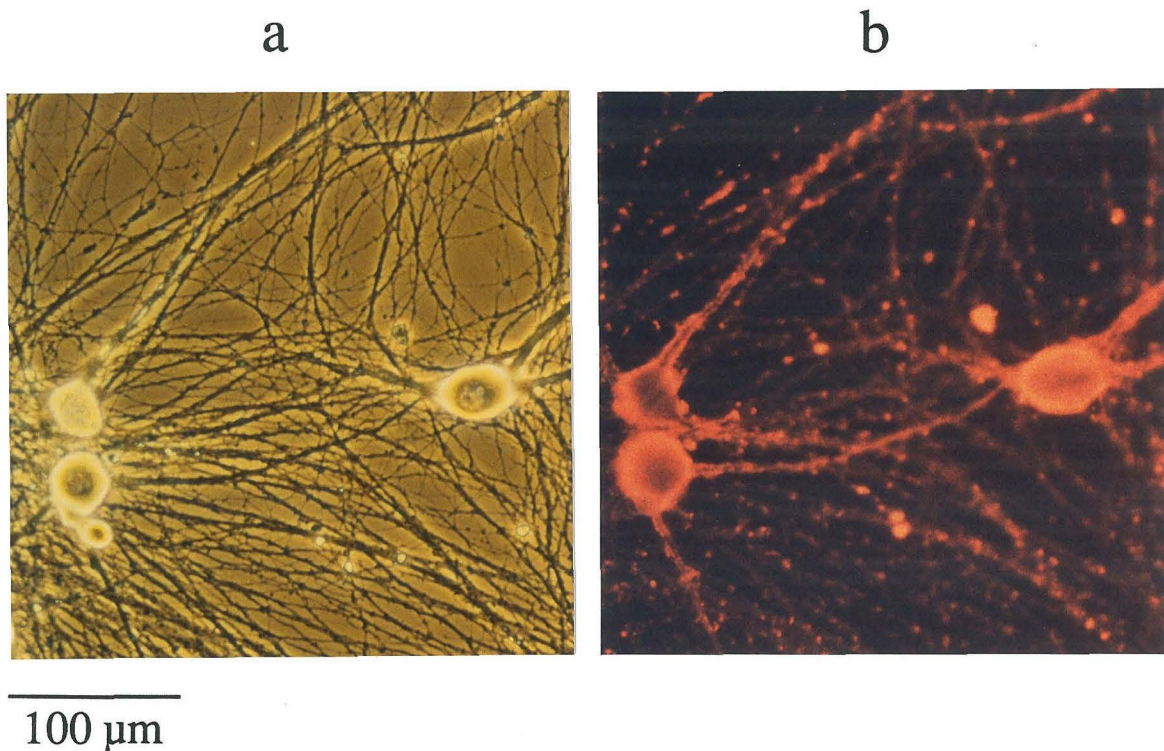
Figure 2.1 Three neurons from the rat superior cervical ganglion, grown in culture for 7 weeks. *a)* Phase-contrast picture. *b)* Fluorescence picture, taken after staining for 5 min with 1 µM RH423. (*b* was taken at a slightly higher plane of focus than *a*.) Fig 2.3 shows an optical recording made from the rightmost cell.

phospholipid bilayer

extracellular solution
(aqueous)

hydrophobic domain
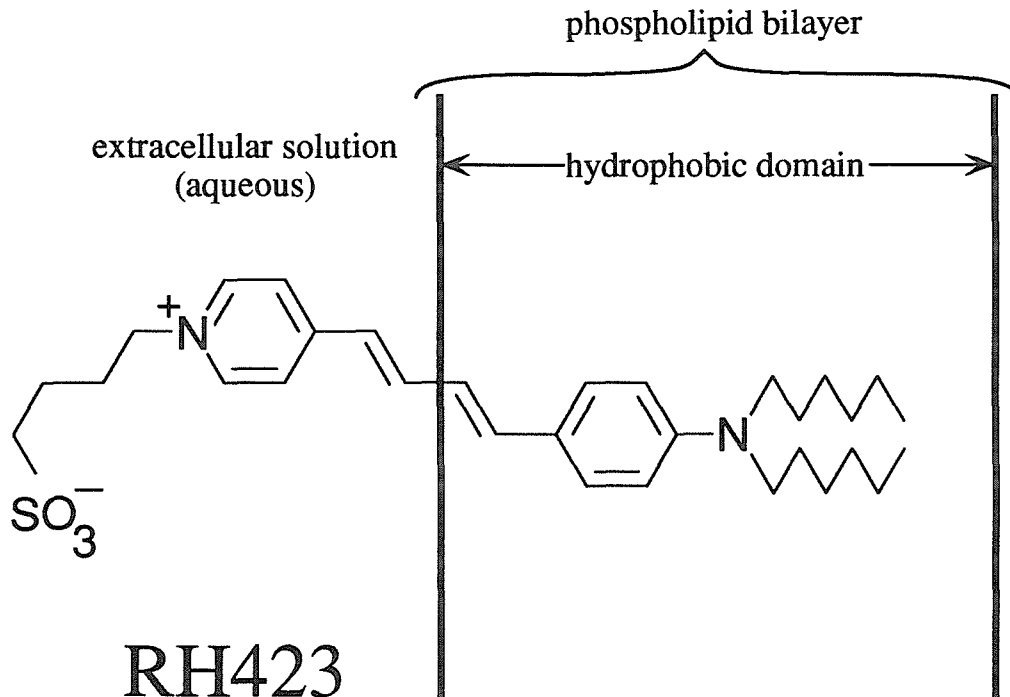
RH423

Figure 2.2 Structure of the styryl dye RH423. The dye molecule is shown bound to the plasma membrane. The position of the dye within the membrane is not meant to be exact, only suggestive.

mass culture that was plated on a polylysine/laminin substrate 7 weeks before the picture was taken; the network of processes is healthy and dense. The staining procedure is very simple: the culture is washed by replacing the external solution thrice, a 1 μM solution of RH423 is applied for 5 minutes, then unbound dye is removed by washing thrice more. Note that the dye stains membranes preferentially, so that the cell bodies show as bright rings. The microscope was focussed on the cell equators, where the rings are particularly bright due to a large area of edge-on membrane. Some of the thicker processes show as unfilled cylinders, again because the dye is staining the membrane. Membranous debris also stains very brightly, and is responsible for the punctate staining.

Fig 2.2 shows the structure of RH423. It is amphipathic, having a hydrophilic end (the charged sulfate group) and a hydrophobic end (the twin alkyl tail). Because of this double-ended nature, the dye molecule is thought to be highly oriented in the membrane:

the sulfate group out in water, where its charge can be effectively solvated, and the alkyl tails in the hydrophobic interior of the membrane bilayer. (The figure is only a cartoon: the exact depth of the molecule in the membrane is not known.) The dye binds very strongly to membranes (as seen in Fig 2.1) because of the long hydrophobic end, but isn't very permeant because of the localized charge at the sulfate. The chromophore—that part of the molecule responsible for absorbing and emitting photons—is bracketed by the two nitrogen atoms: it comprises the two rings, and the polymethine chain that links them.

2.2.3 Fluorescence signals

The rightmost cell in Fig 2.1 was penetrated with a glass microelectrode, then stimulated intracellularly while its fluorescence was recorded. Fig 2.3 shows the result. Scale bars are as marked; the arrow for the optical signal indicates the direction of *increasing* fluorescence. RH423 is a fast dye, whose optical response can follow submillisecond changes in membrane potential. (Slow dyes are mentioned briefly in section 2.3.) The optical signal—a decrease in this case—follows the membrane potential quite well, though the bridge-balance artifacts in the electrical signal make direct comparison a little difficult. The detector used to record the signal was slightly larger than the cell body, and the total photocurrent from this pixel was 0.86 nA. The optical signal at the peak of the action potential is only a 0.8% decrease in this photocurrent, but the signal-to-noise ratio is still quite good (over 20). Under the proper conditions, optical recording can be quite sensitive!

a) intracellular

V_m

50 mV

b) fluorescence

$\frac{\Delta F}{F}$

.5%

20 ms
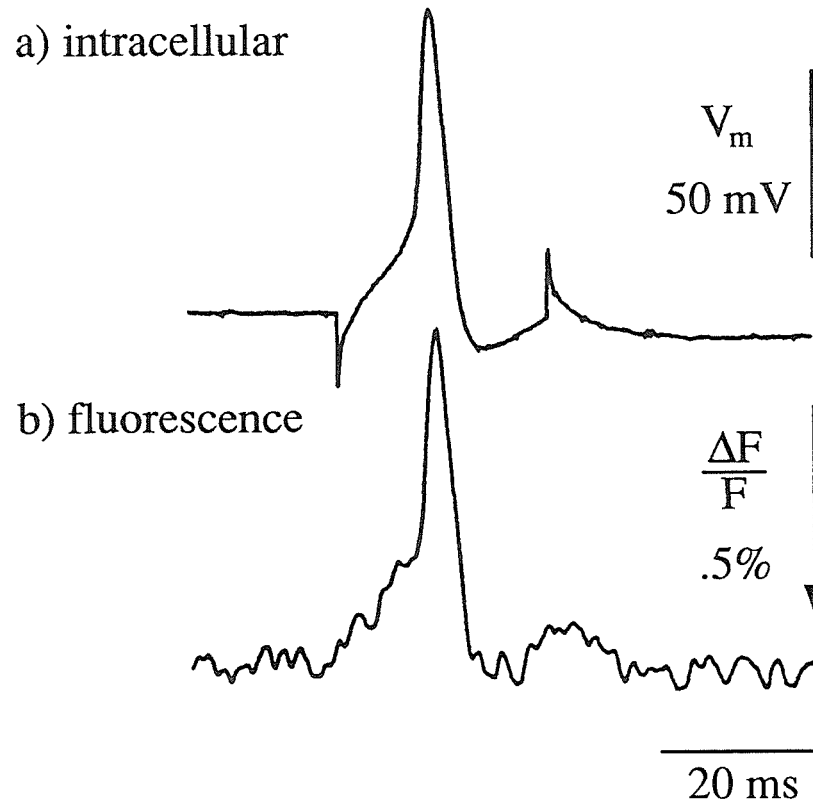
Figure 2.3 Simultaneous electrical and optical recording from the rightmost neuron in Fig 2.1. *a)* Recording from glass intracellular electrode. The cell was stimulated by injecting a square current pulse through this electrode; the duration of this current pulse is indicated by the bridge artifacts. *b)* Optical recording, showing a voltage-dependent decrease in the cell's fluorescence. This is a single, unaveraged record. The *arrow* points in the direction of increased fluorescence.

The sensitivity of a particular dye is often expressed as $\Delta F/F$, where F is the resting fluorescence intensity of a cell, and ΔF the change in fluorescence due to a given voltage change. For this ratio, the following four conditions will usually hold:

1) $\Delta F/F$ is independent of illumination intensity, since ΔF and F are both linear in intensity. It is likely that this independence breaks down at extremely high intensities, when the dye molecule starts absorbing two photons before it has a chance to fluoresce, but this is far outside the regime relevant here.

2) $\Delta F/F$ should be independent of the membrane area being observed, since both ΔF and F should scale as the area.

3) $\Delta F/F$ should also be independent of dye concentration, provided that dye molecules do not interact with each other. This independence will fail for complex dye mechanisms, however: for example, if the voltage-sensing response depends on dye dimerization, $\Delta F/F$ will certainly depend on the concentration.

4) $(\Delta F/F)/\Delta V$ is independent of the size of the voltage change, since the dye response is linear in membrane potential. This linearity holds very well for all of the commonly-used fast dyes for which it has been tested.

These properties make $\Delta F/F$ a useful figure of merit for the sensitivity of a particular dye. ("$\Delta F/F$" is the commonly-used shorthand for $(\Delta F/F)/\Delta V$.) Other things being equal, $\Delta F/F$ should be constant from cell to cell when using a particular dye, regardless of illumination intensity, the size of that cell's action potential, or the degree of staining of that cell (with the reservations stated under condition 3). Thus, it is a useful number to use when comparing different dyes. Take Fig 2.3 as an example: the change from the peak of the action potential to the trough of the afterhyperpolarization is 91 mV, and the change from peak to trough in the optical signal is 0.84%, so $\Delta F/F$ here is 0.92%/100 mV.

In practice, $\Delta F/F$ is *not* constant across cells. The most obvious complication is background staining: for instance, if a piece of bright debris were attached to a cell, it would increase F without changing ΔF, thus reducing $\Delta F/F$. This variation makes it necessary to average $\Delta F/F$ over many cells in order to measure a sensitivity that may be compared between dyes. $\Delta F/F$ is also not the most relevant figure of merit; the signal-to-noise ratio S/N is, since S/N determines the smallest voltage change that can be seen. In

the best case, where shot noise (noise due to photon counting statistics) dominates, $S/N \propto (\Delta F/F) \cdot \sqrt{F}$. However, this figure is highly dependent on the particular apparatus being used (since F depends on both illumination intensity and collection efficiency), and so is difficult to compare between different apparatuses. In the end, $\Delta F/F$ is the handiest (and most widely used) measure of fluorescent-dye sensitivity.

Two limitations of dye recording should be mentioned here. First, voltage-sensitive dyes cannot be used to measure the resting potential, since the signals only show *changes* in fluorescence[1]. Second, dye signals cannot show the absolute magnitude of voltage changes, only their time course and relative sizes. Because of the aforementioned variation in $\Delta F/F$, a 0.2% change might indicate a 100 mV change in one cell, but only 20 mV in another. $\Delta F/F$ is presumably constant when averaged over a given cell, however, and so it is possible to measure the *relative* sizes of changes in the *same* cell, and even to guess absolute sizes by making an assumption about the size of the action potential. For instance, if an action potential in cell X gives a 1% change in fluorescence, and an EPSP gives a 0.2% change, it is safe to say that the height of the EPSP is one-fifth that of the action potential. If it were known that action potentials in healthy cells of cell X's type were always 90 mV high, the height of the EPSP could be estimated as 18 mV. Despite this difficulty in calibration, the speed and linearity of the dye response means that the shape of a dye signal should be an accurate reflection of the time course of the change in membrane potential, even though its absolute magnitude is not known.

---

[1]In theory, it may be possible to measure the resting potential if the dye's response is nonlinear in voltage, or if it exhibits a voltage-dependent spectral shift. Calibrations for these measurements would be extremely difficult, however, and in practice fast dyes have never been used for this purpose.

2.2.4 Optical apparatus

Fig 2.4 shows the apparatus used to record the signals shown in Fig 2.3. Light

from a stabilized mercury arc lamp is captured by a collector lens, focussed by intermediate

lenses, and turned on or off by a shutter. The desired wavelengths of exciting light are

passed by an excitation filter, and then reflected by a dichroic mirror. This mirror has the

property of reflecting light shorter than a cutoff wavelength, and transmitting light longer

than the cutoff. In this case, the excitation filter and dichroic mirror combine to select the

546 nm line of the mercury arc. A high-numerical-aperture objective lens focusses this

light onto the stained cell, and then collects the emitted fluorescence. The emitted light is

now *transmitted* by the dichroic mirror, due to its longer wavelength. The dichroic mirror

and emission filter form a long-pass filter with a minimum wavelength cutoff of 610 nm.
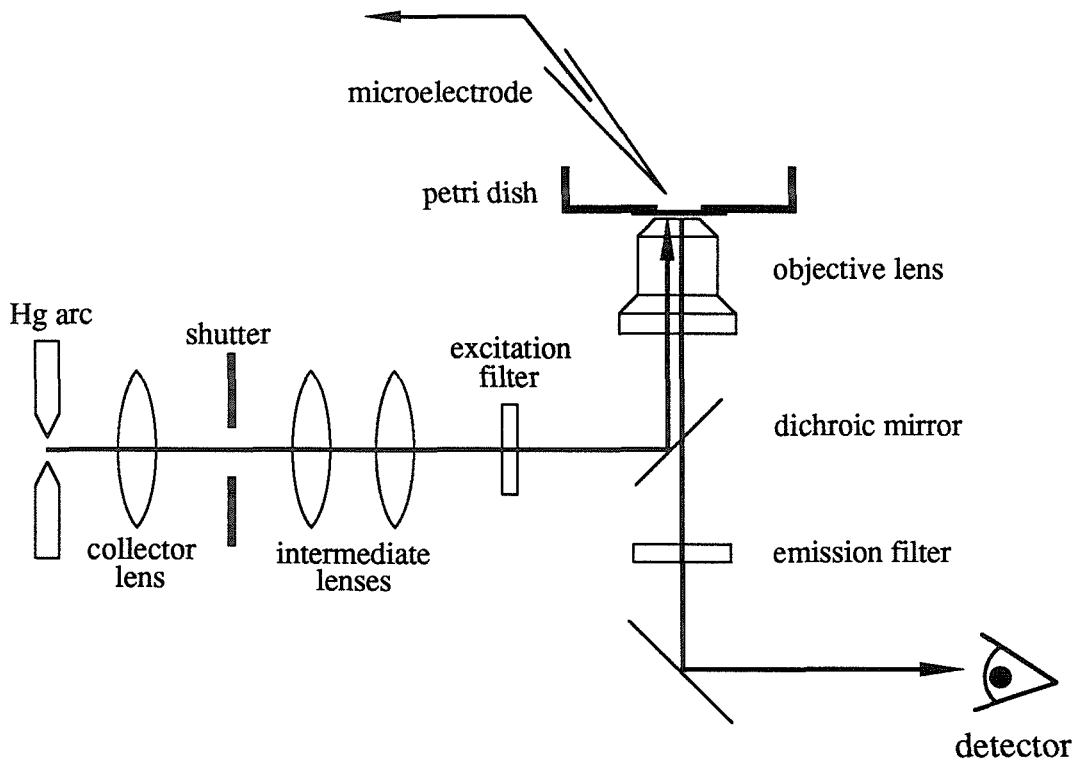
Figure 2.4 Optical apparatus for fluorescence recording. The neuron, not visible at this scale, is in the center of the petri dish, penetrated by the microelectrode and focussed by the objective.

The signals shown in Fig 2.3 were detected by a very low-noise photodiode/amplifier combination, while for Fig 2.1 the detector was just a 35 mm camera.

2.2.5 Signal processing

Fig 2.5 shows the rather complex procedure of data reduction that is necessary to remove the effects of dye bleaching and yield Fig 2.3. Fig 2.5*a* is the raw fluorescence trace, showing the voltage-sensitive signal as a barely-visible downward deflection at 50 ms. This signal is dwarfed by the initial step from 0 to 0.86 nA (the resting fluorescence) when the shutter opens. Fig 2.5*b* shows the same data as *a*, but now inverted and expanded by a factor of 70. The action potential, now clearly visible, is well above the background noise. The finite resolution of the 12-bit analog-to-digital converter is also revealed. Trace *b* shows an overall upward trend, due to photobleaching of the dye (remember that this trace has been inverted, so that an *upward* deflection is a *decrease* in fluorescence). In order to remove this bleaching artifact, a trace without stimulation was recorded (Fig 2.5*c*). Subtracting this bleach trace from the trace recorded with stimulation yields the pure voltage-dependent signal, uncomplicated by bleaching artifacts. However, a simple subtraction would add extra noise; therefore, the bleach trace was fitted by a quadratic function, also shown in *c*, and this smooth curve was subtracted from *b*. Finally, the difference was digitally low-pass filtered at 300 Hz, yielding the final result shown in Fig 2.5*d* (identical to Fig 2.3*b*).
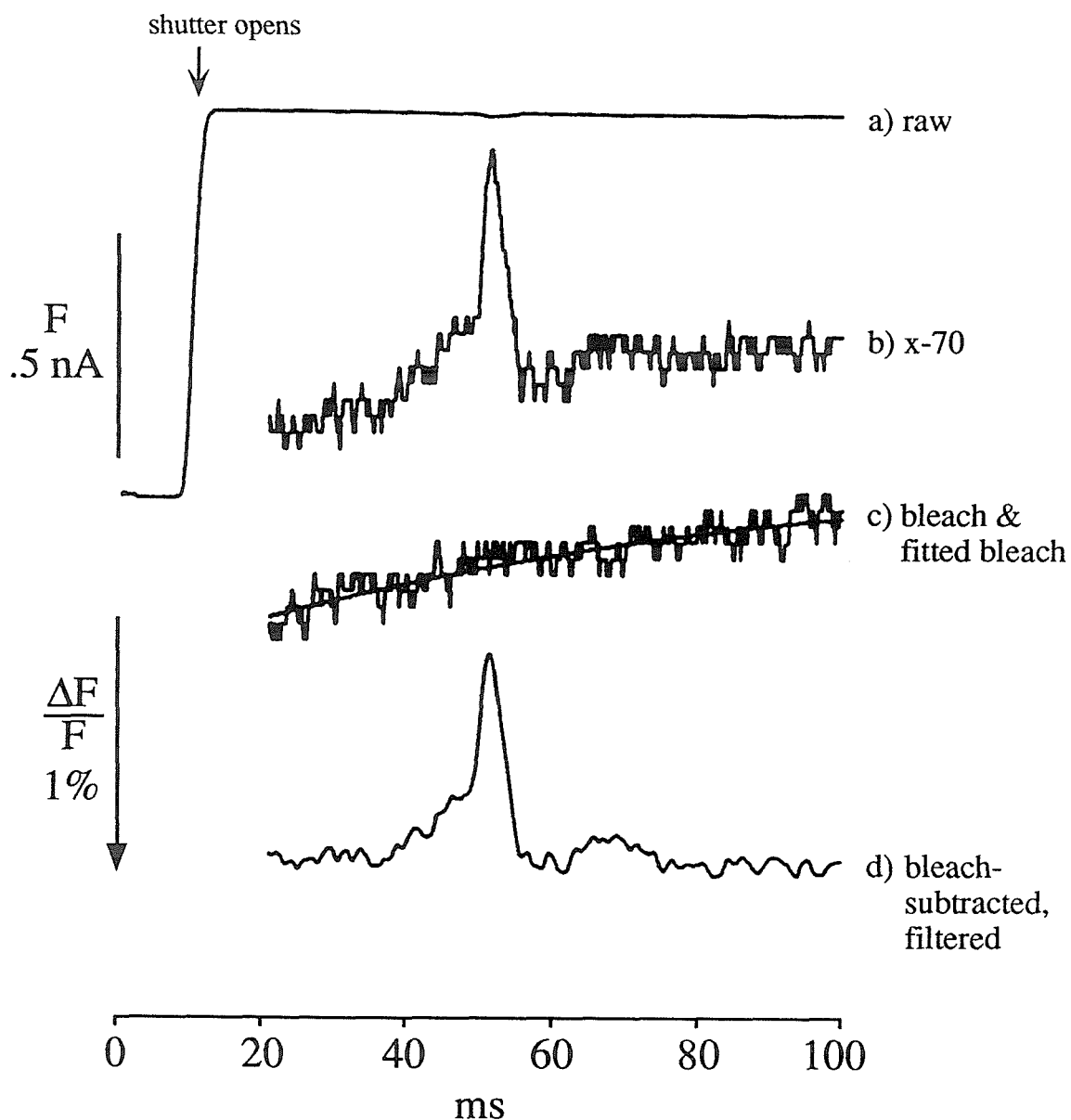
Figure 2.5 Bleach-subtraction and filtering of the optical signal. *a*) Raw fluorescence trace. The *arrow* indicates the opening of the illumination shutter. The optical signal, a small decrease, can just be seen. *b*) Amplified, inverted fluorescence signal. At the scale shown here, the gain is about -70. *c*) Fluorescence signal with no stimulus, showing the bleach artifact only. The *jagged trace* shows the actual bleach, while the *smooth trace* shows a quadratic fit to the bleach. *d*) Bleach-subtracted, filtered trace. The quadratic fit from *c* has been subtracted from *b*, and the difference filtered digitally at 300 Hz. **Scale bars:** *F* is the scale for *a*, while $\Delta F/F$ is the scale for *b*, *c*, and *d*.

2.2.6 Bleaching and phototoxicity

Bleaching is often very rapid, especially with the very bright illumination used for fluorescence measurements. For the dyes that I have used, the bleach rate was quite variable, but usually between 0.1% and 1% per 100 ms. After some tens of seconds of illumination, this significantly reduces the resting fluorescence, and thus the fluorescence signal.

A more serious problem is that of phototoxicity, also known as photodynamic damage. When a stained cell is illuminated for too long, the dye kills the cell, though the same illumination would have no effect on an unstained cell. This toxicity is thought to be due to formation of singlet oxygen by the illuminated dye molecules. For the experiments described in this thesis, using the dye RH423 on rat SCG neurons at the usual level of illumination, photodynamic damage becomes serious after a few tens of seconds. It is also possible for dyes to have pharmacological effects, i.e., to affect the behavior of the neurons even without illumination. I have not noticed any pharmacological effects in these experiments.

In order to limit photodynamic damage and bleaching, it is essential to keep illumination intensity and exposure time to a minimum. This explains the need for the shutter. By limiting exposure to short flashes of about 100 ms, with the shutter opening just before stimulation and closing after all interesting electrical activity has occurred, it is possible to conduct a useful experiment within the time limit set by phototoxicity.

2.2.7 Absorption signals

The optics for absorption measurements are of course quite different from those for fluorescence, but the experiments themselves are carried out in much the same way. The preparation is stained with an appropriate dye, and illuminated in order to measure absorption signals. Photodynamic damage and bleaching are problems for absorption measurements, just as for fluorescence.

-ᴇᴇᴇᴇᴇ- tungsten filament

— shutter

excitation filter

condenser lens

microelectrode

petri dish

objective lens

emission filter

detector
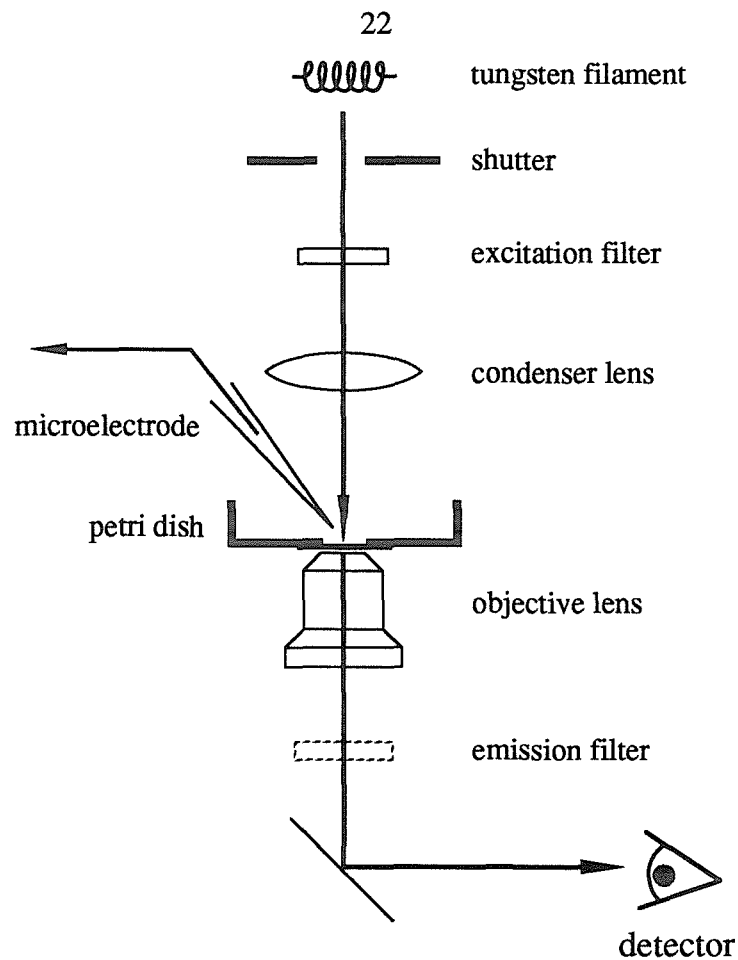
Figure 2.6 Optical apparatus for absorption recording. The emission filter is often omitted.

An example of what an optical system for measuring absorption signals might look like is shown in Fig 2.6. There are several features that differ from the fluorescence setup of Fig 2.4. (1) Transillumination is used instead of epiillumination. For epiillumination, illumination and light collection were from the same side through the same lens. Here, the illumination focussed by the condenser passes through the specimen, and is collected by the objective on the other side. (2) Since the exciting and emitted beams no longer share the same light path, a dichroic mirror is unnecessary. (3) The excitation and emission filters pass identical wavelengths. In fact, if fluorescence and stray light are negligible, the emission filter may be left out altogether. (4) Since fractional changes in intensity are much

smaller for absorption signals, it is important to have a very stable light source. A tungsten-halogen incandescent lamp is usually used instead of a mercury arc.

Terminology for the sizes of absorption signals is somewhat confusing. I will use I_0 for the transmitted intensity before staining, T for the resting transmitted intensity after staining, and ΔT for voltage-dependent changes in transmitted intensity. (If the unstained specimen is transparent, I_0 will just be the illuminating intensity incident on the specimen.) Using these definitions, I_0-T is the steady-state level of light absorbed by the dye, and ΔT is the voltage-dependent change in light absorbed. The analog of $\Delta F/F$ for absorption is then $\Delta T/(I_0$-$T)$, the fractional change in absorption. Just as $\Delta F/F$ is a good measure of intrinsic dye sensitivity, $\Delta T/(I_0$-$T)$ should be independent of illumination intensity, independent of membrane area, and (with luck) independent of dye concentration, and thus should be a parameter useful when comparing dyes.

$\Delta T/(I_0$-$T)$ can be awkward to measure, since the difference between I_0 and T is often quite small. It is common practice to quote $\Delta T/T$ instead, since this fraction can be measured continously during an experiment. Since $S/N \propto (\Delta T/T)\cdot \sqrt{T}$, this ratio is closely related to the signal-to-noise ratio, but $\Delta T/T$ is *not* independent of membrane area or dye concentration. Another term often seen in the literature, ΔA, is closely related to $\Delta T/T$, but its use has been quite inconsistent. Cohen and collaborators, in their papers about screening dyes on squid giant axon (Ross *et al.*, 1977; Gupta *et al.*, 1981), define $\Delta A/A_r = -\Delta T/(I_0 - T)$. Waggoner, on the other hand (Waggoner, 1976) uses $\Delta A = \log_{10}[(T + \Delta T)/T] \cong \Delta T/2.3T$ for small ΔT; this ΔA is the change in the absorbance $A = \log_{10}(I_{\text{incident}}/T)$. I will avoid using the ambiguous ΔA and stick to $\Delta T/T$, converting when necessary.

2.2.8 Dye mechanisms

An understanding of dye mechanisms is useful both for designing new and better dyes, and for using presently available dyes in experiments. Of interest are the dyes'

staining properties, their spectroscopic (absorption and emission) properties, and their voltage-sensing properties. The theoretical bases for all three are described in some detail in appendix A; potentiometric mechanisms are briefly summarized here.

The voltage-sensitive signal from an absorption dye must of course depend on voltage-dependent changes in its absorption properties. For fluorescent dyes, absorptive changes are compounded with emissive changes. These spectroscopic changes may arise from several sources. First, the environment of the dye molecule: for instance, if the molecule moves from the membrane to aqueous solution, its spectra are usually altered. Second, the state of the molecule: for instance, if two dye molecules bind together to form a dimer, their spectra usually change, and their fluorescence is quenched. Third, the orientation of the molecule: for instance, if the molecule rotates so that its transition moment is along the line of illumination, its absorption and fluorescence will both decrease to zero. Finally, the energy levels of the molecule: a change in electric field may directly alter the energy levels of the ground and excited states of the dye.

Three types of potentiometric mechanism are well established: redistribution, reorientation, and electrochromism. For redistribution dyes, changes in membrane potential alter the partitioning of dye between the membrane and aqueous solution. For reorientation dyes, changes in potential rotate the dye molecules, altering their degree of dimerization as well as their orientation. For electrochromic dyes, changes in electric field differentially alter the energies of the ground and excited states, directly altering the transition energy and shifting the absorption and emission spectra. (These mechanisms are more thoroughly explained in Appendix A.)

These mechanisms must all be taken with a grain of salt, since the biophysical experiments that support them have of necessity been carried out in artificial membranes. Since dye sensitivity varies so much between biological systems, it would not be surprising if dye mechanisms also varied between biological membranes and artificial membranes. Indeed, in at least one case this is partially true (Loew *et al.*, 1985).

Electrochromism is the mechanism most relevant here, since it is thought to apply to the styryl dyes that have been used throughout this thesis. If styryls do indeed act electrochromically, a depolarization should simply blue-shift their spectra, and they should have simple bipolar action spectra. Depolarization should increase their absorption below the wavelength of maximal absorption, and decrease it above; emission should be affected similarly. (See Appendix A for details.) Thus, an electrochromic mechanism suggests optimal filters for excitation and emission. Experiments to test these predictions and find the best filters are described in Chapter 6.

2.2.9 Other optical recording techniques

Also of interest are two other optical methods that can also give information about electrical activity: ion-sensitive dyes—especially calcium-sensitive dyes—and intrinsic optical signals. Calcium-sensitive dyes don't measure membrane potential directly, but can see changes in intracellular calcium due to electrical activity. They have several advantages: the signals are very large, with changes on the order of 50% (compared to 1% for fluorescent voltage dyes, and 0.1% for absorption voltage dyes), so that recordings can be made at high spatial resolution. At least in the case of fura-2, the Ca^{++} concentration can be calibrated reasonably well. For a review, see Tsien (1989).

Intrinsic signals are those activity-dependent optical signals that can be seen without any extrinsic dye. In fact, the first optical signal recorded was a light-scattering signal (Hill and Keynes, 1949). Recently, intrinsic signals have been used to record from cortex with high spatial resolution (Grinvald *et al.*, 1986). Slow intrinsic signals appear to be due to light-scattering and absorbance changes, and do not seem to be a direct probe of membrane potential. They do, however, seem to reflect the activity of the small patch of brain that they come from, and intrinsic-signal recording holds great promise for recording the patterns of activity from cortex. A great advantage of this method is that without dyes, there are no pharmacological or phototoxic effects. For a review, see Lieke *et al.* (1989).

2.3 HISTORY

2.3.1 Overview

Voltage-sensitive dye signals were discovered just over twenty years ago. The first ten or fifteen years of dye history were spent on technical improvements, synthesizing better dyes and improving optical systems. The technical difficulties with dye recording are still quite constraining; it's definitely preferable to use conventional electrodes, if possible. (This is mostly a testament to the power and precision of conventional techniques, which also have improved greatly over the last two decades.) Still, there are questions that cannot be addressed with conventional electrodes, and in the last five or ten years, dye recording has matured enough that it can be applied to biological questions, and start to fulfill some of its promise. Before discussing my work in the rest of the thesis, it is instructive to consider the work of those who have gone before. There are three main technical challenges for dye-recording: (1) increasing the sensitivity of the dyes, (2) reducing their phototoxicity, and (3) improving detector optics and electronics.

Improvements in voltage sensitivity have been hampered by an insufficient understanding of the molecular mechanisms involved. Over the years, the voltage-sensing mechanisms for several classes of dyes have been worked out on artificial bilayer membranes (Appendix A), but alas, the behavior on these model systems doesn't necessarily carry over to real biological systems. In the face of this theoretical ignorance, most improvements in dye sensitivity and phototoxicity have been made by a process of organic synthesis, trial, and error. This process is complicated because the sensitivity of any particular dye varies between different biological preparations and species. The original massive screenings of dyes were done on the squid giant axon, which is a very simple and convenient system because of its enormous size (being up to 1 mm in diameter and several cm in length). However, the dyes that were most sensitive for the giant axon

were far less sensitive for vertebrate neurons (Ross and Reichardt, 1979). Even worse, they had different spectral responses on preparations besides the squid giant axon, suggesting that they were operating by a different mechanism. Dyes must therefore be screened on the particular cell type being used. The earliest dyes were developed for invertebrate preparations, but very sensitive dyes have been developed for vertebrates during the last decade. With all the compounds that have been tried, it should be possible to find a reasonably sensitive dye for any preparation.

Photodynamic damage is even less understood. Its effect is simple: stain a cell with almost any dye (including other non-voltage-sensitive dyes used for vital staining), shine a bright light on it, and it dies after a while. Presumably, dye molecules that have absorbed photons become excited, and occasionally react with an oxygen molecule to form extremely reactive free oxygen radicals. That these radicals are toxic is well known. Despite this general understanding, the detailed mechanisms of photodynamic damage are unknown: What is the mechanism of free radical formation (and how would one design a dye to minimize it)? Which sites in the cell are attacked by free radicals to cause damage?

Phototoxicity can be controlled in several ways, but only to a certain degree. First, it is crucial to limit the intensity and duration of illumination as much as possible. Intensity can only be reduced at the expense of the signal-to-noise ratio, however (in the shot-noise-limited case), and the duration of illumination can't be shorter than the duration of the phenomena being studied. Second, removing dissolved oxygen from the bathing solution can greatly reduce phototoxicity (Cohen *et al.*, 1974, Parsons *et al.*, 1989a). Indeed, this is the best evidence that photodynamic damage is caused by oxygen radicals. This remedy can only be carried so far, since cells need oxygen to live. Third, there have been some experiments with antioxidant protection agents that might mop up free oxygen radicals. These experiments have not met with much success (Parsons *et al.*, 1989a). As with voltage-sensitivity, the main improvements in phototoxicity have come from screening many dyes.

While dyes have been improving through hit-and-miss screenings, detection systems have improved through rational design (optics and electronics being relatively well-understood sciences). Especially over the last decade, great progress has been made in designing better optical systems and detector electronics, and the performance of both is fast approaching theoretical limits. The history of optical detectors is reviewed in Chapter 3, for easy comparison with the apparatus described there.

One of the main themes of the next few subsections is the gradual improvement in dye sensitivities over the years. In order to give an idea of the size of these improvements, I give dye sensitivities as $\Delta F/F$ for fluorescence dyes, and $\Delta T/T$ for absorption dyes. The chief value of these two measures is that they are readily calculable from the numbers given in the literature. Keep in mind that they do not directly reflect the signal-to-noise ratio S/N, which depends also on the detected light intensities. Nor are they necessarily intrinsic properties of the dye. In particular, $\Delta T/T$ depends crucially on the degree of staining; $\Delta F/F$, on the other hand, should be relatively independent of dye concentration, and is an intrinsic biophysical parameter of the dye, except for effects of background staining.

2.3.2 Early history

As early as 1949, Hill and Keynes saw small changes in the light scattered from (unstained) nerves after repeated firing (Hill and Keynes, 1949; Hill, 1950). The modern history of optical recording began with the advent of signal-averaging computers, which made it possible to measure very small (but repeated) signals, by averaging away random noise. Cohen *et al.* (1968) reported intrinsic signals (that is, signals with no dye applied) during single action potentials in the squid giant axon; the fractional changes in light-scattering and birefringence were about 5×10^{-6} and 8×10^{-6} per action potential, respectively. Tasaki *et al.* (1968) made the great leap forward to extrinsic signals, staining their invertebrate nerves with the fluorescent dye ANS before measuring changes in

fluorescence, light-scattering, and birefringence. Using ANS, they saw a $\Delta F/F$ of about 10^{-4} per action potential, much larger than any intrinsic signals that had been seen.

The goal of these pioneering studies was to further understand the mechanism of action potential propagation, since the intrinsic optical signals presumably reflected reorientation of membrane lipids, or some other membrane-biophysical process. It had been suggested very early by David Gilbert that "optical signals might be used to follow activity in the nervous system" (see Cohen, 1989), but this seemed very difficult with the small intrinsic signals, for which thousands of sweeps needed to be averaged. The discovery of extrinsic, dye-dependent signals set off a search for dyes that would give larger signals. After screening about 100 dyes, this search paid off (Davila *et al.*, 1973) with the discovery that the dye merocyanine 540 gave $\Delta F/F$ of 0.1% (10^{-3}) per action potential on the squid giant axon. These signals could be easily detected in a single sweep. These large dye signals meant that interest soon shifted away from the biophysics of squid giant axons, and towards recording from the much smaller cells in intact nervous systems.

First, the dye signals had to be understood. In order for dye-recording to replace electrodes, it was desirable that (1) the signals depend linearly on the membrane potential, and (2) that they should be able to follow fast changes in membrane potential. It was soon discovered (Cohen *et al.*, 1974) that dye responses fell into two classes: fast (response times of microseconds), and slow (response times of seconds or slower). Fast dyes were clearly the class of interest for recording action potentials (which last for milliseconds). The structures of six fast dyes that are mentioned below are shown in Fig 2.7; all have given large signals in some preparation.
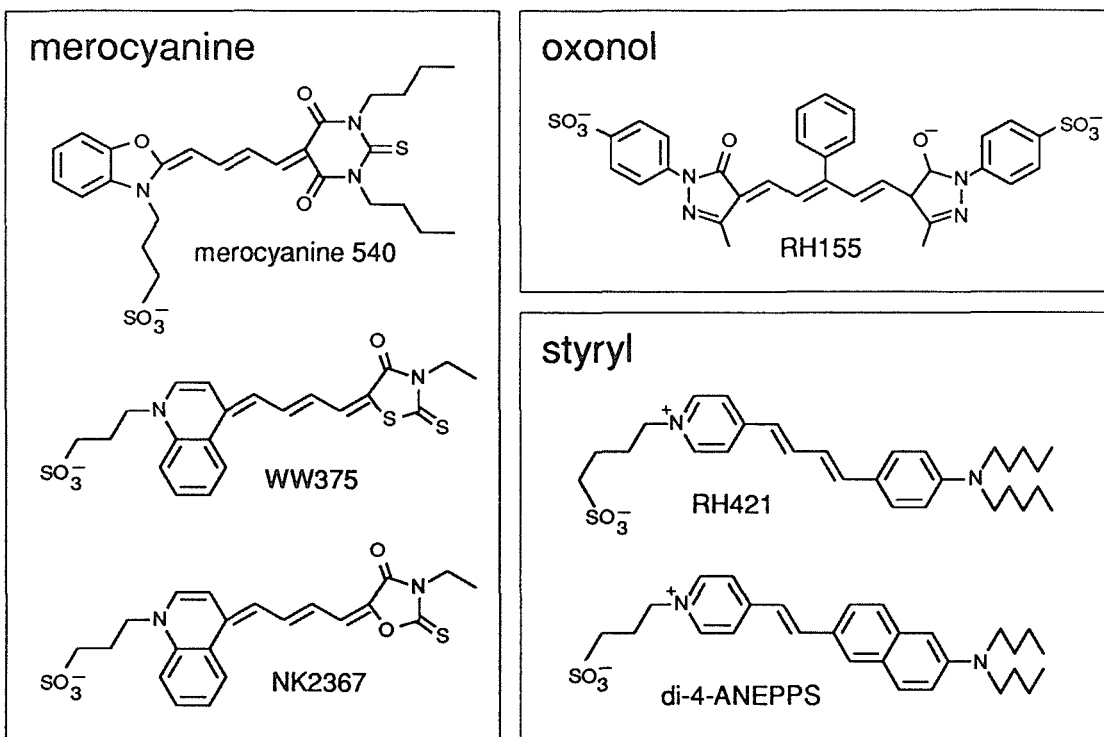
Figure 2.7 Structures for six voltage-sensitive dyes. Sources for structures are as follows: merocyanine 540, WW375, and NK2367 (all from Waggoner, 1979); RH155 (Konnerth *et al.*, 1987); RH421 (Grinvald *et al.*, 1983); di-4-ANEPPS (Fluhler *et al.*, 1985).

Cohen *et al.* (1974) used the squid giant axon to study the properties of merocyanine 540 (dye I in their then-current nomenclature). They found that this dye gave fluorescence signals that were linear with membrane potential over a range of 200 mV, and that these signals responded to membrane potential within microseconds. Originally it was not clear that the dye signals depended on potential, and not some other parameter such as membrane current; they used voltage-clamp experiments to show that while the time course of the dye signal accurately reproduced the course of the membrane potential, it did *not* resemble that of the membrane current.

Slow dyes are worth a short mention here. Although slow, they give much bigger signals than fast dyes. Hoffman and Laris (1974) were the first to use slow dyes to measure membrane potentials from suspensions of cells. They used the slow cyanine dye diO-C$_6$(3) to record from red blood cells, and found changes in fluorescence of up to 1%

per mV change in potential (*i.e.*, roughly 1000 times larger than the fast signal from merocyanine 540 on squid axon). Sims *et al.* (1974) showed that the cyanine dyes, which were membrane-permeant, work by redistributing in response to changes in membrane potential, probably crossing the membrane into and out of the cell, which explains their slow responses. The changes in concentration due to redistribution change the concentration of dye-dye dimers, whose fluorescence is much lower than that of dye monomers, thus leading to the observed change in fluorescence. Despite their enormous signals, slow dyes respond too slowly to be useful for recording action potentials and other fast electrical activity, and I will not discuss them further.

Another major innovation during this early period was the use of absorption rather than fluorescence. Ross *et al.* (1974) made both fluorescence and absorption measurements using a close analogue of merocyanine 540 on squid giant axon. They reported changes in transmission of $\Delta T/T = .02\%/100$ mV, compared with $\Delta F/F = 0.1\%/100$ mV for fluorescence. Even though $\Delta T/T$ was five times lower than $\Delta F/F$, the signal-to-noise ratio was actually twenty times higher for absorption. This is because the resting transmitted intensity T for the absorbance measurements was much higher than the resting fluorescence intensity F. In the shot-noise-limited case, the signal-to-noise ratio goes as $(\Delta I/I) \cdot \sqrt{I}$, where I is the resting intensity, and ΔI is the change in intensity. Ross *et al.* did not quantitate resting intensities, but for example if T was 10^4 times as large as F, this would account for the quoted difference in signal-to-noise (assuming that their apparatus was shot-noise limited). In studies after this one, dyes screened on the giant axon were tested both for fluorescence and for absorbance signals. Some dyes give large signals in both modes, but most are best in fluorescence only or absorption only.

2.3.3 Dye screenings

These early dyes were not particularly sensitive, and were highly phototoxic. For instance, Cohen *et al.* (1974) reported significant damage when giant axons stained with merocyanine 540, in normal (oxygenated) seawater, were illuminated for as little as 10 seconds. In order to improve both sensitivity and reduce phototoxicity, three massive searches (Cohen *et al.*, 1974, already mentioned; Ross *et al.*, 1977; Gupta *et al.*, 1981) were carried out using the squid giant axon as a test preparation. Over a thousand dyes were tried in these screenings. Some of these were preexisting compounds, while others were specifically synthesized as voltage-sensitive dyes in Alan Waggoner's laboratory.

Merocyanine 540, the best dye found in the Cohen *et al.* (1974) screening, has been described above. The best dye found by Ross *et al.* (1977) was a merocyanine-rhodamine, WW375 (their dye XVII), which gave absorbance signals thrice as large as those from merocyanine 540, and caused seventy times less photodynamic damage. Gupta *et al.* (1981) reported several dyes that were as sensitive as WW375, including NK2367, a close analogue of WW375 that has since been used extensively. All of these dyes, however, were more phototoxic than merocyanine 540.

Unfortunately, it now seems that dyes that are very sensitive for the squid giant axon are not necessarily sensitive on other preparations (*e.g.*, Ross and Reichardt, 1979), and dyes that were insensitive on the giant axon give large signals in other systems (*e.g.*, RH414; see Grinvald *et al.*, 1983 and Grinvald *et al.*, 1988, section IV.H.2). The reasons for this variability are not at all understood, but it means that the enormous effort that was put into screening dyes on squid axon has not paid off in a universal dye that works for all cells. This is not to say that the dyes that were tested on squid axon are not useful elsewhere; many are, but these must be ferreted out by further testing. The massive screening on giant axon needs to be replaced by smaller screenings on the specific preparation of interest.

During the days of giant-axon screening, most new dyes were synthesized by Alan Waggoner and two others in his laboratory, Jeff Wang and Ravender Gupta. Since then, the task of dye synthesis has been taken over by others: Amiram Grinvald and Rina Hildesheim (in Grinvald's laboratory), and Leslie Loew's group. Several excellent dyes (especially fluorescent dyes of the styryl class) have come out of this effort. Grinvald's group has synthesized several hundred new dyes; in particular (Grinvald *et al.*, 1982a; Grinvald *et al.*, 1983), they reported screening about twenty new styryl dyes on cultured mouse neuroblastoma cells, looking for fluorescent signals since these have a theoretical advantage over absorption signals for small structures (see Appendix B). This search paid off spectacularly in the discovery of RH421, which gave the highest $\Delta F/F$ ever seen: 21%/100 mV.

Leslie Loew took a novel and promising approach to dye synthesis, making styryl dyes that were specifically designed to operate according to a particular mechanism (charge-shift electrochromism), based on theoretical considerations and on molecular orbital modelling. His reasoning was that since this mechanism was based on intrinsic properties of the dye molecule, rather than on its interaction with the membrane, these dyes were more likely to be insensitive to the preparation. His laboratory synthesized about thirty new styryl dyes (Loew and Simpson, 1981; Fluhler *et al.*, 1985), and screened them on an artificial bilayer system. In this model system, their dyes seem to operate by an electrochromic mechanism (Loew *et al.*, 1979; Loew and Simpson, 1981; Fluhler *et al.*, 1985), and the best of them, di-4-ANEPPS, gave a quite-respectable fluorescence signal of 8%/100 mV.

Alas, variability between preparations once again reared its ugly head. When Loew's di-ASP styryl dyes were tried on squid giant axon (Loew *et al.*, 1985), they gave fortyfold lower sensitivities. Much of this decreased sensitivity was attributable to increased background staining, but it was clear that the signals weren't purely electrochromic. Loew's group also tried RH421 on their artificial bilayer system (the

structure of RH421 being very close to that of the di-ASP dyes), and found that it seemed to operate by electrochromism. The catch: its sensitivity on the bilayer was only 5%/100 mV, compared to the 21%/100 mV that Grinvald's group had found with neuroblastoma cells. On a more encouraging note, Gross *et al.* (1986) tested di-4-ANEPPS on four vastly different cell types, and found large signals on each. A431 human carcinoma cells, rye protoplasts, and rat basophilic leukemia cells all gave responses of about 10%/100 mV, while fungus spores gave 4%/100 mV.

Despite all these complex and unexplained phenomena, it is clear that styryl dyes have given the largest signals for cultured vertebrate neurons, and so these are the dyes that we have tried.

2.3.4 Biological preparations

Fast voltage-sensitive dyes have been used on a wide spectrum of preparations, from cultured cells to cortex. I list here a potpourri of examples, to give the flavor of the field, and then review the work most relevant to this thesis, *i.e.*, recordings from cultured neurons, and recordings that could detect subthreshold postsynaptic potentials.

Salzberg and collaborators (Salzberg *et al.*, 1973) were the first to record optically from single neurons in an intact preparation. They measured fluorescent signals of 10^{-3} from single neurons in the leech segmental ganglion using merocyanine 540, but encountered severe phototoxicity. Using better dyes and more refined technology, Salzberg *et al.* (1977) were able to record simultaneously from 14 neurons in the barnacle supraesophageal ganglion. They obtained signals of up to 6×10^{-4} with the absorption dye NK2367. Woolum and Strumwasser (1978) used the absorption dyes WW375 and NK2367 to record from intact *Aplysia* ganglia. They obtained signals of about 5×10^{-4} from single cells using NK2367, but found that the dye had strong pharmacological effects—not phototoxicity, but effects caused by the dye without light—on the circadian rhythm of the *Aplysia* eye. Grinvald *et al.* (1982b) used absorption dyes to visualize spreading activity in

rat hippocampal slices, seeing signals of about 10^{-4}. Salzberg *et al.* (1983) used *intrinsic* signals (without dyes) to detect action potentials in frog presynaptic terminals. Orbach and Cohen (1983) were the first to record from the *in vivo* vertebrate central nervous system, studying the salamander olfactory bulb. London *et al.* (1987) used absorption signals to record from the buccal ganglion of the mollusc *Navanax*, refining their technique to the point where they could record from 70% of the cells, in a ganglion that contains 200 cells. Ross and Krauthamer (Ross and Krauthamer, 1984; Krauthamer and Ross, 1984) used WW375 and NK2367 to record fluorescent signals from the processes of single neurons in the barnacle supraesophageal ganglion, and interpreted the detailed time courses of their signals in terms of the cable properties of the neuron. (They had to average several hundred sweeps in order to obtain an adequate signal-to-noise ratio, however.) Blasdel and Salama (1986) used fluorescent dyes to record from monkey visual cortex, though it now seems that they may have been measuring intrinsic signals rather than dye signals (Grinvald *et al.*, 1986). Grinvald's group did several sets of experiments recording from the soma and processes of cultured neuroblastoma cells (Grinvald *et al.*, 1981a; Grinvald *et al.*, 1983). More recently, our group has recorded from primary cultures of rat sympathetic neurons (Rayburn *et al.*, 1984; Chien *et al.*, 1987), and Brian Salzberg's group has used an absorption dye to record from cultures of *Aplysia* neurons (Parsons *et al.*, 1989a).

It is fair to say that most of the dye-recording experiments so far, spread across this disparate set of preparations, have been demonstrations of technique. Due to difficulties inherent in dye recording or in the preparations themselves, only a few of these experiments have yet been able to answer real biological questions. However, the questions they have addressed are inherently difficult (else dye recording would not be necessary), and there is great promise for future progress.

2.3.5 Dye recording in culture

Of particular relevance here is optical recording from cells in culture. In the early 1980s, Amiram Grinvald's group did a series of experiments using N1E-115 neuroblastoma cells, a mouse cell line that puts out processes in culture. Under the right conditions many cells will fuse, giving enormous cell bodies over 100 μm in diameter (clearly an advantage for dye recording!). Grinvald, Ross, and Farber (Grinvald *et al.*, 1981a) recorded absorption signals of $\Delta T/T = .05\%$ using a merocyanine dye, and fluorescence signals of $\Delta F/F = 3\%$ using an oxonol. The absorption signals were recorded using a tungsten-halogen lamp and a 10 by 10 photodiode array, which let them record simultaneously from the soma and large processes. For the fluorescence experiments, they used a laser microbeam as an intense light source and a photomultiplier tube as a detector. Using the laser and PMT, they were able to record action potentials from processes 7 μm in diameter, after averaging four sweeps. However, photodynamic damage limited them to only four sweeps per recording site. With this same fluorescence apparatus, Grinvald and Farber (1981) demonstrated the existence of calcium action potentials in the growth cones of neuroblastoma cells. They later (Grinvald *et al.*, 1983) synthesized improved dyes, especially RH421 with its legendary $\Delta F/F$ of 21%/100 mV. Using these dyes and an improved optical system, they were able to record action potentials from a 2 μm neuroblastoma process with a signal-to-noise ratio of 50.

Tom Parsons, David Kleinfeld, and collaborators have followed a path remarkably parallel to ours. They have grown microcultures of a few identified *Aplysia* neurons in culture, and studied their synaptic interactions using the absorption dye RH155 (Parsons *et al.*, 1989a; Parsons *et al.*, 1989b; Kleinfeld *et al.*, 1989). With maximum illumination, their largest signals had a $\Delta T/T$ of about 2×10^{-3}, and they could record action potentials with a signal-to-noise ratio of about 50. However, at this illumination intensity, photodynamic damage killed their cells after about 30 seconds (even with oxygen removed

from the medium), so they reduced the illumination when a lower signal-to-noise ratio was sufficient.

Five other groups have done some preliminary dye-recording in culture. Ross and Reichardt (1979) recorded from rat sympathetic neurons and chick spinal cord neurons in culture, in their study of dye sensitivity across species. Obaid and Salzberg (1982) used NK2367 for absorption measurements from identified leech neurons in culture. Tank and Ahmed (1985) recorded from rat brain cultures using the fluorescent dyes RH237 and RH421, obtaining $\Delta F/F$ of 1%. Ross et al. recorded in absorption, also using RH155, from leech neurons in culture (Ross et al., 1987). This recording was a minor adjunct to the main experiments using the Ca^{++}-sensitive dye arsenazo III, and the voltage-dye signal was only used to show that the processes and soma of the neurons were isopotential. Recently, Bonhoeffer and Staiger have recorded fluorescence signals from organotypic hippocampal slice cultures (Bonhoeffer and Staiger, 1988). Using the styryl dyes RH414 and RH237 and a 12 x 12 photodiode array, they could record action potentials from single cells, with a $\Delta F/F$ of about 0.2%. Except for Bonhoeffer and Staiger, who have gone on to study long-term potentiation (Bonhoeffer et al., 1989), none of these groups have pursued dye-recording in culture any further.

2.3.6 Dye recording of synaptic potentials

Optical recording of postsynaptic potentials from cells in culture has never been reported. Parsons and Kleinfeld had sufficient sensitivity, but could not record PSPs for other technical reasons; mainly, their AC-coupled amplifiers filtered out the very slow PSPs of their *Aplysia* cultures. Grinvald's group certainly had large enough signals from their neuroblastoma cultures, but this is not a culture system where synapses form.

Several groups have reported optical detection of PSPs *in vivo*. Salzberg *et al.* (1977) were able to record large postsynaptic potentials (greater than about 10 mV) in a barnacle ganglion, using NK2367 in absorption. Improving upon this work, Grinvald *et*

al. (1981b) used NK2367 and WW433, now with signal-averaging software, and detected synaptic potentials of about 2 mV (averaging 100 sweeps) in the *Navanax* buccal ganglion. One of the main problems with recording small signals from intact preparations is the background absorption and fluorescence from cells surrounding the cell of interest. Trying to overcome this problem, Grinvald's group (Agmon *et al.*, 1982; Grinvald *et al.*, 1987) designed a set of intracellular styryl dyes, *i.e.*, dyes meant to be injected into the cell of interest. This allows recording from the processes of the injected cell, without fluorescent background from adjacent cells (though there *is* severe background from the staining of *intracellular* membranes). They reported a $\Delta F/F$ of about 0.3% in leech neurons, and recorded a 2 mV PSP from the neuropil of a leech motoneuron (Grinvald *et al.*, 1987).

CHAPTER 2 REFERENCES

A. Agmon, R. Hildesheim, L. Anglister, and A. Grinvald (1982) Optical recordings from processes of individual leech CNS neurons iontophoretically injected with new fluorescent voltage-sensitive dye. *Neurosci. Lett.* **10:**S35.

G. G. Blasdel and G. Salama (1986) Voltage-sensitive dyes reveal a modular organization in monkey striate cortex. *Nature* **321:**579-585.

G. G. Blasdel (1989) Visualization of neuronal activity in monkey striate cortex. *Ann. Rev. Physiol.* **51:**561-581.

T. Bonhoeffer and V. Staiger (1988) Optical recording with single cell resolution from monolayered slice cultures of rat hippocampus. *Neurosci. Lett.* **92:**259-264.

T. Bonhoeffer, V. Staiger, and A. Aertsen (1989) Synaptic plasticity in rat hippocampal slice cultures: Local "Hebbian" conjunction of pre- and postsynaptic stimulation leads to distributed synaptic enhancement. *Proc. Natl. Acad. Sci. U. S. A.* **86:**8113-8117.

C.-B. Chien, W. D. Crank, and J. Pine (1987) Noninvasive techniques for measurement and long-term monitoring of synaptic connectivity in microcultures of sympathetic neurons. *Soc. Neurosci. Abstr.* **13:**1426, abstr. #393.15.

L. B. Cohen, R. D. Keynes, and B. Hille (1968) Light scattering and birefringence changes during nerve activity. *Nature* **218:**438-441.

L. B. Cohen, B. M. Salzberg, H. V. Davila, W. N. Ross, D. Landowne, A. S. Waggoner, and C. H. Wang (1974) Changes in axon fluorescence during activity: molecular probes of membrane potential. *J. Membr. Biol.* **19:**1-36.

L. B. Cohen (1989) Special topic: optical approaches to neuron function. *Ann. Rev. Physiol.* **51:**487-490.

L. B. Cohen, H.-P. Hopp, J.-Y. Wu, C. Xiao, J. London, and D. Zecevic (1989) Optical measurement of action potential activity in invertebrate ganglia. *Ann. Rev. Physiol.* **51:**527-541.

H. V. Davila, B. M. Salzberg, L. B. Cohen, and A. S. Waggoner (1973) A large change in axon fluorescence that provides a promising method for measuring membrane potential. *Nature New Biol.* **241:**159-160.

P. De Weer and B. M. Salzberg, eds. (1986) *Optical Methods in Cell Physiology.* Wiley (Interscience), New York, NY.

E. Fluhler, V. G. Burnham, and L. M. Loew (1985) Spectra, membrane binding, and potentiometric responses of new charge shift probes. *Biochemistry* **24:**5749-5755.

A. Grinvald and I. Farber (1981) Optical recording of calcium action potentials from growth cones of cultured neurons with a laser microbeam. *Science* **212:**1164-1167.

A. Grinvald, W. N. Ross, and I. Farber (1981a) Simultaneous optical measurements of electrical activity from multiple sites on processes of cultured neurons. *Proc. Natl. Acad. Sci. U. S. A.* **78**:3245-3249.

A. Grinvald, L. B. Cohen, S. Lesher, and M. B. Boyle (1981b) Simultaneous optical monitoring of activity of many neurons in invertebrate ganglia using a 124-element photodiode array. *J. Neurophysiol.* **45**:829-840.

A. Grinvald, R. Hildesheim, I. C. Farber, and L. Anglister (1982a) Improved fluorescent probes for the measurement of rapid changes in membrane potential. *Biophys. J.* **39**:301-308.

A. Grinvald, A. Manker, and M. Segal (1982b) Visualization of the spread of electrical activity in rat hippocampal slices by voltage-sensitive optical probes. *J. Physiol. (Lond.)* **333**:269-291.

A. Grinvald, A. Fine, I. C. Farber, and R. Hildesheim (1983) Fluorescence monitoring of electrical responses from small neurons and their processes. *Biophys. J.* **42**:195-198.

A. Grinvald, E. Lieke, R. D. Frostig, C. D. Gilbert, and T. N. Wiesel (1986) Functional architecture of cortex revealed by optical imaging of intrinsic signals. *Nature* **324**:361-364.

A. Grinvald, B. M. Salzberg, V. Lev-Ram, and R. Hildesheim (1987) Optical recording of synaptic potentials from processes of single neurons using intracellular potentiometric dyes. *Biophys. J.* **51**:643-651.

A. Grinvald, R. D. Frostig, E. Lieke, R. Hildesheim (1988) Optical imaging of neuronal activity. *Physiol. Rev.* **68**:1285-1366.

D. Gross, L. M. Loew, and W. W. Webb (1986) Optical imaging of cell membrane potential changes induced by applied electric fields. *Biophys. J.* **50**:339-348.

R. K. Gupta, B. M. Salzberg, A. Grinvald, L. B. Cohen, K. Kamino, S. Lesher, M. B. Boyle, A. S. Waggoner, and C. H. Wang (1981) Improvements in optical methods for measuring rapid changes in membrane potential. *J. Membr. Biol.* **58**:123-137.

D. K. Hill and R. D. Keynes (1949) Opacity changes in stimulated nerve. *J. Physiol.* **108**:278-281.

D. K. Hill (1950) The effect of stimulation on the opacity of a crustacean nerve trunk and its relation to fibre diameter. *J. Physiol.* **111**:283-303.

J. F. Hoffman and P. C. Laris (1974) Determination of membrane potentials in human and *Amphiuma* red blood cells by means of a fluorescent probe. *J. Physiol.* **239**:519-552.

D. Kleinfeld, T. D. Parsons, F. Raccuia-Behling, A. L. Obaid, and B. M. Salzberg (1989) Synaptic interactions in assemblies of cultured *Aplysia* neurons. I: Analysis of optically recorded electrical activity. *Soc. Neurosci. Abstr.* **15**:1140, abstr. #455.11.

A. Konnerth, A. L. Obaid, and B. M. Salzberg (1987) Optical recording of electrical activity from parallel fibres and other cell types in skate cerebellar slices *in vitro*. *J. Physiol.* **393**:681-702.

V. Krauthamer and W. N. Ross (1984) Regional variations in excitability of barnacle neurons. *J. Neurosci.* **4**:673-682.

E. E. Lieke, R. D. Frostig, A. Arieli, D. Y. Ts'o, R. Hildesheim, and A. Grinvald (1989) Optical imaging of cortical activity: Real-time imaging using extrinsic dye-signals and high resolution imaging based on slow intrinsic-signals. *Ann. Rev. Physiol.* **51**:543-559.

L. M. Loew, S. Scully, L. Simpson, and A. S. Waggoner (1979) Evidence for a charge-shift electrochromic mechanism in a probe of membrane potential. *Nature* **281**:497-499.

L. M. Loew and L. L. Simpson (1981) Charge-shift probes of membrane potential: a probable electrochromic mechanism for p-aminostyrylpyridinium probes on a hemispherical lipid bilayer. *Biophys. J.* **34**:353-365.

L. M. Loew, L. B. Cohen, B. M. Salzberg, A. L. Obaid, and F. Bezanilla. (1985) Charge-shift probes of membrane potential: Characterization of aminostyrylpyridinium dyes on the squid giant axon. *Biophys. J.* **47**:71-77.

L. M. Loew, ed. (1988) *Spectroscopic membrane probes,* vols. I-III. CRC Press, Boca Raton, FL.

J. A. London, D. Zecevic, and L. B. Cohen (1987) Simultaneous optical recording from many neurons during feeding in *Navanax*. *J. Neurosci.* **7**:649-661.

A. L. Obaid and B. M. Salzberg (1982) Optical recording of normal electrical activity from identified leech neurons maintained in culture. *Soc. Neurosci. Abstr.* **8**:834, abstr. #239.11.

H. S. Orbach and L. B. Cohen (1983) Optical monitoring of activity from many areas of the in vitro and in vivo salamander olfactory bulb: a new method for studying functional organization in the vertebrate central nervous system. *J. Neurosci.* **3**:2251-2262.

T. D. Parsons, D. Kleinfeld, F. Raccuia-Behling, and B. M. Salzberg (1989a) Optical recording of the electrical activity of synaptically interacting *Aplysia* neurons in culture using potentiometric probes. *Biophys. J.* **56**:213-221.

T. D. Parsons, B. M. Salzberg, A. L. Obaid, F. Raccuia-Behling, and D. Kleinfeld (1989b) Synaptic interactions in assemblies of cultured *Aplysia* neurons. II: Dynamic patterns of effective connectivity. *Soc. Neurosci. Abstr.* **15**:1140, abstr. #455.12.

H. Rayburn, J. Gilbert, C.-B. Chien, and J. Pine (1984) Noninvasive techniques for long-term monitoring of synaptic connectivity in cultures of superior cervical ganglion cells. *Soc. Neuroci. Abstr.* **10**:578, abstr. #171.1.

W. N. Ross, B. M. Salzberg, L. B. Cohen, and H. V. Davila. (1974) A large change in dye absorption during the action potential. *Biophys. J.* **14**:983-986.

W. N. Ross, B. M. Salzberg, L. B. Cohen, A. Grinvald, H. V. Davila, A. S. Waggoner, and C. H. Wang (1977) Changes in absorption, fluorescence, dichroism, and birefringence in stained giant axons: optical measurement of membrane potential. *J. Membr. Biol.* **33**:141-183.

W. N. Ross and L. F. Reichardt (1979) Species-specific effects on the optical signals of voltage-sensitive dyes. *J. Membrane Biol.* **48**:343-356.

W. N. Ross and V. Krauthamer (1984) Optical measurements of potential changes in axons and processes of neurons of a barnacle ganglion. *J. Neurosci.* **4**:659-672.

W. N. Ross, H. Arechiga, and J. G. Nicholls (1987) Optical recording of calcium and voltage transients following impulses in cell bodies and processes of identified leech neurons in culture. *J. Neurosci.* **7**:3877-3887.

B. M. Salzberg, H. V. Davila, and L. B. Cohen (1973) Optical recording of impulses in individual neurones of an invertebrate central nervous system. *Nature* **246**:508-509.

B. M. Salzberg, A. Grinvald, L. B. Cohen, H. V. Davila, and W. N. Ross (1977) Optical recording of neuronal activity in an invertebrate central nervous system: simultaneous monitoring of several neurons. *J. Neurophysiol.* **40**:1281-1291.

B. M. Salzberg, A. L. Obaid, D. M. Senseman, and H. Gainer (1983) Optical recording of action potentials from vertebrate nerve terminals using potentiometric probes provides evidence for sodium and calcium components. *Nature* **306**:36-40.

B. M. Salzberg (1989) Optical recording of voltage changes in nerve terminals and in fine neuronal processes. *Ann. Rev. Physiol.* **51**:507-526.

P. J. Sims, A. S. Waggoner, C.-H. Wang, and J. F. Hoffman (1974) Studies on the mechanism by which cyanine dyes measure membrane potential in red blood cells and phosphatidylcholine vesicles. *Biochemistry* **13**:3315-3330.

D. W. Tank and Z. Ahmed (1985) Multiple-site monitoring of activity in cultured neurons. *Biophys. J.* **47**:476a (abstr.).

I. Tasaki, A. Watanabe, R. Sandlin, and L. Carnay (1968) Changes in fluorescence, turbidity, and birefringence associated with nerve excitation. *Proc. Natl. Acad. Sci. U. S. A.* **61**:883-888.

R. Y. Tsien (1989) Fluorescent indicators of ion concentrations. *Meth. Cell Biol.* **30**:127-156.

A. S. Waggoner (1976) Optical probes of membrane potential. *J. Membr. Biol.* **27**:317-334.

A. S. Waggoner (1979) Dye indicators of membrane potential. *Ann. Rev. Biophys. Bioeng.* **8**:47-68.

J.C. Woolum and F. Strumwasser (1978) Membrane-potential-sensitive dyes for optical monitoring of activity in *Aplysia* neurons. *J. Neurobiol.* **9**:185-193.

Chapter 3
Dye-Recording Apparatus, 1.
System design and performance

3.1 INTRODUCTION

3.1.1 System components

This chapter and the next two describe the design, construction, and performance of a very sensitive dye-recording system. In the dye-recording literature, the emphasis has been on biology, not electronics, and so the design of recording systems has not been described in much detail, nor has their performance been well characterized. In these three chapters, I have taken advantage of the open-ended nature of the Ph.D. thesis to describe the design, testing, and performance of my dye-recording system in some detail. This chapter attempts to emphasize design goals and limitations, both those set by biology and those set by fundamental physics, in order to show the logic behind the design of the system. It is hoped that this discussion may prove useful in the design of future detectors.

Any dye-recording system has four major components: microscope, light source, optical detector, and data acquisition system. The system described here incorporates improvements in the light source, optical detector, and data acquisition system.

Microscope. The essential features of a microscope are a condenser lens to focus illumination on the specimen, filters to select excitation and emission wavelengths, and an objective lens to collect light from the specimen and form a magnified real image. In an epifluorescence microscope such as the one used here, the condenser and objective are the same lens.

Secondary parts of the microscope include a stage for holding and moving the specimen, and various output ports that supply images of the specimen to eyes, camera, or optical detector.

Light source. This is usually either a tungsten-halogen lamp or a mercury arc lamp. Here, it is a mercury arc lamp with a regulated power supply. The lamp is stabilized by a novel feedback regulator that greatly reduces fluctuations in illumination intensity. The illumination is turned on and off by an electromechanical shutter.

Optical detector. This consists of a primary photodetector (*e.g.*, a photomultiplier tube or photodiode array) that transduces light to an electrical signal, and detector electronics that amplify, process, and multiplex the electrical signal. The optical detector is usually made up of many individual photodetectors, each receiving the light from an individual picture element (pixel).

The novel optical detector described here comprises a fiber-optic camera of 256 pixels, discrete photodiode detectors, and very low-noise amplifiers. A real image of the specimen is projected onto the end of a tightly-packed bundle of optical fibers (the input of the fiber-optic camera); each fiber then carries the light from its pixel to a photodiode, where the light signal is transduced into a photocurrent and then amplified. The dark noise of this detector is significantly lower than previous detectors.

Data acquisition. Data acquisition hardware and software convert the optical detector's electrical output signal into digital form, and then convert this data into an intelligible form under the experimenter's control. The data acquisition system used here is a novel one, based on an IBM AT microcomputer and a TransEra MDAS data acquisition box. Its capabilities do not differ significantly from those of previous systems, except perhaps for its low cost.

3.1.2 Design goals

The two main goals for any dye-recording system are to maximize the signal-to-noise ratio (S/N) while minimizing phototoxicity and bleaching. These goals must be balanced against one another, since higher S/N requires more light exposure (brighter illumination or many repeated measurements), while lower toxicity and bleaching require less light exposure. In the simplest terms, S/N is given by

$$S/N = (\Delta I/I)\ (I/i_{rms}),\qquad\qquad (3.1)$$

where I is the detected photocurrent, ΔI is the signal (a change in photocurrent), and i_{rms} is the noise in the photocurrent. This expression can be divided into a biophysical factor, the dye sensitivity $\Delta I/I$, and an instrumental factor, I/i_{rms}. The former is described in Chapter 4; the latter, in this chapter. Maximization of I/i_{rms} requires efficient optics for high I, and quiet photodetectors and a stable light source for low i_{rms}.

In order to reduce phototoxicity and bleaching, unnecessary illumination must be eliminated, and light must be used efficiently. A shutter is used to control illumination, admitting light only while dye signals are being recorded. Efficient use of light mainly requires an efficient optical system, just as for maximization of S/N. As much signal as possible should be squeezed out of each joule of illumination, since each illuminating photon is paid for with phototoxicity.

The technical requirements for the system can thus be summarized as *efficient optics*, *stable illumination*, and *quiet photodetectors*. These are determined by the microscope, light source, and optical detector, respectively.

Section 3.2 covers the theory of noise in photodetection, a necessary background for the rest of the chapter. This section also explains the choice between absorption and fluorescence techniques (the details of this comparison are in Appendix B). Chapters 4 and 5 cover each of the major components (microscope, light source, detector, data acquisition, in sections 4.1, 4.2, 5.1, and 5.2, respectively) in turn, describing both design and real

performance. Section 3.3 gives a brief history of dye-recording instrumentation, for comparison with the present apparatus. Finally, section 3.4 summarizes the performance of this apparatus, as well as possible future improvements that could be made. Detailed technical discussions have been relegated to the appendices. Appendix B compares fluorescence and absorption techniques. Appendix C discusses microscope performance, especially the dependence of illumination intensity and collection efficiency on numerical aperture. Appendix D is a noise analysis for the detector preamplifiers.

Chapters 3 through 5 only discuss instrument design (I/i_{rms}), not dye biophysics ($\Delta I/I$). Chapter 6 describes work on improving $\Delta I/I$ through dye screening, dye staining experiments, and experiments with different excitation and emission filters. (Strictly speaking, filters are part of the microscope, but these experiments belong more naturally with the dye biophysics of Chapter 6.)

3.2 NOISE THEORY

Shot noise is the ultimate physical limit for all optical recording. Light is made up of discrete quanta (photons), and so the intensity of a beam of light formed of randomly-emitted photons, for example the output of a mercury arc lamp or the fluorescence from a stained neuron, inevitably shows statistical fluctuations: shot noise. The noise in a beam of intensity I goes as $\sqrt{I}$, so that the signal-to-noise ratio (S/N) goes as $I/\sqrt{I}=\sqrt{I}$: the brighter the light, the higher the signal-to-noise ratio.

This section discusses the theory of noise for optical recording, starting from first principles. Although quantitative light intensities and noise levels have not usually been quoted in the literature, it is clear that in practice, many dye-recording experiments have not been limited by shot noise, but instead by amplifier noise or fluctuations in illumination intensity. In order to have the maximum possible signal-to-noise ratio, it is important to have quiet amplifiers, a stable light source, and an efficient optical system. This topic has

been discussed in the literature, notably by Grinvald *et al.* (1983), and in good reviews by Cohen and Lesher (1986) and Grinvald *et al.* (1988).

Theoretically, phototoxicity sets the only fundamental restriction on the shot-noise-limited signal-to-noise ratio. I is a product of illuminating intensity, the preparation's fluorescence or transmission, and the optical system's efficiency. Without phototoxicity, I (and thus, S/N) could in principle be increased without limit simply by increasing the illuminating intensity. (In practice, of course, the stability and brightness of available light sources impose a limit.)

Since photodynamic damage does occur, there is a biological limit on the illuminating intensity that may be safely used, and a premium on the efficiency of the optical system. The optical efficiency of detection, rather than illumination, is particularly important. A lossy illumination system decreases both detected intensity and phototoxicity; a lossy detection system, on the other hand, decreases intensity without lowering phototoxicity.

3.2.1 Noise sources

The first step in photodetection, whether the detector is a photodiode, a photomultiplier tube (PMT), or a charge-coupled device (CCD), is to transduce photons into electrons. Since the quantum efficiency of the photodetector (the fraction of photons successfully transduced) is always less than unity, the limiting shot noise is actually not in the light signal, but in the photocurrent: there are fewer electrons than photons[1]. Therefore the following discussion uses I to signify photocurrent (amperes), *not* light power (watts). To convert photocurrent to incident light power, multiply by $h\nu/QGe$, where $h\nu$ is the energy of a single photon, Q is the quantum efficiency of the detector, e is the charge of the

---

[1] For devices with gain, such as PMTs, the correct statement is "fewer electron packets than photons."

electron, and G is the detector's quantum gain (1 for CCDs and photodiodes, large for PMTs).

Along with shot noise, there are two other main types of light noise: dark noise and illumination noise. All three are conveniently classified by their dependence on I: I^0, $I^{1/2}$, or I^1. In the following discussion, a lowercase i indicates a root-mean-square (rms) noise: i_{shot}, i_{dark}, i_{ill}. These noise amplitudes are all referred to the input (given as an equivalent rms photocurrent).

Dark noise, or amplifier noise, is proportional to I^0, *i.e.*, it does not depend on I. Dark noise comes from the amplifier and other parts of the detector electronics, is present even with no incident light, and depends on the particular electronics being used. It is typically white noise, which rolls off at the system's upper frequency limit, but it may have $1/f$ or 60 Hz components.

Shot noise is proportional to $I^{1/2}$. Shot noise is due to the intrinsic statistical fluctuations of the photocurrent, and so is independent of details of electronics. Since shot noise is pure white noise (see Appendix D), it is easily calculated:

$$i_{shot}=G\sqrt{2eIB},\qquad(3.2)$$

where B is the power bandwidth of the system. B should be as narrow as possible, consistent with the time course of the signals being measured. In order to detect action potentials (which have risetimes of about 1 ms) without too much distortion, B must be at least 300 Hz.

Illumination noise, due to fluctuations in the light source or movement of the optical path, is proportional to I^1. I use the term "illumination noise" because this type of noise is equivalent to a fluctuation in the light source intensity[2]. In additional to a true fluctuation in intensity, illumination noise can also be due to motion in the illuminating light path, motion

---

[2]Noise that is linear in I has also been referred to as "extraneous noise" (*e.g.*, Cohen and Lesher, 1986) and "technical noise" (*e.g.*, Parsons *et al.*, 1989).

in the preparation, or motion in the outgoing light path. Illumination noise due to apparatus vibration was a problem up until about five years ago, especially for absorption measurements, but has been eliminated by good mechanical design and vibration isolation (Cohen and Lesher, 1986). Illumination noise due to fluctuations in the light source depends on the lamp used: incandescent tungsten-halogen bulbs are very stable, while mercury arc lamps, though brighter, are less stable due to movements of the arc plasma.

3.2.2 Total noise

Since these three noises are uncorrelated, their amplitudes add in quadrature (their powers sum linearly):

$$(i_{total})^2 = (i_{dark})^2 + (i_{shot})^2 + (i_{ill})^2 \qquad (3.3)$$

Fig 3.1 shows how these noise sources combine, and how the quantum yield of the detector affects their relative contributions. The logarithmic plot shows I/i_{rms} as a function of incident light intensity; the scales have been left off in order to emphasize qualitative features. The thick curve shows the total noise from a detector with significant dark noise and high quantum efficiency (Q). At low intensities, dark noise dominates (the curve has slope 1); at medium intensities, shot noise is dominant (slope 1/2); at high intensities, illumination noise dominates (slope 0). Since noises add in quadrature, a good rule of thumb is that any source less than half the size of another can be ignored.

Clearly, it's best to be in the intermediate regime, where i_{shot} dominates; i_{dark} and i_{ill} should be reduced as far as possible in order to widen this range. This requires quiet photodetectors and stable illumination. In the presence of illumination noise, it is pointless to increase illumination past the point where i_{ill} exceeds i_{shot}, because photodynamic damage will increase without any change in S/N. If illumination noise is completely eliminated, photodynamic damage becomes the upper bound on useful intensity.
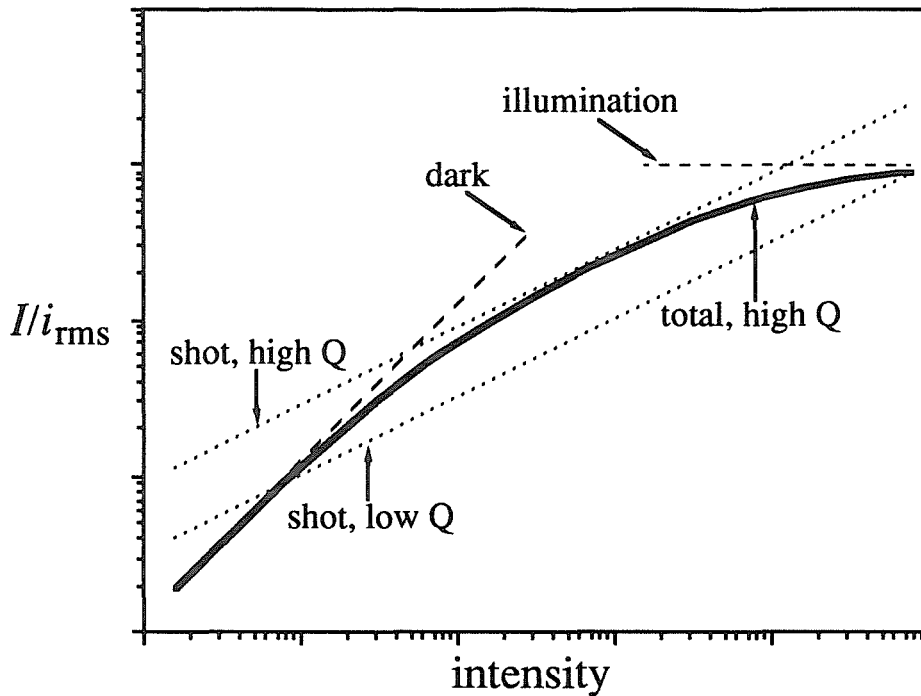
Figure 3.1 Comparison of dark, shot, and illumination noise. The ratio of total photocurrent to photocurrent noise is plotted logarithmically against illuminating intensity; the scales have been left off to emphasize qualitative features. The *dashed lines* show dark and illumination noise; the *dotted lines* show the shot noise from a high and a low quantum-efficiency detector (their Q values differ by a factor of 8). The *solid curve* shows the total noise that results when dark and illumination noise are added to the *high Q* shot noise curve.

A photodiode-amplifier combination has a quantum efficiency of about 80% and has some amplifier noise. Such a combination is modelled well by the high Q total noise curve, which includes dark noise. A photomultiplier, on the other hand, has a high quantum gain and so can have essentially no dark noise, but its quantum efficiency is not much above 10% (Yariv, 1985, p. 349). A photomultiplier is modelled well by the low Q shot noise curve, which includes no dark noise, and assumes a Q eight times lower than that for the high Q curve. Fig 3.1 thus shows that a photomultiplier will outperform a photodiode detector at very low light levels, because of its lower dark noise; at moderate light levels, however, the photodiode detector is better.

In summary, then:

- Amplifier noise should be low enough so that i_{dark} is less than i_{shot} for the lowest detected intensity used.

- Illumination noise should be low enough that i_{ill} is less than i_{shot} for the highest intensity used.

- A photodiode detector operating in a shot-noise-limited regime will always have greater S/N than a photomultiplier at the same intensity.

The apparatus described here uses photodiode detectors to record fluorescence signals from cultured rat SCG neurons. For this case, $G=1$, B is roughly 300 Hz, and the current I from a pixel containing a single cell is typically 1 nA. This gives $i_{shot}=.31$ pA, or expressed as a fraction, $i_{shot}/I=3.1\times10^{-4}$. The noise performance of the apparatus will be optimal if i_{dark} is somewhat lower than i_{shot}, and i_{ill}/I lower than i_{shot}/I. Chapters 4 and 5 show that these two conditions are usually true, so indeed the apparatus operates in the shot-noise-limited regime.

3.2.3 *Fluorescence* versus *absorption*

When beginning to use voltage-sensitive dyes on a new preparation, the first decision is whether to use fluorescence dyes or absorption dyes. This is not a particularly straightforward decision, nor one lightly made, since the hardware for fluorescence measurements and for transmission measurements differ substantially. Of course the optical apparatus must differ, but more significantly, the optical detectors and electronics must be optimized for vastly different light levels. In this case, fluorescence was chosen. Appendix B treats this question in detail, but the qualitative arguments are quite simple.

The choice between the two modes may be determined by mechanical or optical constraints: for instance, a preparation that is not accessible from both sides is inappropriate for absorption, which requires the measurement of transmitted light. More generally, however, this decision depends on the relative signal-to-noise ratios of the two methods. In the shot-noise limit (see the last subsection), $S/N \propto (\Delta I/I)\sqrt{I}$; absorption is

favored by large I, while fluorescence is favored by large $\Delta I/I$. The most important determinant of relative S/N is a, the fraction of light absorbed by the stained specimen.

There are three factors that make T much larger than F. First, a is small: even for the squid giant axon—a thick preparation with a large membrane area—a is only .25 (Ross *et al.*, 1977); for neuronal cultures, a may be as low as 10^{-4}. Second, the quantum yield of the dye is always less than unity. Third, the microscope's collection efficiency is lower for fluorescence. This is due to a simple geometric factor: transmitted light passes through in a small cone, which can be collected completely, but fluorescent light is (roughly speaking) emitted in a sphere, only a fraction of which can be collected. All three factors combine to make the T large and F small. This difference favors absorption, since a higher intensity means a lower fractional shot noise.

Another effect of small a, however, is to make $\Delta F/F$ much larger than $\Delta T/T$. For fluorescence mode, the absorbed light both creates the signal and adds shot noise; the transmitted light has no effect. For absorption mode, it is the absorbed light that creates the signal, while the transmitted light adds shot noise. Therefore, fluorescence is favored in cases of small a, where little light is absorbed and much is transmitted.

In order to resolve these two conflicting effects of a, they must be quantified. For fluorescence, the signal is proportional to a, and the shot noise proportional to $\sqrt{a}$, so $(S/N)_{\text{fluor}} \propto \sqrt{a}$. For absorption, the signal is again proportional to a but the shot noise—determined by the transmitted light intensity—is constant (assuming $a \ll 1$), so that $(S/N)_{\text{abs}} \propto a$. These dependences on a mean that in the shot-noise limit, absorption will have a higher S/N for strongly absorbing preparations, while fluorescence will have a higher S/N for relatively transparent preparations.

This simple dependence on a can be modified if there is background staining, or if shot noise is not limiting. Background staining—staining not associated with the cells of interest—makes absorption more attractive, by increasing fluorescent shot noise without affecting transmission shot noise significantly. If dark noise or illumination noise is large,

it may dominate the total noise and favor one mode or the other. Illumination noise limits $(S/N)_{abs}$ long before affecting $(S/N)_{fluor}$, since $\Delta T/T$ is much smaller than $\Delta F/F$. On the other hand, dark noise limits $(S/N)_{fluor}$ before $(S/N)_{abs}$, since ΔF is smaller than ΔT. Absorption is sensitive to lamp fluctuations, while fluorescence is sensitive to noisy amplifiers.

In summary, absorption dyes are more appropriate for preparations that can be stained heavily: large cells, cells with extensively folded membranes, or ganglia. Fluorescence dyes are more appropriate for small cells, thin preparations, and small subcellular regions such as growth cones. (Appendix B gives an exact formula for comparison.) Remember however that this simple shot-noise analysis cannot take into account the properties of a particular dye: an absorption dye that is especially sensitive for a particular cell type might well outperform the available fluorescence dyes. The shot-noise analysis may also need to be modified in case of background staining or excessive instrumental noise (dark noise or illumination noise).

For rat SCG cultures, fluorescence was the obvious choice. Rat SCG neurons are quite small, and the fluorescent styryl dye RH421 had shown extraordinary sensitivity when tested on cultured mouse neuroblastoma cells (Grinvald et al., 1983). See Appendix B for a quantitative analysis.

3.3 HISTORY

In the original squid giant axon experiments (Cohen et al., 1974) the optical arrangements could be very simple because of the huge size of the preparation: Cohen and collaborators recorded from a section of axon 300 to 800 μm in diameter and 5 mm long. The illumination system consisted of a 100 W tungsten-halogen lamp, a condenser lens, and a quartz lens to focus the light onto the axon. The detection system was just a single photodiode, recording the fluorescence of the axon at 90°. Many technical improvements have been made in order to record from smaller preparations. Recording from single

mammalian neurons in culture is particularly demanding: the cell bodies are at most about 30 μm in diameter, a thousandfold reduction in membrane area compared to the giant axon.

Microscopes. With the first recordings from neurons in an invertebrate nervous system (Salzberg *et al.*, 1973) came the first use of a microscope as an illumination system. Salzberg, Davila, and Cohen used an upright microscope, illuminating the preparation from below with an ordinary brightfield condenser, and recording fluorescence from above with a 20x objective, NA 0.4. This general arrangement was standard for quite some time for both fluorescence and absorption measurements, until Grinvald and coworkers (Grinvald *et al.*, 1983) introduced the use of an epifluorescence inverted microscope, the type used here. An inverted microscope is much more convenient for electrophysiology, since the objective (which must be very close to the specimen in order to have a high NA) is underneath the preparation and out of the way, leaving plenty of elbow room for the electrodes. An epifluorescence mode can give much higher fluorescence, since the illuminating and emitted light both pass through the same high-NA objective. (For transmitted fluorescence, either the condenser or the objective must have a long working distance, and thus a small NA, in order to leave room for electrodes.)

Light sources. The earliest dye-recording experiments used tungsten-halogen incandescent lamps (Cohen *et al.*, 1974). Grinvald's group introduced the use of a mercury arc lamp with a constant-current power supply (Grinvald *et al.*, 1982), and also the use of a He-Ne laser as an extremely bright source for single-pixel experiments (Grinvald *et al.*, 1981a). The main innovation of the present work is the use of a feedback shunt regulator to stabilize a mercury arc.

Optical detectors. The early squid axon experiments used only a single photodetector. Salzberg and coworkers (Salzberg *et al.*, 1977), recording from many cells at once in a barnacle ganglion, introduced the use of multiple detectors. Each of their 14 detectors comprised an optical fiber connected to a photodiode, which was manually

positioned to record the light from a particular cell. Grinvald *et al.* (1981b) improved upon this arrangement by using a fixed 12 x 12 array of photodiodes. Instead of moving their detectors to cover a cell, they simply picked the detectors on which the cell happened to fall. The fiber-optic camera used here can be thought of as a hybrid of these two arrangements. A similar fiber-optic camera has been briefly described by Tank and Ahmed (1985).

Three other detectors have been used for optical recording: photomultiplier tubes (Grinvald *et al.*, 1982), charge-coupled devices (Frostig *et al.*, 1988; Ts'o *et al.*, 1988), and photodiode arrays (Grinvald *et al.*, 1981). Photodiode arrays are the most commonly used, and indeed they are the only other option (besides a fiber-optic camera) for the present experiments. As discussed in subsection 3.2.2, PMTs are inferior to silicon detectors, because of their lower quantum efficiency, whenever shot noise exceeds amplifier noise. For the preamplifiers used here, shot noise exceeds amplifier noise when the photocurrent reaches 100 pA (section 5.1.5). PMTs are also economically impractical for large array detectors, since they are several orders of magnitude more expensive than photodiodes. Commercially available CCDs can only be scanned at video rates (30 ms/frame), and so are far too slow for following action potentials or synaptic potentials.

A photodiode array is not theoretically inferior to a fiber-optic camera (after all, they both use the same detector element, a photodiode), but the fiber-optic camera is more practical. Photodiode arrays must be fabricated as monolithic silicon devices, so large arrays are difficult to make and prone to defects. At the time that the fiber-optic camera was built, a 12x12 square photodiode (Centronics) array was the largest commercially available. Large fiber-optic cameras are much easier to build, since they are assembled from individual photodiodes and fibers; this one has 256 pixels, and much larger arrays are clearly feasible. Making electrical connections to the dense forest of leads on the back of a photodiode array is a daunting task; making connections to a fiber-optic camera is much

easier, since the diodes are widely spaced. The fiber-optic camera has one disadvantage compared to photodiode arrays: the dead space between photodiodes is greater. Even for square fibers, some space is taken up by the fibers' cladding and the adhesive that holds them together; for close-packed circular fibers, another 10% of the area would be lost between fibers.

Detector electronics. There have been two main issues in the design of preamplifiers for dye-recording: the choice between AC-coupled and DC-coupled amplifiers, and reduction of amplifier noise.

One of the main problems for detector electronics is that of seeing a small signal on top of a large resting fluorescence or transmittance, a problem that is especially acute for absorption-dye experiments, where dye signals are typically about 1 part in 1000 or less. Early amplifiers removed the resting level by AC-coupling with time constants of 100 ms or greater (*e.g.*, Cohen *et al.*, 1974). A cost was paid in phototoxicity: after the illumination was turned on, several time constants passed before the amplifiers' outputs settled and signals could be seen, during which time the light was causing photodynamic damage. Nakajima and Gilai (Nakajima and Gilai, 1980) solved the problem in a different way. They used a DC-coupled amplifier with an additional output stage, consisting of a sample-and-hold circuit and a differential amplifier. The sample-and-hold was triggered shortly after illumination started, and thereafter its output was held at the resting light level, which the differential amplifier then subtracted from the signal. This scheme has two advantages. First, the illumination shutter may be opened and closed quite quickly, since it need not wait for the amplifiers to settle. Second, any slow components of the dye signal may now be seen, since they are not removed by AC-coupling. A side effect is that the slow signal due to bleaching is revealed as well, and must be subtracted out digitally.

For the present SCG culture system and styryl dyes, the resting-light-level problem is made moot by large signals and low photocurrents. As explained in subsection 5.2.2, the digitization noise from the 12-bit ADC used here is less than the fractional shot noise

expected from even the brightest cells (2 nA photocurrent). For the apparatus used here, the preamplifiers are DC-coupled, and shutter flashes may be as short as tens of milliseconds.

There have been significant reductions in preamplifier noise (Grinvald *et al.*, 1988, IV.B.2; Bonhoeffer and Staiger, 1988), but since circuit diagrams and noise amplitudes have not been published, these preamplifiers are difficult to compare with the present system. The amplifiers described here are likely to be a zenith; light levels are unlikely to ever be low enough to require quieter amplifiers. The quietest of the amplifiers discussed here are at the Johnson noise limit for 6 GΩ feedback resistors, a limit that is equal to the shot noise in a photocurrent of about 10 pA (very dim indeed).

Data acquisition and analysis. Previous dye-recording systems have used minicomputers such as the PDP-11/34, and acquisition programs written in assembly language (Cohen and Lesher, 1986). The tremendous advances in computer hardware and software have made possible the present system, which uses an IBM AT personal computer and software written in BASIC and C. The software described above was written from scratch, but its capabilities seem quite similar to those of previous systems, except that it is designed for tens of pixels rather than hundreds. Bleach-correction techniques are particularly important for fluorescence recordings. The technique used here is to record a reference trace without stimulation, fit a smooth curve to this reference, then subtract the fitted curve from the experimental trace; this is essentially the same technique used by others (Grinvald *et al.*, 1982).

3.4 SUMMARY OF APPARATUS

3.4.1 Dye-recording apparatus

This chapter, the two following chapters, and the three associated appendices (B through D) describe the theory, design, and performance of an apparatus for dye recording

from rat SCG microcultures using fluorescent styryl voltage-sensitive dyes. The apparatus has four components: microscope, light source, optical detector, and data acquisition and analysis. Several of these have innovative features. This particular apparatus is optimized for SCG microcultures, but many of these new features could be used elsewhere. For those readers not interested in the technical detail of Chapters 4 and 5, the main features and performance of the system are summarized here.

Two main factors compete in the design: high signal-to-noise ratio and low photoxicity. The ultimate limit on signal-to-noise is shot noise; low fractional shot noise requires high detected light intensities. Low phototoxicity, on the other hand, requires low illuminating intensities. Both factors require an efficient optical system.

The apparatus is built around a standard Olympus IMT-2 inverted microscope, with standard phase-contrast and fluorescence illuminators. A video camera is used for alignment of the optical detector with the culture. Using a Nikon 20x objective (NA 0.75), with filters and a dichroic mirror that select the 546 nm mercury line for excitation, and wavelengths longer than 610 nm for emission, the illuminating intensity is approximately 10 W/cm^2 at the specimen. Typical pixels over cell bodies or processes have fluorescence photocurrents of 0.2-2 nA. Assuming a noise bandwidth of 300 Hz, this range of photocurrents gives fractional rms shot noise of .02% to .07%.

The light source is a standard mercury arc lamp, stabilized by a feedback shunt regulator. The regulator monitors lamp fluctuations using a photodiode mounted in the lamphouse. A fast electromechanical shutter turns the illumination off when it is not being used. Even using a poorly regulated Olympus power supply, the shunt regulator reduces fast fluctuations (mostly 60 Hz) to .02% rms at the specimen. Slow fluctuations at about 5 Hz are harder to regulate, since they are not spatially uniform. Slow fluctuations of about 1% p-p persist at the specimen even though they have been suppressed to below 0.1% at the lamphouse photodiode. Trials that are spoiled by these slow lamp fluctuations are identified and rejected during analysis.

The optical detector is a novel fiber-optic camera with discrete photodiodes, which has practical advantages over a monolithic photodiode array. The octagonal array of square optical fibers has 256 pixels, and a field of view 810 μm across. The photocurrents from this detector are amplified by 256 very low-noise transimpedance amplifiers. The main reason for their low noise is the dual-FET input stage that precedes a conventional operational amplifier. The frequency responses of these amplifiers are dominated by stray capacitances, and their bandwidths from about 150 to 650 Hz, compared to the desired bandwidth of 300-500 Hz. The amplifiers are designed to operate at the Johnson noise limit set by their 6 GΩ feedback resistors. In practice, the quietest operates at this limit, while the noisiest is about three times noisier, which is only equivalent to the shot noise in a photocurrent of 110 pA. For the usual range of fluorescences, amplifier noise will be completely masked by shot noise.

Small stray capacitances in the preamplifiers cause two problems: gain peaking and crosstalk between amplifiers. Using a square light pulse as a test, the maximum gain peaking gave an overshoot of 22%, while the maximum crosstalk was 15%. These effects can distort the shapes and sizes of signals, so some care must be taken when interpreting optical signals, but (for reasons explained in subsection 5.1.5) they are unlikely to introduce spurious signals.

The amplifier outputs are multiplexed and digitized under computer control. The acquisition system consists of an IBM AT personal computer and a stand-alone TransEra MDAS acquisition module. The 12-bit analog-to-digital converter of the MDAS should give a maximum digitization noise of .028%. The system uses three sets of software: OPTIK and associated programs capture and manipulate video images for pixel alignment; MULTI acquires optical and electrophysiological data during experiments; DISPLAY and the SCOPE UTILITIES display and analyze the SCOPE data files stored by MULTI.

3.4.2 Threshold for detection

The system achieves its design goal for noise: shot noise is dominant over the three instrumental sources of noise. Amplifier noise is well below shot noise. Illumination noise is just below shot noise at high frequencies, though occasional slow fluctuations must be eliminated by rejecting spoiled trials. Finally, digitization noise is below shot noise (only just below, in unfavorable cases).

With a noise bandwidth of 300 Hz, the detected photocurrents of 0.2 to 2 nA should give rms shot noises of .02% to .07%. For bright pixels, then, it should be possible to detect signals of about 0.1% without signal averaging, and smaller signals with some averaging.

3.4.3 Possible improvements

The apparatus could be improved in several ways:

- The most useful improvement would be better regulation of the mercury arc lamp, since fast illumination noise is close to shot noise at a photocurrent of 2 nA, and the slow fluctuations are quite inconvenient. Better regulation may be as simple as repositioning the lamphouse photodiode.

- A second-generation optical detector with improved detector electronics would be very useful (though a great deal of work), since it should remove crosstalk between amplifiers, and might provide more uniform amplifier frequency responses. Reducing the feedback resistors to 1 GΩ should reduce stray capacitances, and should not add undue noise.

- At present, digitization noise is sometimes significant (though it never exceeds shot noise); a 14-bit or 16-bit analog-to-digital converter would remove any question of this.

- Finally, one can always use more powerful software: on-line bleach-subtraction and an integrated data analysis program are the two most likely improvements.

CHAPTER 3 REFERENCES

T. Bonhoeffer and V. Staiger (1988) Optical recording with single cell resolution from monolayered slice cultures of rat hippocampus. *Neurosci. Lett.* **92**:259-264.

L. B. Cohen, B. M. Salzberg, H. V. Davila, W. N. Ross, D. Landowne, A. S. Waggoner, and C. H. Wang (1974) Changes in axon fluorescence during activity: molecular probes of membrane potential. *J. Membr. Biol.* **19**:1-36.

L. B. Cohen and S. Lesher (1986) Optical monitoring of membrane potential: Methods of multisite optical measurement. In *Optical Methods in Cell Physiology,* eds. P. DeWeer and B. M. Salzberg. Wiley (Interscience), New York, NY. pp.71-99.

R. D. Frostig, E. E. Lieke, D. Y. Ts'o, and A. Grinvald (1988) Infra-red imaging of functional organization of visual cortex through the intact dura using a CCD camera. *Soc. Neurosci. Abstr.* **14**:897, abstr. #362.2.

A. Grinvald, W. N. Ross, and I. Farber (1981a) Simultaneous optical measurements of electrical activity from multiple sites on processes of cultured neurons. *Proc. Natl. Acad. Sci. U. S. A.* **78**:3245-3249.

A. Grinvald, L. B. Cohen, S. Lesher, and M. B. Boyle (1981b) Simultaneous optical monitoring of activity of many neurons in invertebrate ganglia using a 124-element photodiode array. *J. Neurophysiol.* **45**:829-840.

A. Grinvald, R. Hildesheim, I. C. Farber, and L. Anglister (1982) Improved fluorescent probes for the measurement of rapid changes in membrane potential. *Biophys. J.* **39**:301-308.

A. Grinvald, A. Fine, I. C. Farber, and R. Hildesheim (1983) Fluorescence monitoring of electrical responses from small neurons and their processes. *Biophys. J.* **42**:195-198.

A. Grinvald, R. D. Frostig, E. Lieke, R. Hildesheim (1988) Optical imaging of neuronal activity. *Physiol. Rev.* **68**:1285-1366.

S. Nakajima and A. Gilai (1980) Action potentials of isolated single muscle fibers recorded by potential-sensitive dyes. *J. Gen. Physiol.* **76**:729-750.

T. D. Parsons, D. Kleinfeld, F. Raccuia-Behling, and B. M. Salzberg (1989) Optical recording of the electrical activity of synaptically interacting *Aplysia* neurons in culture using potentiometric probes. *Biophys. J.* **56**:213-221.

W. N. Ross, B. M. Salzberg, L. B. Cohen, A. Grinvald, H. V. Davila, A. S. Waggoner, and C. H. Wang (1977) Changes in absorption, fluorescence, dichroism, and birefringence in stained giant axons: optical measurement of membrane potential. *J. Membr. Biol.* **33**:141-183.

B. M. Salzberg, H. V. Davila, and L. B. Cohen (1973) Optical recording of impulses in individual neurones of an invertebrate central nervous system. *Nature* **246**:508-509.

B. M. Salzberg, A. Grinvald, L. B. Cohen, H. V. Davila, and W. N. Ross (1977) Optical recording of neuronal activity in an invertebrate central nervous system: simultaneous monitoring of several neurons. *J. Neurophysiol.* **40**:1281-1291.

D. W. Tank and Z. Ahmed (1985) Multiple-site monitoring of activity in cultured neurons. *Biophys. J.* **47**:476a (abstr.).

D. Y. Ts'o, R. D. Frostig, E. E. Lieke, and A. Grinvald (1988) Functional organization of visual area 18 of macaque as revealed by optical imaging of activity-dependent intrinsic signals. *Soc. Neurosci. Abstr.* **14**:898, abstr. #362.3.

A. Yariv (1985) *Optical Electronics*, 3rd ed. CBS College Publishing, New York.

Chapter 4
Dye-Recording Apparatus, 2.
Microscope and light source

4.1 MICROSCOPE

4.1.1 Introduction

The heart of a dye-recording system is the microscope. The microscope illuminates the specimen, projects its image onto eye, film, video camera, or optical detector, and positions it for electrophysiology and optical recording. The experimentalist is fortunate that this most essential of parts is the easiest to obtain: the microscopes that are presently available commercially are of very high quality, convenient to use, and not too expensive. Also, over the last few years, advances in computerized lens-design techniques have made it possible to have very high numerical-aperture objective lenses with moderate magnifications (*i.e.*, a fairly large field of view).

This section briefly discusses the design of an efficient optical system, then describes the microscope used here. Subsection 4.1.2 describes the requirements for illumination system, objective, and condenser, which lead to high optical efficiency and the maximum signal-to-noise ratio. (Appendix C expounds the theory behind these requirements.) Subsection 4.1.3 then describes the system used in this thesis, which is based on an Olympus IMT-2 microscope.

Alignment and calibration are particularly important for dye recording. When analyzing a dye signal, it is important to know what area of the culture the signal comes from, so the optical detector array must be aligned carefully relative to the microscope.

Subsection 4.1.4 describes the use of a video camera for alignment. In order to compare fluorescence values between pixels, with different filters, and over time, it's important to know the illumination intensity and the output efficiency of the microscope. Subsection 4.1.5 describes calibration devices used to measure these quantities.

4.1.2 Efficiency of optics

As discussed in section 3.1, the optical efficiency of the microscope should be high, in order to maximize S/N and minimize bleaching and photodynamic damage. This means that the microscope should get light into and out of the specimen efficiently, so that the detected photocurrent I is as high as possible. The factors that affect I can be roughly grouped into three parts:

$$I = (\text{illum. intensity}) \times (\text{dye factors}) \times (\text{collection eff.}) \ .$$

The second factor depends not on the microscope, but rather on the staining of the preparation and the properties of the dye; these are discussed in Chapter 6. The first and last factors are properties of the microscope: an optically efficient microscope will have high illumination intensity, and high collection efficiency. The illumination intensity depends on the brightness of the light source, the illumination optics, and the condenser lens. The collection efficiency is simply the fraction of transmitted or fluoresced photons collected by the optical detector; this fraction is determined by the objective lens. Appendix B examines in detail the theoretical bases for improving illumination intensity and collection efficiency; the results are summarized below.

Both illumination intensity and collection efficiency depend crucially on the lenses used; the numerical aperture of the condenser (NA_{cond}) and of the objective (NA_{obj}) must both be large. Illumination intensity depends as well on the illumination system. The light source must be bright, of course, and the intermediate lenses and stops must be arranged for proper illumination. With nonuniform light sources such as tungsten filaments and

mercury arcs, uniform illumination is commonly provided by Kohler illumination. With this illumination method, the light source is imaged onto the back focal plane of the condenser; for maximum intensity, the source's image should just fill the condenser's entrance pupil. Under these conditions, with a perfectly uniform light source, the illumination intensity is proportional to $(NA_{cond})^2$. In practice, the dependence is only roughly quadratic, since real light sources are not uniform, and there are several other modifying factors; still, NA_{cond} should be as large as possible.

Collection efficiency depends primarily on NA_{obj}. For absorption measurements, NA_{obj} need only exceed NA_{cond}, in which case all the transmitted light will be collected. For fluorescence measurements, on the other hand, the emitted light goes in all directions— it's impossible to collect all of it—and NA_{obj} must be as large as possible. The collection efficiency is roughly proportional to $(NA_{obj})^2$, though again this is an approximation, since the angular dependence of fluorescence intensity can be quite complex.

Thus, high numerical apertures for the condenser and objective are the two keys to optical efficiency. More prosaically, it is also important to have well-designed, well-corrected optics, with good antireflection coatings and clean optical surfaces. These are most simply obtained by purchasing a good modern microscope.

4.1.3 Description of apparatus

Fig 4.1 shows an overview of the apparatus. Its main parts are an Olympus IMT-2 inverted microscope; an RCA TC1005/N01 video camera used for alignment; an Olympus OM PC 35-mm camera for taking pictures of cultures; two Leitz micromanipulators for intracellular electrophysiology; a 256-pixel optical-fiber camera that captures the fluorescent light from the culture; and a set of 256 preamplifiers that transduces and amplifies the light from each pixel. These are all mounted on two aluminum plates and partially surrounded by a metal screen that acts as a Faraday cage.
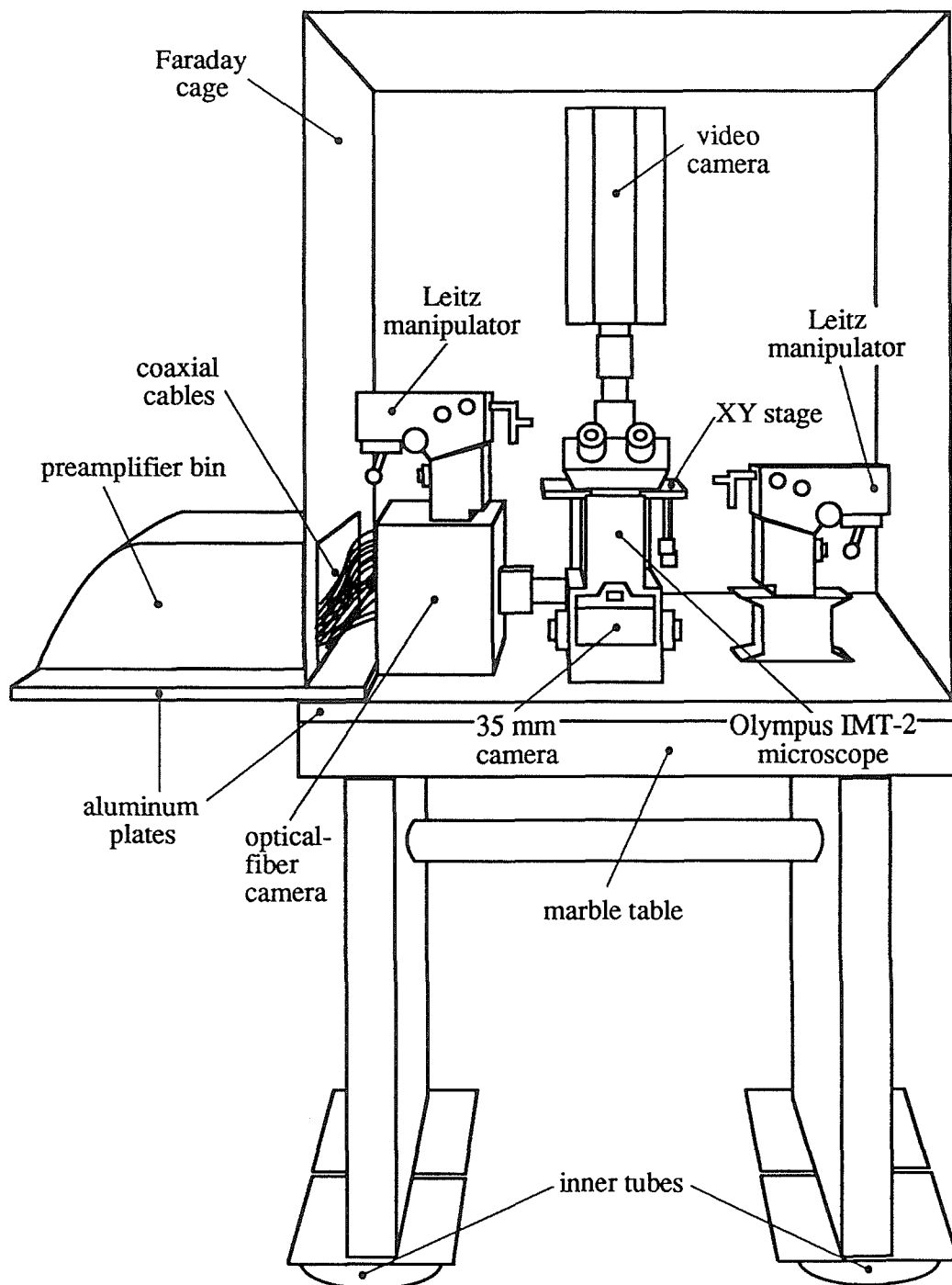
Figure 4.1 Overview of the apparatus, with major components marked.
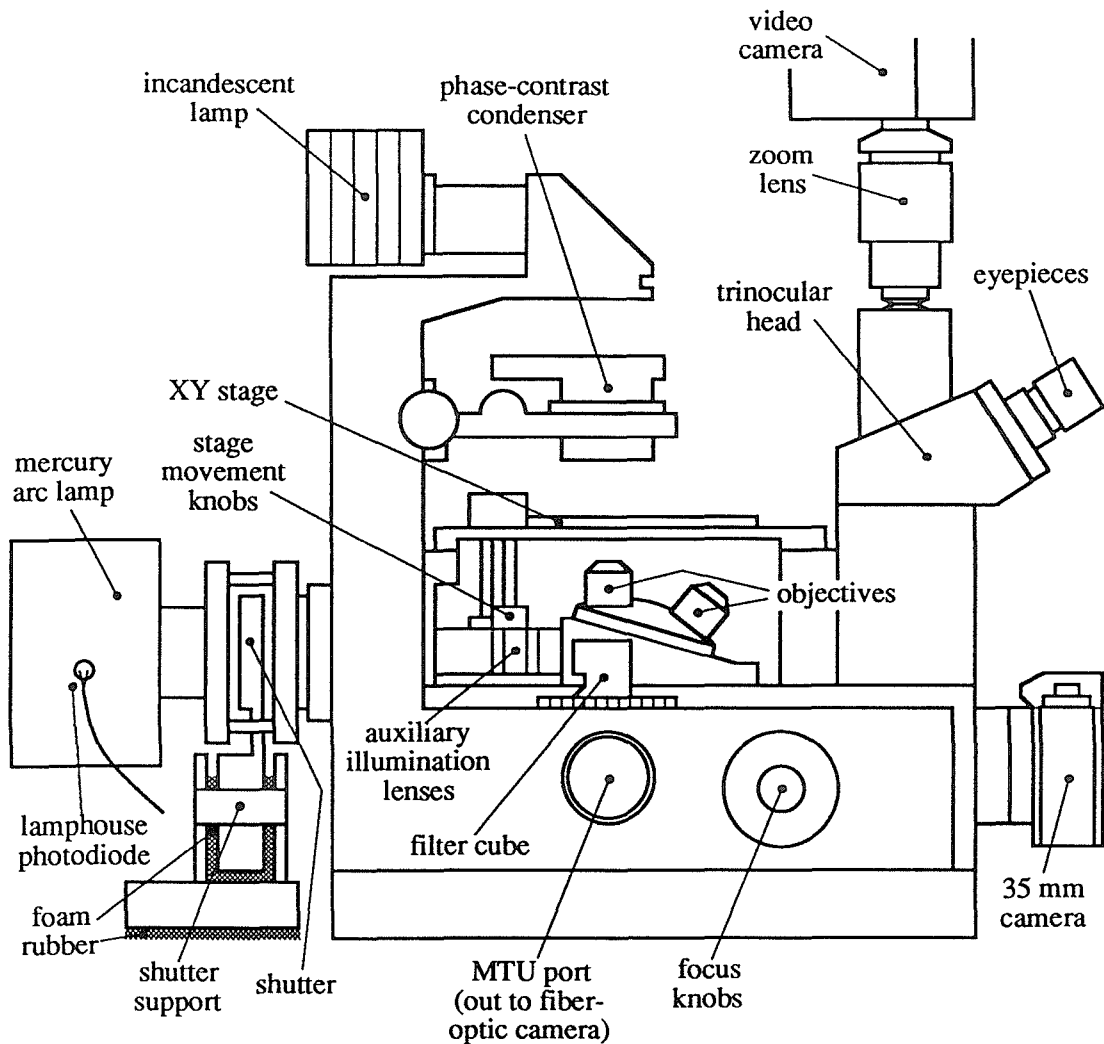
Figure 4.2 Side view of the Olympus IMT-2 microscope, with components marked. The specimen sits on the XY stage, directly below the phase-contrast condenser and above the objective. The IMT-2 can mount up to six objectives at once; only two are shown here.

For vibration isolation, the aluminum plates are mounted on a massive marble table supported by four inflated inner tubes (10 cm i.d., 25 cm o.d.). Various ancillary equipment, mounted on equipment racks, is not shown here: amplifiers for electrophysiology, assorted control electronics, a monitor that shows the output from the video camera, the data acquisition system, and the IBM AT microcomputer that controls the apparatus.

This subsection describes the microscope, its illuminators, and its output paths. The fiber-optic camera and the rest of the dye recording system are described later in this chapter; the electronics for electrophysiology, in Chapter 6.

The IMT-2 microscope is shown in more detail in Fig 4.2. The specimen (not shown) is held and positioned by the XY stage in the center of the diagram. Modern microscopes are like Swiss army knives, with attachments sticking out in all directions: this one has two illumination systems, four image outputs, a rotating nosepiece that holds six objective lenses, and two filter cubes for fluorescence. The specimen may be transilluminated for viewing in phase contrast, or epiilluminated for viewing in fluorescence; it may be viewed by eyes, 35 mm camera, video camera, or an MTU (multi-tube adapter) port, in which the optical detector is mounted. The objectives have different magnifications, and are optimized for either phase-contrast or fluorescence. The filter cubes hold the excitation filter, dichroic mirror, and emission filter required for epifluorescence. Fig 4.3 is a schematic diagram of the light path for epifluorescence. The paragraphs below first describe the optical components along the light path, from lamp to detector, then describe the stage.

Illumination. For phase-contrast microscopy (not illustrated), the microscope is equipped with a standard incandescent lamp and phase-contrast condenser. A field iris can control the area illuminated, and a 550 nm interference filter can be inserted to eliminate chromatic aberration when taking photomicrographs.
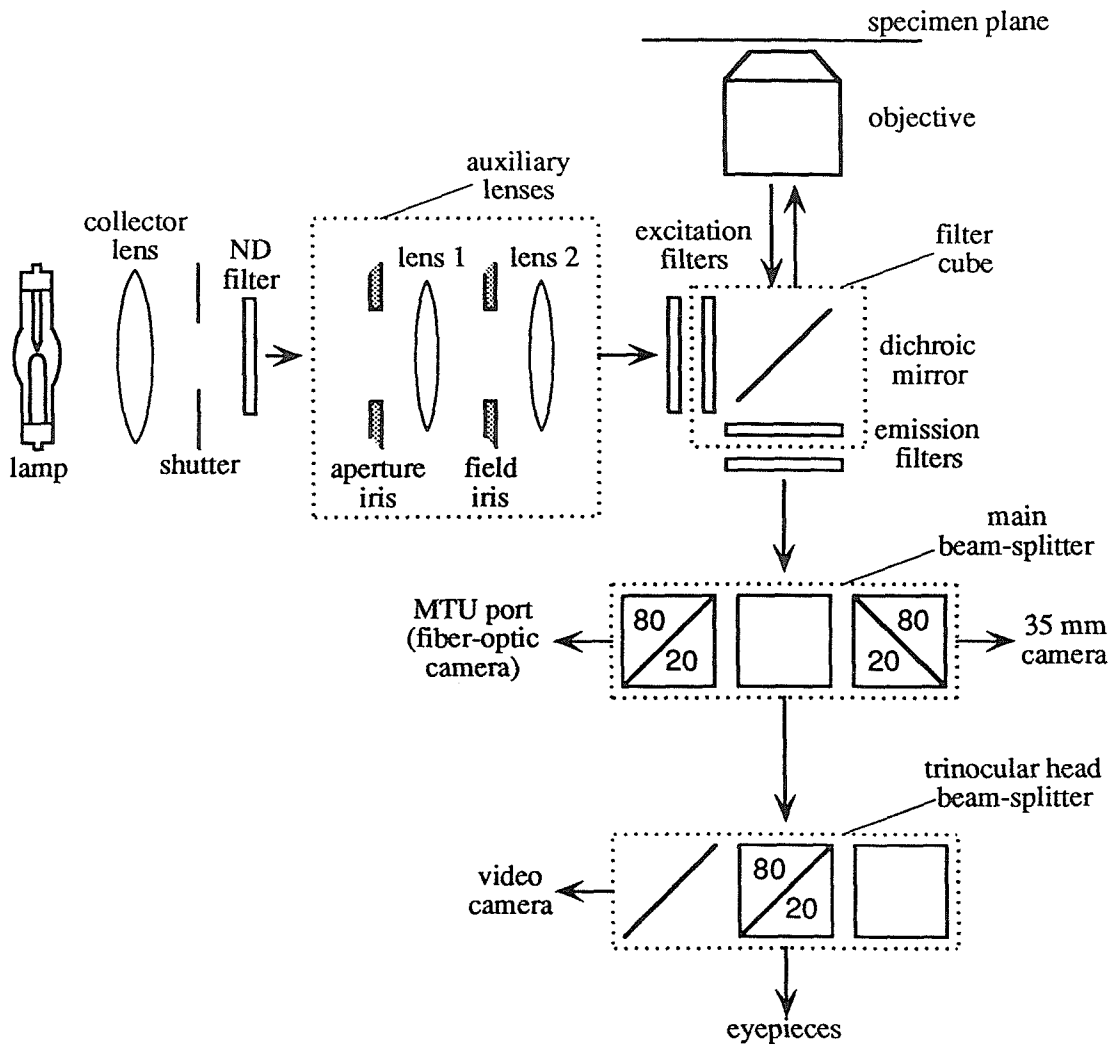
Figure 4.3 Schematic diagram of the light path of the IMT-2, used in epifluorescence mode, showing all important optical components. See text for description.

For fluorescence microscopy and dye recording, the microscope has the standard Olympus fluorescence illuminator, which has been modified by adding a shutter and stabilizing the light source. The light from a mercury arc lamp is gathered by a collector lens, then further focussed by two auxiliary lenses. There are several ways to control the illumination: a neutral-density filter (mounted in a slider) can reduce the intensity by a factor of 4, a field iris controls the area illuminated, and an aperture iris controls the

numerical aperture of the illuminator. The electromechanical shutter turns the illumination on and off; as shown in Fig 4.2, it is padded with foam to insulate the rest of the apparatus from its vibrations. The lamphouse photodiode, also shown in Fig 4.2, monitors the output of the lamp. A feedback circuit uses this signal to regulate the lamp's power supply and stabilize its output. Section 4.2 describes the mercury arc light source in great detail, including the feedback regulator and the shutter control electronics.

Phase-contrast is used for alignment, ordinary photography, and positioning microelectrodes—*i.e.,* whenever fluorescence can be avoided. Phase-contrast illumination is relatively dim, and does not cause significant dye bleaching or phototoxicity. Fluorescence is used for dye recording only, since the fluorescent illumination is very bright (as it must be to maximize signal-to-noise ratio) and causes bleaching and phototoxicity: every second of exposure is precious. Fluorescence micrographs are only taken after the experiment is done and the cells are not needed anymore.

Filters. The excitation filters, dichroic mirror, and emission filters determine the wavelengths of the exciting and observed light, and are especially important for dye recording. The IMT-2 can use several standard filter cubes. Each cube comprises an excitation filter, dichroic mirror, and emission filter; an additional excitation filter may be mounted in front of the built-in excitation filter, and an additional emission filter may be slid in beneath the cube. The standard filters used here were an Olympus G cube (BP545 excitation filter, DM580 dichroic mirror, O590 emission filter) with an additional LP515 long-pass excitation filter. The 545 nm bandpass filter (width 80 nm) and the 515 nm long-pass filter effectively remove all exciting wavelengths except for the 546 nm mercury line; the combination of the dichroic mirror and O590 long-pass filter passes only wavelengths longer than 610 nm.

When aligning and calibrating the fluorescence optics, it is convenient to be able to see nonfluorescent objects: mirrors, photodiodes, etc. Since the G cube is too efficient for this purpose (light passed by the excitation filters is completely blocked by the emission

filters), and so a spare V cube was modified by replacing its dichroic mirror with a plain glass coverslip. The coverslip acts as a very lightly silvered mirror, and with the standard mercury-arc illumination, the emission and excitation filters of this modified cube pass enough light to see nonfluorescent objects easily.

Objectives. Six objectives (all dry lenses) are usually used: an Olympus 4x phase objective for low-magnification alignment; Olympus 10x, 20x, and 40x phase objectives for higher-magnification viewing; and high numerical aperture Nikon 20x and 40x phase objectives for fluorescence. (See Table C.1 for more detailed information on these lenses.)

The choice of objective for dye recordings is determined by two considerations: numerical aperture and field of view. As discussed above, NA_{obj} must be as large as possible for maximum optical efficiency; in general, this will require a high-magnification lens (since high-magnification lenses have higher NA). On the other hand, the magnification must be low enough that an entire microculture can be seen at once: reasonable sizes for SCG microcultures are in the range 0.5 to 0.75 mm. The field of view is determined by the microscope's tube diameter—approximately 20 mm—divided by the objective's magnification. The maximum convenient magnification is thus about 20x. The input to the optical-fiber camera is actually 16 mm across (a little smaller than the tube), so at 20x magnification, the optical detector's effective field of view is about 800 μm in diameter.

The high-NA Nikon 20x lens (Fluor 20 Ph3DL, NA .75) was the objective used for most dye-recording experiments. Occasionally, the Nikon 40x lens or a Zeiss 63x oil-immersion lens were used for experiments that studied a single cell in detail and did not require a large field of view.

Output light paths. As shown in Fig 4.3, the IMT-2 is equipped with two selectable beam-splitters that can direct the image of the specimen into any of four output paths. The first directs light to the MTU port, the trinocular headpiece, and the 35 mm

camera; the three choices are 80:20:0, 0:100:0, and 0:20:80 (MTU:trinocular:35 mm). The second, within the trinocular head, directs light to the eyepieces or video camera; the choices are 100:0, 80:20, and 0:100 (video:eyepieces). The standard arrangement during experiments is to send images to the fiber-optic camera in the MTU port, to the video camera, and to the eyepieces. The first beam-splitter is switched from the MTU port to the 35 mm camera for photography.

Stage. The specimen is held by the IMT-2's standard XY stage. Mounted on the stage is a lucite plate that holds an aluminum heating ring, which in turn holds the 35 mm petri dish containing the culture of interest. The lucite plate has drilled holes for mounting components; the heating ring has attachments for a temperature sensor and ground wires. The stage is mounted on the microscope, and so provides movement relative to the optical detector and the micromanipulators, which are both fixed to the table.

For dye-recording experiments, it is often convenient to mount the stage on the table instead, and place the entire microscope on a sliding plate that can move relative to the table (*e.g.*, Calvet and Calvet, 1981). In this arrangement, after the stage movement is used to position the cells for electrode penetration, the sliding plate can be used to move the microscope to look at various parts of the culture, without disturbing the impaled cells. Unfortunately, the optical-fiber camera and preamplifier bin—which must be fixed to the microscope—are too large for this sliding-plate arrangement to be convenient here.

4.1.4 Detector alignment

Alignment is provided by the video camera, which can record the position of each detector pixel, and then compare these with the positions of each cell in a phase-contrast image. Pixel positions are recorded as follows. The microscope is focussed on a mirror, and the optical-fiber bundle is backlit to produce a reflected image of the fibers. The eight alignment fibers are lit up directly by light-emitting diodes (LEDs); the other 256 fibers are lit up by shining a bright light into the fiber bundle from the side. This light is conducted

along the interstices between fibers, and neatly outlines each one. The output of the video camera goes both to a video monitor and to an image capture board in the IBM AT; the positions of the fibers can be recorded by tracing with a marker on the face of the video monitor, and more accurately by capturing an image with the computer.

During an experiment, the hand-drawn map on the video monitor provides quick, crude alignment: the positions of the pixels overlay the live video image of the culture. For a more accurate archival record, the program OPTIK captures a video image of the culture (see section 5.2.3). Since the video camera and optical fiber camera are both fixed to the microscope, realignment of the fiber camera is almost never required. The map on the video screen is accurate to a few microns (with a 20x objective), if care is taken to avoid parallax errors; the digital map that OPTIK uses is accurate to about two microns.

The present video system has one flaw: its field of view is a little too small. The camera's 1" Nuvicon tube has an active area about 12 mm square. In order to have the same field of view as the 18 mm optical detector array, the image would have to be demagnified by 2/3 between the trinocular head and the video camera. The Nikon zoom lens (shown in Fig 4.2) has a minimum magnification of only 0.9, so that about 20% of the image is lost. Intermediate lenses with lower magnifications are not commercially available, so custom-built optics would be needed to fix this problem.

One may wonder why a reticle is not used instead of this complicated video system. A reticle—simply a piece of glass marked with a map of the detector's pixels—is a simpler alignment method that has been used before. Looking into the eyepieces, one would see this map superimposed on the image of the culture. It is not mere perversity to use a video camera, video monitor, and image capture board instead of a piece of glass. This more complex system (though partially a historical accident) has two advantages. First, the fiber bundle is quite nonuniform, which makes a computerized map easier to build than a reticle. Second, the computerized system makes it very easy to select interesting pixels. OPTIK

displays a captured image of the culture with the pixel array overlaid, as well as the fluorescence level from each pixel; pixels are then selected with the touch of a key.

4.1.5 Optical system calibration

Three characteristics of the microscope are important enough to monitor routinely: stability of the light source, illumination intensity, and output efficiency. For early dye recording experiments with this apparatus, I measured all three before each experiment. After a while, it became clear that they were fairly stable, and thereafter I only checked these characteristics from time to time.

Stability of the light source is monitored with a Hamamatsu S-1087 photodiode— the same photodiode used in the optical detector—mounted in the side of the lamphouse (see Fig 4.2). This photodiode serves a dual purpose: it is part of the feedback loop used to stabilize the mercury arc lamp (see the next section), and also provides a monitor of the lamp's intensity. Its photocurrent is amplified by a transimpedance amplifier in the feedback regulator; the resulting voltage signal is conveniently checked for fluctuations with an oscilloscope.

The illumination intensity is monitored with another S-1087 photodiode, this one mounted in a petri dish. This device, called a "photodiode dish," is a sandwich: a protective coverslip below, a thin metal disk with a 100 μm circular pinhole in the middle, and the photodiode above. The sandwich is mounted in the bottom of a 35 mm plastic culture dish, which substitutes neatly on the stage for a dish with a real culture. The pinhole delimits the area of the diode that is illuminated. To measure the illumination intensity, the microscope is focussed (using the V cube modified for alignments, described in section 4.1.3), and the photocurrent is measured with a digital voltmeter. This current can then be converted to a radiant intensity (units of W/m^2) by using the specified quantum efficiency of the S-1087 and the known area of illumination. The photodiode dish is used

routinely to monitor the brightness of the lamp, and also to measure the effects of different excitation filters.

The output efficiency of the microscope is monitored by replacing the specimen with a light source, the "fake cell." This device, also mounted in a culture dish, comprises a coverslip, a 20 μm pinhole, and an optical fiber that presses against the pinhole. Illuminated with an LED driven by a calibrated current source, the fake cell provides a cell-sized standard light source. (It is not a perfect simulacrum: the light emitted from the optical fiber is well-collimated, whereas the fluorescent light from a stained cell is nearly isotropic.) The relative output efficiencies of different photodetector pixels are measured by positioning the pinhole over the pixels; the signal from a reference pixel can also be measured from day to day, to guard against dirty optical surfaces or unnoticed misalignment. The current source that drives the fake cell can be controlled by a TTL signal as well as manually; a TTL pulse can produce a pulse of light that rises in less than 10 μs. Such light pulses can be used to measure the temporal responses of the optical detector's preamplifiers (whose responses are on the order of milliseconds).

4.2 LIGHT SOURCE

4.2.1 Choice of light source

The apparatus described here uses for illumination a mercury arc lamp with a regulated power supply. The mercury arc lamp is standard for fluorescence microscopy, and is the light source most commonly used for fluorescence dye recording (Grinvald et al., 1982). Other light sources that may be used include xenon arc lamps (Salzberg et al., 1973), He-Ne lasers (Grinvald and Farber, 1981), and tungsten-halogen incandescent lamps. For a discussion of light sources in general, see Carlson and Clark (1965), later updated by Eby and Levin (1979). For discussions of light sources for dye recording, see

the reviews by Grinvald *et al.* (Grinvald *et al.*, 1988, section IV.A) and Cohen and Lesher (Cohen and Lesher, 1986, section 5.3).

Briefly, here are the major features of different light sources, as compared to mercury arc lamps (this comparison is by no means exhaustive). Mercury arc lamps are bright, but not stable. Their total light output is high, and mostly concentrated in a few narrow emission peaks. Especially for narrowband excitation, they are brighter than xenon arc lamps, whose emission is broad-band, and much brighter than tungsten-halogen lamps, which are broad-band *and* dimmer overall. Mercury arc lamps are certainly dimmer than lasers, but have several strong emission lines, and so may be more convenient than a single-wavelength laser. The brightness of the mercury arc, however, must be weighed against its instability. The arc (being a hot plasma) is susceptible to arc wander, which causes fluctuations in the lamp's intensity and is impossible to control. Xenon arcs are somewhat more stable (Grinvald *et al.*, 1988, section IV.A.2); tungsten-halogen lamps, having solid filaments, are much more stable. Lasers are usually quite noisy, and also have high coherence, which is undesirable because it causes speckle.

When choosing a light source for dye-recording, one wants the brightest source that is sufficiently stable. As explained below, a mercury arc lamp is as bright as is useful, since its illumination intensity is high enough to start causing significant photodynamic damage. When stabilized with an optical feedback regulator, it is sufficiently stable for the present experiments. A tungsten-halogen bulb would be slightly more convenient because of its increased stability, but would be too dim; a laser would require complex apparatus for reducing coherence, and its extra intensity would not be useful anyway, because of phototoxicity.

The following subsections describe the properties of the mercury arc lamp used here (subsection 4.2.2), the optical feedback circuit used to reduce its fluctuations (subsection 4.2.3), software methods that compensate for fluctuations (subsection 4.2.4),

and the shutter used to control illumination (subsection 4.2.5). Subsection 4.2.6 summarizes the properties of the light source.

4.2.2 Properties of the mercury arc lamp

The apparatus described here uses an Osram HBO 100W/2 high-pressure mercury arc bulb, mounted in the standard lamp housing for the Olympus IMT-2 microscope. Fig 4.4*a* is a sketch of this bulb. It comprises two electrodes, a sharp cathode and a large blunt anode, surrounded by a quartz envelope (required in order to withstand the high operating temperature). The lamp is ignited by vaporizing the mercury contained in the bulb, which ionizes to form an arc that conducts current and gives off light. The spectral distribution of this light is shown in Fig 4.4*b*; the marked 546 nm line is the illumination wavelength used for most of the dye recording described here. The arc is initially about 1 mm long, but spreads over a few mm as the bulb ages and the electrodes erode. (The bulb is rated for a lifetime of 200 hours.)
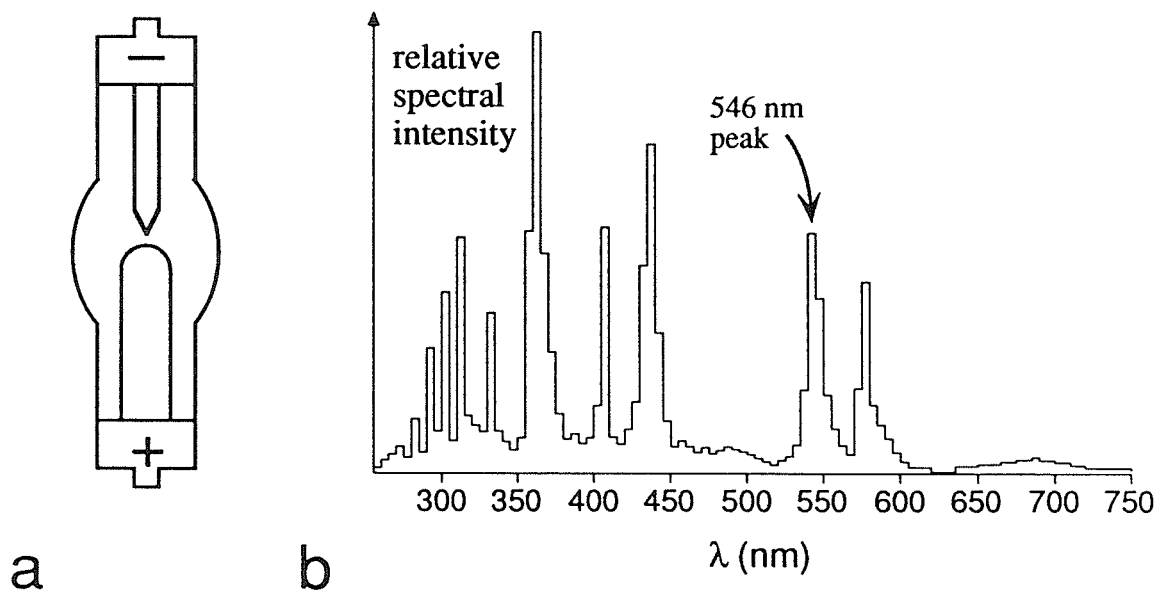
Figure 4.4 The Osram HBO 100W/2 mercury arc bulb. *a*) Schematic of the bulb. *b*) Spectral distribution of light from the bulb. The 546 nm mercury line is marked. (Spectrum provided by McBain Instruments.)

I have used two different power supplies for this bulb, which is rated at 100 watts and runs at approximately 4.5 A at 22 V. The first was a Lambda LE-101 DC supply, used in current-regulated mode. This supply required an Oriel 68705 igniter, which applies 30 kV sparks in order to vaporize the mercury in the bulb. This igniter had a distressing tendency to damage other electronics in the room, so more recently I have used an Olympus BH2-RFL-T2 power supply, which has a built-in RF igniter that does not seem to damage electronics. This power supply is not well current-regulated, and has considerably more 60 Hz ripple than the Lambda supply, but this ripple is removed by the optical feedback circuit described below.

The two most important properties of a light source are its brightness (the illumination intensity available) and stability (its illumination noise). With a Nikon 20x Fluor objective and filters that select the 546 nm mercury line (see subsection 4.1.3), this bulb provides an illumination intensity of 10 W/cm^2 at the specimen. This intensity falls nicely into the range of desirable intensities set by the signal-to-noise ratio and phototoxicity. The upper limit is set by phototoxicity, which starts to be significant at 10 W/cm^2 (see Chapter 6), and would reach unacceptable levels if the light source were much brighter.

The lower limit of desirable intensities is set by S/N considerations: if the illumination were much dimmer, the shot-noise-limited S/N would be too low, and amplifier dark noise would start to intrude. This apparatus is designed to measure postsynaptic potentials of perhaps 5-10 mV; since the sensitivity of the dyes used here is about 1%/100 mV, $\Delta F/F$ for PSPs is likely to be roughly .05% to 0.1%. When illuminated at 10 W/cm^2, a typical SCG neuron gives a fluorescent photocurrent of 1 nA, which has a shot noise of 0.3 pA rms, or .03% (with a 300 Hz noise bandwidth; see section 3.2.2), for S/N of 2 or 3. At this light level, some signal averaging is already required; if illumination were much dimmer, the required averaging would become

prohibitive[1]. The mean preamplifier dark noise is .08 pA rms (see section 5.1), so if the illumination were a factor of 10 lower, the noise would start to be dominated by dark noise instead of shot noise. In summary, the illumination intensity from the HBO 100W/2 is not too dim, not too bright (Goldilocks would be pleased).

Illumination noise in the output of the HBO 100 W/2 takes two forms. First, there is line frequency ripple, at 60 Hz and higher harmonics. With the Lambda power supply, line frequency ripple was 0.2% p-p (peak-to-peak); with the Olympus supply, it is 1.5% p-p. Second, there are nonperiodic slow fluctuations, consisting of occasional spikes in intensity (at least some of which are presumably due to arc wander). The spikes typically rise in tens of milliseconds and decay in hundreds of milliseconds, and have amplitudes ranging from too small to detect, through 0.1%, to 3% or larger. Bulbs seem to go through noisy and quiet periods, lasting for minutes or tens of minutes, in an unpredictable pattern. During a typical quiet period, spikes exceeding 0.1% arrive at 0.1/s; during a typical noisy period, these spikes arrive at 2/s, and half of them exceed 0.5%. These fluctuations seem to depend on the age of the bulb: one new bulb (the only one that was carefully observed) was very quiet.

The effects of illumination noise can be reduced in three ways, one a hardware method and the other two software methods:

- *Optical feedback regulator.* The lamp regulator circuit described in the next subsection reduces lamp fluctuations using a negative feedback loop. The lamphouse photodiode samples the illumination, and whenever it senses a rise or fall in intensity, the current supplied to the bulb is correspondingly reduced or increased. This method can suppress global fluctuations that affect the overall intensity, but not local fluctuations that only affect part of the specimen.

---

[1]It might be possible to compensate for a lower illumination intensity with more intense staining, but these cells are already stained extremely heavily (see section A.4.4).

- *Correction for illumination intensity.* If the intensity fluctuations can be measured independently of the fluorescence signals, they may be corrected in software. In principle, even local fluctuations could be corrected, provided that the illuminating intensity could be monitored at many points in the specimen. In practice, these corrections are difficult: it's not necessarily easy to measure the fluctuations.

- *Rejection or averaging of data.* Illumination noise is not, of course, correlated with true fluorescence signals. If several fluorescence records are taken consecutively, illumination fluctuations that appear in one record will not appear in others. These fluctuations usually have certain characteristic shapes that can be distinguished from true optical signals. Records that have a nonrepeatable waveform of the right signature can be marked as contaminated and rejected. Alternately, the effect of these fluctuations can be reduced by signal averaging.

I have used only the first and last of these methods; they are discussed in the next two subsections.

4.2.3 Optical feedback regulator

Fig 4.5 is a schematic of the regulator circuit[2]. The photocurrent from the lamphouse photodiode (see subsection 4.1.5) is converted to a voltage by a transimpedance amplifier, then further amplified and used to drive a transistor that parallels the lamp. When a fluctuation increases the lamp intensity, the transistor shunts more current, reducing the intensity and creating negative feedback. The standing current through the transistor determines the maximum output swing of the circuit, but during ignition this current shorts the Olympus power supply and prevents it from lighting this lamp, so a switch is used to disconnect the regulator during ignition. In order to check how well the regulator is working, the output of the transimpedance amplifier (REG) can be monitored while the gain of the circuit is adjusted between zero and full gain using the potentiometer after the x11 amplifier.

---

[2]An earlier version of this circuit has been previously cited in the literature (Cohen and Lesher, 1986). For historical reasons, the circuit shown is somewhat more complicated than necessary.
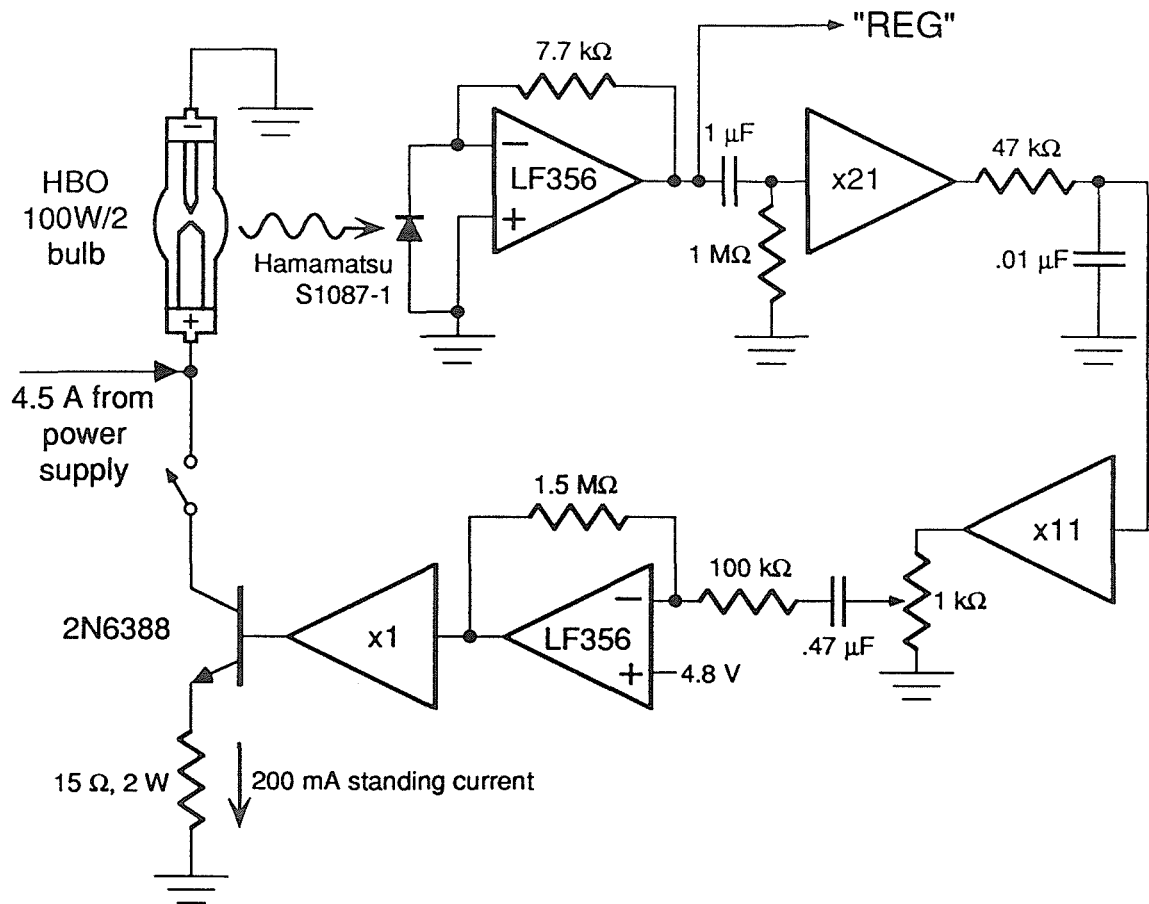
Figure 4.5 Optical feedback regulator circuit. The output of the lamphouse photodiode is amplified and used to drive a shunt regulator. The 2N6388 Darlington power transistor in parallel with the lamp shunts more current when the lamp intensity increases. The circuit passes frequencies between 3.2 and 320 Hz, and its gain may be varied from zero to full, in order to check the effects of regulation. The *REG* output provides a monitor of the lamp intensity.

The bandwidth of the regulator is 3.2-320 Hz (3 dB-down frequencies)[3]. Those fluctuations that fall within this range should be suppressed by a factor equal to the loop gain. The gain from the output of the photodiode to the current shunted through the transistor is (7.7 kΩ)(21) (11)(15)/(15 ohm)=1.8x10^6. At the lamp's operating current of

---

[3]During the design of a feedback regulator, some care must be taken to avoid unnecessary phase shifts, which can cause oscillations. "Motorboating" (oscillation at very low frequencies) was especially troublesome for this circuit.

about 4.5 A, the photocurrent from the lamphouse photodiode is about 0.7 mA. Taking

the approximation that the lamp's light output is linearly proportional to the lamp current,

the overall gain of the feedback loop is $(1.8 \times 10^6)(0.7 \text{ mA})/(4.5 \text{ A}) = 280$. Fig 4.6$a$ shows

the effect of the regulator on line frequency ripple, as measured by the REG output.

Without regulation, the fluctuations are 1.5% p-p (0.47% rms); with regulation, they are

reduced to .0082% p-p (.0023% rms), a 200-fold improvement. This is slightly less than

the loop gain, probably due to a small amount of ripple within the feedback circuit itself.

Fig 4.6b shows REG on a slower timescale with the 60 Hz ripple filtered out, in order to

see the slow nonperiodic fluctuations. These are not completely removed (the time

response of the regulator is too slow), but their peak amplitude is reduced by an order of

magnitude.

REG is not a good measure of the illumination intensity at the specimen, since the

lamphouse photodiode does not directly sample the light going to the specimen (it is

a) 60 Hz ripple

unregulated

regulated

20 ms

b) slow fluctuations

unregulated

regulated

1 s
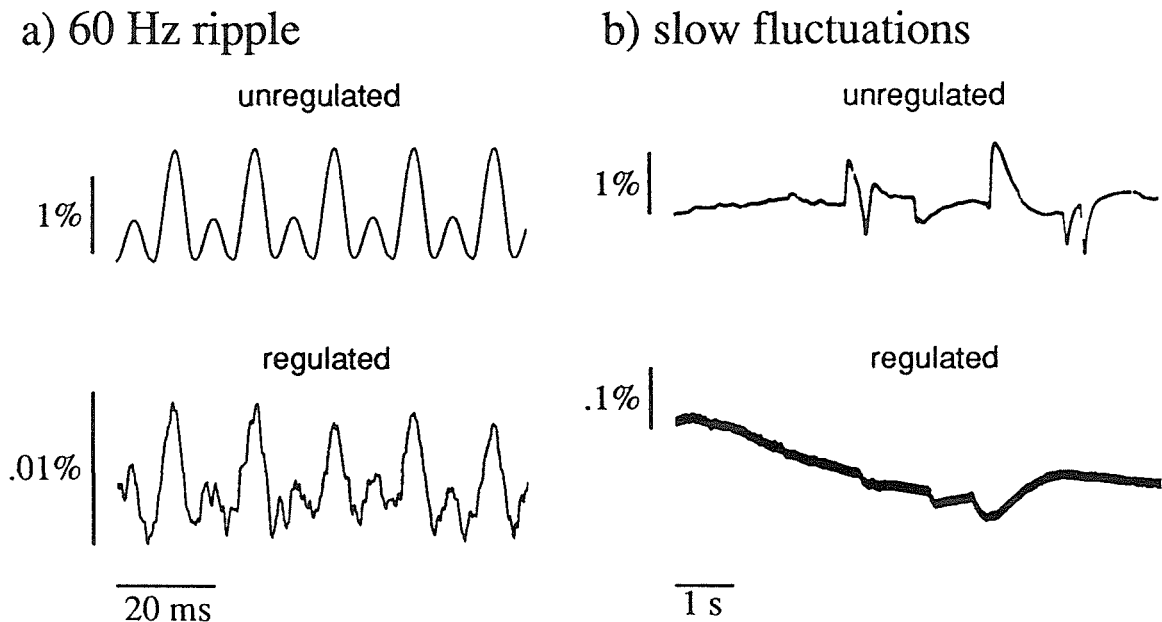
Figure 4.6 Regulation of fluctuations as measured by the lamphouse monitor *REG*. The regulator circuit's gain was zero for the *unregulated* traces, and full for the *regulated* traces. *a*) 60 Hz ripple, filtered with a passband of 0.16-320 Hz. *b*) Slower fluctuations, filtered with a passband of 0.16-5.3 Hz.

mounted at right angles to the illumination path). Indeed, one expects movement of the arc to produce fluctuations that are spatially nonuniform, giving rise to intensity changes that are different at the lamphouse photodiode and at the specimen. Fig 4.7 and Fig 4.8 compare REG with the signal SPEC measured with the photodiode dish (see subsection 4.1.5) mounted in the specimen plane. Fig 4.7 shows that line frequency fluctuations were suppressed in both places: the peak-to-peak ripple decreased from 1.5% to .008% in REG, and from 1.8% to less than .05% in SPEC. The total rms noise decreased from .5% to .002% in REG, and from .6% to .02% in SPEC. Fig 4.8 shows the effects of regulation on slow nonperiodic fluctuations. Looking at the unregulated traces in Fig 4.8a, it's clear that some spikes are common to REG and SPEC, but others differ. It is thus not surprising that with regulation (Fig 4.8b), slow fluctuations are still present in SPEC, despite being heavily suppressed in REG. These spikes presumably reflect some spatially nonuniform change in the lamp, such as arc movement.

a) unregulated

REG

1% \N\N\N\N\N

SPEC

1% \N\N\N\N\N

20 ms

b) regulated

REG

.01% \N\N\N\N\N

SPEC

.1% \N\N\N

20 ms
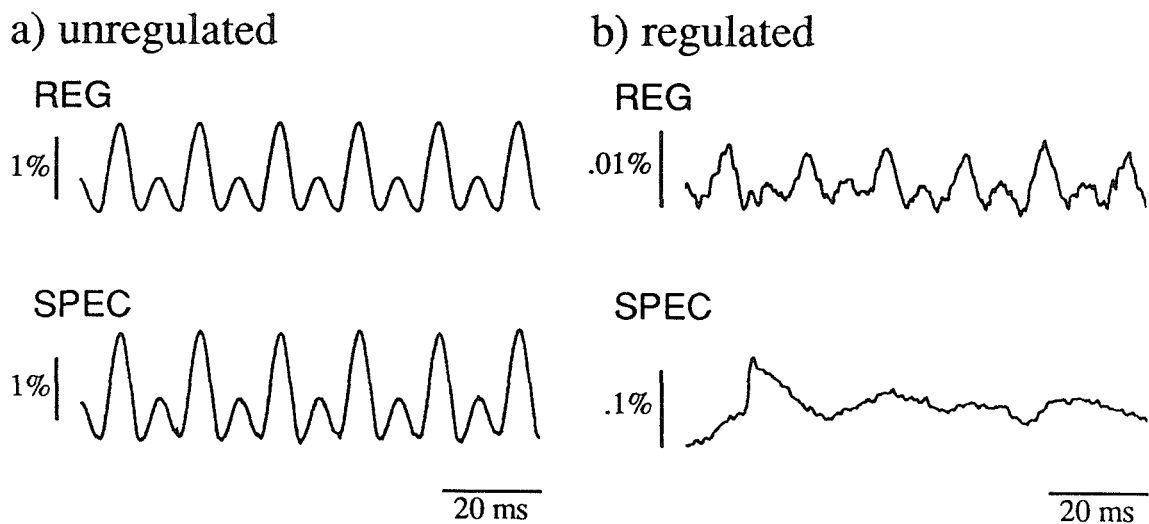
Figure 4.7 Comparison of line-frequency fluctuations at the lamphouse photodiode (*REG*) and the specimen (*SPEC*). *SPEC* was measured by the photodiode dish (see subsection 4.1.5), illuminated as if for dye recording, with a Nikon 20x Fluor objective and the usual filters. All signals have been filtered with a passband of .16-320 Hz. a) Unregulated. b) Regulated.

a) unregulated   b) regulated

REG

1%|

SPEC

1%|

1 s
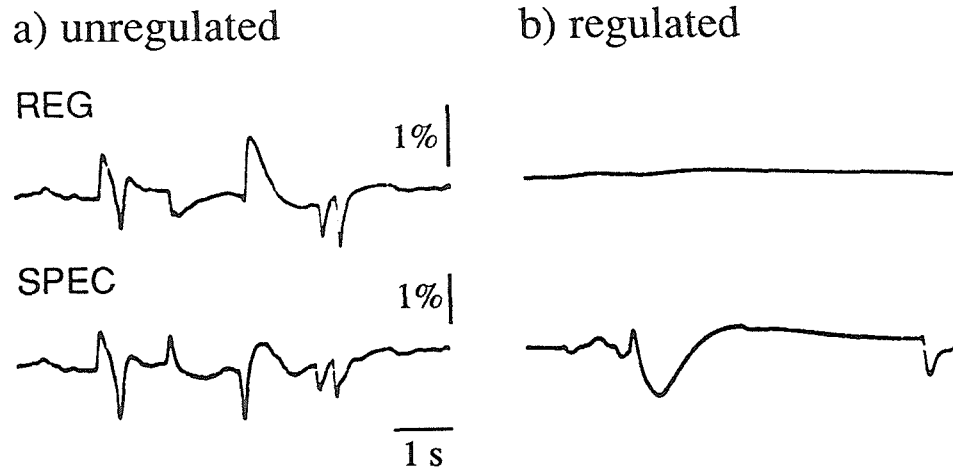
Figure 4.8 Comparison of slow nonperiodic fluctuations at *REG* and *SPEC*. All signals shown have been filtered with a passband of .16-5.3 Hz. *a*) Unregulated. *b*) Regulated. Scales for *b* are identical to those shown for *a*.

It is quite conceivable that intensity fluctuations that differ between REG and SPEC might nevertheless be uniform across the illuminated part of the specimen. While the lamphouse photodiode is quite far from the illumination path, the cone of rays that leaves the bulb to illuminate the specimen is relatively small, and Kohler illumination is meant to produce a uniform intensity. In order to check for variations in intensity across the specimen, the multifiber detector was used to measure illumination reflected off a mirror. Fig 4.9 shows signals from 3 pixels that span the field of view of the detector. Intensity spikes are usually relatively uniform across the field, as seen in Fig 4.9*a* and *b*, but are sometimes quite nonuniform, as in Fig 4.9*c*. Nonuniformities occur not only between the lamphouse monitor and the specimen, but also within the specimen plane itself.

The frequency of fluctuations was quantified by observing 10 pixels spread over the detector for 50 periods, each lasting 200 ms—a typical length for an experimental record. In 7 records there was an intensity spike that was uniform across the specimen, in 3 a nonuniform spike, and in the remaining 40 either no fluctuation or a slow uniform
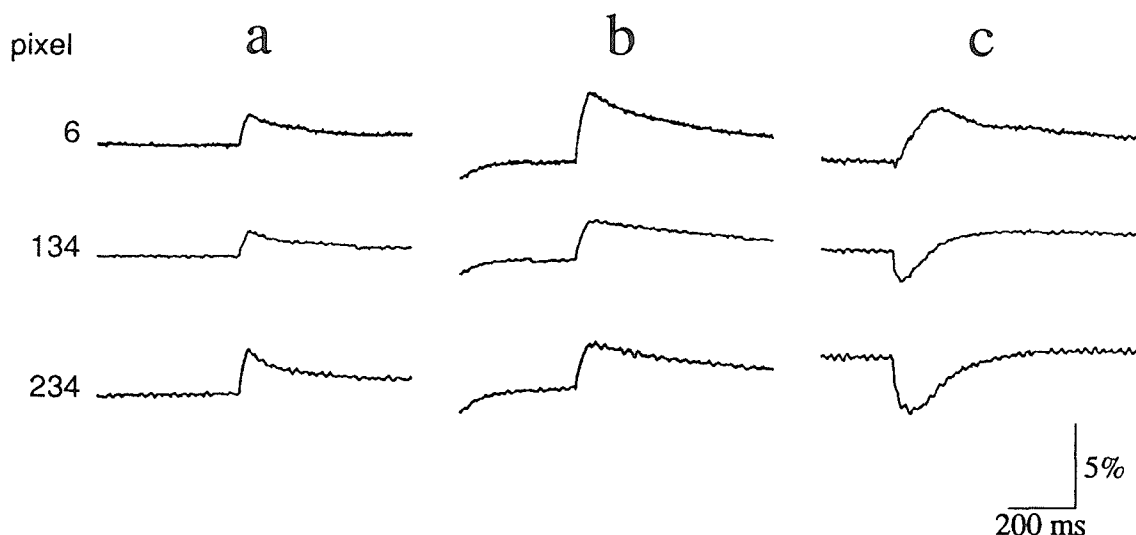
Figure 4.9 Spatial variations in intensity fluctuations. The microscope was focussed on a mirror, which was illuminated as for dye recording. The reflected light was reduced by a combination of neutral density and long-pass filters, to avoid saturating the multifiber detector. The pixels shown are at the upper left (6), center (134), and lower right (234) of the detector array. a) and b) Uniform fluctuations. c) Nonuniform fluctuation. Scale bars apply to all traces.

change that was nearly linear in time. This incidence of illumination noise is typical, though it varies greatly when the bulb is in a particularly noisy or quiet phase.

4.2.4 Compensating for fluctuations

Software can partially compensate for uniform illumination fluctuations. They are identified quite easily, since they have a characteristic shape and do not repeat from trial to trial. At present, records that contain fluctuations are simply rejected. It should be possible to go further and subtract the effects of uniform fluctuations in software, but this would require a good reference signal. A photodiode placed at an appropriate point in the illumination pathway should faithfully record uniform fluctuations.

Nonuniform fluctuations are more troublesome. Software correction would require a spatially resolved reference for illumination intensity. Alas, the only available reference, the fluorescence signal from a nearby background pixel, is not a very good one. Such a signal is quite noisy from shot noise, shows dye bleaching as well as illumination changes,

and is also likely to show some voltage-dependent signals (pixels are rarely completely free of neurites). It seems likely that software correction of nonuniform fluctuations is not feasible, and the best one can do is to reject records with nonuniform fluctuations; this is the strategy presently used.

Fluctuations might also be reduced with improved hardware. Note that the intensity at the regulated point (REG) is much quieter than the intensity at the specimen. If the regulated point was at the specimen—if REG reflected the specimen intensity more accurately—then the specimen intensity should be more stable. This might be achieved by a modification as simple as moving the lamphouse photodiode closer to the illuminating light path. A more sophisticated method would use a lightly-silvered mirror to sample the entire area of the illuminating beam, then use a lens to focus this onto a photodiode.

Another practice that might help would be to run new bulbs for 10-15 hours continously when they are first turned on (Grinvald *et al.*, 1988, section IV.A.2). The idea behind this practice is that the bulb electrodes selectively erode where the arc contacts them. A long, continuous run "seats" the arc in a particular place on the electrodes, so that it is not tempted to jump around during future lightings. I have only burnt-in bulbs for a few hours, so the longer times that Grinvald *et al.* suggest may yield stabler arcs.

4.2.5 Shutter

Specimen illumination is turned on and off by an Ilex No. 1 Synchro iris shutter (Ilex Optical Co., Rochester, NY) interposed in the light path (see Fig 4.2). This electromechanical shutter is carefully mounted in a foam-packed support, to avoid vibrating the apparatus when it opens and closes. The circuit that controls the shutter allows it to be opened and closed either manually or by a TTL input. During dye-recording experiments, the shutter is usually flashed by driving the TTL input with a timer circuit; a ten-turn knob allows the length of the TTL pulse to be adjusted from 10 ms to 500 ms.

4.2.6 Summary

The two important properties of a light source for dye-recording are illumination intensity and stability. The mercury arc lamp system described here is appropriately intense: it is bright enough to give a reasonable signal-to-noise ratio, but not so bright that it causes excessive phototoxicity. It provides 10 W/cm^2 at the specimen, which gives a typical fluorescent photocurrent of 1 nA; the shot noise in this photocurrent is .03% rms, which should give a signal-to-noise ratio of 2 or 3 for large postsynaptic potentials.

The stability of this lamp is also reasonable, though not all that could be desired. The feedback regulator reduces fast intensity fluctuations to about .02% rms (slightly below shot noise for a typical cell), but does not regulate slow fluctuations as well. Slow fluctuations can be very large (up to several percent), and seem to be due to arc movement, since they are often spatially nonuniform. This nonuniformity makes these fluctuations very hard to regulate and compensate; at present, trials that are spoiled by fluctuations are simply rejected (not included in the analysis). It might be possible to improve the stability of the lamp by repositioning the lamphouse monitor, or by burning new bulbs in for a long time.

CHAPTER 4 REFERENCES

J. Calvet and M. C. Calvet (1981) A simple device for making a standard inverted phase-contrast microscope movable. *J. Neurosci. Meth.* **4:**105-108.

F. E. Carlson and C. N. Clark (1965) Light sources for optical devices. In *Applied Optics and Optical Engineering,* vol. I, ed. R. Kingslake. Academic Press, New York. pp.44-109.

L. B. Cohen and S. Lesher (1986) Optical monitoring of membrane potential: Methods of multisite optical measurement. In *Optical Methods in Cell Physiology,* eds. P. DeWeer and B. M. Salzberg. Wiley (Interscience), New York, NY. pp.71-99.

J. E. Eby and R. E. Levin (1979) Incoherent light sources. In *Applied Optics and Optical Engineering,* vol. VII, eds. R. R. Shannon and J. C. Wyant. Academic Press, San Diego. pp.1-46.

A. Grinvald and I. Farber (1981) Optical recording of calcium action potentials from growth cones of cultured neurons with a laser microbeam. *Science* **212:**1164-1167.

A. Grinvald, R. Hildesheim, I. C. Farber, and L. Anglister (1982) Improved fluorescent probes for the measurement of rapid changes in membrane potential. *Biophys. J.* **39:**301-308.

A. Grinvald, R. D. Frostig, E. Lieke, R. Hildesheim (1988) Optical imaging of neuronal activity. *Physiol. Rev.* **68:**1285-1366.

B. M. Salzberg, H. V. Davila, and L. B. Cohen (1973) Optical recording of impulses in individual neurones of an invertebrate central nervous system. *Nature* **246:**508-509.

Chapter 5
Dye-Recording Apparatus, 3.
Detector and data acquisition

5.1 OPTICAL DETECTOR

5.1.1 Introduction

The optical detector for the apparatus described here incorporates significant innovations in its primary photodetector—an optical-fiber camera with discrete photodiodes—and in its very low-noise preamplifiers. This section describes its design, testing, and performance.

Several constraints are imposed on the design of a detector by the biological preparation for which it is optimized. The important parameters of preparation are the size of the cells and of the culture, the speed of the cells' electrical responses, and the resting light levels expected. This detector was designed to record from microcultures of rat SCG neurons that are 400-800 μm in diameter, and have somewhere between one and ten cells, each 20-40 μm in diameter. These sizes determine the dimensions of the detector array. The action potentials of SCG neurons are typically 1 to 5 ms wide (depending on the temperature); in order to follow their electrophysiology, the detector's bandwidth must be about 300 Hz, and the sampling rate for recording should be about 2 kHz per cell. Finally, the detected fluorescent photocurrent from a typical SCG neuron, with 10 W/cm^2 illumination and a 0.75 NA objective, is about 1 nA; this determines the characteristics of the detector's preamplifiers.

The overall design of the detector, including the reasons for using a fiber-optic camera, is described in subsection 5.1.2. The next three subsections are devoted to the design and performance of the detector electronics. Subsection 5.1.3 describes the design of the preamplifiers; the detailed noise design is covered in Appendix D. Section 5.1.4 describes the design of the support electronics, and the construction of both the preamplifiers and the support electronics. The performance of the preamplifiers is then described in subsection 5.1.5. Possible future improvements to the detector are summarized in subsection 5.1.6.

5.1.2 Fiber-optic camera

Optical detectors for dye recording tend to look more like physicists' instruments than biologists'; this detector is no exception. Fig 5.1 shows a schematic diagram. An image of the culture is focussed onto a close-packed array of 256 square optical fibers; each
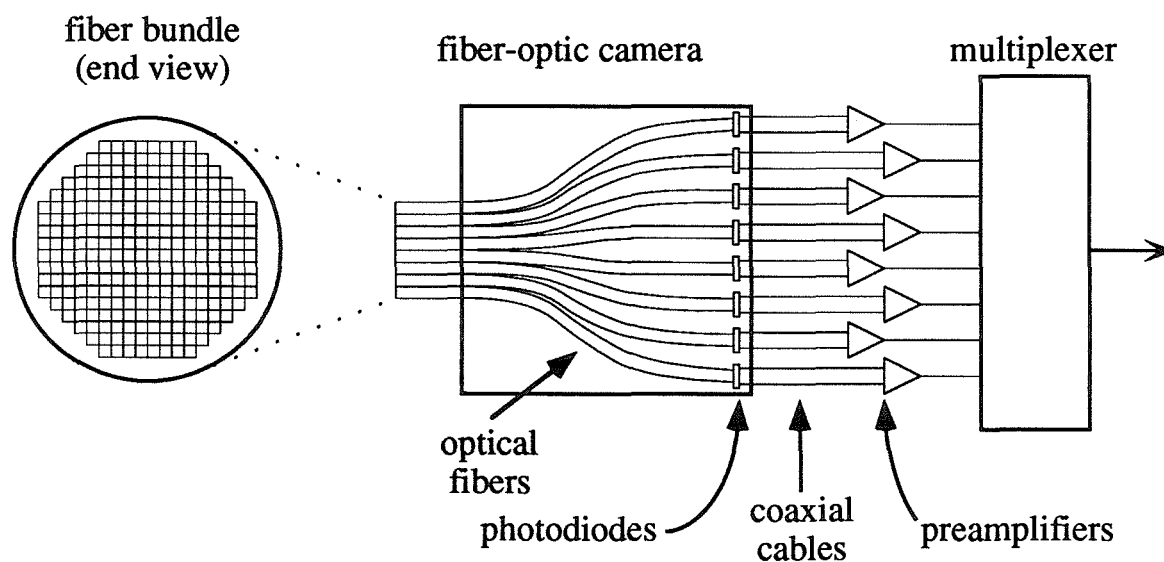
Figure 5.1 Schematic overview of the optical detector. The image of a culture is focussed onto the end of a bundle of 256 optical fibers; within the fiber-optic camera, these fibers splay out to individual photodiodes (only eight fibers and diodes are shown here). Each pixel's light is transduced to a photocurrent by its photodiode, then carried by a coaxial cable to a transimpedance preamplifier, where it is converted to a voltage, multiplexed with the signals from other pixels, then sent to the data acquisition system.

optical fiber conducts the light from its pixel to a discrete photodiode, where it is transduced into a photocurrent. A coaxial cable carries the photocurrent to one of 256 low-noise preamplifiers, where it is further transduced into a voltage. The voltage signal from this pixel is then multiplexed with signals from other pixels, and fed into the data acquisition system.

The optical fibers and the photodiodes compose an "optical-fiber camera," quite a different beast than an ordinary 35 mm camera. The optical fibers fill the role of the lens (the imaging element) in an ordinary camera, while the photodiodes replace the grains in a photographic emulsion (the photodetectors). The resulting detector is coarse-grained, but fast and ultra-sensitive. The optical-fiber camera has nowhere near the resolution of a 35 mm camera or a video camera, but operates at much lower light levels, and has a much faster response time.

An idealized view of the input plane of the fiber-optic camera is shown in Fig 5.2. (The real fibers are neither this uniform in size nor so regularly packed.) The octagonal array is 18 fibers across; there are 256 fibers that lead to photodiodes, plus 8 alignment fibers that are connected to LEDs. The alignment fibers may be back-illuminated with the LEDs, making them quite useful for alignment and focussing. The array is 16 mm across, with an average center-to-center fiber spacing of 0.9 mm. With a 20x objective, the detector has an 800 μm field of view with 45 μm pixels. This field of view is well matched to the size of SCG microcultures, and the pixel size comfortably contains a single SCG neuron (though in a culture with several cells, some will usually fall on pixel boundaries).

The fiber-optic camera was assembled as follows. Its body—including the mold that holds the fiber bundle and the backplane that holds the photodiodes—was machined from Lucite. Each optical fiber (Poly-Optical, Santa Ana, CA) was cut to an appropriate length with a fresh razor blade, both ends were polished, then one end was epoxied to an S-1087 photodiode (Hamamatsu). (For the eight alignment fibers, a plastic connector was
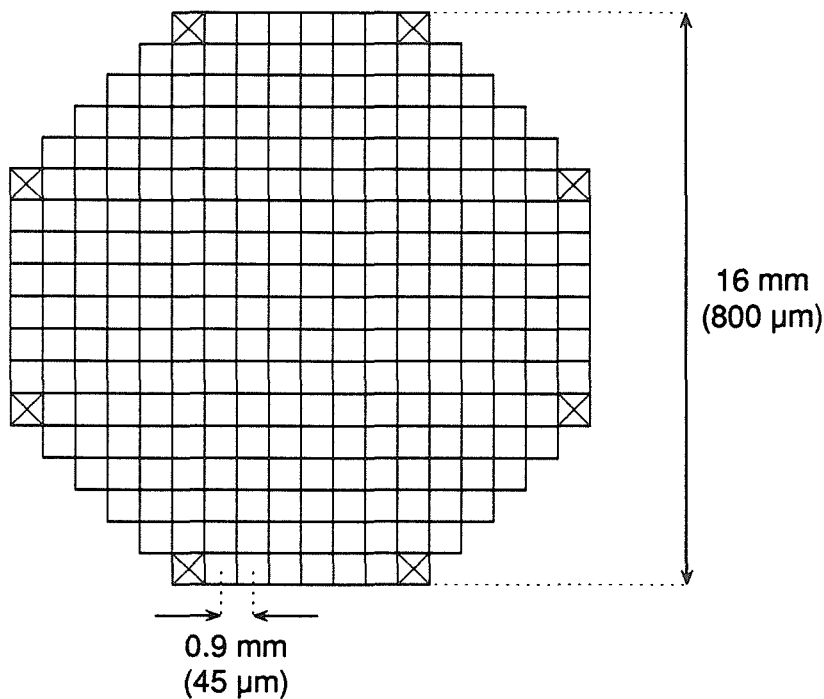
Figure 5.2 Schematic end view of the fiber bundle. The *crosses* indicate the eight alignment fibers; the other fibers go to photodiodes. The dimensions shown are projected sizes at the specimen with a 20x objective.

glued onto the free end, so it could be connected to an LED.) The fibers were then laid into one half of the Lucite mold, one row at a time, with layers of .001" (25 μm) Mylar tape separating the rows. As each row was laid, the photodiodes at the other end of the fibers were inserted into the backplane, in rows of 16 photodiodes each. The photodiode leads were inserted through the backplane and press-fitted into 25-pin connectors that had coaxial cables soldered to their far sides. Two of these connectors per row each held eight photodiodes (only 16 of the 25 pins were used). Finally, the two halves of the camera were screwed together to form the complete array. The finished camera thus connects an octagonal bundle of 256 fibers to a square array of 16 rows of 16 photodiodes.

					D	77	91	105	136	154	172	E					
				45	61	76	90	104	137	155	173	190	206				
			27	44	60	75	89	112	138	156	174	191	207	217			
		16	26	43	59	74	88	113	139	157	175	183	199	216	236		
	6	17	25	42	58	73	96	114	140	158	167	182	198	209	237	248	
C	7	18	24	41	57	72	97	115	141	159	166	181	197	208	238	249	F
0	15	19	32	40	56	80	98	116	142	151	165	180	196	210	239	250	245
1	14	20	33	48	64	81	99	117	143	150	164	179	195	211	231	251	244
2	13	21	34	49	65	82	100	118	135	149	163	178	194	212	230	252	243
3	12	22	35	50	66	83	101	119	134	148	162	177	193	213	229	253	242
4	11	23	36	51	67	84	102	127	133	147	161	176	192	214	228	254	241
5	10	30	37	52	68	85	103	126	132	146	160	200	222	215	226	255	240
B	9	31	38	53	69	86	111	125	131	145	184	201	223	232	227	247	G
	8	29	39	54	70	87	110	124	130	144	185	202	221	233	225	246	
		28	47	55	71	95	109	123	129	168	186	203	220	234	224		
			46	63	79	94	108	122	128	169	187	204	219	235			
				62	78	93	107	121	152	170	188	205	218				
					A	92	106	120	153	171	189	H					

Figure 5.3 Corrected map of multiplexer addresses for the fiber-optic camera. Multiplexer addresses run from 0 to 255; alignment fibers are lettered A through H. Fibers 240 through 245 are not connected to photodiodes: these addresses are used instead for auxiliary inputs to the data acquisition system.

During use, the camera is placed inside a square aluminum tunnel so that a Leitz micromanipulator may sit on top (see Fig 4.1). The fiber bundle and the open ends of the tunnel are shrouded in black conductive plastic (3M); this shroud blocks out stray light and serves as a Faraday cage. The RG174/U coaxial cables run back to the preamplifier bin,

where 16 cables (a row from the photodiode backplane) connect to each amplifier card. The preamplifiers are discussed in the next subsection.

The laying of the optical fibers inside the camera is quite complex, since it involves mapping 18 rows of variable length at the fiber bundle into 16 even rows at the photodiode backplane. In order to check this mapping, the fake cell (a small light source mounted in a petri dish; see subsection 4.1.5) was used to illuminate each pixel in turn, and responses were recorded from all 256 preamplifiers. This procedure found several wiring mistakes inside the camera. Fig 5.3 shows the corrected map of multiplexer addresses for each pixel, with the alignment fibers lettered A-H. The multiplexer addresses 240 through 245 have been coopted for auxiliary inputs such as electrophysiological signals, etc. (see the next subsection).

The fake-cell mapping test also served to check for crosstalk between pixels, and measure the relative transmittance of each fiber. There was no gross crosstalk: each pixel gave a large response in only one preamplifier, with a little light leakage (1 or 2%) to neighboring pixels. Fig 5.4 shows the distribution of photocurrents measured from each photodiode as the end of its optical fiber was illuminated with the fake cell. The distribution of transmittances is asymmetric, with a standard deviation of 20% of the mean. The three extremely low values probably represent badly damaged fibers; the noticeable shoulder on the low side of the mean may represent nicked fibers or fibers that were poorly joined to their photodiodes. The rest of the variation may be due to variations in joins to the photodiodes, or to variable losses in the fibers themselves. These square fibers are nonstandard and not of the best plastic: over the lengths used here (about 30 cm), their rated light loss is 10%. In principle, one of the advantages of a fiber-optic camera is that individual pixels may be repaired; for instance, a damaged photodiode could be replaced. In practice, the mechanical design of this camera makes repairs difficult, and in case of damaged fibers, impossible.
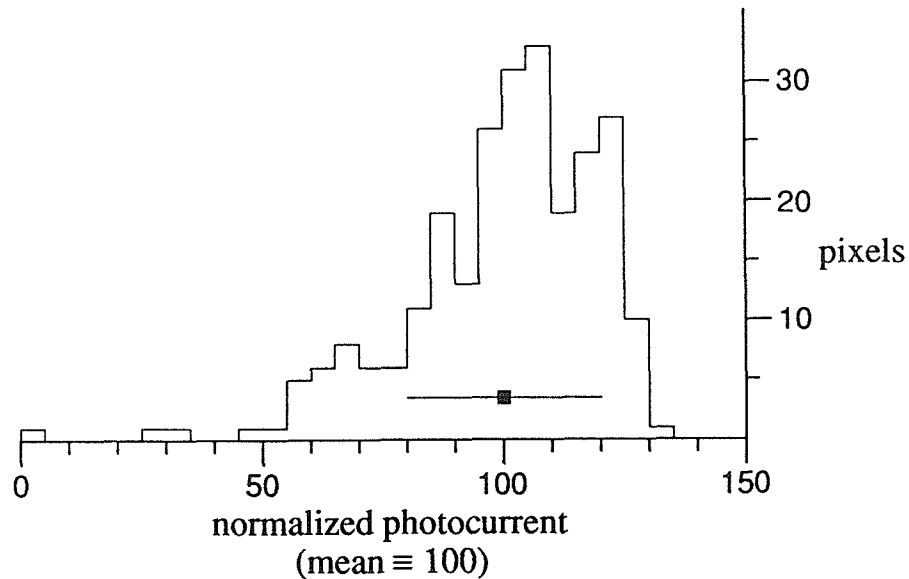
Figure 5.4 Distribution of fiber transmittances. Each fiber was illuminated in turn with the fake cell, and the detected photocurrents recorded. The *square* and *bar* indicate mean ± s.d.

5.1.3 Preamplifier design

The preamplifier is designed to minimize amplifier noise, given a desired bandwidth and a desired range of detected light intensities. For the preparation used here, a bandwidth of about 300 Hz is optimal: this is the lowest bandwidth that will not greatly decrease the amplitude of SCG neuron action potentials (though it will distort their shape). With the light source and microscope described above, typical fluorescence levels from these cells are between 0.2 and 2.0 nA per pixel. One hopes that at typical intensities, amplifier noise may be made smaller than shot noise; for the preamplifier described here, this hope is realized.

This subsection describes the main features of the preamplifier design; Appendix D has a detailed analysis. For an extremely useful reference, see Sigworth's article on the design of patch-clamp amplifiers (Sigworth, 1983). The preamplifier for fluorescence dye recording has much in common with a patch-clamp amplifier: both are very low-noise, low-current transimpedance amplifiers. (A *transimpedance* amplifier is simply a circuit that amplifies an input *current* and produces an output *voltage*; in contrast, a transconductance

amplifier amplifies an input voltage into an output current.) The main differences are that

the patch-clamp amplifier is faster and amplifies smaller input currents, while the dye-

recording preamplifier has more stringent signal-to-noise requirements, and must be

produced by the hundreds. The preamplifiers described here are quite similar to those

described by Sigworth.
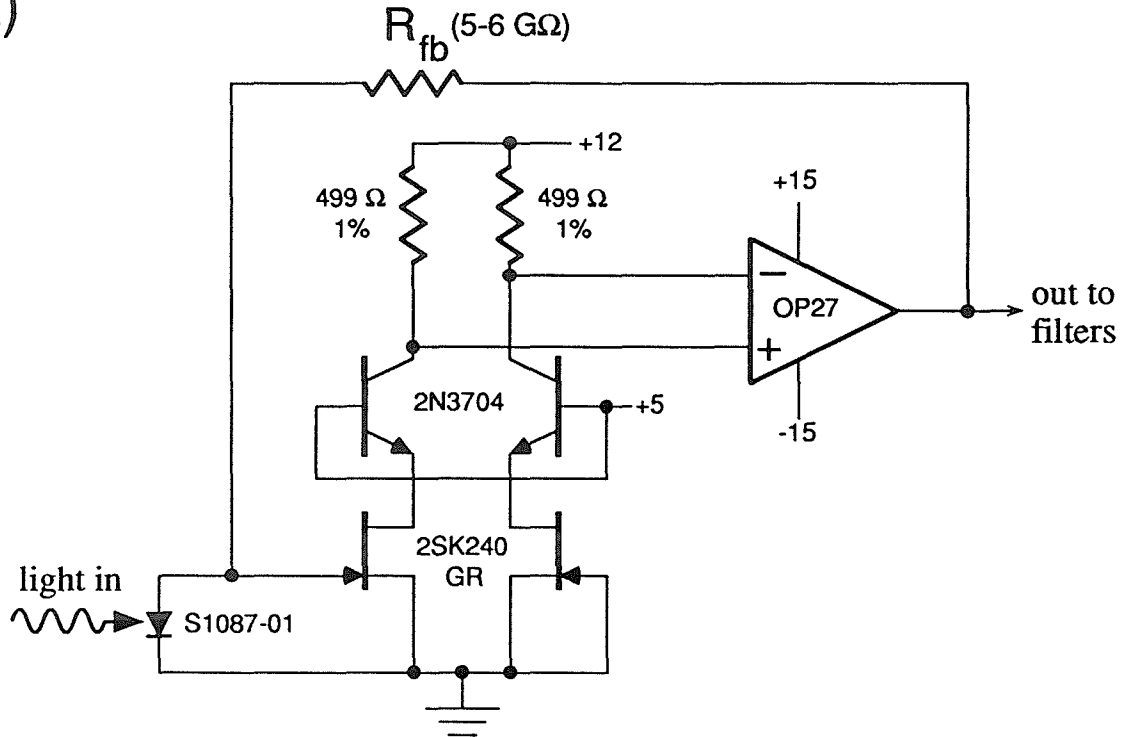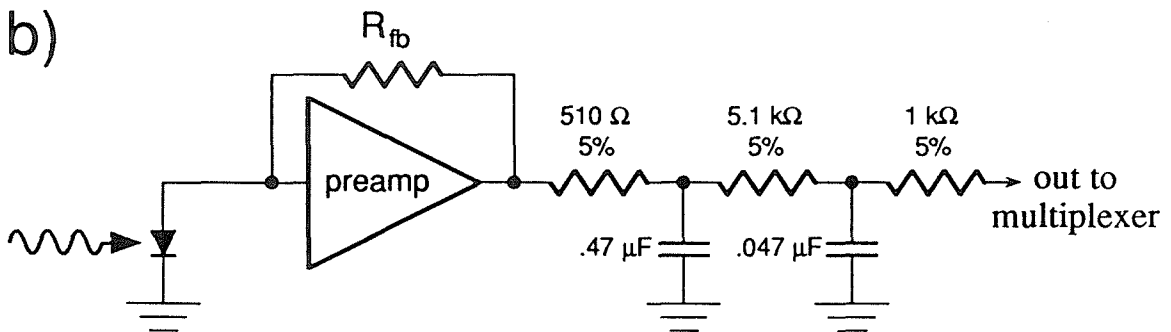
Figure 5.5 Preamplifier and filter circuits for the optical detector. *a*) Preamplifier circuit. A dual FET input stage and an OP27 form a high input-impedance inverting amplifier. Together with a feedback resistor (R_{fb}), they form a low-noise, low-input-current transimpedance amplifier. *b*) Output filters for the preamplifier. The dual FET and OP27 from *a* are represented as the amplifier *preamp*.

Fig 5.5a shows the preamplifier circuit. The basic circuit is quite simple: the current from a photodiode is fed into a transimpedance amplifier, comprising a high input impedance amplifier with a large feedback resistor. The amplifier forces the photocurrent I to flow through the feedback resistor R_{fb}, giving an output voltage IR_{fb}. Before it is multiplexed, this output voltage is passively filtered, as shown in Fig 5.5b. For good design, the amplifier cannot be considered alone: the photodiode, connecting cable, feedback resistor, and filters are all important as well.

Photodiode and cable. The photodiode and cable have two requirements. First, they must not add excess noise of their own. Second, their capacitances must not be too large, since they add to the input capacitance of the amplifier, which couples the amplifier's input voltage noise to the input current. The larger the input capacitance, the larger the effect of the amplifier voltage noise. The S1087-01 photodiode used here (Hamamatsu) is intrinsically very quiet, and has a capacitance of 200 pF; the RG174/U coaxial cable used to connect the photodiodes to the amplifiers does not have excess noise, and has a capacitance of 60 pF (100 pF/m over 60 cm).

Feedback resistor. The choice of feedback resistor is extremely important. R_{fb} has three effects: it sets a lower limit on the noise of the amplifier, determines its dynamic range, and determines its frequency response. First, the Johnson noise of R_{fb} sets an irreducible minimum for the amplifier noise. (Johnson noise or thermal noise is a fundamental physical property of a resistor in contact with a heat bath.) The equivalent Johnson noise current of a resistance R is proportional to $1/\sqrt{R}$, so R_{fb} should be made as large as possible. Second, R_{fb} sets the dynamic range. Since the output voltage cannot exceed the power supplies of the amplifier, and so saturates at about 12 V, the maximum input current is 12 V/R_{fb}. The feedback resistance must be small enough to accommodate expected photocurrents. Third, R_{fb} determines the amplifier's frequency response. Small stray capacitances combine with the very large resistances used here to dominate the frequency response. In order that the effects of these capacitances may be controlled, R_{fb}

cannot be too large. The resistors used here, made by Victoreen, are about 6 GΩ; they are described in detail in subsections 5.1.5 and 5.1.6. These feedback resistors are large enough that their Johnson noise is below shot noise for currents as low as 10 pA; they allow input currents of up to 2 nA, a reasonable range for the fluorescences from these cells; finally, their frequency response is reasonable (see subsection 5.1.5).

Amplifier. The amplifier has two parts: a junction field-effect transistor (JFET) input stage, and a conventional operational amplifier. The 2SK240-GR dual JFET (Toshiba) provides extremely high input impedance, with correspondingly low leakage current, and a moderate gain. The OP27 op-amp adds its high gain, and after the gain of the first stage, its noise is insignificant. The 2N3704 bipolar transistors are used to form a cascode configuration, where they serve two purposes: they control the drain-source voltage of the JFETs, and they prevent voltage noise later in the amplifier from feeding back to the input through the JFET's gate-drain capacitance.

Filters. The RC filters on the output of the preamplifier serve two purposes: they help to reduce any gain peaking in the amplifier, and they prevent aliasing by the multiplexer. Stray capacitance from the feedback resistor to ground sometimes causes gain peaking (a resonance in the amplifier at a certain frequency), which both distorts the signal and increases the noise. These RC filters will help to filter out any gain peaks above about 600 Hz. Aliasing is a distortion of the signal inherent in the process of sampling. Since the signals are to be digitized, they must be sampled at some frequency f_s. Aliasing affects any frequency components in the output signal that are above $f_s/2$, folding them down below $f_s/2$. This adds extra noise and distorts the signal, so it's desirable that the output filters remove most frequency components above $f_s/2$. With a typical sampling frequency of 3 kHz, $f_s/2$ is 1.5 kHz, well above the 3 dB frequency of these RC filters.

The 1 kΩ series resistor after the RC filters serves an important purpose: it eliminates transients feeding back from the multiplexer, which were a frustrating problem before this resistor was added. These transients, a well-known problem when using

multiplexers, can be simply explained as follows. There are finite capacitances within the multiplexer chip, connecting address lines to the analog inputs. Whenever the address is changed, capacitative transients through these capacitances will deposit a small charge on the input lines. The filter's output impedance is not small (5.1 kΩ in parallel with .047 µF), so without the 1 kΩ resistor, this small charge would be deposited on the .047 µF capacitor, altering the preamplifier's output voltage. The 1 kΩ resistor impedes the flow of this small charge, and prevents it from reaching the .047 µF capacitor, thus preventing multiplexer artifacts, including a complex form of crosstalk between the outputs of different preamplifiers.

5.1.4 Other detector electronics

Apart from the individual preamplifiers, the detector electronics has several other components: multiplexers, amplifiers for auxiliary inputs, and control electronics. These are described below, along with the physical realization of all these circuits. Each 16 amplifiers, corresponding to a single row of photodiodes in the backplane of the fiber-optic camera, are grouped together on a printed-circuit (PC) card. The detector electronics consists of 16 of these amplifier boards, together with a controller card; the 17 cards are mounted in a modified STD-bus card rack.

Multiplexers. The detector is designed to record from up to 30 pixels at once, with a sampling rate of 3 kHz/pixel, for a total sampling rate of 90 kHz. Assuming an average of two pixels per cell, this is enough for cultures of up to 15 cells. A two-stage multiplexer combines the signals from the selected pixels for data acquisition; the circuits are shown in Fig 5.6. First, a pair of CD4051 multiplexers on each amplifier card switches the board's 16 amplifier outputs into a single card output (see Fig 5.6*a*), which is buffered with an LM310 follower. The 16 card outputs travel along the motherboard of the STD bin to a controller card, where another pair of CD4051s multiplexes them into a single signal (see Fig 5.6*b*). This signal is then multiplied by 0.8 by a voltage divider, low-pass filtered

with a time constant of 1.4 μs to remove high-frequency noise, and finally buffered by an

LM310 for output to the data acquisition system.
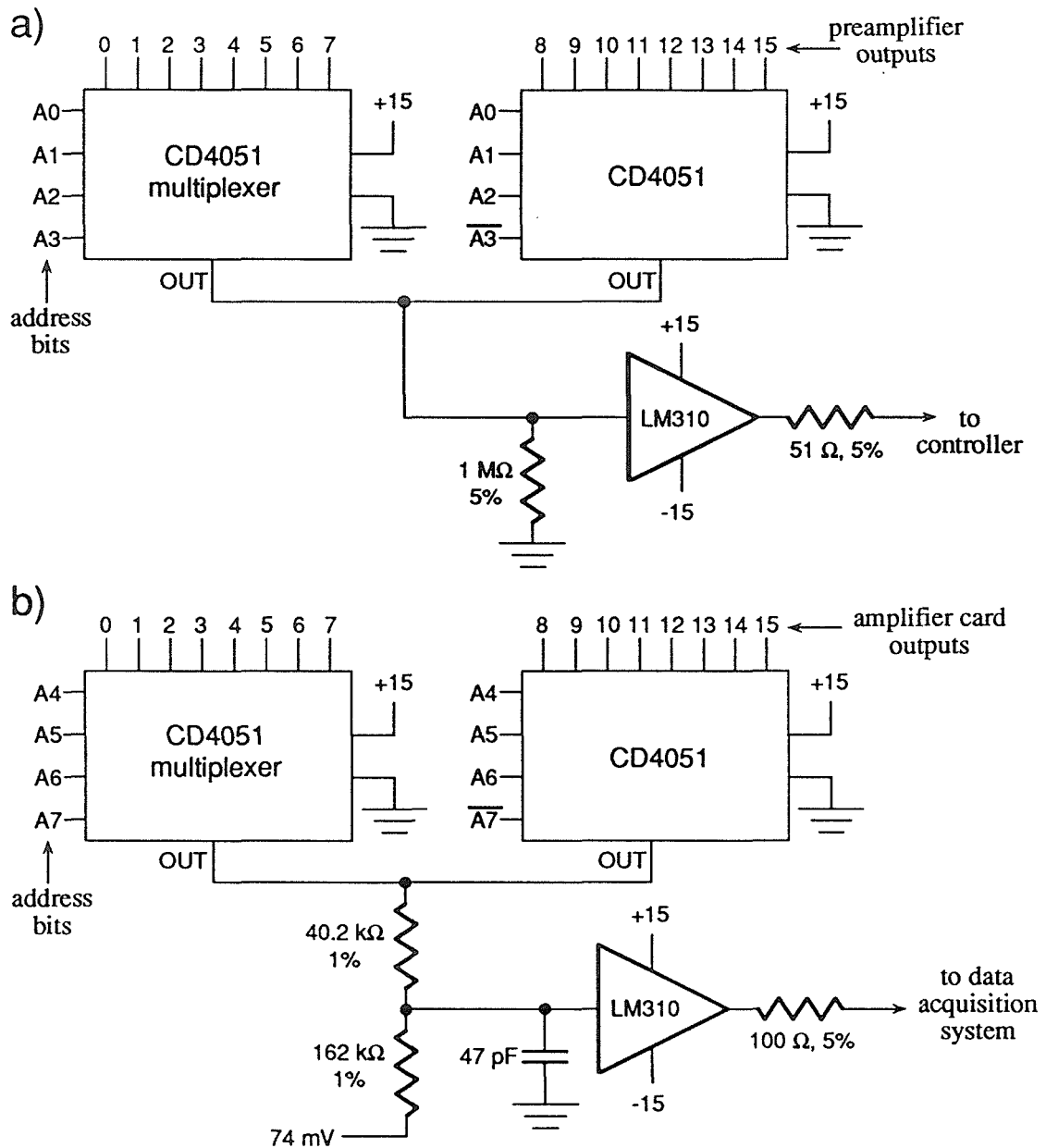
Figure 5.6 Multiplexers for the optical detector. *a)* The board multiplexers combine the signals from the 16 preamplifiers on a single amplifier board. *b)* The controller multiplexers combine the 16 board outputs into a single signal, which is then multiplied by 0.8, filtered, and buffered. The 74 mV DC offset at the lower end of the voltage divider is a historical appendix; it's not necessary.
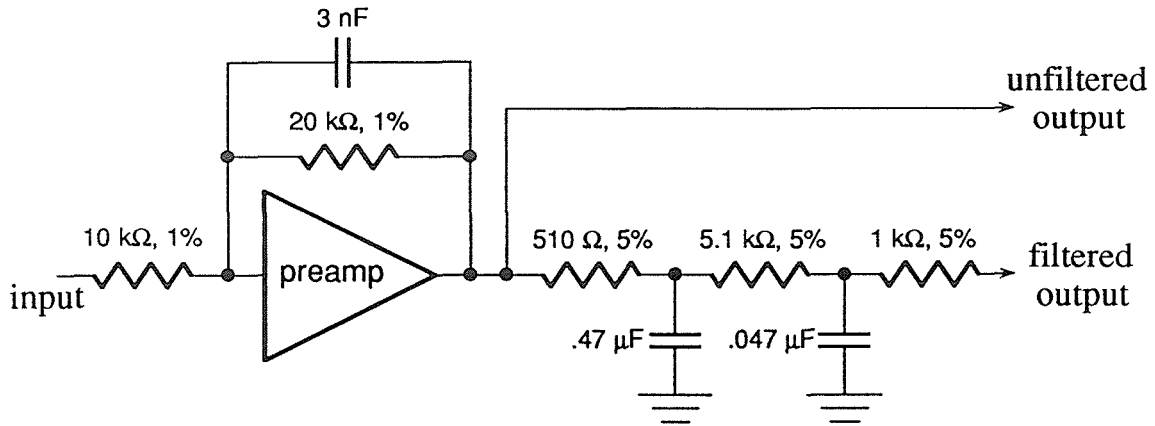
Figure 5.7 Amplifiers for auxiliary inputs. The inverting amplifier *preamp* is the same as for the optical inputs (the circuit is shown in Fig 5.5a). The three unfiltered amplifiers take their output from *unfiltered output*; the filtered amplifiers take their output from *filtered output*.

Auxiliary inputs. During dye-recording experiments it is often necessary to record other signals besides optical signals: intracellular potential, stimulus current, illumination intensity. To allow for such signals, six of the optical fibers (multiplexer addresses 240 through 245) have been disconnected, and their amplifiers modified as shown in Fig 5.7. Three of these have unfiltered outputs, and the other three have filtered outputs. The unfiltered channels are used for most purposes; the filtered channels can be used to test how the output filters used on the photodiode channels affect the shape of a particular signal.

Using a few of the optical detector's channels is a simple solution for multiplexing auxiliary inputs, but is slightly inconvenient because the preamplifiers only take monopolar inputs. The auxiliary inputs must be carefully manipulated, usually by adding a negative offset voltage, to insure that they are always negative.

Amplifier cards. The amplifier cards are 4.5" by 6.5" PC boards (custom-made by Pacific Bonde Co., Pacoima, CA) mounted in a modified STD-bus card rack (Vector). Each card holds 16 preamplifiers (Fig 5.5); two CD4051 multiplexers and an LM310 follower (Fig 5.6a); a hex inverter for buffering the address lines; and a voltage regulator

that produces 12 V, from which a zener diode in turn produces 5 V. Additional voltage regulation is provided by passively filtering all supply voltages at each amplifier.

Controller card. The controller electronics is wire-wrapped on a prototype board, also mounted in the STD-bus card rack. The controller card holds the multiplexers and follower shown in Fig 5.6*b*, as well as latches and buffers for the address lines. During experiments, the multiplexer address is generated by the data acquisition system; for testing, it can be set using a manual control box.

Card rack. All of the cards snap into a modified STD-bus card rack, whose motherboard provides power and carries signals. The rack has slots for 16 preamplifier cards, plus three controller cards. Only one of the controller slots is used, leaving space for test equipment. The STD motherboard has been modified to provide +15 V and -15 V analog supply voltages, and a +5 V digital supply voltage. It carries the low four bits of the multiplexer address from the controller card out to the amplifier cards, and carries back the 16 card outputs. (The high four bits of the multiplexer address need not be sent to the amplifiers, since these bits are only used on the controller card, where they select amongst the 16 card outputs.)

5.1.5 Preamplifier performance

The performance of the preamplifiers may be divided into three parts: DC responses (offsets and gains), AC responses (responses to light pulses), and noise.

DC performance. Theoretically, the output offsets of the amplifiers should have a range[1] of about 30 mV, but the actual offsets vary over about 200 mV. Channel 0 on each card tends to have an especially large negative offset, which seems to be due to leakage over the surface of the PC board from a power line that is near channel 0's input. The leakage is due to traces of moisture on the board: when the moisture is removed by

---

[1]This figure depends on the tolerance of the FETs' characteristics and on the tolerance of the 499 Ω drain resistors.

scratching the board or by turning the detector on and thus heating the board, the offset is reduced. (At the picoampere level, even a very faint coating of moisture can leak significantly!) These offsets would not be important, except that the detector electronics is monopolar and cannot handle negative signal voltages. In particular, a negative input to a CD4051 multiplexer will crosstalk to other inputs, which is highly undesirable. During experiments, there is usually at least a little light in every pixel, so all the outputs are positive and the offsets do not matter.

The gains of the preamplifiers depend purely on the feedback resistors. For historical reasons, three sorts (all from Victoreen) are used. A few are 5 GΩ; of the rest, about half are 6 GΩ and the other half are 10 GΩ resistors surgically reduced to about 6 GΩ. This was done by carefully scraping away part of the resistor's insulation, and using conductive paint to short out part of the helical resistive element. The altered resistors range from 4.3 GΩ to 6.9 GΩ. The three types are roughly equivalent, though their stray capacitances differ slightly. The resistors were all calibrated against one of the 5 GΩ resistors (tolerance 1%), by using a photodiode driven by an LED to inject a carefully adjusted current into each amplifier. This calibration is important because the resistances are used to convert amplifier output voltages into the photocurrents that are quoted throughout this thesis.

There is no detectable DC crosstalk between preamplifiers, though there is light leakage between adjacent fibers at the level of 1-2%.

AC performance. Ideally, the AC characteristics of the preamplifier would be set by its design. In this circuit, for instance, the frequency response would be determined by the output RC filters. Unfortunately, when working with 5 GΩ feedback resistors at a timescale of 0.5 ms, the inevitable stray capacitances (on the order of 0.1 pF) become dominant. These capacitances have two main effects: they set the frequency responses of the individual preamplifiers, limiting bandwidth and causing gain peaking; and they cause crosstalk between nearby amplifiers.
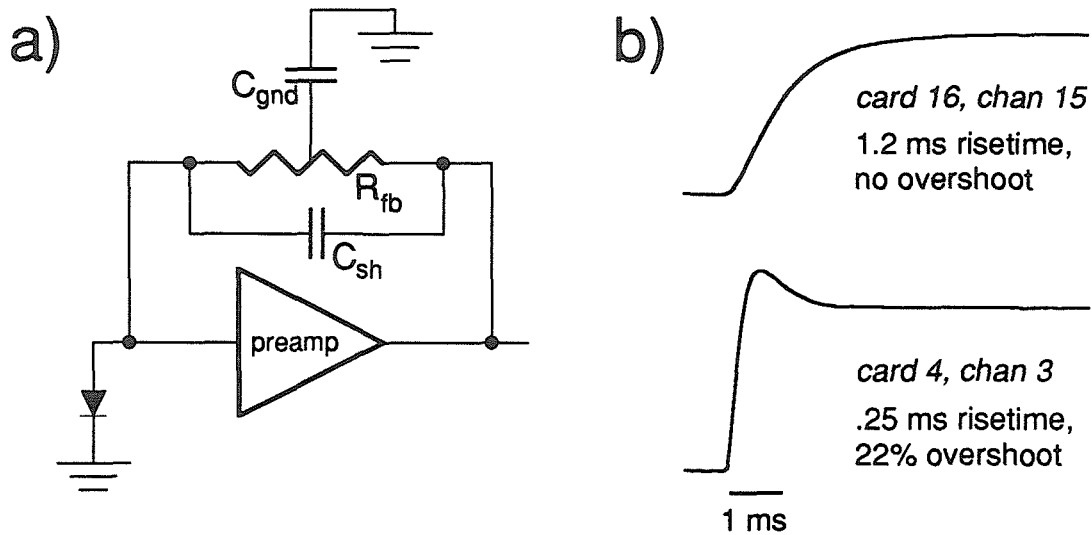
Figure 5.8 Stray capacitances that limit preamplifier bandwidth and cause gain peaking. *a*) Diagram showing shunt capacitance in parallel with the feedback resistor, and capacitance from within the resistor to ground. *b*) The responses of the slowest and fastest amplifiers to a step increase in light. Channel 16-15 has the slowest risetime of the amplifiers; channel 4-3 has the largest overshoot.

Fig 5.8*a* schematizes the capacitances that set frequency response: shunt capacitance in parallel with the feedback resistor (C_{sh}), and stray capacitance from the resistor to ground (C_{gnd}). The figure approximates these as lumped capacitances, but in truth they are complicated distributed capacitances that depend intimately on the way in which the circuit is laid out. C_{sh} and C_{gnd} are strongly affected by such factors as the length of the resistor's leads and the proximity of the neighboring amplifier card's ground plane. The effect of these stray capacitances can be explained as follows. Consider the current through the feedback network at a given voltage across R_{fb}: the ratio of voltage to current gives the effective feedback impedance, which is equal to the gain of the transimpedance amplifier. At high frequencies, C_{sh} increases the current, since it provides a low-impedance path in parallel with R_{fb}, and thus decreases the effective feedback impedance. Conversely, C_{gnd} decreases the current that flows through the feedback network by shorting some of it to ground, and thus increases the effective feedback

impedance. Thus, the two capacitances have opposing effects: C_{sh} reduces the gain of the amplifier at high frequencies, while C_{gnd} causes gain peaking.

After the amplifiers were constructed, their stray capacitances were hand-tailored to optimize their frequency response. Each preamplifier in turn was fed a square pulse of light. While watching the preamplifier's response to this signal, the leads of its feedback resistor were carefully bent, minimizing the overshoot of the response while keeping the risetime short. After this optimization, there was still a range of amplifier responses, of which Fig 5.8*b* shows the two extremes: the amplifier with the slowest risetime (amplifier 16-15), and the amplifier with the largest overshoot (4-3). Overall, the overshoot varied from 0% to 22% of the steady-state level, while the risetime (defined as the time to reach 63% of the steady-state level) varied from 0.25 ms to 1.2 ms. Crudely speaking, these correspond to bandwidths of 650 to 150 Hz. The 5 GΩ resistors are short-bodied and have a large C_{sh}, so they tended to have slow risetimes but no overshoot. The two other resistor types are longer-bodied, and have faster responses. The 6 GΩ resistors have fast risetimes and usually have overshoots, while the modified 10 GΩ resistors have intermediate risetimes and no significant overshoot.

For dye-recording experiments, slow amplifier responses and gain peaking are inconvenient, since signal amplitudes will vary slightly depending on the amplfier that records them. These variations will not, however, be as severe for real fluorescence signals with finite risetimes (at least 0.5 ms) as for the instantaneous steps used to test amplifier responses. These effects will be quantitative, not qualitative: the amplitudes of fast signals such as action potentials will be decreased by slow amplifiers or increased by overshooting amplifiers, but action potentials will not be created or destroyed. For experiments where accurate quantitative results are required, the amplifier responses must be corrected by digital filtering after data acquisition. Each amplifier's time response can be measured and stored, then used to deconvolve signals from that amplifier's pixel.

A greater inconvenience apparently caused by stray capacitances is that of crosstalk between channels. Slight capacitances from a premplifier's output to the inputs of its neighbors can inject small currents into the neighbors' inputs whenever the preamplifier's output changes, giving rise to crosstalk. Three sorts of coupling seem to be important; Fig 5.9a shows two. On each amplifier card, the sixteen preamplifiers are arranged in two rows of eight. The first sort of coupling is from an amplifier to its immediate neighbors in the same row. The second sort is from amplifiers in the first row to amplifiers in the second row. The third (not shown) is from amplifiers in the first row of one card to amplifiers in the second row of the next card. Fig 5.9b shows a typical example of crosstalk. The pixel for channel 6-8 (amplifier card 6, channel 8) was illuminated with a square pulse of light, and responses recorded from both 6-8 and 7-6. Channel 6-8 shows a
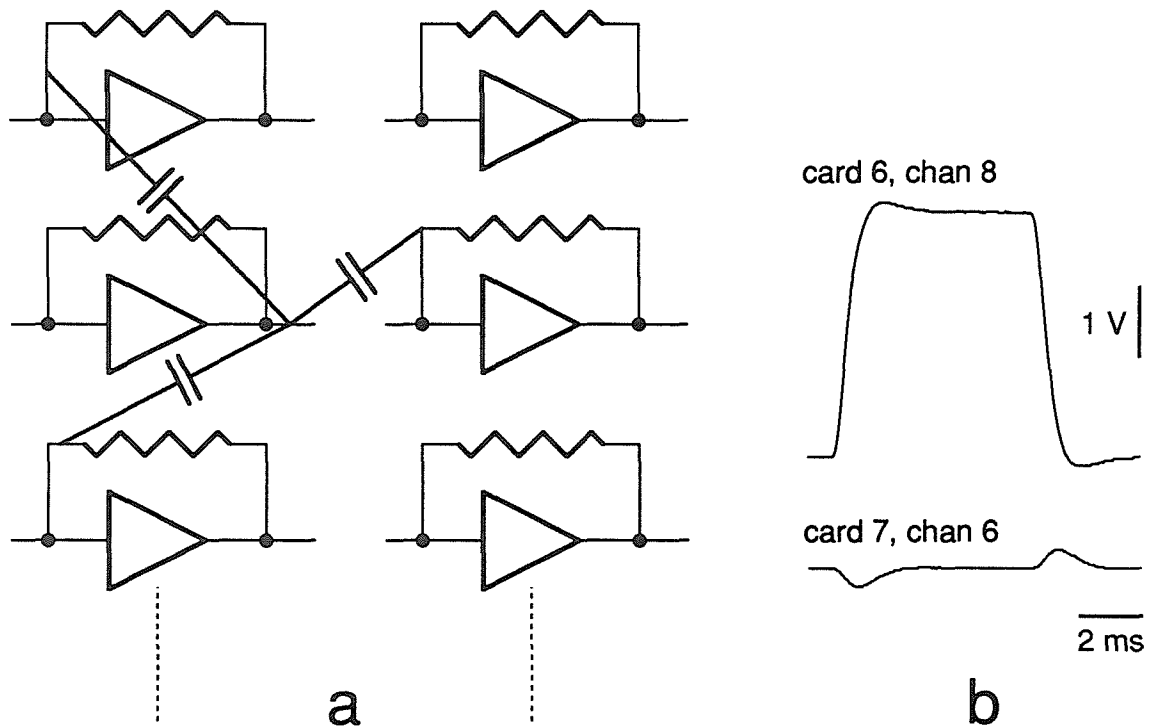
Figure 5.9 Crosstalk caused by stray capacitances. a) Schematic showing stray capacitances from the output of one amplifier to the inputs of its neighbors. There are two rows of eight amplifiers on each board; only six amplifiers are shown here. b) An example of crosstalk, presumably due to stray capacitances. Channel 6-8 was illuminated with a square pulse of light; the peak crosstalk in channel 7-6 was 7% of the plateau level in 6-8.

typical amplifier response with slight overshoots, while channel 7-6 shows a typical crosstalk signal: an inverted, differentiated version of the response from 6-8, with peaks that are 7% of the amplitude of 6-8's response. For the largest crosstalk signals, this figure is 15%. The time course and sign of these crosstalk signals, as well as their spatial distribution on the amplifier cards, point very strongly to a capacitive origin. The proof of this pudding is in the removing: the crosstalk could presumably be eliminated in a future generation of amplifiers with better layout and shielding.

As with gain peaking, crosstalk is inconvenient, not insurmountable. Since it is a capacitive effect, it is again somewhat alleviated by the slowness of real signals: dye signals do not rise as fast as the square pulse used for testing, and so will crosstalk less. The vast majority of amplifiers have no crosstalk, or crosstalk at the level of a few percent, which is not detectable above noise; only a few amplifiers on each board have crosstalk above 10%. For a typical action potential with a 1% signal, 10% crosstalk will give a spurious 0.1% signal in another pixel. There are three reasons that such crosstalk is unlikely to be mistaken for a true dye signal: rarity, polarity, and timing. First, crosstalk is rare: as noted above, only a few pairs of amplifiers on each card exhibit significant coupling. Second, crosstalk has the wrong polarity. In SCG cultures, EPSPs as well as action potentials are depolarizations, while crosstalk signals are inverted (they look like hyperpolarizations). Third, crosstalk is coincident in time with the signal that causes it. As long as the pixel causing the crosstalk is being monitored, this timing can be used to distinguish crosstalk. Signals large enough to cause significant crosstalk usually occur in pixels over cell bodies, and these are precisely the pixels that are monitored during a dye-recording experiment. Despite these ameliorating factors, if crosstalk happens to superimpose itself on a real signal, it can distort that signal's shape. Care must be taken when interpreting signals from these amplifiers, especially when quantitative results are desired.

Noise performance. Besides their transimpedance and time response, the third important characteristic of the amplifiers is their dark noise. Appendix D describes amplifier noise in detail; those results are summarized here.

A theoretical minimum for noise is set by the Johnson noise of the feedback resistor. A typical preamplifier has a feedback resistor of 6 GΩ and a power bandwidth of 400 Hz, for which the Johnson noise is 33 fA, expressed as an equivalent rms input current. Expressed the same way, the measured amplifier noise is 78 ± 13 fA (mean ± s.d. for 240 amplifiers[2]), with a range of 54-117 fA. Thus, the average measured noise amplitude is just about twice that expected from Johnson noise. The power spectra in Appendix D show that the quietest amplifier is actually right at the Johnson noise limit, though with some extra line-frequency harmonics.

The comparison with Johnson noise is merely a test of how well the amplifier noise is understood; for practical use, the comparison with shot noise is the important one. Again assuming a power bandwidth of 400 Hz, the mean amplifier noise of 78 fA is equal to the shot noise from a photocurrent of 48 pA. That is, the noise for any pixel whose fluorescence is much brighter than 48 pA will be shot-noise dominated. Even the noisiest amplifier has an input noise (117 fA) equivalent to the shot noise from a photocurrent of only 110 pA. Thus, one of the main design goals for the detector is fulfilled: it is shot-noise limited for typical photocurrents of 0.2 to 2 nA.

5.1.6 Future improvements

This detector is the first built in our laboratory, and is in most ways a first-generation device. Though usable, it has a few annoying flaws. The following

---

[2]This set of amplifiers excludes the card with auxiliary inputs (card 16), since the photodetector inputs on this card pick up large line-frequency components from the six auxiliary inputs.

improvements would yield a second-generation detector that would truly be a pleasure to use.

Fiber bundle. The plastic fibers used here were chosen because they are square, and so can be packed more closely than conventional round fibers. They are less than satisfactory for two reasons. Their dimensions are not very uniform, so that packing was difficult, and the final fiber bundle is not very regular. They are also quite lossy, with losses specified at 10%/foot. If better square fibers cannot be found, ordinary round fibers should be considered, since they have very good properties, and a close-packed array of circles only has 10% dead space.

When connecting the fibers to photodiodes, it might be better to devise a spring-loaded positive contact, rather than using epoxy, which was quite fragile. Not only would such a spring-loaded connection be mechanically robust, it would allow easy replacement of photodiodes in case of broken leads, etc.

Amplifier circuit. The present amplifier circuit seems generally satisfactory, though its layout leaves something to be desired (see below). The most difficult part of this circuit is the feedback resistor, whose stray capacitances are very hard to control. A lower value such as 1 GΩ might have some advantages: the maximum input current would be raised to 10 nA, and gain peaking might be eliminated. The 1 GΩ resistors available from Victoreen have short bodies and consequently high shunt capacitance; their frequency response would have to be tested. As for noise, the present circuit is very quiet, even though there is some excess noise above Johnson noise. If the excess noise stayed constant, changing R_{fb} to 1 GΩ might not increase the mean amplifier noise much at all.

A useful and cheap addition would be a buffer op-amp at the output of every preamplifier, before the multiplexer. The passive filters in the present circuit do not have a very low output impedance, making them susceptible to multiplexer transients (though these have been eliminated by the 1 kΩ series resistor) and other problems. A buffer amplifier would be a simple solution.

Multiplexers. The present multiplexers have power supplies of 0 and 15 V. They have the problem that any input that goes even slightly below 0 V starts to crosstalk to the other multiplexer inputs. Such negative inputs can arise either from a large amplifier offset, or from an undershoot from an amplifier with gain peaking. (These do not often occur during normal use, but were confusing during testing of the electronics.) This limitation requires that the auxiliary inputs be always positive, which is not always convenient to arrange. For the next-generation detector, it would be desirable to use multiplexers with power supplies of -5 V and +15 V.

Supply voltages. In the present arrangement, the -15 and +15 V analog supply voltages for the OP27 op-amps are regulated once for the whole card rack. A better arrangement would be to have the rack supply -18 and +18 V, and use a pair of voltage regulators on each card to generate -15 and +15 V. (The +5 and +12 V analog supplies are already regulated individually for each card.) Presently, all analog supply voltages have an extra stage of passive filtering at the point of use. The effects of these filters on noise performance should be tested: it is not clear that they are necessary, and they take up nearly 100 components per card.

PC board layout. The most egregious problem with the present detector electronics is that the PC boards are extremely overcrowded. The RC filters on the output of each amplifier were not included in the original board layout, and are piggybacked awkwardly on top. The next-generation detector should use much larger boards, with a single row of sixteen amplifiers instead of the two rows of eight presently used. Such a cleaner layout should by itself eliminate most of the crosstalk that presently exists; it should be possible to eliminate the rest with wider spacing between amplifiers and a judicious use of grounded lines for shielding. Wider spacing should also make all stray capacitances easier to control, and shield lines should eliminate offsets due to leakage over the surface of the PC boards.

5.1.7 Summary

This section has described the most technically demanding component of the apparatus, the optical detector. It uses a fiber-optic camera to break an image into an octagonal array of 256 square pixels. The size of the pixels and the detector array (45 μm and 810 μm at the specimen, respectively) are determined by the sizes of rat SCG neurons and of SCG microcultures. The light from each pixel is detected by a discrete photodiode/preamplifier combination. The preamplifiers are low-noise, low-current transimpedance amplifiers, comprising a JFET input stage, a conventional op-amp, and a feedback resistor of several gigohms. The choice of feedback resistor is crucial to the properties of the preamplifiers, as it determines their dynamic range and frequency response, and sets a lower limit for their noise. The frequency response is made complex by the presence of stray capacitances at the level of 0.1 pF; these capacitances also cause some crosstalk between neighboring amplifiers. The feedback resistors used here are about 6 GΩ, giving a maximum photocurrent of 2 nA, varying amplifier bandwidths from about 150 to 650 Hz, and an average amplifier noise equal to the shot noise in a photocurrent of 50 pA. These bandwidths fit reasonably well with the speed of the electrophysiology of SCG neurons, and this range of useful photocurrents fits well with the fluorescences observed from SCG neurons with standard staining and illumination. Some of the amplifiers have gain peaking, and some have crosstalk; these phenomena can change the amplitudes of signals, but cannot introduce spurious signals. The next-generation optical detector should have amplifiers with equally low noise, uniform frequency response, and no crosstalk.

5.2 DATA ACQUISITION AND ANALYSIS

5.2.1 Introduction

The data-acquisition requirements for dye recording are much greater than those for conventional electrophysiology, primarily because of the large number of input channels. It is not enough to simply acquire this data; some degree of real-time data analysis and display are required as well, since many choices during an experiment depend on knowledge of the signals detected. Displaying these signals quickly and intelligibly is usually more difficult than the acquisition of the data itself.

Fortunately, cells in culture are sparse, so the present system can be much simpler than a system for recording from cortex or a large ganglion. In a typical SCG microculture, cell bodies might fall on 15 pixels, requiring a sampling rate of about 50 kHz. Recordings from extended preparations usually use over 100 pixels, requiring sampling rates on the order of 500 kHz. The modest requirements of recording in culture can be cheaply satisfied with a personal-computer-based system, such as the one described in this section.

Dye recording experiments with SCG microcultures have two information-gathering phases followed by a data analysis phase. After the culture is stained with dye and washed, the first stage is to set its spatial alignment: a video picture of the culture is captured, and the pixels on which cells fall are noted. This video picture and alignment information are stored on disk. The second stage is the experiment itself: one or more cells are penetrated with glass electrodes and stimulated, while dye signals are recorded from all the cells. The data acquired during this stage is also stored on disk. Finally, in the third stage, data that has been stored on disk is reduced and analyzed. Subsection 5.2.2 first describes the hardware used for all three phases: a personal computer, a data acquisition system, and an image capture board. The next three subsections describe, in turn, the

software used in each of the three phases. During electrophysiological experiments, time is often at a premium, so it is important that the data acquisition programs be both powerful and easy to use.

I have not attempted to include the source code for this software in this thesis, for several reasons. The programs are long and polyglot: the source code adds up to 840 kilobytes, and is written in a mixture of C, BASIC, and assembly language. The acquisition software is also intimately designed for this particular hardware configuration. For those interested, the source code is available on floppy disk, either from me or from Jerry Pine. The descriptions below do not try to explain the software in too much detail, but rather try to give a flavor for its main capabilities and limitations.

5.2.2 Hardware

This data acquisition and analysis system is based on a 8 MHz IBM AT personal computer. The AT sends commands to a data acquisition subsystem, and receives digitized data in return; it also controls an image capture board that digitizes images from the video camera described in subsection 4.1.4.

Data acquisition system. The data acquisition subsystem is a TransEra 7000-MDAS (Modular Data Acquisition System, TransEra Corp., Provo, UT; currently manufactured by Acurex), which has its own 68000 microprocessor, and communicates with the AT via an IEEE-488 bus. This intelligent subsystem is a particularly elegant device, since it relieves the AT of direct responsibility for data acquisition. It requires only a simple ASCII command to acquire several thousand data points, and then returns these data, neatly packaged, to the AT. The AT uses a National PC-IIA IEEE-488 interface card (National Instruments) to communicate with the MDAS.

The MDAS has a 12-bit analog-to-digital converter (ADC). A custom software routine—Analog Input with External Multiplexer (AIM), written by TransEra—acquires data from the multifiber detector, while simultaneously selecting the desired pixels by

writing their multiplexer addresses to the detector's controller card. This software routine has a maximum data sampling rate of 90 kHz. The ADC has a programmable-gain amplifier, which can amplify the input signal by any power of 2 between 1 and 128. The AIM command sets programmed gains individually for all the pixels from which it records.

The 12-bit ADC really only provides 11 bits for the signal from the multifiber detector, since the signal is always positive, but the ADC takes bipolar inputs; this number of bits is just sufficient. Digitization noise, caused by rounding off to the nearest ADC count, has an rms amplitude of $1/\sqrt{12}$ times the size of the ADC count. Different pixels can have very different steady-state photocurrents, but the programmable-gain amplifier allows one to ensure that the steady-state photocurrent of each pixel yields between 1024 and 2047 ADC counts. The maximum rms digitization noise is thus $(1/\sqrt{12})/1024=.028\%$, which is equal to the fractional shot noise in a 2 nA photocurrent with a bandwidth of 500 Hz. Thus, in the range of fluorescences for which the multifiber detector is designed (.2 to 2 nA), shot noise will always be greater than digitization noise.

Image capture board. The AT contains a Chorus PC-Eye 4-bit image capture board and a Tecmar Graphics Master graphics adapter. This combination can acquire and display video images with up to 640 by 400 pixels and 16 gray levels, with an acquisition time of about one-third of a second.

IBM AT computer. The AT is equipped with 1.7 megabytes of random-access-memory, a 20-megabyte hard disk, and 360-kilobyte floppy drive, and a 60-megabyte tape drive. The hard disk is used to store data during experiments; floppy disks and tapes are used for permanent data storage. During experiments, an Epson FX-80 dot-matrix printer is used to print out certain data for inclusion in lab notebooks.

5.2.3 Image alignment software

The first phase of a dye-recording experiment is to align the culture relative to the optical detector's fiber bundle, and select the pixels from which to record. These tasks use

the program OPTIK, following a three-step procedure. First, the culture is crudely aligned

using the video monitor (see subsection 4.1.4). Second, it is aligned carefully. OPTIK

acquires a video image of the culture and overlays this with an image of the fiber bundle.

The specimen stage is then moved so that the cells fall just so, within a single pixel if

possible. Third, pixels are selected for recording. OPTIK measures the fluorescence from

each pixel, using the MDAS; this information is useful for avoiding pixels with bright

debris. Pixels can be selected very easily using cursor keys and then outlined in the video

image.
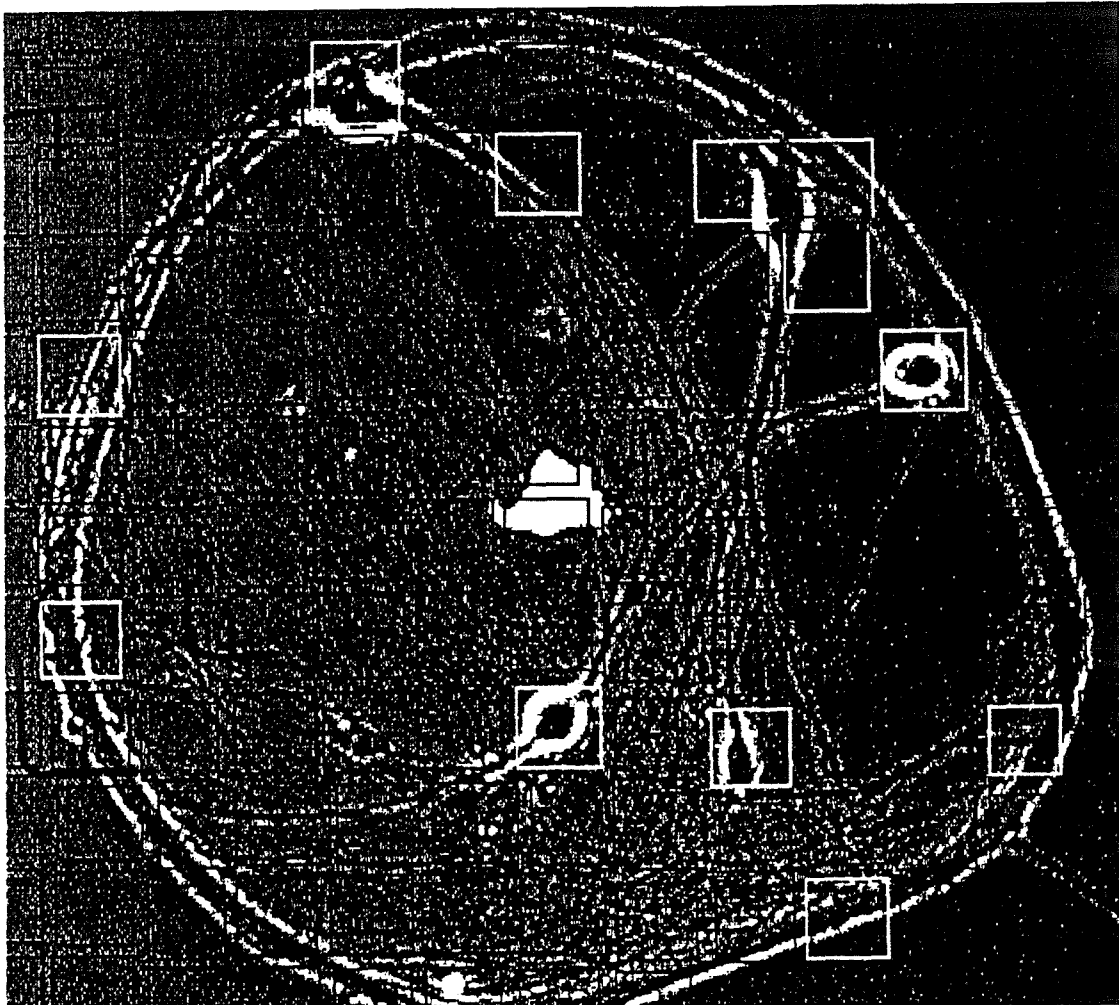
Figure 5.10 Sample video image acquired by OPTIK, showing the cell bodies and processes of a five-neuron microculture. The *squares* indicate the positions of optical fibers: *highlighted squares* are the pixels selected for recording, and *dark squares* are unselected pixels.

After pixels are selected, OPTIK stores several types of data about the culture. It writes the list of selected pixels to a disk file GROUPS.LST, for MULTI to use later; it stores a video image of the culture, with the fiber array overlaid and selected pixels highlighted, for later reference; finally, it prints out the list of selected pixels, along with the fluorescences of all pixels in the array, for inclusion in a notebook. Stored video images are later recalled and printed out on a Hewlett-Packard LaserJet II laser printer; Fig 5.10 shows an example. Despite the poor quality of this xeroxed image, the cell bodies and processes can be seen, as can the fiber bundle (dark squares) and the selected fibers (bright squares).

A technical aside about field of view: as described in subsection 4.1.4, the video camera's imaging element is only 12 mm square. With a 20x objective and 0.9x demagnification before the video camera, this gives a field of view 670 µm square, compared to the field of view of the multifiber detector, which is 810 µm across. The image capture board further reduces this field of view: OPTIK can only display part of the video image at any time, and this window is 530 µm wide by 450 µm high. This window may be panned, but it is highly inconvenient to have a culture that is larger than this size.

Table 5.1 lists several auxiliary programs. The fiber bundle is not quite regular, so OPTIK displays it as a collection of squares, whose positions and sizes are stored in a file FIBER.CFG. This file can be edited—indeed was originally generated—using the program EDFIB, which captures a video image of the fiber bundle, produced by backlighting the fiber array, and then allows a human to tweak the squares to match the video image. The other five programs listed are solely for printing out hardcopies of video images. DR. HALO III (Media Cybernetics) does the actual printing; the other four programs are involved in a complex dance of file formats, converting back and forth between .PIC and .CUT files (which deserve to be described only in a thesis even longer than this one).

Program	Version	Language	Purpose
OPTIK	3.0	QB3	Aligns culture, selects pixels.
EDFIB	1.0	QB3	Edits fiber array description file.
SHOWPIC		QB4	Displays .PIC video files.
SHOWCUT		QB4	Displays .CUT video files.
CUT2PIC		QB4	Converts .CUT files to .PIC files.
PIC2CUT		QB4	Converts .PIC files to .CUT files.
Dr. HALO	III	comm.	Prints video images on HP LaserJet.

Table 5.1 Programs for acquiring, storing, and manipulating video alignment images. Current version numbers are shown where applicable. Dr. HALO is a commercial program; the other programs are written in Microsoft QuickBASIC 4.0 (*QB4*) and QuickBASIC 3.0, coprocessor version (*QB3*).

These programs were written in two different versions of Microsoft QuickBASIC, as indicated in Table 5.1; some of them use assembly-language subroutines, as well. Both OPTIK and the auxiliary programs use the HALO library of graphics functions (HALO v2.26, Media Cybernetics). OPTIK also uses software libraries to run the image capture board (PC-Eye v2.24, Chorus Systems) and the IEEE-488 interface card (GPIB-PC vC.7, National Instruments).

5.2.4 Data acquisition software

Once the multifiber detector has been aligned and pixels have been selected for recording, there comes the second phase of an experiment, which is really the critical one: recording optical signals while a cell or cells are stimulated. The program MULTI records fluorescence signals from the detector, as well as recording electrophysiological signals using the detector's auxiliary inputs.

MULTI can record from up to sixteen channels, with a total sampling rate of up to 90 kHz; the sampling rate is usually set at 3 kHz per channel. Sixteen channels is not a fundamental limit, but rather the most that fit conveniently onto the computer screen; the maximum sampling rate is set by the speed of the MDAS AIM command. Data can be

stored to disk automatically, or under manual control. MULTI can display the signals from up to sixteen channels at once, and can perform two types of elementary on-line analysis.

The first type of processing makes small signals visible. Raw fluorescence data consists of a large intensity step, due to the opening of the shutter and the start of illumination, with a small signal—of the order of 1%—superimposed. If the raw trace were simply displayed on the screen, the signal would be totally invisible. Therefore, for channels designated as optical signals, MULTI subtracts off the resting fluorescence, and multiplies the difference by 100.

The second type of processing is signal averaging. Putative action potentials or post-synaptic signals need to be confirmed by repetition, and some are too small to see above background noise without averaging. MULTI can average up to 32 trials (limited by available memory), displaying the data for individual trials as they come in, or else showing the final average only. The averaged data can of course be saved to disk, but individual trials may be as well. In cases where one of the trials has been marred by a fluctuation in illumination, the trials are all saved, then the good trials averaged off-line.

The user interface is organized into three screens. The first, the display screen, displays the data as it is acquired, and uses a command-line interface. The second screen is for changing global parameters such as the number of channels acquired, sampling rate, or trial length; the third is for changing channel parameters, such as the multiplexer address, programmed gain, or display range. The second and third screens use a simple point-and-change interface: the parameter to be changed is chosen with cursor keys, then the new value is typed in.

The display screen is used for most of an experiment. Table 5.2 lists the most important commands of the display screen. An experiment is typically a cycle of acquiring data, saving it to disk if useful, adjusting acquisition or display parameters, adjusting the electrophysiology electronics, then acquiring new data. Commonly-used commands are assigned to function keys for easy access.

The other two screens are only used when parameters need to be adjusted. When MULTI is started, it automatically sets the number of channels and the pixels they represent, using the file GROUPS.LST generated by OPTIK. This makes it very easy to select interesting pixels: they're picked out from a video image with cursor keys in OPTIK, then automatically used by MULTI. The display range for each channel is usually set automatically, as is its programmed gain. All of these parameters can be set manually when necessary, using the global parameters and channel parameters screens.

MULTI stores its data in SCOPE files (so named after an earlier data-acquisition program). These files comprise three types of records: a file header, trace headers for each trace, and the traces themselves (the data from each channel). The file header contains

Command	Function
edit global	Go to global parameters screen.
edit channel	Go to channel parameters screen.
help	Show on-line help.
shell	Spawn a DOS shell.
quit	Exit MULTI.
acquire	Acquire a single trial.
average	Average the specified number of trials.
display	Display the specified channels.
autoscale	Set display scales for specified channels.
autorange	Set programmed gains for specified channels.
plot	Set time interval to be displayed.
store	Save data to disk.
print	Dump screen image to dot-matrix printer.

Table 5.2 Important commands for MULTI's display screen.

global information, including the number of traces, sampling rate, trace length, date and time of acquisition, and a brief note describing the data. The trace headers contain trace-specific information, such as equivalent ADC count size and a trace name; the traces are stored as a list of integers, representing values at successive time points. These SCOPE files are used by all of the display and analysis software, described in the next subsection.

The latest edition of MULTI is version 3.60. In addition to the standard program, which uses the MDAS for data acquisition, there is a version whose acquisition routines have been replaced by simulation routines that generate realistic (but not *too* realistic) data. This simulated-data version is very useful for debugging MULTI without having to perform a dye-recording experiment. MULTI is written in Microsoft QuickBASIC version 3.0, coprocessor version, and has several assembly-language subroutines. It uses the same HALO graphics library, image-capture routines, and IEEE-488 routines that OPTIK does.

5.2.5 Data analysis software

Off-line data analysis is performed using DISPLAY and a battery of analysis programs. These are listed in Table 5.3, along with brief descriptions of their functions. A few of the more-complex and more-used deserve comment:

DISPLAY is a graphical display program for SCOPE data files that performs some simple analysis functions. In addition to displaying traces at any desired timescale or amplitude scale, it can add, subtract, and average traces; change trace names; measure means and standard deviations; and bleach-subtract traces. Routine hardcopies for lab notebooks are made using DISPLAY, by capturing screen images and dumping them to a dot-matrix printer.

Program	Version	Function
written in Lattice C		
DISPLAY	2.1	Displays data files, and does simple analysis.
FFT		Performs fast Fourier transforms.
SCRUNCH		Converts FFT files into power spectra.
written in QuickBASIC		
ADD	2.1	Adds traces within a data file.
ASC	2.4	Translates data files to ASCII format for export.
BLSUB	1.1	Bleach-subtracts optical traces.
COLLECT	2.1	Gathers traces from several files into one.
DERIV	1.0	Differentiates traces discretely.
FAVG	1.0	Averages several files together.
FILTER	4.0	Time-filters traces, using standard or custom filters.
INTERP	1.1	Interpolates to change file's sampling rate.
LENGTH	1.0	Truncates or extends files.
LINTRANS	2.1	Performs linear transforms on traces.
LOOK	2.4	Shows file header and trace header information.
MKDAT	1.0	Makes step functions (for test files).
SCALELSQ	1.2	Finds least-squares-fit scaling factor for two traces.
TF	1.0	Measures total fluorescence (resting fluorescence) for traces.
UNITS	2.3	Changes trace units (linear scaling).

Table 5.3 Data display and analysis programs for SCOPE files. Languages (Lattice C v3.15 and Microsoft QuickBASIC 4.0) and latest version numbers are indicated.

For bleach-subtraction, one of its most important functions, DISPLAY generates a bleach-fit trace, then subtracts it off from the raw trace, yielding a bleach-subtracted trace. Generating the bleach-fit trace requires a reference trace that exhibits bleaching only, with no voltage-sensitive signals. The reference can be either (a) a trace recorded in the absence of stimulation, or (b) those parts of a trace—recorded with stimulation—that seem to exhibit no voltage-dependent signals. Method (b) allows a trace to be its own reference, but is more susceptible to artifacts than method (a), which uses an independently-recorded reference. A smooth bleach-fit trace is generated from the reference by fitting a quadratic function to the reference using the method of least squares.

BLSUB bleach-subtracts many files at a time, using method (a). That is, it bleach-subtracts the fluorescence traces in a file by using a reference file recorded without electrical stimulation.

FILTER performs two sorts of filtering: simple low-pass filtering in order to remove high-frequency noise, and custom filtering to adjust the effective frequency response of a signal. Both sorts of filtering are done using time-domain convolution. (Filtering in the frequency domain is faster in principle, but too complicated in practice.) For standard low-pass filtering, the signal is filtered with a "symmetrized RC filter," by convolving it with the following time response $R(t)$:

$$\begin{cases} R(t) = \frac{1}{2}\exp(t / \tau) & [t \le 0] \\ R(t) = \frac{1}{2}\exp(-t / \tau) & [t \ge 0] \end{cases}$$

This is equivalent to filtering first with an RC filter of time constant τ, then with a time-reversed version of the same filter. This filter has the advantages that it is simple, and has zero phase shift at all frequencies, $i.e.$, it does not introduce any time delays. For custom filtering, the signal is convolved with a filter time response from a stored data file. Custom filtering is typically used when making detailed comparisons of time course for an optical signal and an electrophysiological signal (see Chapter 6).

FAVG averages several files together. It is useful when MULTI records a sequence of trials for averaging, but one is spoiled by an illumination fluctuation, so that MULTI calculates a faulty average. After saving the trials as disk files, FAVG can calculate a clean average that excludes the spoiled trial.

ASC converts SCOPE files to ASCII files—lists of scientific-notation numbers. It is used to export data files to commercial plotting or analysis programs.

In a typical experiment, data is taken by MULTI, partially reduced using FILTER, BLSUB, and possibly FAVG, then displayed and analyzed with DISPLAY. Quick-and-dirty hardcopies are made with DISPLAY; publication-quality graphs are made by exporting data to SigmaPlot (Jandel Scientific) on the IBM PC, or Igor (WaveMetrics) on the Macintosh.

DISPLAY is written in Lattice C v3.15. A few early analysis programs were written in C as well, but most were converted to BASIC, and later programs were all written in BASIC. The programs listed as "written in QuickBASIC" in the table are all written in Microsoft QuickBASIC v4.0, and constitute Revision 2.60 of the SCOPE UTILITIES. Fast-Fourier transforms do not translate easily into any BASIC, and so FFT and SCRUNCH remain written in C. A few of the programs in the SCOPE UTILITIES use assembly-language subroutines. DISPLAY uses the same HALO graphics library as OPTIK and MULTI.

5.2.6 Summary and improvements

The data acquisition hardware described here fulfills its design requirements: it can record from up to thirty pixels at a time with a sampling rate of 3 kHz per pixel. The current software can only record from sixteen pixels, though. The 12-bit ADC has sufficient resolution that digitization noise should be less than shot noise. The programs for image alignment and data acquisition work well and are quite easy to use (see Chapters 6 and 7 for results).

No software is above a few improvements, however. MULTI could use two: better on-line analysis software, and more channels for data acquisition. On-line bleach subtraction would be quite useful, as would a routine that automatically summed the signals from the group of pixels that covers a particular cell. At present, only sixteen pixels can be recorded from at once; this number could easily be increased to thirty or so, especially if a pixel-group-summation routine reduced the number of signals that had to be displayed on the same screen.

The data analysis software consists of a display program (DISPLAY) with limited analysis functions, and a hodgepodge of individual analysis programs. If these individual programs were integrated into DISPLAY, especially with some sort of macro facility, data analysis would be simpler and more powerful. Finally, a few technical suggestions: DISPLAY should be upgraded to a newer C compiler, MULTI should be upgraded to use

QuickBASIC 4.0, and the present version of the HALO library should be replaced with a newer one.

CHAPTER 5 REFERENCES

F. J. Sigworth (1983) Electronic design of the patch clamp. In *Single-Channel Recording*, eds. B. Sakmann and E. Neher. Plenum, New York. pp.3-35.

Chapter 6
Technical Dye-Recording Experiments

6.1 INTRODUCTION

A host of factors can influence the effectiveness of dye recording: the particular dye used, dye concentration, staining time, excitation wavelength, and emission wavelength, certainly; also perhaps the composition of the medium, temperature, or the phase of the moon. When starting to use dye recording, one soon discovers that the technique is a morass of variation: dye staining and voltage sensitivity vary widely between cultures and between cells, often for no apparent reason. The experiments in this chapter explore the effects of some of these factors, in an attempt to reduce this variability.

The most important properties of a voltage-sensitive dye are staining and voltage-sensitivity; without these, there is no signal to be recorded. Section 6.3 describes the initial dye screening, which selected the best of about 25 styryl dyes on the basis of good staining and high voltage sensitivity for SCG neurons. In this screening, the dyes RH237, RH421, and RH423 gave the best staining and largest signals. Even before the screening, RH237 and RH421 were known to be good candidates, since they had given huge $\Delta F/F$ values of 14%/100 mV (RH237; Grinvald *et al.*, 1982) and 21%/100 mV (RH421; Grinvald *et al.*, 1983) on mouse neuroblastoma cells in culture. The dye di-4-ANEPPS was developed by Leslie Loew's group after we had completed our initial screening, and gave $\Delta F/F$ of about 10%/100 mV on several different cell types (Gross *et al.*, 1986). The four dyes RH237, RH421, RH423, and di-4-ANEPPS were selected for further study.

During the screening on SCG neurons, the signals from the three RH dyes were typically about 1%/100 mV, and occasionally as large as a few percent per 100 mV. Di-4-

ANEPPS was later found to give similar signals. These signals were disappointingly small compared to the signals reported from other cell types; this is an example of the variability between preparations for which voltage-sensitive dyes are notorious. Signals are quite variable within a single preparation, as well. I have used RH421 and RH423 most extensively; at some times, these dyes routinely gave 1%/100 mV signals on SCG neurons, but at other times, they routinely gave less than 0.25%/100 mV.

The next two sections explore some of the factors that affect staining and sensitivity, and might contribute to this variability. The experiments described in section 6.4 tested how staining is affected by serum contained in the bathing medium. Those in section 6.5 measured dye sensitivities with different excitation and emission filters. The primary purpose of these experiments was to find the optimal filter set for each dye, and insure that the mediocre signals observed were simply due to a poor choice of filters. A secondary purpose was to test the electrochromic mechanism (see Appendix A) that has been proposed for styryl dyes.

The experiments in section 6.6 checked the linearity of RH423's response with respect to membrane voltage, using isolated neurons with no processes. Fast dyes tested in other systems have been shown to be linear over wide ranges of voltage (see chapter 2), but it is reassuring to confirm this result with the particular dyes and cells used here. These experiments with isolated neurons also served to test the idea that variations in $\Delta F/F$ might be due to varying background staining. Since these neurons do not have background fluorescence from the mat of processes usually present in a mature culture, they might be expected to give larger signals.

Besides staining and sensitivity, bleaching and phototoxicity are also important for dye recording. Section 6.7 presents a few measurements of both. These phenomena have not been much studied, though there is a report (Bonhoeffer and Staiger, 1988) that phototoxicity can be reduced by spreading illumination out over time.

Section 6.2 lists technical details of materials and methods; section 6.8 summarizes and discusses the results of 6.3 through 6.7. Lunar effects have not yet been studied.

6.2 MATERIALS AND METHODS

6.2.1 Dyes and dye staining

Amiram Grinvald and Leslie Loew kindly provided the dyes used here. All of the RH dyes came from A.G., while di-4-ASPPS, di-6-ASPPS, di-4-ASPBS, and di-4-ANEPPS came from L.L. Some additional supplies of RH160 and RH421 were purchased from Molecular Probes; many of the dyes used here are available from this company. Dyes were supplied as dry powder; stock solutions were made up in ethanol, usually at 1 mM, and stored in tightly-capped vials. Stocks were kept at 4°C for long-term storage, but during experiments were often left out at room temperature for several weeks. The stability and concentrations of the ethanol stocks were monitored by diluting a small amount to 1 µM in ethanol, and measuring the absorbance spectrum of this dilution in a spectrophotometer. By this criterion, the ethanol stocks seem quite stable: the absorption spectra did not change in shape, though their amplitude changed slightly due to evaporation.

Working dilutions were made fresh for each culture by diluting the stock solution into electrophysiological saline. The usual staining protocol was to wash the culture three times with saline, change into the working dye dilution for 5-10 minutes, then wash three times more with saline. The concentration of ethanol in the working dilution, between 0.1%-0.5% (v/v), is known to affect the electrophysiology of neurons, but it is presumably diluted to harmlessness by the three final washes.

In early experiments, cultures were presoaked in serum-free medium for at least one day prior to use, since this seemed to improve staining. (Serum-free medium is simply

normal culture medium with the horse serum omitted.) Later, this presoak was found to be unnecessary (see section 6.4).

6.2.2 Cell culture

Neurons from the rat superior cervical ganglion (SCG) were cultured using standard techniques. Neonatal rat pups (0-3 days old) were killed by decapitation, and their SCGs removed to a petri dish containing Hanks' balanced salt solution with penicillin/streptomycin and no divalent cations. The ganglia were cleaned of extraneous tissue, then incubated for 20-30 min at 37°C with 0.125% trypsin. The trypsin was neutralized by placing the ganglia in medium with 30% serum for ten minutes; the ganglia were then removed to culture medium, shredded, triturated 20-40 times, and the resulting cell suspension diluted to plating density. The suspension of diissociated cells was sometimes filtered through 44 µm nylon mesh in order to remove clumped cells. The yield from each ganglion was typically 20,000 neurons; mass cultures were usually plated at 3000 cells/dish. Cells were plated into a petri dish with a central 6 mm well (see below) either in a single 100 µl drop in the central well, or in a glass cloning ring in a dish flooded with medium.

Each culture dish contained 2-3 ml of complete L-15/CO_2 culture medium (see below). Cultures were maintained at 37°C in a 5% CO_2 atmosphere, and fed every two or three days by replacing 1 ml of the volume with fresh medium. At times, culture dishes were kept inside a closed 150 mm culture dish together with an open petri dish full of water to maintain humidity, and fed once a week. Nonneuronal cells were removed from cultures by treatment with the antimitotic agent 5-fluoro-2-deoxyuridine (FUdR; Sigma). One or two days after plating, FUdR was added at a concentration of 20 µM, along with 20 µM uridine (Sigma); it was not removed, but diluted out by subsequent feedings. This treatment was usually sufficient to completely remove all nonneuronal cells.

Media. The culture medium used for SCG neurons was that of Mains and Patterson (1973), except for the omission of methocel and BSA, and the replacement of rat serum with horse serum. Basal L-15/CO_2 was made by adding 5 ml/l of stable vitamin mix and 29 ml/l of 7.5% sodium bicarbonate (Gibco) to liquid L15 medium (Whittaker MA Bioproducts), and stored for months at 4°C. Complete L-15/CO_2 culture medium was made by supplementing each 100 ml of basal L-15/CO_2 with 10 ml horse serum (Whittaker MA Bioproducts), 1 ml of 200 mM L-glutamine (Gibco), 1 ml of penicillin/streptomycin (10,000 units/ml penicillin, 10 mg/ml streptomycin; Sigma), 2 ml of a 30% (w/v) glucose solution, 1 ml fresh vitamin mix, and 7S nerve growth factor (0.5 μg/ml final concentration). Complete L-15/CO_2 was stored at 4°C, and usually used within one week. Stable vitamin mix was made by adding 0.3 g L-aspartic acid, 0.3 g L-glutamic acid, 0.3 g L-proline, 0.3 g L-cystine, 0.4 mg d-biotin, 0.1 g *p*-aminobenzoic acid, 8 mg coenzyme A, 0.1 g β-alanine, 40 mg vitamin B-12, 0.2 g myo-inositol, 0.2 g choline chloride, 10 mg DL-6,8-thioctic acid, and 0.5 g fumaric acid (coenzyme A from P-L Biochemical; all others from Sigma) to 100 ml H_2O. Fresh vitamin mix was made by adding 1 mg 6,7-dimethyl-5,6,7,8-tetrahydropterine, 5 mg glutathione, and 100 mg ascorbic acid (all from Sigma) to 20 ml H_2O, then adjusting to *p*H 5-6 with KOH. Stable vitamin mix, fresh vitamin mix, horse serum, glucose, glutamine, penicillin/streptomycin, and NGF were all aliquotted and stored frozen at -20°C.

SCG cultures were sometimes grown on extracellular matrix (ECM) made from bovine endothelial corneal (BEC) cells. BEC cells were grown in Dulbecco's modification of Eagle's medium (DMEM; Flow Laboratories), supplemented with 10% fetal bovine serum (HyClone), 5% calf serum (Whittaker MA Bioproducts), 2 ng/ml fibroblast growth factor (FGF; Collaborative Research), and the same glucose, glutamine, and penicillin/streptomycin that were used for complete L15/CO_2.

Culture dishes. Culture dishes with a central 6 mm well were made from 35 mm tissue-culture plastic petri dishes (Falcon or Corning) by drilling a 6 mm hole through the

bottom of the dish, then glueing a glass coverslip across this hole with Sylgard (Dow Corning).

Some experiments used gridded dishes, made by glueing an extra coverslip to the bottom of a normal culture dish; the extra coverslip was covered with a pattern of numbered 100 μm squares, made by depositing gold/chrome on the coverslip with integrated-circuit fabrication techniques. This grid pattern provided a coordinate system that allowed identification and repeated location of individual cells.

Substrates. Three substrates proved successful for long-term mass culture of SCG neurons: dried collagen, extracellular matrix (ECM) made from bovine endothelial corneal (BEC) cells, and polylysine-laminin. Early experiments used dishes coated with double-layer dried collagen (Johnson and Argiro, 1983). These dishes were prepared by spreading a small drop of rat-tail collagen solution over the central well, gelling this collagen by exposure to ammonia fumes, drying, then applying and spreading a second drop of collagen, which was dried without gelling. Collagen was found unsuitable for making microcultures, and so was given up in favor of ECM.

Later experiments used ECM from BEC cells (Gospodarowicz *et al.*, 1981; MacCallum *et al.*, 1982). BEC cells (a kind gift of Dr. W. Bleisch) were plated at 50,000 cells/6 mm well, grown to confluency, then after two or three days at confluency were lysed by exposure to 20 mM NH_4OH for about 15 min. The ECM that remained after lysis of the BECs was kept wet and stored at 4°C. BEC cells were found to adhere and spread best on a substrate of polyimide (Selectilux 50; EM Industries); this serendipitous discovery came from using polyimide as an insulation for multielectrode dishes (Regehr *et al.*, 1989). BEC cells were grown up in modified DMEM (see above); when plated to make ECM, 3-5% dextran (39 kd) was added to the medium to help the cells form smooth layers. ECM often contained a great deal of membranous debris, and so gave high background during dye recording experiments; it was given up in favor of polylysine-laminin.

Most of the experiments described in this chapter and the next used dishes coated with polylysine and laminin. Dishes were flooded with an 0.5-1 mg/ml solution of poly-DL-lysine (roughly 20 kd; Sigma) in Dulbecco's phosphate buffered saline (DPBS; Flow Laboratories), and left overnight at 4°C. The next day, the dishes were rinsed twice with distilled water, the water was aspirated off, then the dishes were air-dried. The central wells of the dishes were then coated with laminin by filling them with 10-20 µg/ml laminin (Sigma) in DPBS, and letting this solution sit for at least 45 min. The dish was rinsed at least twice with DPBS before plating. It was important to keep the laminin wet; it became a poor substrate if it dried out.

Collagen substrates gave good long-term survival, though the network of neurons in a dish would sometimes roll up and detach after a few weeks in culture. ECM from BECs gave the healthiest cultures: initial neurite outgrowth was very fast, neurons were round and phase-bright, and often had several short, fat processes (presumptive dendrites); the cultures routinely survived for five or six weeks, and sometimes for as long as three months. Polylysine-laminin gave good initial outgrowth and healthy cells, but the neurons usually started acquiring phase-bright inclusions after two or three weeks in culture, and often looked sick at five or six weeks.

6.2.3 Electrophysiology

Electrophysiological stimulation and recording used amplifiers modified from a commercial design (Getting Microelectrode Amplifier) and home-built stimulators that generated square pulses with variable amplitudes, lengths, delays, and repetition rates. The stimulators could be "60 Hz-synchronized" so that they always fired in phase with the line frequency; this made recordings less sensitive to line frequency pickup. Electrode holders were mounted on Leitz micromanipulators. Intracellular electrodes were pulled on a Brown-Flaming P-77 horizontal puller (Sutter Instruments) from omega-dot glass (0.58 mm i.d., 1.0 mm o.d., WPI), filled with 3M KAc, and typically had resistances

of 80-100 MΩ. Whole-cell patch pipettes were pulled from KG-33 borosilicate glass

(0.8 mm i.d., 1.6 mm o.d., Garner Glass Co.) on a homemade vertical puller, whose

use was kindly provided by Henry Lester. A typical whole-cell pipette had a bubble

number of 4 (corresponding to a diameter of about 0.6 μm), and a resistance of 15 MΩ

when filled with intracellular solution. The intracellular solution (modified from Marty and

Neher, 1983) was 140 mM KCl, 2 mM $MgCl_2$, 11 mM EGTA-KOH, 1 mM $CaCl_2$,

and 10 mM HEPES, pH adjusted to 7.2 with KOH and osmolarity adjusted to

340 mOsM with sucrose.

Early experiments used a modification of Freschi's high-calcium recording solution

(Freschi, 1983): 140 mM NaCl, 5 mM KCl, 6.25 mM $CaCl_2$, 0.5 mM $MgCl_2$,

11 mM glucose, 10 mM HEPES buffer, adjusted to pH 7.3 with NaOH and to

340 mOsM with sucrose. Later experiments used high-Ca^{++} L15/Air as a recording

solution; this is very similar to the medium used for culturing SCG neurons, and the switch

was made in the hope that the cells would better tolerate long electrophysiological

experiments. High-Ca^{++} L15/Air was made by adding stable vitamin mix, fresh vitamin

mix, glucose, glutamine, and penicillin/streptomycin (all in the same proportions as for

complete L15/CO_2; see above) to L15, adding 5 mM $CaCl_2$ for a final Ca^{++} concentration

of 6.3 mM, and setting the pH to 7.3. Both the modified Freschi's solution and L15/Air

had elevated calcium in order to facilitate stable penetrations. Healthy SCG neurons

typically had resting potentials of 55-60 mV when penetrated. No difference in dye

properties was noticed between modified Freschi's and L15/Air.

A stainless-steel ring inserted in the culture dish provided a bath ground, used both

as a reference for recordings and as a return path for injected currents. The culture dish

was mounted inside another stainless-steel ring, which provided resistive heating, and

incorporated an AD590 integrated temperature sensor (Analog Devices) for monitoring

temperature. The temperature in the center of the culture dish was calibrated against the

EMISSION FILTERS			EXCITATION FILTER SET			
filter	passband (nm)	peak trans	set	filters	passband (nm)	peak trans
RG610	>612	95%	A	BP490	416-486	96%
RG630	>628	95%	B	BP490+Y455	452-486	81%
RG645	>653	95%	C	BP545+BP485/20	474-494	48%
RG665	>668	95%	D	BP545 only	474-550	98%
RG695	>696	95%	E	BP545+LP515	520-550	83%
RG715	>713	95%	F	BP545+G546	540-550	36%
RG780	>789	95%				

Table 6.1 Emission filters and excitation filter sets used for testing dependence of dye sensitivity on wavelengths, with passbands and peak transmissions. The endpoints given for the passbands are wavelengths of half-maximal transmission.

temperature at the heating ring. Some experiments were carried out at room temperature (22-25°C in our laboratory), while others were carried out at 30-33°C.

6.2.4 Optical recording

The dye screening used an early version of the optical recording apparatus, comprising a Zeiss Invertoscope D inverted microscope, with a Zeiss 63x Neofluar oil objective (NA 1.25) and a single-pixel detector. All other experiments used the apparatus described in Chapters 3 through 5. The light source was a mercury arc lamp throughout.

Various filters were used to test the wavelength dependence of dye sensitivity. Excitation filter experiments used the dichroic mirror and emission filter of the standard Olympus IMT-2 G cube, with either the G cube's BP545 excitation filter or a BP490 excitation filter transplanted from a B cube. These excitation filters were sometimes supplemented with one of the following: Y455, LP515 (both from Olympus), G546 (Ealing), and BP485/20 (source unknown). Emission filter experiments used long-pass filters obtained from Melles Griot: RG610, RG630, RG645, RG665, RG695, RG715, and RG780; small circles were cut from the original 2-inch squares and mounted in plastic emission filter holders (Olympus), which could be inserted underneath the filter cube.

Table 6.1 summarizes the properties of the emission filters (RG610 through RG780) and the excitation filter sets (A through F).

6.3 EARLY DYE SCREENING

The initial screening of dyes on the rat SCG culture preparation was done in our laboratory by Dr. Helen Rayburn. Only a passing mention of this screening has been published (Rayburn *et al.*, 1984), and so its results are summarized briefly here.

There are (at least) seven criteria for a good fluorescent voltage-sensitive dye. The first four are staining criteria. (1) The most important is that stained cells should show nice bright rings of fluorescence, indicating a dye that binds to the membrane (where it provides signal), but does not enter the cell (where it only adds background). (2) The dye should not enter the cell on a timescale of hours (the length of a typical experiment). (3) The dye should not stain debris, since stained debris adds background. (4) The dye also should not stain nonneuronal cells; stained nonneuronal cells also add background. It is surprising that some dyes can differentiate between cell membranes and membranous debris, or between neuronal and nonneuronal membranes; this presumably reflects differences in lipid or protein composition among the different membranes.

There are three other important criteria besides staining properties. (5) Most, importantly, the dye must give large voltage-sensitive signals. (6) The dye should bleach slowly. (7) The dye should have low phototoxicity.

For this initial screening, dyes were selected primarily on the basis of bright rings and large voltage-sensitive signals (criteria 1 and 5), and secondarily on the basis of other staining properties (criteria 2, 3, and 4). Bleaching and phototoxicity (criteria 6 and 7) were not taken into account. (Phototoxicity is especially difficult to assay.) The screening was performed in two phases: dyes were first checked for good staining, and then the dyes that stained well (and a few of those that didn't) were tested for voltage sensitivity.

a)

$$Y\text{---}(CH_2)_n\text{---}\overset{+}{N}\text{---}(C{=}C)_m\text{---}N(C_lH_{2l+1})_2$$
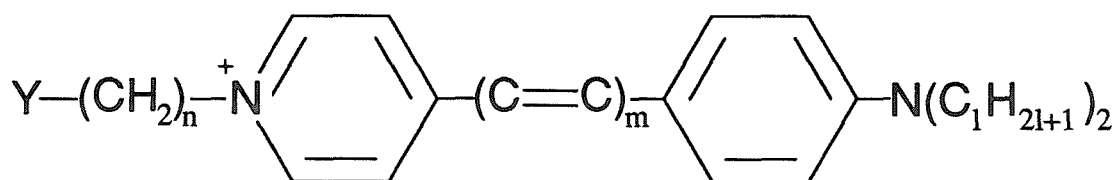
b) GOOD STAINING

dye	Y	n	m	l
RH160	SO_3^-	4	2	4
RH237	SO_3^-	4	3	4
RH292	$(Et)_3N^+$	3	2	4
RH376	PO_3^{2-}	4	2	4
RH415	$(Et)_3N^+$	3	2	3
RH421	SO_3^-	4	2	5
RH423	SO_3^-	4	2	6
RH425	$(Me)_3N^+$	3	2	4
RH429	$(Et)_3N^+$	4	2	4
RH477	SO_3^-	4	3	5
RH725	PO_3^{2-}	3	2	4
RH749	$(Et)_3N^+$	6	2	4
di-4-ASPBS	SO_3^-	4	1	4
di-6-ASPPS	SO_3^-	3	1	6

c) POOR STAINING

dye	Y	n	m	l
RH293	SO_3^-	4	2	3
RH295	SO_3^-	4	2	2
RH332	SO_3^-	3	2	1
RH414	$(Et)_3N^+$	3	2	2
RH437	$(Me)_3N^+$	3	2	3
RH461	$(Me)_3N^+$	3	2	2
RH528	PO_3^{2-}	3	2	4
RH687	$(Me)_3N^+$	4	2	4
RH743	$(Et)_3N^+$	5	2	4
di-4-ASPPS	SO_3^-	3	1	4

Table 6.2 Partial list of styryl dyes screened. *a)* Common structure for styryl dyes. *b)* Dyes that gave good staining. *c)* Dyes that gave poor staining.

Table 6.2 lists most of the styryl dyes that were screened by H.R. for staining properties, with their structures indicated (a few dyes have been left out due to incomplete data). This first phase of screening was quite crude. Mass cultures of SCG neurons grown on dried collagen were stained with a micromolar dye solution for five to ten minutes, then staining was assayed by eye, with no attempt at quantitating fluorescence. The dyes in the table are grouped roughly into dyes that stained well and dyes that stained poorly, on the basis of staining criteria 1 through 4. One generalization stands out from

these results: the length of the twin alkyl tail is crucial. Dyes whose tail had 3 or less carbons almost always stained poorly, while dyes whose tail had 4 or more carbons usually stained well. This result makes intuitive sense: the alkyl tails anchor the dye molecules in the membrane.

The next round of screening tested the voltage sensitivity of all of the dyes that stained well (except for di-4-ASPBS and di-6-ASPPS), and a few of those that stained poorly. Each dye was used to stain a mass SCG culture, then optical signals were observed as individual neurons were stimulated intracellularly. The measured voltage sensitivities were, as usual, quite variable between cells and between cultures, and so no quantitative results are quoted here, but three dyes emerged as the clear victors: RH237, RH421, and RH423 had peak sensitivities ($\Delta F/F$) of a few percent per 100 mV, and for cells with good staining, fluorescences of about 1 nA per cell. In the biophysical experiments described in the rest of this chapter, I used these three dyes and di-4-ANEPPS (provided by Leslie Loew after the initial screening was completed).

Dye screenings cannot be as complete as one would like. With the large number of dyes tested, for most dyes it is only feasible to test a few cells with one or two staining conditions. It is always conceivable that a given dye did not perform well because it was not tested at its optimal concentration or staining time. In order to partially address this concern, many dyes were tested by first penetrating a neuron intracellularly, then perfusing in dye solution. In this manner, the cell's fluorescence F and its signal ΔF could be observed as it stained over time. F usually seemed to plateau within a few minutes, though it sometimes increased slowly after this time. $\Delta F/F$, on the other hand, would often be quite high during the first minute, decrease by a factor of two or three within the next minute or so, then settle to a nearly stable level, with perhaps a slow steady decline. Presumably, this behavior of $\Delta F/F$ reflects rapid staining of voltage-sensitive sites, followed by slower staining of background (non-voltage-sensitive) sites. This phenomenon has not been explored further.

6.4 STAINING EXPERIMENTS

Early on in our experiments with voltage-sensitive dyes, we found that dye staining was inhibited by the serum normally present in $L15/CO_2$ culture medium. Initially, we found that cell fluorescences were increased approximately tenfold by presoaking in serum-free medium (SFM), *i.e.*, by changing the culture to SFM at least one day before staining; this result has been reported in abstract form (Rayburn *et al.*, 1984; Chien *et al.*, 1987). The experiments described in this section show that this presoak is not necessary.

Mass cultures were grown on gridded dishes (see section 6.2), which allowed individual cells to be mapped and located repeatedly. The dishes were stained (with or without an SFM presoak) and then the fluorescences of individual cells measured. In some experiments, the fluorescences of the mapped cells were followed over time.

SFM PRESOAK		NO PRESOAK	
dish #	net F (nA)	dish #	net F (nA)
1	0.40 ± 0.12	2	0.46 ± 0.22
3	0.46 ± 0.17	6	0.51 ± 0.14
5	0.75 ± 0.24		

Table 6.3 Effect of SFM presoak on staining. Cultures were stained with 2 μM RH423 in L15/Air for 7 min. Net fluorescences are given as mean ± s.d. (13 cells for each dish).

Table 6.3 shows fluorescences from a set of five sister cultures. Three dishes had been presoaked in SFM for one day, and two had not. The dishes were washed three times with L15/Air (which does not contain serum), stained for 7 min with 2 μM RH423, then washed three times more. The net fluorescences shown in the table are means from 13 cells in each dish, after correction for background fluorescences. The presoaked dishes are not significantly different from the non-presoaked dishes. Similar results were found in three other experiments with a total of 13 dishes.

Serum *does* interact with the dye, however. After dish 1's net fluorescences were measured, the dish changed back into complete L15/CO$_2$. After 1 hour in this serum-containing medium, all 13 mapped cells were much dimmer: their net fluorescence decreased from 0.40 ± 0.12 nA (mean ± s.d.) before exposure to serum to .04 ± .01 nA afterwards. This decrease is not due to bleaching, since the dish was kept carefully in the dark; presumably, the serum took up dye from the cells, reducing their fluorescence. Such binding of dye by serum would not be surprising, since serum contains large globular proteins. Such proteins have hydrophobic interiors, and thus have hydrophobic-hydrophilic boundary regions—the perfect environment for binding styryl dyes. Though it has not been tested, this phenomenon seems likely to hold for other styryls besides RH423. The early observation that good staining required an SFM presoak was probably due to traces of serum left by inadequate washing.

This measurement shows that serum-containing medium removes dye bound to cells; what happens if no serum is added? In another experiment, a dish was stained, then left in SFM for one day. The average fluorescence of 13 cells increased from 0.43 ± 0.13 nA immediately after staining to 1.03 ± 0.39 nA on the second day. This increased staining did not show up as bright membrane rings; instead, the dye concentrated inside the cell bodies. Intracellular staining is quite undesirable for dye recording, and so for long-term experiments that require repeated dye recording on successive days, the best policy is to use serum-containing medium to destain each culture after each recording session, then restain it with fresh dye for the next session.

6.5 FILTERS

6.5.1 Introduction

This section describes experiments that measured dye sensitivity with different excitation and emission filters, using the styryl dyes RH237, RH421, RH423, and di-4-

ANEPPS. The three RH dyes were the best to emerge from the initial screening (section 6.3); in addition, RH237, RH421, and di-4-ANEPPS were known to give large signals on other cell types (see section 6.1).

These experiments had two purposes. The primary aim was to find an optimal filter set for each dye. During the initial screening, $\Delta F/F$ for the three RH dyes was typically 1%/100 mV, and at the very most a few times this. Compared to the published results on other cell types ($\Delta F/F$ greater than 10%/100 mV), these signals were quite disappointing, and it seemed possible that at least some of the discrepancy might be due to a less-than-perfect choice of excitation and emission wavelengths. These experiments measured both F and ΔF for each filter combination; in the shot noise limit, the signal-to-noise ratio is proportional to $\Delta F/\sqrt{F}$. Once optimal filter sets were found, each dye could be seen at its best, and a single dye chosen for microculture experiments.

The secondary aim was to shed some light on the biophysical mechanism underlying the dye signal. In artificial membrane systems, styryl dyes have been shown to operate primarily by an electrochromic mechanism (see Appendix A). The signals reported with RH421 and RH237 for neuroblastoma cells are, however, too large to be accounted for by electrochromism (Fluhler *et al.*, 1985).

In an electrochromic model, the electric field across the membrane directly alters the energies of the dye molecule's ground and excited states, thus shifting the dye's excitation and emission spectra; the action spectra for excitation and for emission should both be biphasic, with similar signs (see Fig A.5). $\Delta F/F$ can be split into contributions from excitation and emission: $\Delta F/F = f_{exc}(\lambda_{exc}) + f_{em}(\lambda_{em})$, where the excitation component f_{exc} depends on the excitation wavelength used, and the emission component f_{em} depends on the emission wavelength. (In the notation of Appendix B, $f_{exc} = bs_A$ and $f_{exc} + f_{em} = bs_F$.) f_{exc} should be positive for $\lambda_{exc} < \lambda_{exc,max}$ and negative for $\lambda_{exc} < \lambda_{exc,max}$, where $\lambda_{exc,max}$ is the peak of the excitation spectrum; f_{em} should have a similar dependence on

140

λ_{em} and $\lambda_{em,max}$. These predictions of electrochromism are crudely tested by experiments with different filters.

6.5.2 Experimental protocol

The mass cultures used here were grown either on ECM or on polylysine-laminin. Cultures were stained for (typically) 5 minutes with 1 μM dye, individual neurons were penetrated intracellularly and stimulated to fire action potentials, and dye signals were recorded with different filter combinations. Filters were changed *during* the penetration by removing then replacing the filter cube, or removing then replacing the emission filter holder. With a steady hand, these filter changes did not affect the penetration. In cases of low fluorescence (especially with excitation filter sets B and C), signals were averaged in order to improve the signal-to-noise ratio. Action potentials, fluorescences (F), and signals (ΔF) from stored data files were measured in the program DISPLAY.

6.5.3 Excitation filters

Fig 6.1 shows the spectrum of a mercury arc lamp: it is very bright at a few mercury-line wavelengths, but dim in between. Mercury arcs give a high signal-to-noise ratio for fluorescence dye recording because they are very bright; however, they are less than optimal for studying excitation spectra because of their poor spectral coverage. The figure also shows the passbands of the six excitation filter sets (see Table 6.1) in relationship to the arc's spectrum. Filter sets B and C gave especially dim illumination, since their passbands do not include any of the mercury lines. All experiments with excitation filters used the Olympus G cube; the dichroic mirror and emission filter built into this cube combined to form a long-pass filter with a 610 nm cutoff.
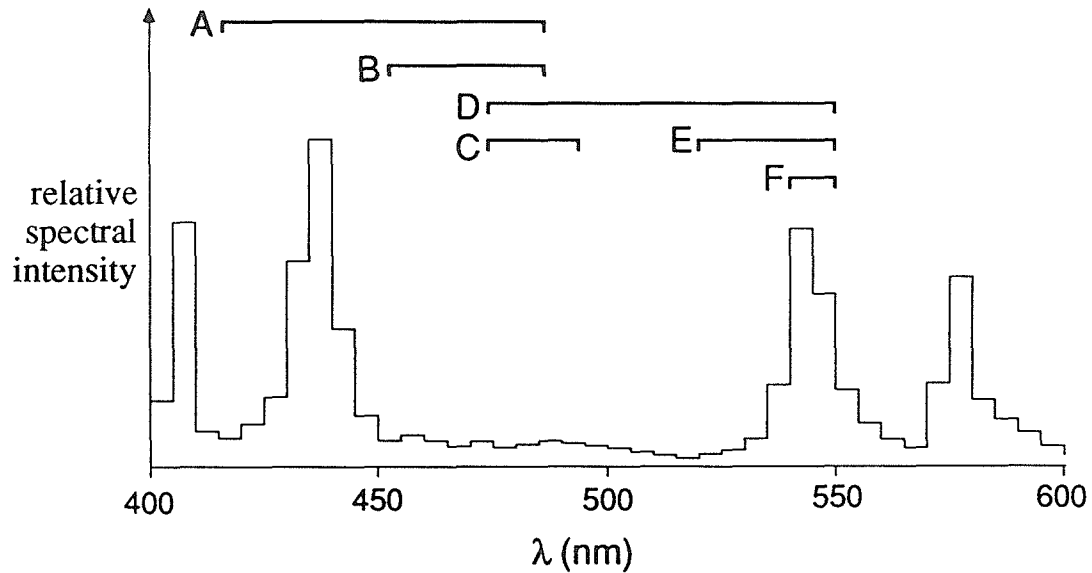
Figure 6.1 Excitation filter sets. Brackets indicating the passbands of filter sets *A* through *F* (see Table 6.1) are shown together with the output spectrum of a mercury arc lamp, which has peaks at 435, 546, and 577 nm. (Spectral data obtained from McBain Instruments.)

Fig 6.2 shows voltage sensitivities measured from four cells stained with RH423. There is variability between cells, but three main features are apparent. (1) $\Delta F/F$ was always negative. (2) As the excitation wavelength was increased by going from set A to set F, the magnitude of $\Delta F/F$ increased, reaching a maximum with E and F. (3) For sets A, B, and C, the signal was often small enough to be undetectable. This was especially common for B and C, since their low illumination intensity gave very little fluorescence.

The results for RH237 and RH421 (not shown) were very similar: sensitivity increased from A through F, and signals were usually undetectable for A, B, and C. A positive $\Delta F/F$ was seen once: a cell stained with RH237 gave a signal of +0.2%/100 mV with filter set A. With di-4-ANEPPS, the signals with filter sets A, B, and C were usually detectable, but the results were otherwise the same as those for RH423: sensitivity increased from A through F, and there were no positive signals.
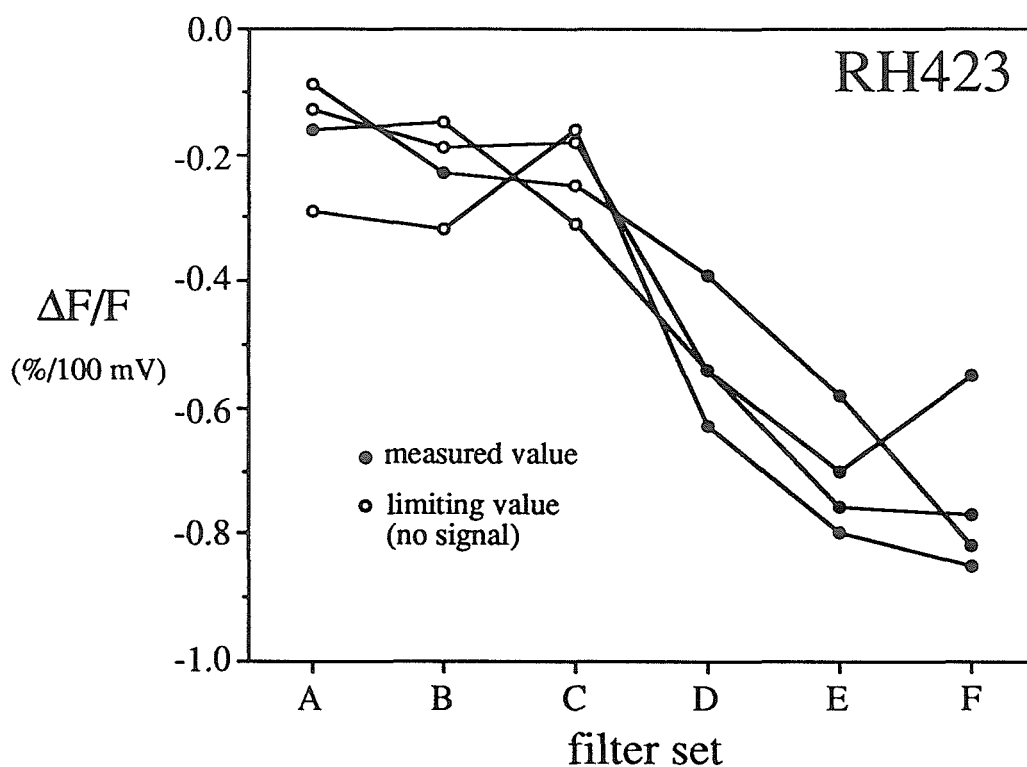
Figure 6.2 Δ*F/F* for RH423 with six different excitation filters, measured from four cells. Each curve represents Δ*F/F* values measured from a single cell with the six filter sets. *Solid circles* are true data points, while *open circles* are upper bounds in cases where no signal was observed above noise.

Optimal filter set. The shot-noise-limited signal-to-noise ratio is proportional to $\Delta F/\sqrt{F}$. For RH423, this figure of merit was highest for filter sets D and E (data not shown). The signals from A, B, and C were very small, and the low peak transmittance (36%) of set F offsets its high $\Delta F/F$. Set E (BP545 bandpass and LP515 long-pass) gave a slightly higher $\Delta F/F$ than set D (BP545 alone), but its illumination was somewhat dimmer, so $\Delta F/\sqrt{F}$ was roughly equal for both D and E. Given this equivalence in terms of signal-to-noise ratio, E is preferable, since it passes a lower illumination intensity and so should cause less photodynamic damage.

The results for the other three dyes were the same: filter sets D and E gave roughly comparable S/N, so E is preferable since it gives less light and therefore less phototoxicity.

Potentiometric mechanism. As described in subsection 6.5.1, electrochromism predicts that the excitation action spectrum $f_{exc}(\lambda_{exc})$ should be positive below $\lambda_{exc,max}$, and negative above. In order to interpret the results of excitation-filter experiments, it is necessary to know $\lambda_{exc,max}$. Loew's group has measured absorption spectra (equivalent to excitation spectra) for dyes bound to lipid vesicles (Fluhler *et al.*, 1985); they measured $\lambda_{exc,max}$ of 468 nm for di-4-ANEPPS, 467 nm for di-4-ASPPS, and 471 nm for di-4-ABPPS (the latter two are close analogs of the RH dyes used here). Therefore, $\lambda_{exc,max}$ should be roughly 470 nm for the four dyes used here, and should fall in the middle of the wavelength range covered by the six filter sets. Since $\Delta F/F$ is the sum of f_{exc} and f_{em}, it need not switch sign, but an electrochromic model predicts that $\Delta F/F$ should become more negative from A through F. For all four dyes, the data from excitation-filter experiments is consistent with this prediction, provided that f_{em} is assumed to be about -0.5%/100 mV for the 610 nm long-pass emission filter.

6.5.4 Emission filters

Experiments that studied the emission dependence of sensitivity used the Olympus G cube, supplemented by additional emission filters. The dichroic mirror and emission filter of the cube form a 610 nm long-pass filter; the additional emission filters were simple long-pass filters whose cutoff wavelengths (see Table A.1) ranged from 610 nm (RG610) to 780 nm (RG780). These experiments used excitation filter set E, which was shown in the last subsection to give maximal signals. These experiments used only RH237, RH423, and di-4-ANEPPS; RH421 was not tested.

Fig 6.3 shows fluorescences and voltage sensitivities from a cell stained with RH237. The measured F values indicate the shape of the dye's emission spectrum. The resting fluorescence of the cell decreases steadily from RG610 to RG780, as more and more of the emission spectrum was cut off by the emission filter. The RG610 and RG630 filters gave essentially the same fluorescence, so most of the emitted light was at
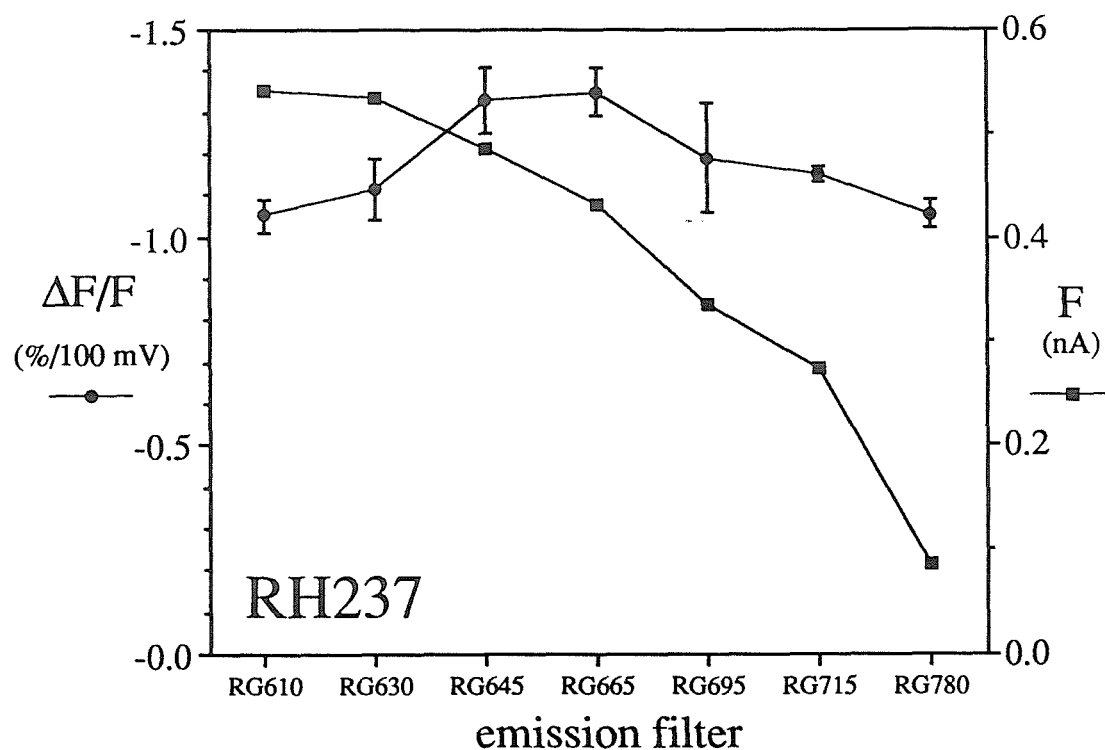
Figure 6.3 Voltage sensitivity and fluorescence for RH237 with seven different emission filters, measured from a single cell. *Circles* are Δ*F/F* values; note the inverted axis. The error bars represent the range of two measurements. *Squares* are *F* values. *RG610* is a 610 nm long-pass filter; the other filters are named similarly (see Table 6.1 for exact cutoff wavelengths).

wavelengths longer than 630 nm. The fluorescence decreases to below half of its initial value with the RG715 filter, so $\lambda_{em,max}$ is about 700 nm (assuming that the emission spectrum is symmetrical). The results of fluorescence measurements with RH423 and di-4-ANEPPS were similar, except that their emission maxima were about 660 nm.

The most interesting feature of the Δ*F/F* curve is that it is nearly flat: the voltage sensitivity has no significant dependence on the cutoff wavelength. The results from another cell stained with RH237 and several other cells stained with RH423 and di-4-ANEPPS were more variable, but essentially similar: Δ*F/F* was independent of the emission filter used.

Optimal filter. The practical consequence of the $\Delta F/F$ results is that the best emission filter is no emission filter. The dichroic mirror and emission filter built into the G cube already form a 610 nm long-pass filter, and any additional emission filter would only decrease F without changing $\Delta F/F$, decreasing the signal-to-noise ratio.

Potentiometric mechanism. When using a long-pass emission filter with cutoff wavelength λ_{cut}, an electrochromic model predicts that f_{em}, the emission component of $\Delta F/F$, will be negative and proportional to the dye's emission at λ_{cut}. Thus, f_{em} should be zero when λ_{cut} is short enough to pass the entire emission spectrum, should peak (at a negative value) when $\lambda_{cut}=\lambda_{em,max}$, and should be zero again when λ_{cut} is long enough to block the entire emission spectrum. The $\Delta F/F$ spectrum should show a peak at $\lambda_{em,max}$, but Fig 6.3 shows no significant peak. These crude action spectra for emission do not support an electrochromic mechanism.

6.5.5 Best dye

The four dyes that emerged from the initial screening and were then tested extensively with different filters, had voltage sensitivities that fell within a factor of two. RH423 and di-4-ANEPPS seemed slightly more sensitive than RH237 and RH421, but this is by no means definitive, since $\Delta F/F$ varied considerably among cells and cultures. RH423 was chosen, somewhat arbitrarily, for use in microculture experiments.

6.6 LINEARITY

During dye-recording experiments with microcultures, synaptic potentials were often not visible in the optical signal, even though—extrapolating from the size of the optical signal for an action potential—they should be. (See Chapter 7 for examples of optical recording of synaptic potentials.) This raised the question of the linearity of the dye response.

Defining nonlinearity as a lack of correspondence between the optical signal and the membrane potential recorded by an intracellular electrode, it could arise in at least two ways. The first possibility is that the dye is intrinsically nonlinear: $\Delta F/\Delta V$ may not be constant over the normal range of membrane potentials. The second possibility is that the cell's cable properties cause apparent nonlinearity. The dye signal samples the potential of all stained membrane in the pixel, while the intracellular electrode measures only the membrane potential at the cell body. These two signals can differ, since the cell's dendrites and axons are often at different potentials from the cell body and may be included in the pixel. In the most extreme case, the optical detector and glass electrode can measure signals from entirely different cells: for instance, if cell B's axon passes over cell A's soma, a pixel centered on A's soma may show a small dye signal when B's axon fires, while of course an intracellular electrode in A's soma will show nothing.

In order to check for the first, intrinsic, type of nonlinearity, I recorded dye signals from six SCG neurons freshly plated on glass coverslips and stained with RH423. Bare glass is a very poor substrate for these cells, so they do not extend neurites; however, they will stick to it for a few hours, and it is possible to stain and record from them during this period. These neuriteless cells are nearly spheres (the physicist's ideal cell shape!), and questions of cable properties do not arise. After making a gigohm seal on a cell with a patch pipette, the patch was broken with pressure, and the cell stimulated in whole-cell current clamp. In order to test a large voltage range, a pair of current pulses was used: the first was hyperpolarizing, the second depolarizing. The filters used were the G cube with the LP515 excitation filter (*i.e.*, excitation filter set E, with no additional emission filter).

Fig 6.4 shows the average of four trials recorded from one of these cells. The cell fired an action potential during the depolarizing pulse. Note the close correspondence between the resulting voltage trace and the fluorescence trace. A least-squares fit of these two curves gives a voltage sensitivity of 1.89%/100 mV, and the bottom trace in Fig 6.4 shows a difference plot calculated by multiplying the voltage trace by 1.89%/100 mV, then

subtracting it from the fluorescence trace. The fit is quite good. Fig 6.5 shows the

linearity of the dye response in another way: each time point from Fig 6.4 has been

replotted on a scatterplot of $\Delta F/F$ versus V_m. Over this voltage range, the dye response

seems to be linear to within a few percent. (A proper statistical analysis would be

complicated by the fact that the values at successive time points are not independent, and so

no quantitative analysis was undertaken.) The other five cells gave similarly linear

responses.

A note on filtering: the electrophysiology electronics is very fast, but the
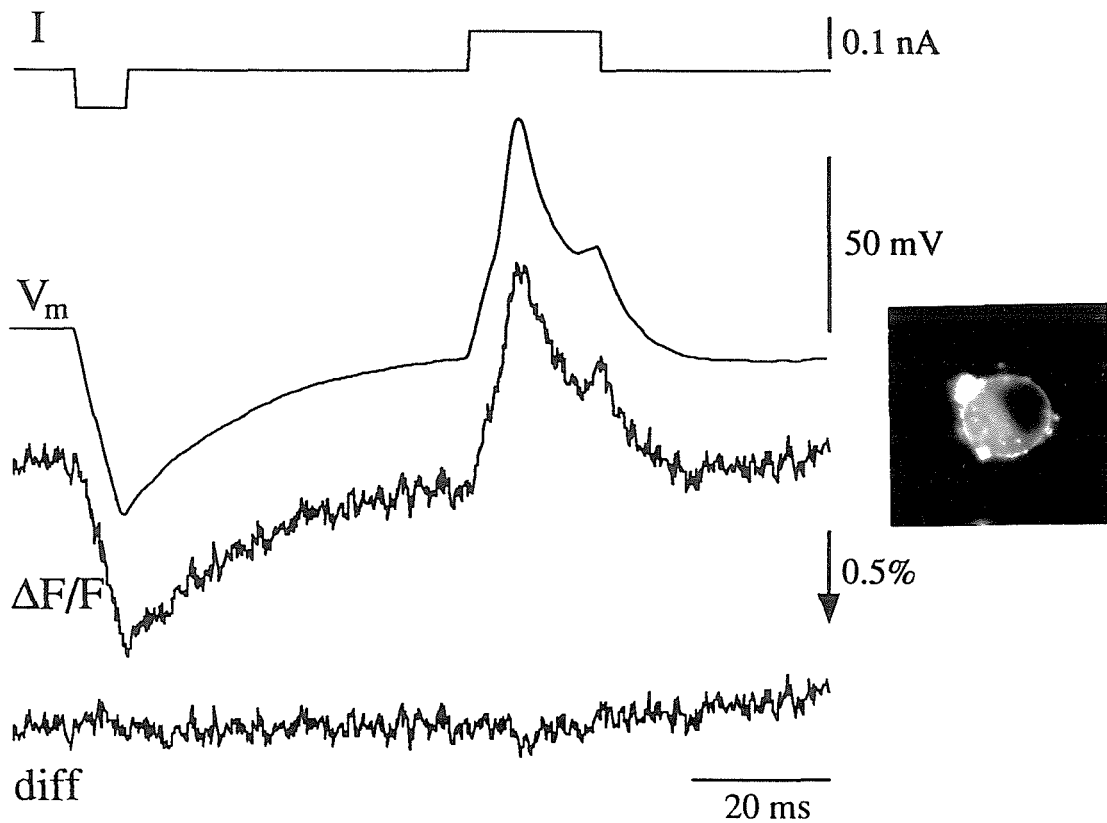
Figure 6.4 A test of dye linearity (see text for explanation). I is the current injected into the cell, V_m is the cell's membrane potential, and $\Delta F/F$ is the resulting fluorescence signal. The membrane potential and fluorescence trace match almost perfectly. *diff* is the difference between the fluorescence trace and the (scaled) voltage trace. The 0.5% scale bar applies to both lower traces; note that the fluorescence signals are inverted, as usual (the *arrow* points down). These data are the average of four trials; the voltage trace has been filtered to match the time response of preamplifier 134. The *inset* is a fluorescence micrograph of the cell, taken immediately after the dye signal was recorded.
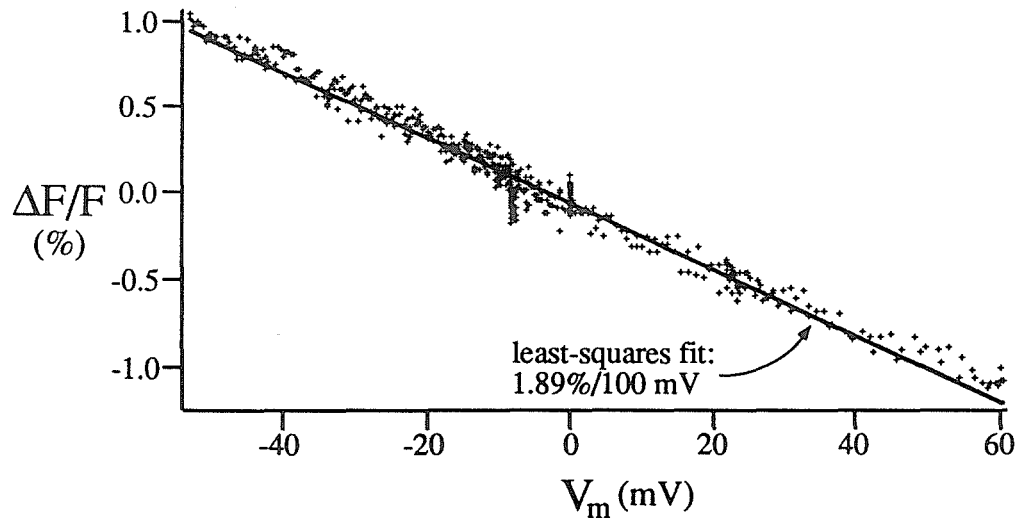
Figure 6.5 The voltage and fluorescence data from Fig 6.4, plotted as a scatterplot in order to show linearity. The *small crosses* are individual time points; the heavy line shows a least-squares-fit, whose slope is -1.89%/100 mV. V_m is given relative to the cell's resting potential.

preamplifier for pixel 134, which recorded the fluorescence signal, has a noticeable

response time of about 0.4 ms. In order to match the filtering of the voltage and

fluorescence signals so they could be fairly compared, the voltage signal was convolved

with a stored record of amplifier 134's response, using the program FILTER. The flatness

of the difference plot shows that this procedure worked well.

One explanation for variations in $\Delta F/F$ is that they are due to varying background

staining. If this is so, then one might expect these freshly-plated cells to give high $\Delta F/F$,

since there is no network of neurites to add background. This is indeed true: the $\Delta F/F$

values for these six cells were 1.2, 1.9, 2.1, 2.3, 2.4, and 2.5 %/100 mV, quite good

compared to the 1%/100 mV that was typical for recordings from microcultures or mass

cultures. It is clear from fluorescence micrographs that even these freshly-plated cells still

have substantial background fluorescence (see Fig 6.4), so the intrinsic sensitivity of

RH423 may be much higher than these $\Delta F/F$ values. In another experiment, a freshly-

plated SCG neuron that was stained with RH423 gave the largest signal that I have ever seen, about 7%/100 mV.

6.7 BLEACHING AND PHOTOTOXICITY

6.7.1 Dye bleaching

Bleaching rates were measured for RH237, RH421, RH423, and di-4-ANEPPS, from 4 to 10 cells stained with each dye. RH421 and RH423 bleach much faster than RH237 and di-4-ANEPPS. For SCG neurons with typical staining (about 1 μM dye for 5-10 minutes), using standard filters (filter set E) at the standard illumination intensity, the ranges of bleach rates for each dye were: RH423, 1-2.6%/100 ms; RH421, 1.6-2.4%/100 ms, di-4-ANEPPS, 0.3-0.5%/100 ms; and RH237, 0.3%/100 ms or lower.

In a few experiments that repeatedly measured cell and background fluorescences, the background bleached much more quickly than the stained cell. It is quite conceivable that dye bound to the substrate or to debris may be more susceptible to bleaching than dye bound to cells, but no quantitative study has been made of this phenomenon.

6.7.2 Pharmacological effects of the dyes

No toxic effects of these dyes have been seen without exposure to light. For instance, in one experiment that looked at the effects of serum on staining, cells were stained for 7 minutes with 2 μM RH423. The mapped cells were illuminated very briefly (a few hundred ms) to measure their fluorescences, then switched back to complete L15/CO$_2$ (which presumably removed the bound dye), and returned to the incubator. The cells were exposed to dye for a total of about 30 min. When 52 mapped cells were observed in phase-contrast four days later, all 52 were still alive.

No pharmacological effects of the dyes have been noticed, but this is not to say that they do not exist. Such effects are always a possibility, especially considering the very

high concentration of dye in the membrane (see Appendix A), and any dye-recording experiment must control for them.

6.7.3 Phototoxicity

On the other hand, dye staining combined with light exposure clearly causes cell death. Anecdotal observations during dye-recording experiments suggested that for normal staining with RH421 or RH423, using filter set E for a standard illumination intensity of 10 W/cm^2, somewhere between 10 and 30 seconds of illumination caused deterioration of the cells' electrophysiological properties.

Table 6.4 summarizes an experiment that measured phototoxicity by staining and exposing cells, then looking at their survival over a few days. Two mass cultures were grown on gridded dishes for four weeks. In each culture, the position of every cell in ten 500 μm squares was mapped, so that every cell could be identified later. The cultures were stained for 5 min with 2 μM RH423, and the fluorescences of the cells were typical: 0.5-1.0 nA per cell with full illumination. The cells in each square were illuminated for 5, 20, 80, or 320 seconds, either with full illumination (assumed here to be 10 W/cm^2) or through a neutral-density filter for one-quarter illumination (2.5 W/cm^2). The dishes were then switched back to complete L15/CO$_2$ and returned to the incubator. The survival of the

exposure (J/cm^2)	survived/total intensity	
	10 W/cm^2	2.5 W/cm^2
12.5		15/15
50	22/22	20/20
200	18/18	23/24
800	2/18	15/23
3200	4/11	

Table 6.4 Cell survival during a phototoxicity experiment. The table entries show the ratio of (cells which survived at day 1) to (cells which were initially mapped), for each illumination condition. *Exposure* is the product of *intensity* and exposure time.

mapped cells was then assessed in phase-contrast at 1, 4, and 8 days. Table 6.4 shows the lumped data from both dishes at day 1. (All of the cells that were dead at day 8 had already died by day 1.)

At full exposure, nearly all cells illuminated for 20 seconds survived, while most cells illuminated for 80 or 320 seconds died. The lethal dose of light seems to be between 20 s and 80 s at full illumination. Three other experiments (169 cells total) found lethal doses of between 10 s and 30 s at full illumination; there seemed to be some variability in threshold between dishes.

In addition to the toxicity threshold at full illumination, Table 6.4 shows a tantalizing result. Of the cells exposed to full illumination for 80 s, only 2 of 18 survived. Of the cells exposed to one-quarter illumination for 320 s, however, 15 of 23 survived. This suggests that phototoxicity may not be determined by the total light dose alone,but may depend on the time over which this dose is spread. This experiment should be repeated, preferably using a more definitive test of cell survival such as Trypan Blue exclusion. Some of the exposed cells seemed to become sick without dying, making them hard to score in phase contrast.

6.8 DISCUSSION

Chapters 3,4, and 5 described the engineering of a detector apparatus for dye recording; this chapter describes experiments for refining and understanding the practical application of the technique to cultured rat SCG neurons.

6.8.1 Practical hints

Sifting through the results of these experiments, a few hard nuggets of practical knowledge emerge:

Best dye. After the initial screening, four dyes seemed most promising: RH237, RH421, RH423 and di-4-ANEPPS. The latter two gave slightly larger voltage signals;

RH423 was chosen arbitrarily as the dye for microculture experiments. Since these dyes had roughly similar voltage sensitivities, one of the other three might be preferable for a secondary reason such as bleaching or phototoxicity.

Staining. Cultures are usually stained by washing thrice to remove the culture medium, adding dye at a concentration of 0.5-5 μM for 5-10 min, then washing thrice more to remove unbound dye. Dye concentration and staining time have not been studied systematically, but they do not have obvious effects on the final $\Delta F/F$. In experiments during the initial screening that stained cultures by perfusing dye, cell fluorescences seemed to plateau within a few minutes; $\Delta F/F$ was sometimes very high for the first minute of staining, then decreased.

Serum clearly binds RH423 and destains SCG neurons. This is probably a general property of large soluble proteins: in experiments with the dye RH155, Brian Salzberg's group has found that bovine serum albumin efficiently removes dye from cultured *Aplysia* neurons (T. Parsons, personal communication). It is therefore important to wash cultures thoroughly before staining, but long presoaks in serum-free medium are unnecessary.

Filters. For the four dyes tested (RH237, RH421, RH423, and di-4-ANEPPS), excitation filter set E gave the best signal-to-noise ratio. The filter set passes wavelengths from 520 to 550 nm; it selects the 546 nm line of the mercury arc, with very little broadband excitation. Filter set D (474 to 540 nm) gave a roughly similar S/N but a higher illumination intensity. E should cause less photodynamic damage.

For all four dyes, long-pass emission filters had little consistent effect on $\Delta F/F$. Since these filters reduce F and thus reduce S/N, they should be omitted.

Dye toxicity. RH423 seems to have no toxic effects in the absence of light. Under standard conditions of illumination and staining, the phototoxicity from RH423 becomes lethal at about 20 s. If an experiment uses 100 ms flashes for illumination, this allows approximately 200 trials before the cells die.

6.8.2 Potentiometric mechanism

In order to measure action spectra, one should ideally have a broadband light source with a monochromator for excitation, and another monochromator for measuring emission. Such an apparatus is rarely found attached to a microscope, which explains the poor understanding of potentiometric mechanisms in real cells. The experiments of section 6.5 were quite crude, and mainly aimed at finding the best filters for practical use, but the results make it very unlikely that the four styryl dyes tested operate by a pure electrochromic mechanism on SCG neurons. At best, the results can be interpreted as showing an electrochromic absorption shift compounded with a wavelength-independent signal, with no electrochromic emission shift.

6.8.3 Intrinsic voltage sensitivity

The property of these voltage-sensitive dyes that is most important for the signal-to-noise ratio is their voltage sensitivity. Increasing $\Delta F/F$ from a typical level of 1%/100 mV to 5%/100 mV would directly increase S/N fivefold, obviating the need for signal averaging when recording small potentials, and allowing much lower illumination levels (and thus lower phototoxicity) when recording action potentials. Given the 21%/100 mV signals that have been seen with RH421 on other cells (Grinvald et $al.$, 1983), the question arises: why are the signals from RH421 and related dyes so much smaller on SCG neurons?

Each dye presumably has some intrinsic sensitivity s_F (see Appendix B) that may depend on membrane composition or the ionic composition of the medium; s_F is reduced by background staining to give the observed sensitivity, $\Delta F/F$. One reason for low $\Delta F/F$, then, might be high background staining. Experiments with isolated, neuriteless neurons (section 6.6) support this idea: despite a large amount of obvious background fluorescence, these cells gave signals of 2%/100 mV. If sensitivity variations are purely due to variations in background, the highest observed $\Delta F/F$ will be the best estimate of s_F.

One cell gave 7%/100 mV, so the intrinsic sensitivity of RH423 is at least this. The fluorescence of a cell that gives a signal of 1%/100 mV is presumably at least six-sevenths background.

It would be extremely interesting to try to increase $\Delta F/F$ by reducing background staining. Background staining comes from three sources: other neurons, extracellular staining, and intracellular staining. Staining from other neurons cannot be removed, but the other two sources might be reduced. Cleaning cultures in some way might reduce background staining, or another dye might penetrate cells less readily than RH423, or stain debris less brightly.

6.8.4 Bleaching

It is desirable that bleaching be as slow as possible, because of two adverse effects. First, the slow fluorescence decrease due to bleaching superimposes itself on every fluorescence record, and must be subtracted off in order to see the voltage-dependent signal. The slower the bleaching, the easier and more accurate this bleach-subtraction. The second effect is simply that as a cell is bleached, its fluorescence and so its dye signal decrease. With slower bleaching, the original S/N is maintained for a longer time. Bleach rates were not taken into account when RH423 was chosen as the dye for microculture recordings, but when choosing a dye for future experiments, the low bleach rates of RH237 and di-4-ANEPPS would be points in their favor.

6.8.5 Phototoxicity

It is desirable that phototoxicity be as low as possible because, of course, it kills cells. Also, at sublethal exposure levels, photodynamic damage may alter the very electrophysiological responses that the dyes are meant to measure. Such effects, if subtle, may be very hard to detect. When a stained cell is monitored with an intracellular electrode while it is illuminated, the main symptom of photodamage is that the cell's stimulation threshold progressively increases, until it finally stops firing altogether. The experiments

in section 6.7 show that under standard conditions, SCG neurons stained with RH423 seem to die after about 20 s exposure at 10 W/cm^2. Anecdotal observations give a roughly similar threshold for observable electrophysiological effects.

There are two ways to reduce photodynamic damage: find a better dye or reduce illumination. The gridded-dish assay for phototoxicity (section 6.7) could be used to test the phototoxicity of RH237, RH421, and di-4-ANEPPS; if one of these has much lower phototoxicity than RH423, it would be preferable, since all four dyes have roughly similar voltage sensitivities.

At the present illumination intensity, the signal-to-noise level is just large enough to easily record postsynaptic potentials (see Chapter 3), so illumination cannot be reduced unless dye sensitivity were improved. However, it may be possible to reduce phototoxicity by spreading illumination out over time. Bonhoeffer and Staiger (1988), using RH237 and RH414 on hippocampal cultures, reported that 20 s of continuous illumination was much more harmful than 100 flashes of 200 ms, with flashes separated by 30 s. Cells are known to have mechanisms for dealing with damage from free radicals, including membrane turnover (as Bonhoeffer and Staiger suggest), and free radical scavengers. These damage-control mechanisms may be able to handle occasional short flashes, where they would be overwhelmed by continuous illumination.

It would be quite useful to measure the effects of various illumination protocols. The gridded-dish phototoxicity assay is particularly suited to such measurements, since it provides in-dish controls. Different illumination protocols are used for different cells in the same culture dish, so any improvement in survival rates can be attributed to differences in illumination rather than between-dish variability. The experiment of Table 6.4 showed that cells exposed at one-quarter illumination for 320 s died less often than cells exposed at full illumination for 80 s. This anecdotal result is reminiscent of Bonhoeffer and Staiger's claim, and it would be interesting to repeat and extend it. During microculture experiments, cultures are usually exposed in flashes of 100-150 ms, repeated every 5 or 10 s during

signal averaging, or less frequently without signal averaging. This 1-2% duty cycle is already far below continous illumination, but it would be interesting to know if a somewhat lower duty cycle would reduce toxicity.

CHAPTER 6 REFERENCES

T. Bonhoeffer and V. Staiger (1988) Optical recording with single cell resolution from monolayered slice cultures of rat hippocampus. *Neurosci. Lett.* **92**:259-264.

C.-B. Chien, W. D. Crank, and J. Pine (1987) Noninvasive techniques for measurement and long-term monitoring of synaptic connectivity in microcultures of sympathetic neurons. *Soc. Neurosci. Abstr.* **13**:1426, abstr. #393.15.

E. Fluhler, V. G. Burnham, and L. M. Loew (1985) Spectra, membrane binding, and potentiometric responses of new charge shift probes. *Biochemistry* **24**:5749-5755.

J. E. Freschi (1983) Membrane currents of culture rat sympathetic neurons under voltage clamp. *J. Neurophysiol.* **50**:1460-1478.

D. Gospodarowicz, I. Vlodavsky, and N. Savion (1981) The role of fibroblast growth factor and the extracellular matrix in the control of proliferation and differentiation of corneal endothelial cells. *Vision Res.* **21**:87-103.

A. Grinvald, R. Hildesheim, I. C. Farber, and L. Anglister (1982) Improved fluorescent probes for the measurement of rapid changes in membrane potential. *Biophys. J.* **39**:301-308.

A. Grinvald, A. Fine, I. C. Farber, and R. Hildesheim (1983) Fluorescence monitoring of electrical responses from small neurons and their processes. *Biophys. J.* **42**:195-198.

D. Gross, L. M. Loew, and W. W. Webb (1986) Optical imaging of cell membrane potential changes induced by applied electric fields. *Biophys. J.* **50**:339-348.

M. I. Johnson and V. Argiro (1983) Techniques in the tissue culture of rat sympathetic neurons. *Meth. Enzymol.* **103**:334-347.

D. K. MacCallum, J. H. Lillie, L. J. Scaletta, J. C. Occhino, W. G. Frederick, and S. R. Ledbetter (1982) Bovine corneal endothelium in vitro: elaboration and organization of a basement membrane. *Exp. Cell Res.* **139**:1-13.

R. E. Mains and P. H. Patterson (1973) Primary cultures of dissociated sympathetic neurons. I. Establishment of long-term growth in culture and studies of differentiated properties. *J. Cell Biol.* **59**:329-345.

A. Marty and E. Neher (1983) Tight-seal whole-cell recording. In *Single-Channel Recording*, eds. B. Sakmann and E. Neher. Plenum, New York. pp.107-122.

H. Rayburn, J. Gilbert, C.-B. Chien, and J. Pine (1984) Noninvasive techniques for long-term monitoring of synaptic connectivity in cultures of superior cervical ganglion cells. *Soc. Neuroci. Abstr.* **10**:578, abstr. #171.1.

W. G. Regehr, J. Pine, C. S. Cohan, M. D. Mischke, and D. W. Tank (1989) Sealing cultured neurons to embedded dish electrodes facilitates long-term stimulation and recording. *J. Neurosci. Meth.* **30**:91-106.

Chapter 7
Microculture experiments

7.1 INTRODUCTION

The preceding chapters and the appendices have described a series of technical developments: screening of voltage-sensitive dyes, design and construction of an optical detector, refinements of filter sets and staining procedures. The goal of this long arc of technique was of course to dye-record—in particular, to dye-record from microcultures of rat superior cervical ganglion (SCG) neurons. This chapter describes a final technical development—a reliable method for growing microcultures of SCG neurons—and then presents recordings made from microcultures using the dye RH423. These data form a basis for evaluating the usefulness of dye recording for mapping synaptic connections in these and other microcultures.

Neurons in microculture are grown in much the same way as those in mass culture, except that microcultures use patterned substrates. (Another difference is that the low density of cell in microcultures makes them more fragile and generally harder to grow.) The coverslips on which microcultures are grown have islands of favorable substrate surrounded by a sea of unfavorable substrate. Neurons attach only on the islands, and their growing processes remain confined therein. Previous methods for growing microcultures of SCG neurons (Furshpan et al., 1976; Higgins et al., 1984) used small dots of dried collagen as the favorable substrate, on an unfavorable substrate such as the plastic Aclar; neurons were either grown by themselves, or cocultured with cardiac myocytes. In our laboratory, this collagen-dot method was tedious and unreliable, and so I

have developed a succession of other methods that use a pattern of silastic adhesive to define the microculture islands. Section 7.3 describes these microculture methods.

Rat SCG neurons were chosen for the present experiments because they are known to form synapses with each other in culture (O'Lague *et al.*, 1974). *In vivo*, these neurons receive cholinergic inputs, and (like most sympathetic neurons) have adrenergic outputs. *In vitro*, under certain culture conditions (especially under the influence of nonneuronal cells), they switch to using acetylcholine as a transmitter (Patterson and Chun, 1977), and so can form cholinergic synapses on each other or on themselves (O'Lague *et al.*, 1974; Higgins *et al.*, 1984). Section 7.4 describes some preliminary two-electrode experiments using intracellular physiology on SCG microcultures; these experiments show that cholinergic synapses form under the culture conditions used here.

The dye recording system described in Chapter 3 should have a typical rms noise level of about .03% (the shot-noise limit for a photocurrent of 1 nA with a bandwidth of about 300 Hz). Using the dye RH423, which typically gives 1%/100 mV signals (Chapter 4), this system should certainly be able to detect action potentials (APs) in cell bodies, and may be able to detect large postsynaptic potentials (PSPs), especially with signal-averaging. The detection limits of dye recording were studied in microcultures by recording dye signals from cell bodies and neurites while single neurons or pairs of neurons were stimulated with intracellular electrodes. As well as stimulating the penetrated cells, the intracellular electrodes provided a reliable measure of membrane potential against which the dye signals could be compared. When recording dye signals from cell bodies, detection of APs was routine, but detection of PSPs was not. Though APs recorded intracellularly always gave significant peaks in the fluorescence trace, in general the dye signals did not closely follow the membrane potential measured by the intracellular electrodes. Since the RH423 dye signal is intrinsically linear in membrane potential (section 6.6), these differences appear to be due to dye signals from APs propagating in axons, which obscure the dye signals from cell bodies.

Section 7.5 shows detailed data from two microcultures, one with a single neuron and the other with five neurons. For the one-cell culture, dye signals were recorded from the cell's soma and neurites (presumptive dendrites and axons): the propagating AP was visible in all pixels monitored. Such signals from processes are undesirable for synaptic mapping: if a process passes over the cell body, its signal will contribute to and distort the cell-body signal. For the five-cell culture, dye signals were mostly recorded from cell bodies. This culture was strongly connected, and its suprathreshold synaptic potentials were easily detected with dye recording. Smaller dye signals seemed to be due to propagating APs rather than synaptic potentials.

Section 7.2 lists technical details of materials and methods; section 7.6 summarizes and discusses the results of the chapter.

7.2 MATERIALS AND METHODS

Most methods were as described in section 6.2; only the major points are summarized here.

Cell culture. Methods for microcultures were generally the same as for mass cultures. Section 7.3 describes the fabrication of microculture substrates using silastic adhesive (silastic MDX4-4210 medical grade elastomer, Dow Corning); this silastic was usually cured for 1 hour at 70°C. The protocols of section 6.2 were used to coat these substrates with collagen, polylysine, extracellular matrix (ECM) from bovine endothelial corneal (BEC) cells, or polylysine-laminin. Feeder layers of 1000-3000 neurons were usually grown outside the central well (on the plastic petri dish) in order to condition the medium and improve survival of the microcultures.

Electrophysiology. Early experiments (section 7.4) used Freschi's high-Ca^{++} recording solution and were carried out at room temperature (22-25°C); later experiments (section 7.5) used L15/Air, and were carried out at 30-33°C. For experiments using the cholinergic blocker hexamethonium, a 1 mM stock solution was made by dissolving

hexamethonium chloride (Sigma) in Freschi's recording solution; the desired concentration of drug was made up by diluting this stock solution. Recording solutions with and without drug were perfused into the dish using a gravity-feed system for input, and a vacuum-pump driven aspiration system for output.

Dye recording. Dye recording used the apparatus and software described in Chapter 3. Cultures were washed thrice, stained for 5-8 min with 2 μM RH423, then washed thrice more. Illumination was from a mercury arc lamp, with the Olympus G cube, LP515 excitation filter, and no additional emission filter. The excitation filters (filter set E from Table 4.1) passed wavelengths within 520-550 nm; the emission filters passed wavelengths longer than 610 nm. Most of these experiments used a Nikon Fluor 20 Ph3DL microscope objective (NA 0.75), though a Nikon Fluor 40 Ph3DL (NA 0.85) was occasionally used for smaller islands.

Data analysis. Recorded fluorescence traces were routinely analyzed by digital filtering with a "symmetrized RC filter" of time constant 0.5 ms (see subsection 5.2.5), followed by bleach-subtraction using for a reference a trace taken without stimulation. Culture schematics (Figs 7.5*d* and 7.7*d*) were made from acquired video alignment images by scanning the video images with a Macintosh II running an Abaton FB/300 scanner, then tracing the scanned image in the drawing program Canvas 2.1 (Deneba Software).

7.3 MICROCULTURE METHODS

Microculture dishes were made by glueing coverslips with patterned substrates to the bottom of plastic 35 mm dishes with drilled holes, forming a 6 mm well in the usual way. Each coverslip had about 16 islands of adhesive substrate, each roughly 700 μm in diameter, surrounded by a nonadhesive substrate. Cells plated on such a dish fall to the bottom at random, but only attach to the adhesive islands. The number of cells in each island varies, but plating at the appropriate density insures that several islands in each dish

have the desired population. The target was usually between one and five neurons per island.

Collagen dots. We initially tried the collagen-dot method of Furshpan *et al.* (1976), but had little success. In this method, the islands are formed by drying a small drop of collagen solution on a nonadhesive substrate. Placing each drop of collagen by hand was quite tedious, and the microcultures often "rolled up." When this rolling-up occurred, cells initially attached well to the island, put out extensive neurites, and formed a fascicle (bundle of processes) that girdled the island. Over the next one or two weeks after plating, however, the neurites gradually pulled in, until the cells formed a little lump in the center of the island, which eventually fell off. (Rolling-up was a common problem with other microculture substrates, as well.)

Several different substrates and patterning methods were tried to replace collagen dots. The four most successful methods are briefly outlined here: masked collagen, masked polylysine, nonadhering BEC cells, and polylysine-laminin liftoff. (The particular properties of each substrate determine the methods that can be used to pattern it.)

All four methods define the island boundaries using a pattern of silastic adhesive (Dow medical elastomer; see section 7.2), which is quite hydrophobic and a poor substrate for cell attachment. Fig 7.1 shows a schematic of the central 6 mm well of a typical microculture dish. The clear circles are the islands of exposed substrate; the hatched pattern that separates them is the silastic. (One corner of the pattern is notched for convenient record-keeping.) There is also exposed substrate outside the silastic pattern; cells fall there as well as on the islands, forming a

Figure 7.1 Typical microculture pattern. *White* areas are exposed substrate; *hatched* areas are silastic adhesive. The outer circle is the central 6 mm well of the culture dish.

feeder layer and providing convenient controls for electrophysiology.

The silastic is applied using a "rubber stamp," a thin square of plastic with a pattern of holes drilled in it. A glass microscope slide coated with a thin layer of wet silastic serves as an "ink pad." Using forceps under a dissecting microscope, the rubber stamp is "inked" by placing it on the slide and pressing gently; it is then placed briefly on a glass coverslip and pressed gently again. When the rubber stamp is removed from the coverslip, it leaves behind a thin pattern of silastic, which is then cured for 1 hour at 70°C. For the masked-collagen and masked-polylysine methods, the silastic is applied to a coverslip already coated with substrate molecules; for the nonadhering-BEC-cells and polylysine-laminin-liftoff processes, the silastic is applied to a plain coverslip and the substrate added afterwards.

Fig 7.2 shows the four methods for making substrates using these silastic patterns:

Masked collagen and *masked polylysine*. The first two methods use collagen or polylysine as substrates. A silastic pattern is applied to a coverslip already coated with dry substrate, and acts as a mask to prevent neurons from attaching outside the islands. The masked-collagen method was tried first; it proved unworkable because the collagen layer was thick enough that processes could grow underneath the silastic and connect neighboring islands. Masked polylysine, tried next, was not a good long-term substrate: the microcultures were healthy initially, but rolled up after one or two weeks.

Nonadhering BEC cells. This method uses extracellular matrix (ECM) produced by bovine endothelial corneal (BEC) cells as a substrate. Since ECM loses its potency when dried, and the silastic can only be applied to a dry coverslip, the silastic could not be used to mask an already-coated coverslip, as for collagen and polylysine. Instead, the silastic pattern is applied directly to the polyimide-coated coverslip on which the BEC cells are grown, and BEC cells are plated on top of the silastic. The BEC cells only attach to exposed polyimide, not to silastic; after they grow to confluency and are lysed, extracellular matrix is left only on the islands.

a) masked collagen

silastic adhesive

dried collagen   glass coverslip

b) masked polyL

polylysine

c) nonadhering BEC cells

BEC cells

lyse BECs

ECM

d) polyL-lam liftoff

polylysine + laminin

peel off silastic
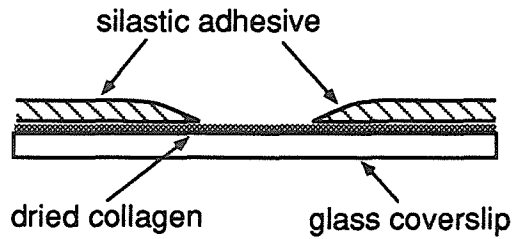
Figure 7.2 Four methods for making microculture substrates. *a)* Masked collagen. *b)* Masked polylysine. *c)* Nonadhering BEC cells. *d)* polylysine-laminin liftoff. Each panel shows a single island in cross-section (vertical dimensions not to scale). The glass coverslip is shown as *white,* and the silastic adhesive, *hatched.*

ECM produced by BECs was an excellent substrate for SCG neurons, and gave good microcultures that lasted for months. Islands occasionally rolled up, especially if their diameter was small, but this did not usually occur until four or five weeks after plating. A disadvantage of ECM was that it contained membrane fragments from the lysed BEC cells, which added to background fluorescence during dye recordings.

Polylysine-laminin liftoff. The final method uses polylysine-laminin as a substrate. As for ECM, laminin is damaged by drying, so a silastic mask cannot be used. Instead, the polylysine-laminin is patterned using a liftoff process, in which silastic is used not as a mask to prevent neuronal attachment, but rather as a way of removing unwanted substrate.

The silastic is applied to a bare glass coverslip, the coverslip is coated with polylysine and laminin, then the silastic is simply peeled off[1] with forceps, leaving behind islands of polylysine-laminin. Bare glass serves as the nonadhesive substrate for this method.

Polylysine-laminin was a very good substrate for SCG neurons (though not quite as good as ECM); these cultures survived routinely for four weeks, and occasionally for months. Polylysine-laminin microcultures had less fluorescent background than ECM microcultures, and were much easier to prepare, since they did not require the extra step of growing BEC cells.

100 µm
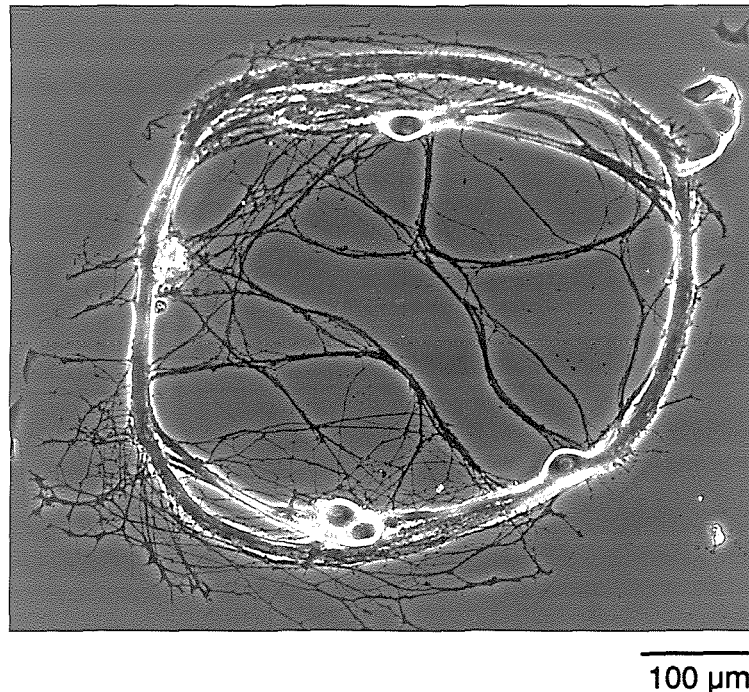
Figure 7.3 Microculture grown on polylysine-laminin, 22 days after plating.

The earlier experiments described in this chapter (section 7.4) used microcultures grown on polylysine and ECM, while the later experiments (section 7.5) used cultures grown on polylysine-laminin. Although polylysine-laminin cultures were slightly less

---

[1]The silastic peels off surprisingly easily, in a single piece, provided that the coverslip has not been cleaned. A thin film of oil or some other contaminant is apparently left on the coverslips during their manufacture; if this film is removed by cleaning, the silastic adheres too tightly to the glass and cannot be peeled off.

healthy than ECM cultures, and had fewer synaptic connections (see section 7.4), they had less fluorescent background, and could be prepared much more easily and consistently.

Fig 7.3 shows a microculture grown on polylysine-laminin, 22 days after plating. This island shows some common features of these microcultures: phase-bright cell bodies, an extensive network of thin axon-like processes, and a large fascicle that runs around the perimeter of the island. Also common (though not seen in this island) are short, thick, dendrite-like processes, which extend from the cell bodies. Microcultures grown on polylysine, ECM, and polylysine-laminin all had the same general morphology, though there were slight differences between substrates, particularly in the degree of fasciculation.

7.4 INTRACELLULAR PHYSIOLOGY

Excitatory synapses were very common in these SCG microcultures. Preliminary experiments characterized the synaptic physiology of these cultures by penetrating pairs of neurons with intracellular electrodes, stimulating the cells one at a time, and recording any resulting excitatory postsynaptic potentials (EPSPs).

Fig 7.4 shows recordings made from two microcultures grown on ECM. Fig 7.4a shows recordings from two cells in a five-cell island. Stimulating cell 2 gave a very complex pattern of synaptic activity, including two suprathreshold PSPs in cell 1 and a suprathreshold PSP in cell 2. This activity was completely suppressed by perfusing in a 300 µM concentration of the nicotinic antagonist hexamethonium, and returned when the drug was washed out.

In order to map the synaptic connections of a microculture, it is important to be able to distinguish between monosynaptic connections (a direct synapse A->B) and polysynaptic connection (an indirect connection A->C->B through another cell C, with A->C a suprathreshold connection). A complete characterization of the monosynaptic PSPs defines the connectivity of the culture; polysynaptic connections are merely results of the direct synapses.

a) five-cell island

b) one-cell island

before

before

1

2

$|20\,mV$

300 μM hex

100 μM hex

1

2

after

after

1

2

20 ms

20 ms
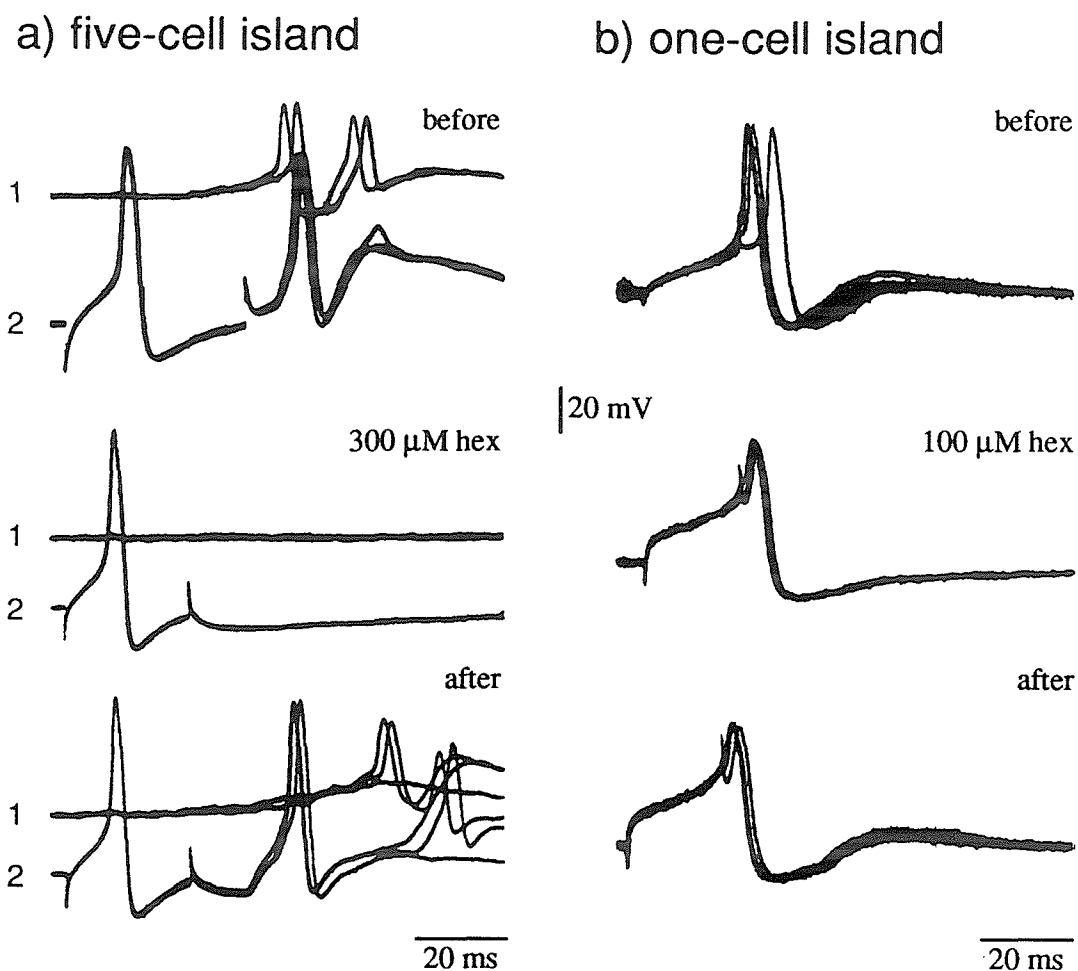
Figure 7.4 Synaptic physiology of SCG microcultures grown on ECM. *a)* Recordings from two cells in a five-cell island, 52 days after plating. The three panels show responses to stimulation of cell 1 before, during, and after application of 300 μM hexamethonium. Each panel shows three traces taken at 0.2 Hz. *b)* Recording from the cell in a one-cell island, 36 days after plating. The panels show responses to stimulation of the cell before, during, and after application of 100 μM hexamethonium. Each panel shows four traces taken at 0.2 Hz. All traces in all six panels have the same vertical scale.

Since only two cells were monitored in the five-cell island of Fig 7.4*a*, it is not possible to distinguish unequivocally between monosynaptic and polysynaptic PSPs. One possible criterion is PSP failure (PSPs that sometimes do not appear): polysynaptic PSPs are likely to fail occasionally, when an intervening connection falls below threshold. PSPs that never fail are most likely monosynaptic, while those that fail even occasionally must be polysynaptic. For instance, the earliest PSP in cell 1—the PSP that began 10 ms after the

peak of cell 2's first AP—was always present and so was most likely monosynaptic. Definitive classification of PSPs as monosynaptic or polysynaptic requires a partially blocking concentration of hexamethonium to bring all PSPs below threshold, coupled with simultaneous recording from all cells in the island (*e.g.,* with voltage-sensitive dyes) to confirm that the stimulated cell is the only cell firing.

Fig 7.4*b* shows recordings from the only cell in a single-cell island. Stimulation of the cell revealed an autapse—a synapse that the cell made on itself—which was evident as a distortion of the normal shape of the AP's afterhyperpolarization. This bump was indeed a cholinergic PSP, as shown by its disappearance upon the application of 100 μM hexamethonium, and its subsequent reappearance upon washing out the drug.

Table 7.1 summarizes the results of similar experiments that tested five islands grown on ECM for 26 to 52 days in culture (including the two shown in Fig 7.4), and seven islands grown on polylysine for 17 to 27 days in culture.

	substrate	
	ECM	polylysine
a) islands tested	5	7
b) days in culture	26-52	17-27
c) cells per island	1-5	1-15
d) islands with PSPs	5	5
e) pairs tested	3	12
f) definitely monosynaptic PSPs	2	4
g) presumed monosynaptic PSPs	1	3

Table 7.1 Incidence of synaptic connections in microcultures grown on ECM and polylysine. *d* counts all islands where PSPs were seen, whether monosynaptic or polysynaptic. *f* and *g* count only monosynaptic PSPs.

For the purposes of this table, PSPs were counted as monosynaptic if they satisfied one of two criteria. (1) In islands with one or two neurons, any PSP was counted as definitely monosynaptic (line *f*), whether it was an autapse or a synapse between different cells. It is impossible to have a polysynaptic chain with fewer than three cells! (2) In

larger islands, PSPs that occurred repeatedly with no evidence of failure were presumed to be monosynaptic (line *g*). This no-failure rule is only circumstantial, since a polysynaptic chain with very strong suprathreshold links might never fail, and so be mistaken for a direct connection.

All five islands grown on ECM showed synaptic connections of some sort, *i.e.*, connections seen with two electrodes, or returning activity seen with a single electrode. Three pairs of cells were tested by penetrating both cells; all three pairs were connected monosynaptically. Two of the three pairs had reciprocal connections, while the third pair was only connected in one direction. In addition, the one single-cell island tested showed an autapse (Fig 7.4*b*), which was of course monosynaptic.

Five of seven islands grown on polylysine showed some synaptic activity. Seven of twelve pairs tested showed presumptive monosynaptic PSPs in at least one direction. No autapse was seen in the one single-cell island tested. The incidences of synaptic connections listed as Table 7.1*d, f*, and *g* are only lower limits, since not every cell was penetrated, and some responses could not be classified as due to monosynaptic or polysynaptic connections.

The vast majority of connections seen in these cultures were fast EPSPs; electrical synapses were occasionally seen, but were very rare. These EPSPs were presumably cholinergic: hexamethonium reduced or eliminated the PSPs in the four islands tested. PSP amplitudes varied from about 1 mV (near the limit of detection) to well above threshold. These synapses fatigued quickly: small PSPs decreased in size unless stimulation rates were held below 0.1 Hz or even .01 Hz, while even the strongest suprathreshold PSP fell below threshold after a few hundred firings. At room temperature, synaptic latencies (measured from the peak of the presynaptic AP to the onset of the PSP) varied from 5-30 ms. These long latencies presumably reflected propagation delays in the small unmyelinated axons. Synaptic connections were seen in microcultures as soon as 11

days after plating; cultures younger than this were not studied because the cells were too small for intracellular penetration.

The frequency of synaptic connections seen in cultures grown on polylysine-laminin was somewhat lower than for ECM or polylysine. One set of dye-recording experiments used 24 polylysine-laminin islands, grown for 14 to 64 days in culture. Of eleven single-cell islands, three showed autapses; of thirteen multi-cell islands, PSPs were seen in seven.

Though the number of cultures tested is small, this difference between substrates seems to be real. The incidence of synaptic connections seemed to correlate with the health of the culture; islands with healthy-looking, smooth, round neurons were more likely to show PSPs. Cultures grown on polylysine-laminin usually seemed to deteriorate after about four weeks in culture, and the highest incidence of synapses was seen with cultures that were two or three weeks old.

7.5 DYE RECORDINGS FROM MICROCULTURES

7.5.1 Introduction

The previous two sections discussed the general behavior and synaptic physiology of microcultures; this section illustrates the dye recordings that can be obtained from them.

The goal of dye recording from microcultures is synaptic mapping, *i.e.*, determination of the complete matrix of N^2 connections in an N-cell island. The main advantage of dyes over intracellular electrodes is that they can record simultaneously from all the cells in an island. Simultaneous recording is useful at two levels of sensitivity: that sufficient for detecting APs, and that sufficient for PSPs.

If dye recording can detect APs, it can be used in conjunction with pairwise intracellular penetrations to determine whether observed PSPs are monosynaptic or polysynaptic. In a strongly-connected culture, this determination is impossible with

intracellular electrodes alone; see Fig 7.4. (In a *very* strongly connected culture, even detection of all APs may not be enough, and it may be necessary to reduce PSPs below threshold using drugs.) Complete mapping of an island in this way is quite tedious, requiring many repetitive penetrations.

If dye recording can detect postsynaptic potentials as well as APs, it can be used in conjunction with a single intracellular electrode to completely map a culture. Each cell is penetrated once and stimulated with the glass electrode, and dye signals reveal its synaptic outputs. This method requires only six penetrations for a six-cell island (one per cell).

Unfortunately, for SCG microcultures only APs can be detected reliably in the dye signal, because signals from neurites obscure the subthreshold signals from cell bodies. Synaptic mapping thus requires pairwise intracellular penetrations in conjunction with dye recording. Subsection 7.5.2 shows data recorded from a single-cell island; this simplest of microcultures is the best for detailed study of the dye signals from neurites. Subsection 7.5.3 shows intracellular and dye signals from a strongly connected five-cell island. This island was partially mapped using pairwise intracellular penetrations; a partial synaptic matrix is shown. Though PSPs cannot be detected *reliably* with dye recording, they can be seen in favorable cases that have no obscuring signals from neurites. Subsection 7.5.4 shows an optically recorded PSP from such a case. Subsection 7.5.5 summarizes the results of dye recordings from 24 microcultures grown on polylysine-laminin.
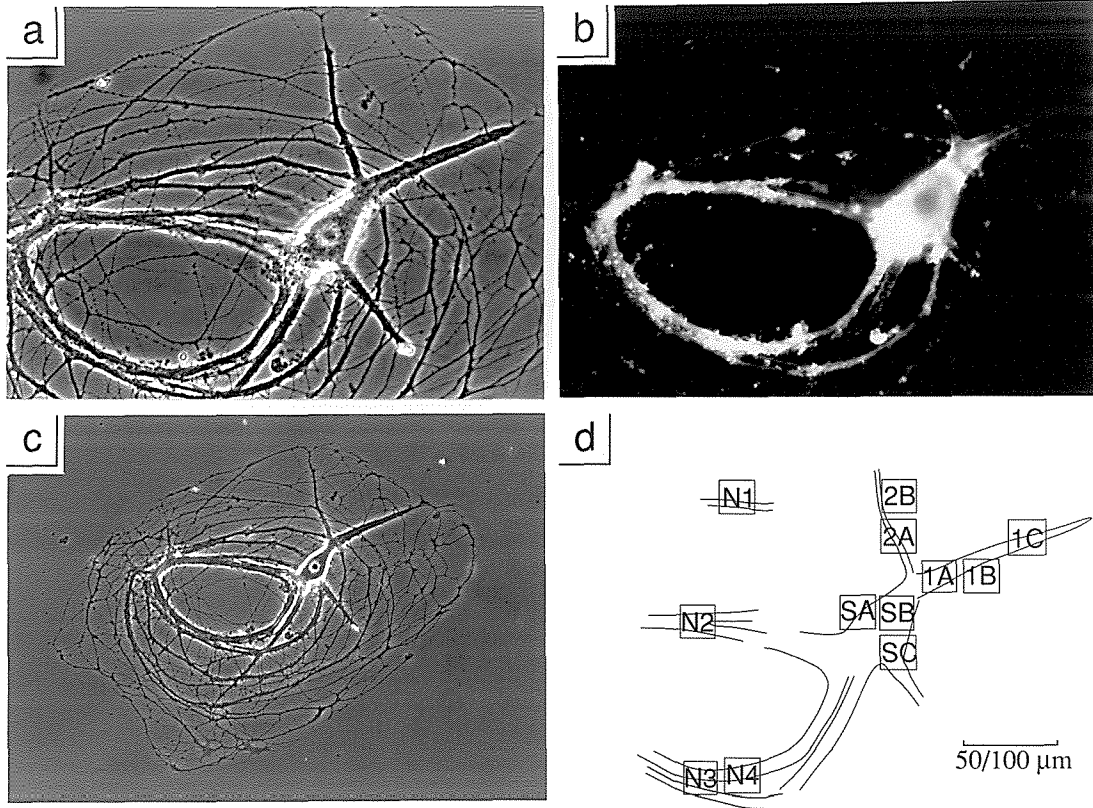
Figure 7.5 Four views of a single-cell microculture, grown on polylysine-laminin for 21 days in culture. *a*) Phase-contrast, 40x objective. *b*) RH423 fluorescence, 40x (focussed on the plane of the processes). *c*) Phase-contrast overview, 20x. *d*) Culture schematic, made by tracing stored video image. *Squares* show the locations of pixels used for dye recording: over the soma (*S1-S3*), presumptive dendrites (*1A-1C, 2A-2B*), and thinner neurites (*N1-N4*). The *scale bar* represents 50 μm for *a*, *b*, and *d*, 100 μm for *c*.

7.5.2 One-cell island

Fig 7.5 shows phase contrast and fluorescence micrographs (*a*, *b*, and *c*) of a single-cell island, and a culture schematic (*d*) showing the locations of 12 pixels from which dye signals were recorded. Several short thick dendritelike processes are seen in phase contrast; dye signals were recorded from presumptive dendrites 1 and 2 (pixels 1A-1C, to the upper right of the soma; pixels 2A-2B, above the soma). The fluorescent membrane staining of RH423 shows the presumptive dendrites as unfilled cylinders; notice

that process 1 seems to be *two* dendrites side-by-side. The island also has a complex network of fine neurites, presumably branched and fasciculated axons; dye signals were recorded from four pixels over this network (N1-N4). Finally, three pixels were chosen over the cell soma (SA-SC). Brightly-stained debris was attached to some parts of the network, and some dye entered the cell during the experiment (the fluorescence picture was taken after all dye recording was done).

After the culture was stained for 7 min with 2 μM RH423, the neuron was penetrated intracellularly, stimulated, and dye signals recorded from the twelve pixels shown (because the island was small, a 40x objective replaced the normal 20x). An average of the data from four trials is shown in Fig 7.6. The dye signals fall into two main classes: those from the soma and presumptive dendrites (SA-SC, 1A-1C, 2A-2B), and those from thick fascicles (N2-N4).

Soma and dendrites. Consider first the dye signals from the soma and dendrites. These have two phases: an early response before the peak of the intracellular AP, and a late response after the peak. The early responses follow the intracellular potential quite well: they all show an initial slow rise during the first part of the stimulus, before the cell passes above threshold, followed by a fast rise once the cell crosses threshold. The initial peaks of the optical signals lag the peak of the intracellular AP by 0.5-1.0 ms; this delay is probably attributable to the time constants of the optical detector's preamplifiers. The late responses deviate significantly from the potential measured by the intracellular electrode: some pixels show late peaks, while others have shoulders following the initial peak. These late responses are probably due to APs propagating in axons that curve back over the cell body and dendrites.

Fascicles. Consider next pixels N2 through N4, which cover fascicles. Their dye signals all show a single peak, with the characteristic shape of a propagating AP (somewhat broadened). Since these pixels cover a length of axon, and also cover many axons whose propagation velocities may differ, some broadening is expected. The peaks of pixels N2,

N3, and N4 lag the peak of the intracellular AP by about 3 ms. (The delay cannot be specified more accurately without carefully accounting for the time constants of the particular preamplifiers used.)
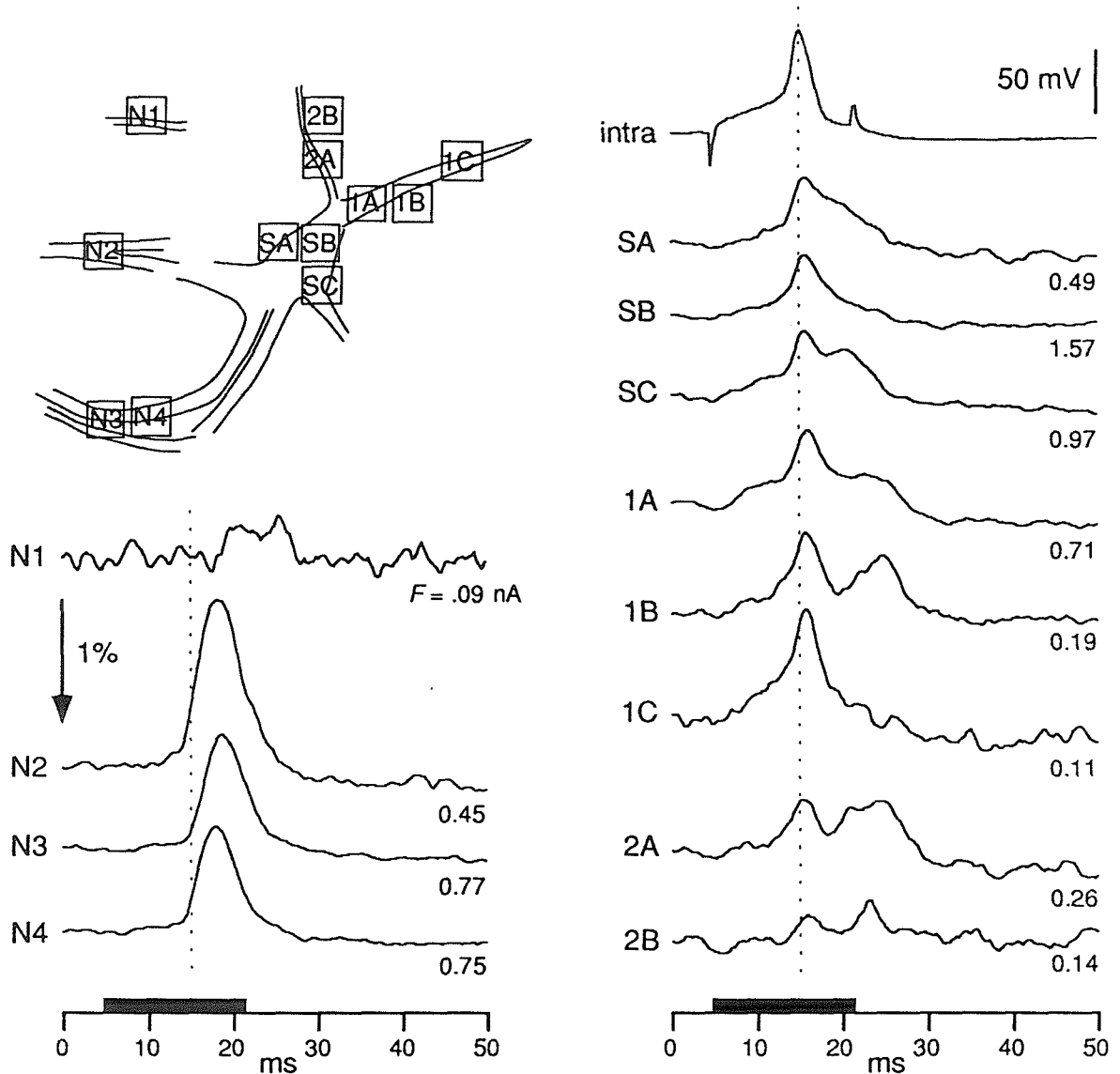
Figure 7.6 Dye recording from a single-cell island; average of four successive stimuli. The *culture schematic* shows pixel locations. The membrane potential from the intracellular electrode is labelled *intra*. Optical signals ($\Delta F/F$, filtered and bleach-subtracted) are labelled on the *left* by pixel, and on the *lower right* by the photocurrent (F, in nA) from that pixel. The *arrow* is the scale for all optical traces; it shows a 1% increase in fluorescence. The *solid bars* on the time axis show the period of intracellular current injection; the *dotted line* is drawn through the peak of the intracellular AP.

Pixel N1. Pixel N1 covers several thin processes in the periphery of the network. Its dim fluorescence means that its signal is quite noisy, but there is a small bump— between 3 and 13 ms after the peak of the intracellular AP— which repeated from trial to trial. This bump is presumably the sum of several small AP signals with different propagation delays.

Sensitivity. The variations in signal size from pixel to pixel correspond well with the amount of background seen in Fig 7.5*b*. Pixel N2 has less background fluorescence than N3 and N4, and has a correspondingly larger signal. The pixels over the cell body show a fair amount of background fluorescence, and have correspondingly mediocre signals.

Summary. When this cell is stimulated, one expects its soma and dendrites to respond essentially simultaneously (the dendrites are quite short and should be electrotonically very close to the soma). The action potential should then spread out through the branching axonal network at some finite velocity (for these small unmyelinated axons, the propagation velocity should be quite small). Thus, the expected signature of a dye signal from the soma or a dendrite is a peak simultaneous with the intracellular AP, while the signature of an axonal signal is a delayed peak. These predictions fit the observed dye signals very well, allowing for the axons that curve back over the cell body and dendrites.

This explanation was further tested by injecting a hyperpolarizing current pulse into the cell (data not shown), which hyperpolarized it by about 30 mV. Averaging 4 trials with this hyperpolarization, distinct dye signals were seen in pixels SA-SC and 1A-1C, no signal was seen in N2-N4, and the results from N1, 2A, and 2B were inconclusive. One expects that the injected current should hyperpolarize the soma and the electrotonically-close dendrites, but not the axons. The signals from SA-SC, 1A-1C, and N2-N4 match these predictions well. (Pixels N1, 2A, and 2B were quite dim, so their signals were noisy and no conclusion could be made.)
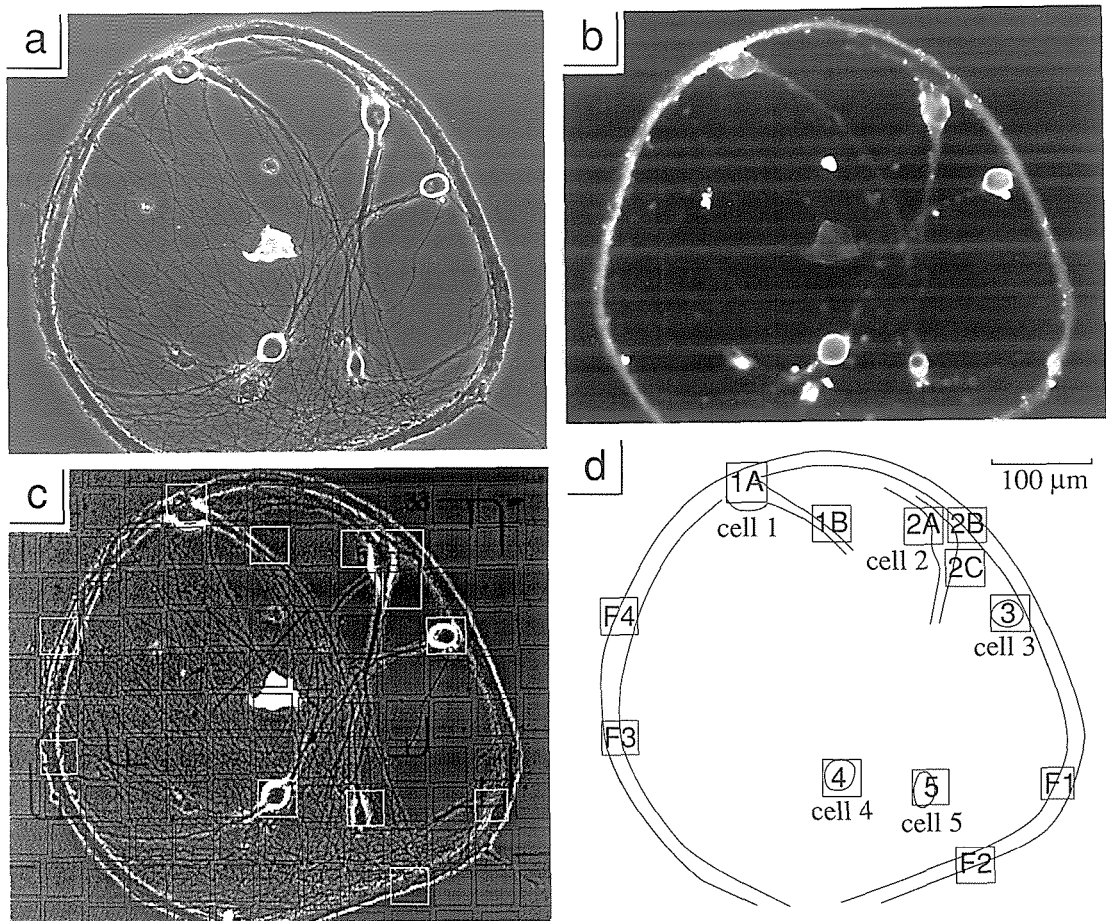
Figure 7.7 Four views of a five-cell microculture, 21 days after plating on polylysine-laminin. *a)* Phase-contrast. The irregular object in the center is a piece of debris. *b)* RH423 fluorescence (focussed on the cell bodies, as for dye recording). *c)* Stored video image. *White squares* show selected pixels; *dark squares* show unused pixels. *d)* Culture schematic, made by tracing the video image. Cells 1 through 5 are numbered. *Squares* show the locations of pixels used for dye recording: over the cell bodies (*1A, 2A-2C, 3-5*), presumptive dendrite (*1B*), and girdling fascicle (*F1-F4*).

7.5.3 Five-cell island

Fig 7.7 shows phase contrast and fluorescence micrographs (*a* and *b*) of a five-cell culture, and a culture schematic (*d*) showing the 12 pixels from which dye signals were recorded. It also shows the video picture (*c*) from which the culture schematic was traced. (Fig 7.5*d* was traced from a similar video picture.) These cells do not have such prominent dendritelike processes as the cell of Fig 7.5, but they do have a distinct
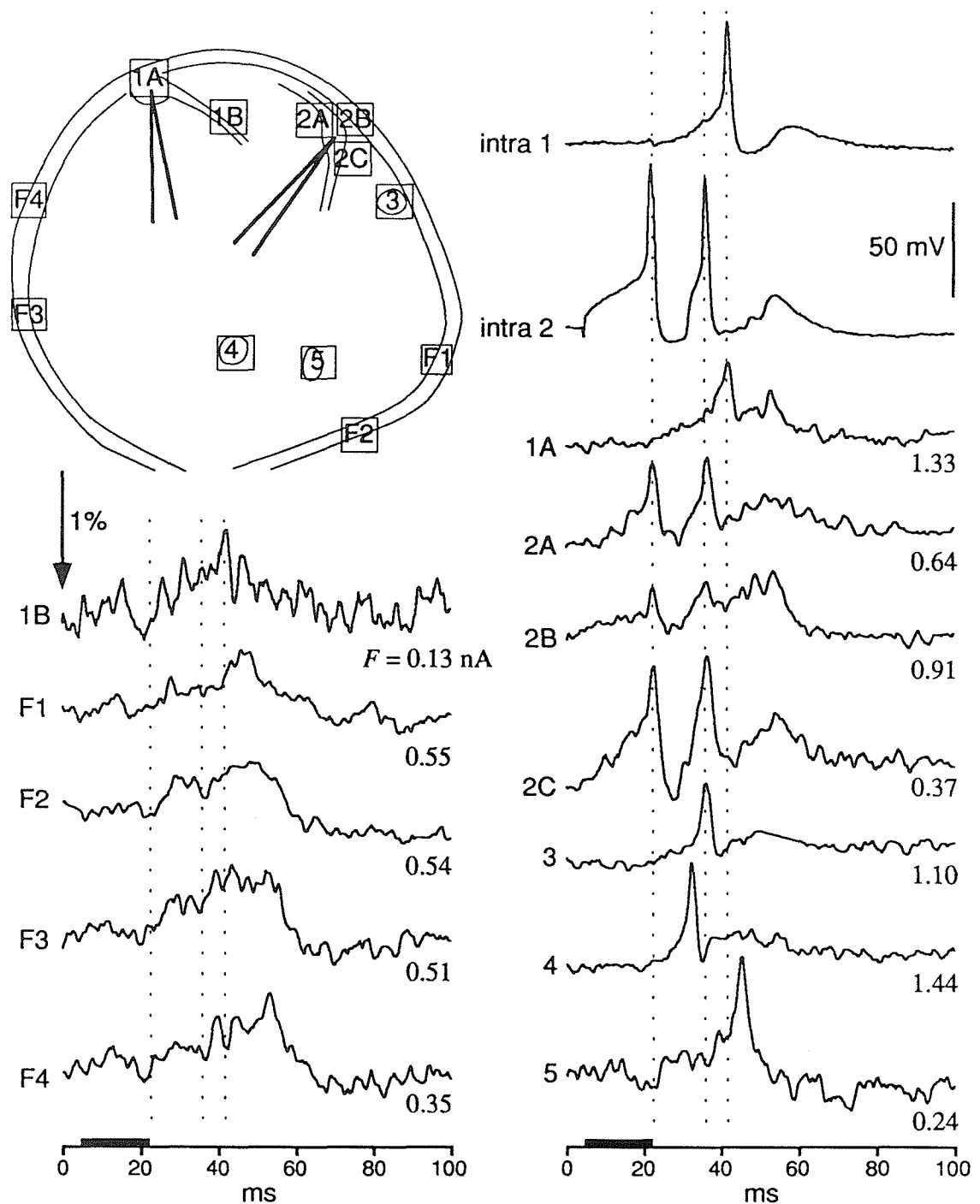
Figure 7.8 Dye recording from a five-cell island, showing a single trial (no signal-averaging) during which cell 2 was stimulated. The *culture schematic* shows pixel locations. Cells 1 and 2 were penetrated intracellularly; their membrane potentials are labelled *intra 1* and *intra 2* (the 50 mV scale bar applies to both). Optical signals ($\Delta F/F$, filtered and bleach-subtracted) are labelled on the *left* by pixel, and on the *lower right* by the photocurrent (F, in nA) from that pixel. The *arrow* is the scale for all optical traces; it shows a 1% increase in fluorescence. The *solid bars* on the time axis show the period of intracellular current injection; the *dotted lines* are drawn through the peaks of the three APs recorded intracellularly from cells 1 and 2.

perimeter fascicle over which four pixels (F1-F4) were chosen. Seven of the other pixels (1A, 2A-2C, 3-5) were chosen over cell bodies, and the last (1B) was chosen over cell 1's presumptive dendrite. Cells 1 through 4 showed nice rings of staining, but cell 5 filled with dye during the experiment.

After the culture was stained for 8 min with 2 µM RH423, the following pairs of neurons were penetrated, changing pairs by moving one electrode at a time: (1,2), (3,2), (3,4), and (2,4). For every pair, each neuron was stimulated several times, and the resulting dye signals recorded. Fig 7.8 shows a data set taken while cells 1 and 2 were penetrated, and cell 2 stimulated. The responses can be divided into signals from processes, and signals from cell bodies.

Processes. When cell 1 was stimulated intracellularly, the signal in pixel 1B was less than 0.2% (data not shown), so not much signal is contributed by the presumptive dendrite under this pixel, if it is indeed a dendrite. The general shapes of the signals shown here for pixels F1-F4 and 1B—broad humps lasting about 30 ms—were repeated from trial to trial, and presumably represent sums of several APs with different latencies. These signals are too small and complex to be interpreted in terms of specific neuronal firing patterns.

Cell bodies. All of the pixels over cells 1 and 2 show clear peaks corresponding to the intracellularly-recorded APs; in 2A and 2C, these optically-recorded APs are clearly distinguishable above the signals from passing axons. Cells 3 and 4 also showed large signals; intracellular penetrations later confirmed that these signals indeed reflected APs in their respective cells. Cell 5 shows a large dye signal in this figure, but was never penetrated. This peak in cell 5 never repeated, and so probably represents a synaptic potential that was just barely suprathreshold for this trial, and fell below threshold later.

Thus, the dye signals from cell bodies are good indicators of APs in those cells. They are, however, poor indicators of subthreshold responses: compare the late PSPs recorded intracellularly from cells 1 and 2 with the corresponding dye signals. Again, this

lack of correspondence between optical and intracellular recording seems to be due to signals from passing axons. The signal from pixel 2B, which straddles the perimeter fascicle, is particularly muddied.

It is clear that this culture was very strongly connected. Later stimulations of cell 2 gave similar sets of dye signals, except that the synapses gradually fatigued so there were fewer suprathreshold responses. Stimulation of cells 1 and 3 gave no obvious dye signals (*i.e.*, no suprathreshold responses) in cells other than the cell directly stimulated. Stimulation of cell 4 gave APs in cells 2, 3, and 4 (the latter two probably due to polysynaptic connections through cell 2).

The combination of intracellular and dye recording can usually determine which PSPs are monosynaptic. The intracellular recordings give detailed information about synaptic responses, while the dye signals give detailed timing for APs in other cells. For instance, looking at the intracellular data in Fig 7.8, consider the PSP that starts at 28 ms in cell 1. The directly-stimulated AP in cell 2 peaks at 22 ms; the next cell to fire is cell 4, whose AP peaks at 32 ms. Since cell 2 is the only cell to fire before the PSP, the PSP must be due to a monosynaptic connection 2->1.

Similar information was obtained by intracellularly penetrating the pairs (3,2), (3,4), and (2,4). Figure 7.9 shows a summary of the connections in this island. Definite absence or presence of a connection (*PSP* or *no PSP*) was usually established from combined intracellular and dye signals. Connections labelled *not supra* showed no suprathreshold PSP; connections labelled with a question mark were not tested.

PSP matrix entries signify PSPs seen intracellularly or (if suprathreshold) with dyes, and confirmed to be monosynaptic using dye signals for AP timings. The above argument for the existence of the connection 2->1 is an example. PSPs have not been classified as sub- or suprathreshold because there was significant synaptic fatigue during the experiment.

postsynaptic cell

	1	2	3	4	5
1	no PSP	no PSP	not supra	not supra	not supra
2	PSP	PSP	PSP	PSP	not supra
3	not supra	no PSP	no PSP	no PSP	not supra
4	not supra	PSP	no PSP *	no PSP	not supra
5	?	?	?	?	?

presynaptic cell

Figure 7.9 Summary of monosynaptic connections mapped in the five-cell island of Fig 7.7. *Solid boxes* indicate pairs tested with intracellular penetration; for *dashed boxes*, at least one cell of the pair was not penetrated. *PSP* and *no PSP* indicate the confirmed presence or absence of the synapse. *not supra* indicates that no dye signal was visible in the postsynaptic cell when the presynaptic cell fired. Cell 5 was never penetrated, and so its outputs were not determined (*question marks*). See text for explanation of the connection 4->3.

No PSP entries indicate that when the pair was penetrated intracellularly, stimulating the presynaptic cell gave no PSP in the postsynaptic cell. The "no" for 4->3 comes with a reservation. When this connection was tested by penetrating both cells and stimulating cell 4, there *was* a very late PSP in cell 3. Since cell 2 fired before this PSP, and from other evidence 2 is known to synapse on 3, this PSP was presumably due to the disynaptic connection 4->2->3; however, it is possible that this PSP included a contribution from a direct connection 4->3.

No supra entries indicate that when the presynaptic cell was fired, no suprathreshold PSP was seen in the dye signal. These connections might have existed nonetheless, since subthreshold PSPs were not visible in the dye signal.

Question marks indicate a complete lack of knowledge. Since cell 5 was never penetrated, its outputs were never tested. In a single trial (that of Fig 7.8), cell 5 showed a suprathreshold PSP in the dye signal; however, this input could not be assigned to a particular cell.

To sum up: though synaptic potentials were not visible in the dye signals, this culture could be synaptically mapped by combining dye recording with pairwise electrode penetrations (the map is only partial because not all possible pairs were penetrated). Four out of five synapses detected were outputs from cell 2, and the complex pattern of activity seen in Fig 7.8 seems to be mostly due to these outputs.

7.5.4 Optically-recorded PSPs

In the five-cell experiment of the last subsection, PSPs could not be detected optically at the cell bodies, since they were obscured by signals from propagating APs. This example does not show that PSPs can *never* be detected, only that they cannot be detected reliably. Fig 7.10 shows an example of an optical recording of a PSP.

A five-cell island, grown on polylysine-laminin for 20 days, was stained for 6 min with 2 μM RH423, and then cells 1 and 3 were penetrated. Stimulation of cell 1 resulted in two superimposed PSPs in cell 3, indicated by arrows in Figs 7.10*a* and *b*. These PSPs were sometimes subthreshold (*a*), and sometimes summed to fire the cell (*b*). Dye signals from the other three cells suggested that the first PSP was due to a direct connection 1->3, while the second was disynaptic: 1->2->3. The optical signals from pixels 3R and 3L reproduced quite faithfully the intracellular recording from cell 3. There are some small deviations between the dye and intracellular signals: for instance, in Fig 7.10*a* the optical
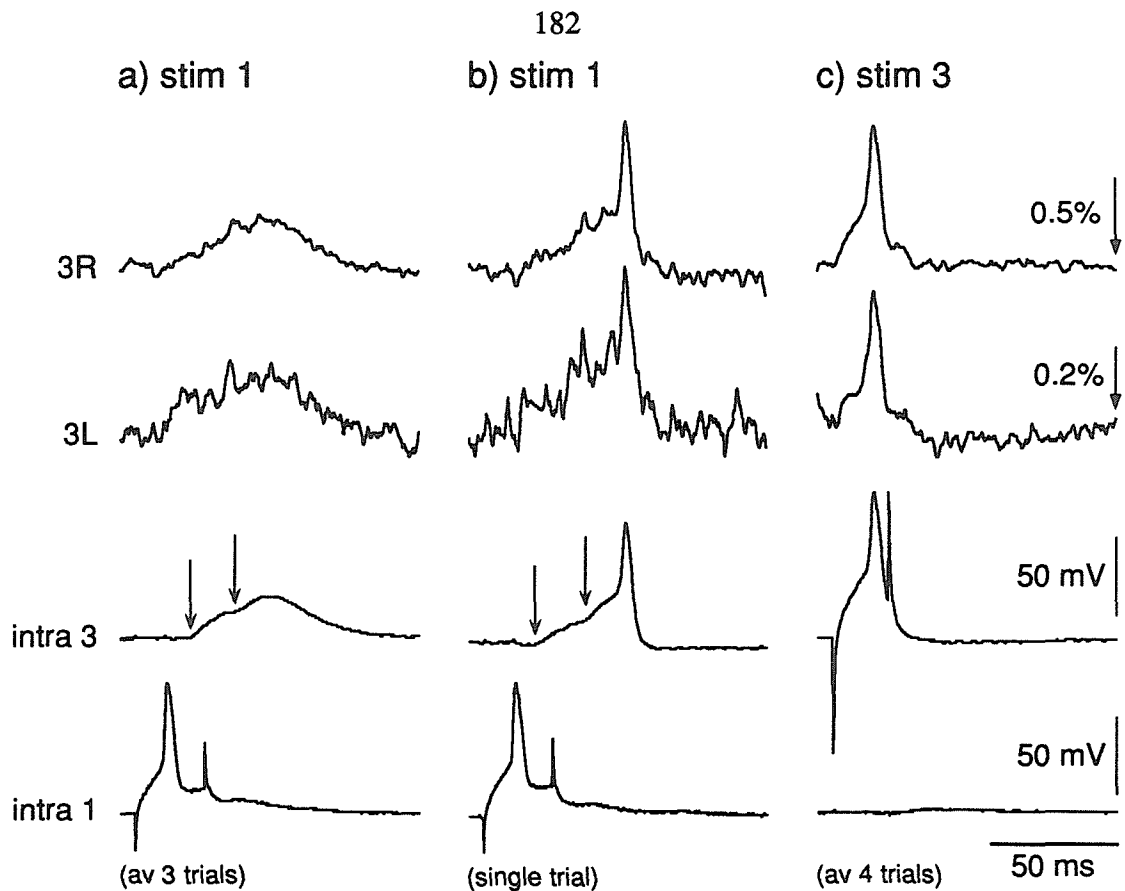
Figure 7.10 Optical recordings of PSPs from a five-cell island, grown in culture for 20 days on polylysine-laminin. Cells 1 and 3 were penetrated intracellularly; their membrane potentials are labelled *intra 1* and *intra 2*. Optical signals ($\Delta F/F$, filtered and bleach-subtracted) are shown from two pixels over the soma of cell 3. Pixel *3R* had photocurrent F=0.75 nA; *3L* had F=0.58 nA. The scale bars apply to all three panels. The four *arrows* indicate the onsets of PSPs in cell 3. *a)* Stimulating cell 1, subthreshold PSP in cell 3 (average of 3 trials). *b)* Stimulating cell 1, suprathreshold PSP in cell 3 (single unaveraged trial). *c)* Stimulating cell 3 directly (average of 4 trials).

signal in 3L starts rising before the first PSP in cell 3. These small deviations are plausibly explained as dye signals from propagating APs.

7.5.5 Summary of microculture recordings

The three microcultures described in the last three subsections displayed the complete range of dye signals seen in microculture experiments. Three main conclusions about dye recording from microcultures can be drawn:

- Action potentials can be detected reliably from cell bodies.

- Action potentials can be detected in presumptive dendrites and axons. Dendrites show an early component of the dye signal, which is simultaneous or nearly simultaneous with the intracellular AP; signals from axons, showing a propagation delay, lag the intracellular AP. Pixels over axons sometimes show distinct peaks from propagating APs, but complex signals—presumably the sum of many APs—are more common. Pixels over cell bodies and dendrites also show complex delayed signals, presumably due to APs propagating in axons that pass through them.

- Synaptic potentials cannot be detected reliably with dye recording in these microcultures. There is sufficient sensitivity to detect large PSPs in cell bodies, but the dye signals from PSPs are often obscured by complex signals from axons that pass through the pixel.

These three conclusions are confirmed by dye recordings taken from 24 islands grown on polylysine-laminin. Of 49 cells penetrated, 46 showed a clear dye signal in the cell body when stimulated. Of 31 pixels that covered presumptive dendrites, 29 showed dye signals simultaneous with the intracellular AP of the corresponding cell. Of 45 pixels that covered axons, 39 gave clear dye signals (single peaks, multiple peaks, or complex signals) upon stimulation of the culture.

7.6 DISCUSSION

7.6.1 Microculture substrates

In order to replace the finicky collagen-dot microculture system of Furshpan (Furshpan et al., 1976), I developed several different procedures (section 7.4) using a pattern of silastic adhesive to define the boundaries of the microculture islands. Masking or liftoff, as appropriate, is used to pattern one of the four substrates collagen, polylysine, BEC extracellular matrix, or polylysine-laminin. ECM (patterned by masking) and

polylysine (patterned by liftoff) were the most successful substrates. Microcultures grown on ECM were the healthiest, and seemed to have more synapses, but polylysine-laminin had less fluorescent background, and was much more convenient to apply. Cultures grown on polylysine-laminin were chosen for routine work; they were quite healthy when used in the first four weeks of culture. The liftoff process is quite general, and should be applicable to nearly any substrate; it would be interesting to try collagen again, patterning it by liftoff.

7.6.2 Microculture electrophysiology

Under the appropriate culture conditions, SCG neurons undergo a transmitter changeover, becoming cholinergic and forming synapses with each other; indeed, such synapses were the first clue to the phenomenon of transmitter changeover (O'Lague et al., 1974). Other groups have seen extensive neuron-neuron synapses in SCG microcultures: Furshpan et al. (1986) reported that cholinergic autapses were common in single-neuron microcultures grown on islands of heart cells, and Higgins et al. (1984) reported seeing cholinergic synapses in microcultures grown on collagen dots. The intracellular-electrode experiments of section 7.5 merely confirm that cholinergic synapses occur frequently under the present culture conditions, and to characterize the properties of the PSPs. In four cultures, the nicotinic antagonist hexamethonium was used to confirm the cholinergic nature of the PSPs; thereafter, all PSPs were assumed to be cholinergic.

Synaptic connections were less common in cultures grown on polylysine-laminin than for those grown on polylysine alone or ECM; this may reflect the fact that the polylysine-laminin cultures started to deteriorate after about four weeks, and sometimes were assayed past their peak, or it may signal a more significant effect of substrates on transmitter changeover. Such an effect would not be without precedent (Hawrot, 1980).

The study of Higgins et al. showed a high incidence of electrical synapses, which was due to the serum-free medium used (see also Higgins and Burton, 1982). The

presence of electrical synapses in addition to chemical synapses would considerably complicate the microculture-mapping experiments, but under the conditions of the present study, the incidence of electrical synapses (defined operationally as nonfatiguing reciprocal synapses that pass hyperpolarizing currents) was very low, perhaps a few percent.

7.6.3 Dye signals from processes

Due to considerations of membrane area, I originally expected that dye signals might be visible from dendrites, but certainly not from axons. That dye signals from processes are significant is the most surprising result of these microculture experiments. In these cultures, a typical cell body is about 30 μm in diameter, and a typical dendritelike process is about 5 μm in diameter. The axons cannot be resolved with light microscopy, but in the electron micrographs of SCG microcultures shown by Furshpan *et al.* (1986), the axons have a typical diameter of about 0.5 μm. The fluorescence values of Fig 7.6 show that pixels over the fascicles give nearly as much fluorescence as pixels over the cell body. This must be due to the large number of axons that make up any given fascicle.

It seems eminently reasonable to assume that RH423 molecules are equally voltage-sensitive whether they are in axonal, dendritic, or somatic membrane. Further, section 6.6 showed that RH423 fluorescence signals are linear in membrane potential. Therefore, the dye signal from a pixel should reflect the weighted average of the membrane potentials of the various cell compartments within that pixel, with weights roughly proportional to membrane area. This is impossible to check directly except for the cell body, since most processes are too small to be penetrated intracellularly. The best that can be done is to check the dye signals against the predictions of basic electrophysiology.

The cell body should of course have a membrane potential equal to that measured by the intracellular electrode. Pixels over cell bodies showed a signal that followed the intracellular potential, sometimes followed by delayed signals that were presumably due to background neurites.

For axons, the action potential should propagate through with some delay after the cell body fires. Indeed, pixels over thin neurites (presumptive axons) consistently showed delayed signals only. In some cases (*e.g.*, Fig 7.6), these signals had the distinctive shapes of propagating APs. In other cases, they had more complex shapes, presumably due to the sum of several different APs. Hyperpolarization of the cell body should have no effect on the axon, except for segments very close to the cell body. In experiments where the cell body was hyperpolarized, pixels over thin neurites showed no signal.

Short dendrites should have membrane potentials essentially identical to the the cell body potential. Signals from pixels over presumptive dendrites (short thick processes) usually showed an early component that rose simultaneously with the intracellular action potential, and a delayed component with a complex shape. The early component was never seen in pixels over thin neurites, while the delayed component was similar to signals from pixels over thin neurites; therefore the early component comes from the dendritelike process, and the late component comes from thin background neurites. In several experiments, hyperpolarization of the cell body gave dye signals in pixels over dendritelike processes. These results from firing and hyperpolarizing the cell body both confirm that the short thick processes are electrotonically close to the cell body. This constitutes electrophysiological evidence that these processes are indeed dendrites, though they could equally well be proximal axon segments.

Furshpan *et al.* (1986) used electron-micrographic serial-sectioning and reconstruction to show that the short, thick neurites seen in phase contrast have dendritic ultrastructure, and that the other thin neurites have axonal ultrastructure. They found synapses only on the cell body and presumptive dendrites, never on presumptive axons. It is thus not surprising that the dye signals seen from presumptive dendrites and presumptive axons are just those expected from true dendrites and true axons.

7.6.4 Microculture dye recording

The goal of developing dye-recording for SCG neurons was to synaptically map SCG microcultures. Intracellular electrodes are inadequate for two reasons: they cannot simultaneously monitor more than two or three neurons, and repeated intracellular penetrations damage cells. The first problem could be solved by reliable optical detection of action potentials; the second, by reliable optical detection of synaptic potentials.

On these microcultures, dye recording can detect APs reliably, but not PSPs. Based on the sensitivity of RH423 (typically 1%/100 mV) and the noise level of the present optical apparatus (about .03% for a typically-stained cell body), one would expect to detect APs from cell bodies, and with a little averaging, PSPs as well. APs were indeed detected reliably from nearly all cells tested, but PSPs were detected optically in only one or two cases; they were usually masked by AP signals in axons that passed back over the cell body.

It is clear that dye recording would be much more useful, for studying either synaptic connections or cable properties, if only the anatomy of the microcultures were not so complex. The main problems are the sheer length of the axons, and the thick fascicles they form. If the axons were shorter, and fascicles did not curve back over the soma and dendrites, PSPs could be detected optically in the soma, and optical signals from the different processes could be distinguished. It might be possible to manipulate the axonal arbor by changing substrates, but under all microculture conditions in which SCG neurons have grown well, I have found that the total length of axon per cell is clearly many millimeters. This is not surprising when it is remembered that the axons of SCG neurons *in vivo* must run at least the distance from the rat's neck to its eye (the iris muscle of the eye is one of the targets of the SCG), a distance of several millimeters. A different cell type that put out less exuberant processes in culture should be much more amenable to experimentation.

CHAPTER 7 REFERENCES

E. J. Furshpan, P. R. MacLeish, P. H. O'Lague, and D. D. Potter (1976) Chemical transmission between rat sympathetic neurons and cardiac myocytes developing in microcultures: Evidence for cholinergic, adrenergic, and dual-function neurons. *Proc. Natl. Acad. Sci. U. S. A.* **73**:4225-4229.

E. J. Furshpan, S. C. Landis, S. G. Matsumoto, and D. D. Potter (1986) Synaptic functions in rat sympathetic neurons in microcultures. I. Secretion of norepinephrine and acetylcholine. *J. Neurosci.* **6**:1061-1079.

E. Hawrot (1980) Cultured sympathetic neurons: Effects of cell-derived and synthetic substrata on survival and development. *Dev. Biol.* **74**:136-151.

D. Higgins and H. Burton (1982) Electrotonic synapses are formed by fetal rat sympathetic neurons maintained in a chemically-defined culture medium. *Neuroscience* **7**:2241-2253.

D. Higgins, L. Iacovitti, and H. Burton (1984) Fetal rat sympathetic neurons maintained in a serum-free medium retain induced cholinergic characteristics. *Dev. Brain Res.* **14**:71-82.

P. H. O'Lague, K. Obata, P. Claude, E. J. Furshpan, and D. D. Potter (1974) Evidence for cholinergic synapses between dissociated rat sympathetic neurons in cell culture. *Proc. Natl. Acad. Sci. U. S. A.* **71**:3602-3606.

P. H. Patterson and L. L. Y. Chun (1977) The induction of acetylcholine synthesis in primary cultures of dissociated rat sympathetic neurons. I. Effects of conditioned medium. *Dev. Biol.* **56**:263-280.

Chapter 8
Conclusions

The aim of this work was to develop an apparatus for recording with voltage-sensitive dyes from cultured mammalian neurons, and explore how this technique could be used to map out the synaptic connections of microcultures—small, isolated networks of cultured neurons. Using this apparatus and the optimized dye-recording conditions which were developed for rat superior cervical ganglion (SCG) neurons, it should be possible under favorable conditions to detect changes in membrane potential as small as 5 or 10 mV; this sensitivity is quite sufficient for synaptic mapping. Unfortunately, conditions are rarely favorable in SCG microcultures; the axons run everywhere, and dye signals from axons that pass back over the cell body usually obscure any subthreshold signals that might otherwise be seen. It would be very interesting to use this apparatus on a microculture system that had less profuse axons and fewer axon fascicles.

8.1 SUMMARY

Good system design is especially important for a dye-recording apparatus: since the desired signals are usually quite close to the noise, it is important not to add unnecessary illumination or dark noise. The apparatus described here was designed for recording from rat SCG neurons in culture. It usually uses the 546 nm line of a stabilized mercury arc for illumination, a Nikon 20x objective (0.75 numerical aperture), a 610 nm longpass emission filter, discrete photodiode detectors (pixel size 45 μm at the specimen), and preamplifiers with 6 GΩ feedback resistors. Under these conditions, the illumination intensity at the specimen is approximately 10 W/cm^2, and a typical SCG neuron stained with the fluorescent dye RH423 gives a detected photocurrent of 1 nA. With a bandwidth

of 300 Hz, the shot noise in such a photocurrent is .03% rms, compared to illumination noise of .02% rms from the stabilized mercury arc (not counting large slow fluctuations that can be rejected), and amplifier noise of .008% rms.

The system design was successful: the signal-to-noise ratio is shot-noise limited, which is the best that can be done. The major improvements over previous systems were the feedback regulator for the mercury arc lamp, the fiber-optic camera detector, and the paired-FET input stage for the preamplifiers.

Two theoretical questions important for the dye-recording technique are discussed: the relative advantages of fluorescence and absorption, and the dependence of illumination intensity and collection efficiency on the numerical aperture of the microscope objective. Appendix B derives a general formula for comparing the signal-to-noise ratios for fluorescence and absorption; fluorescence is favored for preparations that absorb only a small fraction of the incident light when stained. The staining level at which fluorescence and absorption give equivalent signal-to-noise levels is determined by the voltage sensitivities of the particular dye, its quantum yield for fluorescence, and the relative detection efficiencies for the two modes. For the SCG neurons used here, fluorescence is clearly preferred. Using theoretical arguments as well as direct measurements, Appendix C shows that illumination intensity and collection efficiency are proportional to the square of the numerical aperture (Grinvald *et al.*, 1983) only under certain ideal conditions; in general, these quadratic dependences are only very approximate.

An extensive series of experiments found the best conditions for dye-recording with optimal signal-to-noise ratio. In an initial screening, approximately 25 styryl dyes were tested for staining and voltage sensitivity; the best four dyes were RH237, RH421, RH423, and di-4-ANEPPS. These four dyes were tested with different emission and excitation filters; for all four, it was found that narrowband excitation (520-550 nm, mostly the 546 nm mercury line) and broadband emission (610 nm longpass) gave the best results. The results of these filter experiments were inconsistent with a purely

electrochromic mechanism for these dyes. RH423 was chosen (somewhat arbitrarily) for routine use. Staining experiments showed that serum-containing medium bound RH423 and could remove dye from already-stained cells; thus, it is important to wash cultures thoroughly before staining. Upon close examination, a day's presoak in serum-free medium—which we earlier reported to enhance staining (Chien *et al.*, 1987)--proved to be unnecessary. Dye recordings from freshly-plated, neuriteless SCG neurons showed that the fluorescence signals from RH423 are linear over a range of more than 100 mV.

Several different methods were developed for patterning microculture substrates into islands. The most reliable deposits a polylysine-laminin substrate on top of a pattern of silastic adhesive, then removes unwanted substrate by peeling off the silastic. SCG microcultures on polylysine-laminin islands grew routinely for four weeks in culture, and developed extensive cholinergic synapses. (Microcultures grown on polylysine alone or extracellular matrix made by bovine endothelial corneal cells had a somewhat higher degree of connectivity, but were not as reliable.)

After the apparatus and dye-recording conditions were developed, they were used to record dye signals from SCG microcultures while individual neurons were stimulated intracellularly. After such careful system design and optimization of dye-recording conditions, it was ironic that the limits of detection were set not by technical factors, but by the preparation itself. At .03% rms shot noise for a typical cell, the system is theoretically capable of optically detecting large postsynaptic potentials (PSPs). In practice, it can easily detect action potentials in cell bodies, but not subthreshold PSPs. In the complex anatomy of these microcultures with their dense nets of axons, optical signals from action potentials propagating in returning axons usually confuse or obscure any signals from subthreshold PSPs.

These cultures can be synaptically mapped using an intracellular electrode to stimulate the presynaptic neurons, another intracellular electrode to record any postsynaptic activity, and dye recording to monitor the firing of other cells. Dye recording and an

extracellular stimulating electrode would not, however, be sufficient, and so SCG microcultures are not suitable for chronic experiments that follow long-term changes in synaptic connectivity.

8.2 FUTURE TECHNICAL IMPROVEMENTS

The signal-to-noise ratio of this dye-recording system is already quite high enough, and does not need to be increased. In fact, if only action potentials are to be detected, the illumination level could be safely reduced by a factor of ten. There are always technical improvements to be made, of course; some are listed below. Improvements in dye sensitivity or collection efficiency would be particularly useful, since they would allow a lower illumination level (and lower phototoxicity) for the same signal-to-noise ratio.

Dyes. The single most fruitful improvement would be a large increase in dye voltage sensitivity. Large signals were occasionally seen with RH423: often as large as 2%/100 mV, once even 7%/100 mV. If these large signals indeed reflect variations in background fluorescence rather than some perverse variation in intrinsic voltage sensitivity, it is tantalizing to speculate about the source of this background and ways to eliminate it. Background dye could be bound to membrane fragments, proteins on the extracellular surface of the cell, or some other site, but these possibilities are very hard to test by eye or with a fluorescence micrograph. It would be interesting to dye-record from several cells, then measure their fluorescence quantitatively at high spatial resolution, perhaps with a confocal microscope. It might also be possible to synthesize new, more sensitive dyes, but it is difficult to design for higher sensitivity when the potentiometric mechanism is not understood. The level of dye staining probably cannot be increased further, since the present staining protocol already gives a molar fraction of dye of the order of 1% (Appendix A). Less phototoxic dyes would also be useful; low phototoxicity might be more amenable to rational structural design, since it only depends on interaction of the dye molecule with a single oxygen molecule, rather than a complex lipid membrane.

Illumination. No increase in illumination intensity is needed (it would raise phototoxicity to undesirable levels), but a more stable light source would be useful. These might be achieved by improving the feedback regulator as described in Chapter 4.

Objective lens. For fluorescence, any increase in collection efficiency is always useful. The present 20x air objective has a numerical aperture of 0.75, and so collects 9% of the light from an isotropic source in water. Though less convenient, a glycerine- or water-immersion lens would give a higher numerical aperture; better air objectives might also be developed in the future.

Detector. The fiber-optic camera with discrete photodiodes has three advantages over a photodiode array: the pixel number can be scaled up more easily, making electrical connections to the photodiode leads easier, and since any photodiode can be used, the photodiodes can be picked for low noise and low capacitance. It has two disadvantages: it has greater dead space (especially for circular fibers), and requires tricky optical joints from fibers to photodiodes. Though the fiber-optic camera was the optimal solution when this detector was built, it may soon be overtaken by large photodiode arrays or fast charge-coupled devices. Centronics is currently building a 400-pixel photodiode array for Larry Cohen (H. Orbach, personal communication).

Amplifiers. The main problems with the present preamplifiers—crosstalk and gain peaking—are second-order effects that should be solved by a better layout of the printed circuits. Their noise is quite low enough, and in fact in the next generation of amplifiers, it might be best to lower the feedback resistors to 1 GΩ, reducing the effects of stray capacitance at the cost of an increase in Johnson noise.

8.3 FUTURE MICROCULTURE EXPERIMENTS

Since the present experiments are limited by the characteristics of the culture rather than technical considerations, it would be very interesting to study microcultures of other neuronal cell types. Pyramidal neurons from the hippocampus would be particularly

interesting, since the hippocampus is widely thought to be important for long-term memory, and in other contexts (*in vivo* and in hippocampal slices), these neurons are known to show a very interesting form of synaptic change, long-term potentiation (MacNaughton and Morris, 1987). Indeed, Bonhoeffer *et al.* (1989) have dye-recorded from (mass) organotypic cultures of hippocampal neurons. Though some of their dye signals are rather puzzling, they interpret them as reflecting synaptic changes.

In preliminary experiments (data not shown), I have grown hippocampal neurons in microculture, and Wade Regehr measured dye signals from a few of these cells. Two prerequisites need to be established before proceeding with synaptic-mapping experiments.

First, hippocampal microcultures should be checked to see that their anatomy is simpler than that of SCG microcultures: in particular, the cell bodies should be clearly separate from the network of axons. At least superficially, mass cultures of hippocampal cultures look promising in this respect. This separation is clearly important for dye recording of PSPs without interference from axonal signals. Further, a clear separation might make it possible to stimulate the cell body with an extracellular electrode, rather than an intracellular electrode. For SCGs (data not shown), extracellular stimulation was not effective, since nearby axons usually fired before the chosen cell body did. A combination of reliable extracellular stimulation with dye recordings that could detect PSPs would completely obviate the need for intracellular penetrations, thus making long-term plasticity experiments much more practical.

Second, hippocampal microcultures should be studied thoroughly with intracellular recording before extensive optimization of dye recording. It is quite possible that synaptic changes could be seen in two- or three-cell cultures using intracellular electrodes. (Thinking about the SCG microcultures in hindsight, a demonstration of synaptic plasticity with intracellular electrodes would have made the lengthy development of dye recording much more interesting!) If synaptic changes were found with two or three neurons, it

would be very interesting to use dye recording to scale up to larger microcultures, and to

perform chronic synaptic mapping experiments to look for long-term changes.

CHAPTER 8 REFERENCES

T. Bonhoeffer and V. Staiger (1988) Optical recording with single cell resolution from monolayered slice cultures of rat hippocampus. *Neurosci. Lett.* **92**:259-264.

T. Bonhoeffer, V. Staiger, and A. Aertsen (1989) Synaptic plasticity in rat hippocampal slice cultures: Local "Hebbian" conjunction of pre- and postsynaptic stimulation leads to distributed synaptic enhancement. *Proc. Natl. Acad. Sci. U. S. A.* **86**:8113-8117.

C.-B. Chien, W. D. Crank, and J. Pine (1987) Noninvasive techniques for measurement and long-term monitoring of synaptic connectivity in microcultures of sympathetic neurons. *Soc. Neurosci. Abstr.* **13**:1426, abstr. #393.15.

A. Grinvald, A. Fine, I. C. Farber, and R. Hildesheim (1983) Fluorescence monitoring of electrical responses from small neurons and their processes. *Biophys. J.* **42**:195-198.

B. L. MacNaughton and R. G. M. Morris (1987) Hippocampal synaptic enhancement and information storage within a distributed memory system. *Trends Neurosci.* **10**:408-415.

Appendix A
Theory of voltage-sensitive dyes

A.1 INTRODUCTION

It would be extremely useful to understand how voltage-sensitive dyes do their job. A theoretical understanding of mechanisms of voltage-sensitivity could lead to rational design of more sensitive dyes; similarly, an understanding of bleaching and phototoxicity could lead to new dyes that bleached less and were less toxic. Within the more limited scope of this thesis (which does not include any organic synthesis), some understanding of how dyes work is useful for understanding the relative merits of absorption dyes and fluorescence dyes (Appendix B), for trying to optimize dye sensitivity by choosing excitation and emission filters (Chapter 6), and for trying to understand phototoxicity (Chapter 6).

This appendix discusses what is known about the mechanisms of voltage-sensitive dyes in general, and about styryl dyes in particular. (All of the dyes used in this thesis are styryls.) The discussion concentrates on mechanisms of staining and of voltage sensitivity. There is little knowledge about the mechanisms of bleaching and phototoxicity, and so these are not discussed.

First, section A.2 describes the phenomenon of fluorescence (absorption is covered along the way), and defines basic spectral quantities such as the extinction coefficient and quantum yield. Section A.3 is a quick survey of the known potentiometric mechanisms for both absorption and fluorescence dyes. Section A.4 discusses styryl dyes in particular: their staining properties, and the mechanism by which they are thought to work (electrochromism).

For a good introduction to fluorescence microscopy in general, see Taylor and Salmon (1989); for a more sophisticated treatment of the phenomenon of fluorescence, see Loew (1988a). For reviews of dye mechanisms, see Waggoner and Grinvald (1977), Waggoner (1979), or Loew (1988b).

A.2 FLUORESCENCE

There are many ways to calm an excited molecule; for our purposes, fluorescence is the most interesting. A molecule that absorbs a photon may become excited and undergo a transition from its ground electronic state to its first excited electronic state. If it returns to the ground state by emitting a photon within about 1-100 ns, the phenomenon is called fluorescence. (Slower emission is called delayed fluorescence or phosphorescence.)

Besides electronic states, the molecule also has vibrational and rotational states, as well as interactions with solvent molecules. As shown in Fig A.1a, these additional
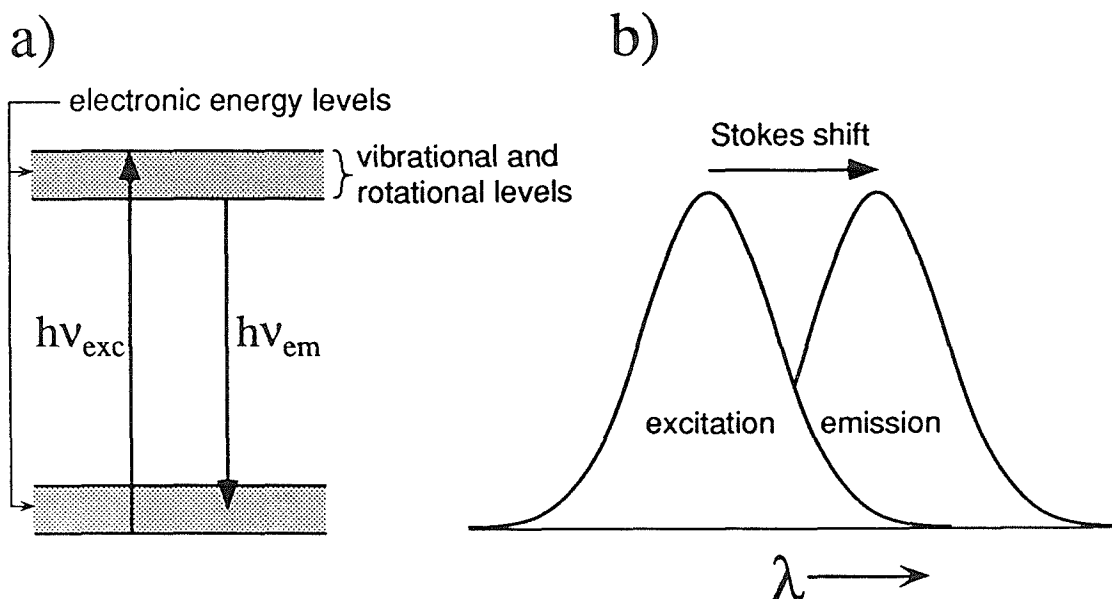
Figure A.1 *a)* Energy-level diagram for fluorescence. Upon excitation, the molecule absorbs a photon and goes from its ground state into its first electronic excited state. It then loses vibrational and rotational energy before emitting a photon and returning to the ground state. *b)* The Stokes shift. The loss of vibrational and rotational energy before fluorescence shifts the emission spectrum to longer wavelengths (lower energies).

interactions smear the electronic energy levels into bands, so that the absorption and emission spectra of the molecule are broad peaks rather than sharp lines. They are also responsible for the *Stokes shift*. When the molecule absorbs a photon, it typically picks up vibrational and rotational energy as well as entering an electronic excited state. This vibrational and rotational energy is rapidly lost through nonradiative interactions, so that by the time the molecule fluoresces, the transition energy is less than the energy initially absorbed. This results in an emission spectrum redshifted with respect to the excitation spectrum, as shown in Fig A.1*b*. This Stokes shift is very important for practical applications of fluorescence, since it allows emitted light to be separated from exciting light by the use of colored filters.

Polarization is important both for excitation and for emission. For any chromophore (the part of a dye molecule that interacts with light), there is a transition moment associated with the transition from the ground state to the first excited state. Linear molecules such as the styryl dyes used in this thesis usually have transition moments that are roughly parallel to the long axis of the molecule. Intuitively, this means that when the molecule absorbs a photon, the resulting redistribution of its electric charge occurs mainly along its length. A chromophore only absorbs light with a component polarized parallel to its transition moment. This is easy to understand for a linear chromophore: the electric field must be oriented to push the molecule's charge along its length. If a chromophore is illuminated with plane-polarized light whose electric field is at an angle θ to the transition moment, the resulting absorption will be proportional to $\cos^2\theta$.

Similarly, the polarization of a fluoresced photon will be parallel to the molecule's transition moment for emission. If the fluorescence is observed through a plane polarizer oriented at an angle θ to the transition moment, the detected fluorescence will again be proportional to $\cos^2\theta$. The transition moments for absorption and emission are parallel, except for unusual molecules. (If the molecule is in solution, however, it may have time to

rotate before it emits a photon, so that the transition moment for emission is no longer parallel to the original transition moment for absorption.)

It is useful to define here two parameters: the quantum yield, which I will call q (Φ is also common), and the extinction coefficient, ε. The quantum yield, a measure of how efficiently the molecule fluoresces, is defined simply as the average number of photons emitted per photon absorbed. Useful fluorophores have quantum yields greater than .1; a good fluorophore might have $q=.5$. The extinction coefficient is a measure of how efficiently the molecule absorbs light. For a sample of concentration c and path length l illuminated with intensity I_0, the extinction coefficient is defined by

$$\varepsilon c l = OD = \log_{10}(I_0/I)$$

where the optical density OD is defined as the logarithm of the fraction of light I/I_0 that is transmitted by the sample. ε has the dimensions of an area, and is usually given in units of $M^{-1}cm^{-1}$; good chromophores have extinction coefficients of about $10^5\ M^{-1}cm^{-1}$. (By multiplying by the natural logarithm of 10 and applying Avogadro's number, ε may be translated into a cross section: for instance, $10^5\ M^{-1}cm^{-1}$ corresponds to a cross section of $3.8\ \text{Å}^2$.)

A.3 POTENTIOMETRIC MECHANISMS

The task of sorting out potentiometric (voltage-sensing) mechanisms has not been an easy one: there is a huge range of dye structures, and many possible mechanisms. Dye sensitivities vary drastically between preparations (*e.g.*, Ross and Reichardt, 1979), and also between biological preparations and the model systems used for studying potentiometric mechanisms (Loew *et al.*, 1985). The experiments necessary for testing potentiometric mechanisms are complex and lengthy, and so the theoretical understanding of dyes has always lagged behind the experimental cycle of syntheses and trials that has constantly produced new dyes.

Just as new dyes have only been synthesized by a few groups, dye mechanisms have only been extensively studied by a few groups, mainly the laboratories of Alan Waggoner and Leslie Loew. The potentiometric mechanisms for several different types of dyes have been understood (at least for model systems) and fall into three general classes: redistribution, reorientation, and electrochromism. The specific causes of bleaching and phototoxicity, on the other hand, are not understood to any significant degree.

This section first discusses the model membrane systems and types of experiments used to test various potentiometric mechanisms, and then describes the three known mechanisms.

A.3.1 Model systems

Ideally, dye mechanisms would be studied using real biological preparations. Unfortunately, these are technically intractable, and artificial membrane systems must be used instead. Two different systems are widely used: solutions of phospholipid vesicles, and hemispherical lipid bilayers.

Vesicle solutions are used to study *steady-state behavior:* how the dye binds to the membrane, whether it forms dimers or higher-order aggregates, and its absorption and fluorescence spectra in the membrane. These measurements are usually made by mixing a dye solution with a suspension of phosphatidylcholine vesicles; the optical properties of the resulting suspension of stained vesicles can be conveniently measured in a spectrophotometer.

A dye's absorption spectrum typically shifts when it binds to a membrane or binds to another dye molecule to form a dimer; also the fluorescence of dimers is often strongly quenched. Vesicle experiments can measure the spectra of aqueous, membrane-bound, and dimerized dye, as well as measuring the relative proportions of each of these forms.

Hemispherical bilayers are used to study *voltage-dependent behavior:* the action spectra of voltage-dependent absorption and fluorescence changes, and voltage-dependent

changes in membrane binding. A hemispherical bilayer is basically a half-bubble of oxidized cholesterol blown on the end of a tube, with saline both inside and out. The voltage across the membrane can be easily changed, since the inside of the tube provides access to one side of the membrane, and the bathing solution provides access to the other. Voltage-dependent optical signals are then studied by illuminating part of the bubble with a laser, and measuring the transmitted or fluoresced light.

In order to elucidate the potentiometric mechanism of a dye, it is essential to know the action spectra and polarization dependence of the voltage-sensitive signals. (An action spectrum is simply a plot of signal size versus excitation or emission wavelength.) Voltage-dependent absorption signals are due to changes in the dye's absorption spectrum. For a redistribution mechanism, for instance, the voltage change might push membrane-bound dye molecules off the membrane, into aqueous solution, thus changing the overall absorption spectrum. If the spectra of aqueous and membrane-bound dye are known from vesicle measurements, this model makes a specific prediction about the action spectrum of the absorption signals. Thus, measurements of the action spectrum with a hemispherical bilayer may support or rule out a particular mechanism.

Voltage-dependent fluorescence signals may be due to changes in the dye's absorption spectrum, fluorescence spectrum, or quantum efficiency. For fluorescence dyes, then, there are two sorts of action spectra: one for which the exciting wavelength is varied, and another for which the observed emission wavelength is varied. With both fluorescence dyes and absorption dyes, knowing the action spectrum is essential not only for understanding the dye's mechanism, but also for picking a set of filters that will give the largest optical signals.

Reorientation mechanisms may depend on the dye reorienting within the membrane, rather than moving between membrane and aqueous solution. To test these, part of a hemispherical bilayer is illuminated with polarized light. If the illuminated area is sufficiently small, it will be nearly planar, and effects of dye orientation will be easy to see.

Conclusions from these artificial systems must be drawn with some care, since they differ significantly from real membranes. Biological membranes usually contain both phosphatidylcholine and cholesterol, along with other phospholipids and membrane proteins; their inner and outer leaflets are also known to have distinct compositions (Op den Kamp, 1979).

A.3.2 Known potentiometric mechanisms

The three potentiometric mechanisms that have been reasonably well established are redistribution, reorientation, and electrochromism. Fig A.2 schematizes each mechanism, and shows exemplary dyes that have been shown to operate by each mechanism in a model system. All three are further explained below. For a fast voltage-sensitive dye to be useful, its signal must be rapid and linear in membrane voltage. Therefore, the speed of response and linearity for the mechanisms are mentioned where known.

Redistribution. Redistribution is the mechanism for membrane-impermeant oxonols such as the one shown, the absorption dye RGA461 (George *et al.*, 1988a,b; Nyirjesy *et al.*, 1988). RGA461 is thought to operate by the "on-off" mechanism shown in Fig A.2*a*. The dye exists in equilibrium between two pools, one membrane-bound and the other aqueous. When the potential inside the bilayer is lowered, the negatively charged dye is driven off; if the potential is raised, the dye is pulled on. The dye's absorption spectrum differs between the membrane and aqueous solution, so this voltage-dependent redistribution causes an absorption change. The size of the absorption signal depends on the average membrane potential, since this determines the amount of dye that is bound.

These studies by Waggoner's group showed that the signals from RGA461 are linear over 500 mV (George *et al.*, 1988b); however, they did not measure its response to rapid voltage changes. Waggoner *et al.* (1977) showed that *permeant* cyanine and oxonol dyes operate by a similar on-off mechanism. They measured response times for the absorption changes of these dyes, and found them to be less than 10 µs.

a) redistribution

RGA461
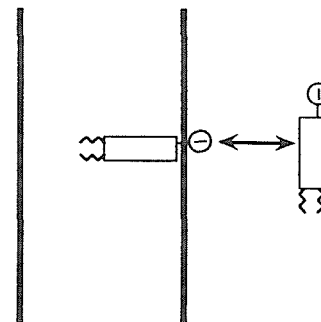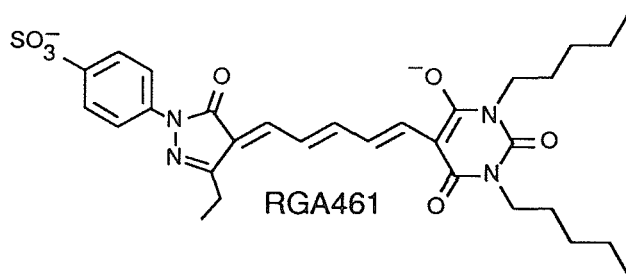
b) reorientation
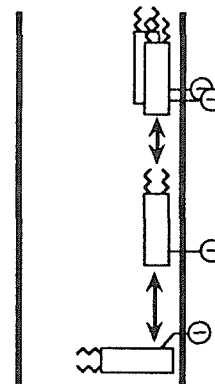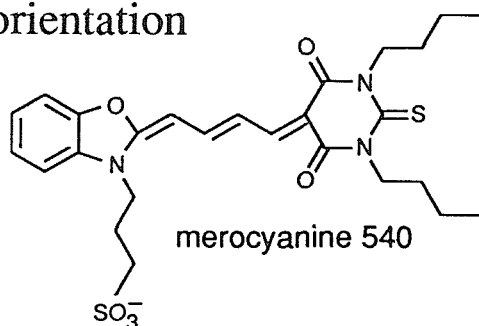
merocyanine 540

c) electrochromism

di-4-ANEPPS
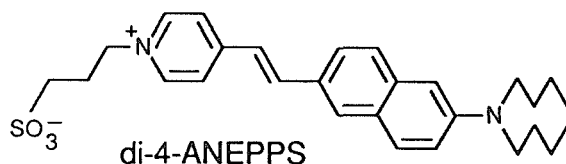
no movement

$$h\Delta\nu = \Delta\mathbf{p} \cdot \Delta\mathbf{E}$$

Figure A.2 The three established potentiometric mechanisms, and the structures of dyes which obey them. *a)* RGA461, an impermeant oxonol dye, works by redistribution. *b)* Merocyanine 540, a merocyanine dye, works by reorientation. *c)* Di-4-ANEPPS, a styryl dye, works by electrochromism. The equation is explained in the text (boldface denotes vectors). Sources for structures: RGA461 (George *et al.*, 1988a); merocyanine 540 (Waggoner, 1979); di-4-ANEPPS (Fluhler *et al.*, 1985). Diagrams adapted from George *et al.* (1988a) and Wolf and Waggoner (1986).

Reorientation. The fluorescence dye merocyanine 540 was one of the first dyes that gave large signals, and its mechanism has been studied the most extensively of any voltage-sensitive dye (*e.g.*, Dragsten and Webb, 1978; Wolf and Waggoner, 1986). It is thought to operate by the reorientation mechanism shown in Fig A.2*b*. The dye exists in three forms: dimers, and monomers oriented either parallel or perpendicular to the plane of the

membrane. When the membrane potential changes, some of the dye molecules rotate from a parallel to a perpendicular position; this rotation has two effects on the dye fluorescence. The first is to break up dimers, which fluoresce much less than monomers. The second is to rotate the transition moments of the dyes, so that they respond differently to different polarizations. In an anisotropic cell, such as a long cylindrical axon, this rotation can contribute to fluorescence changes, even when illuminating with unpolarized light (Dragsten and Webb, 1978).

In their early studies on squid giant axon, Cohen *et al.* (1974) found that the fluorescence signals from merocyanine 540 (which they then called "dye I") were linear over 200 mV. They measured its response time at 13°C to be 30 µseconds; at 26°C, the response was too fast for them to detect.

Electrochromism. Many styryl dyes (all of them used in fluorescence) have been synthesized by Amiram Grinvald's group and by Loew's group. Rina Hildesheim in Grinvald's laboratory synthesized styryls by the traditional method of picking new structures by trial and error; some of these, most notably RH421, gave extremely large signals on mouse neuroblastoma cultures (Grinvald *et al.*, 1983). The styryl dyes designed by Leslie Loew, including di-4-ANEPPS, are unique in having been consciously designed to operate by a specific mechanism: electrochromism. Loew's group has shown that several of these dyes are indeed electrochromic in the artificial hemispherical bilayer system (Loew *et al.*, 1979; Loew and Simpson, 1981; Fluhler *et al.*, 1985). See the next section for a description of their behavior on the squid giant axon.

For an electrochromic (Stark shift) mechanism, the dye molecule does not change its absorption or fluorescence spectra by moving between two different environments or orientations. Instead, the change in electric field acts directly on the dye molecule, changing the relative energies of the ground and excited states of the molecule, and thus shifting the excitation and emission spectra. Take Δp as the difference between the dye's dipole moment in its first excited state and its ground state (**boldface** denotes a vector).

This includes any movement of net charge as the dye moves between the two states, as well as any changes in polarization. If the dye is subjected to a change in electric field ΔE, then the voltage-dependent shift in exciting or emitting frequency, Δv, is given by $h\Delta v = \Delta E \cdot \Delta p$. Loew's dyes were designed to maximize Δp by having a large charge shift between the ground state and first excited state.

The linearity of these dyes has not been tested extensively, but on HeLa cells di-4-ANEPPS is approximately linear over 200 mV (Ehrenberg et al., 1987). Theoretically, electrochromism should be faster than other mechanisms, since it only involves electronic rearrangements, not molecular movement. The response of di-6-ASPPS has been measured on the squid giant axon, and is faster than 1.2 µs (Loew et al., 1985). In practice, however, all three mechanisms are capable of microsecond response times, which are more than fast enough for neurobiology.

One of Loew's original motivations in designing electrochromic dyes was the hope that since the mechanism was intrinsic to the dye molecule and didn't depend on interactions with the surrounding membrane, electrochromic dyes might give uniform signals across preparations. Alas, this has not proved to be true. When some of these styryls were tested on squid giant axon (Loew et al., 1985), their sensitivity was much lower than in the artificial bilayer system, partly due to high background staining. The sensitivity of di-6-ASPPS was about 0.1%/100 mV, compared to 2%/100 mV for the artificial bilayer. Even worse, the action spectra no longer looked perfectly electrochromic. Conversely, when RH421 was tried on hemispherical bilayers during the same set of experiments, its action spectrum looked electrochromic, but its sensitivity was only 5%/100 mV, compared to the 21%/100 mV that had been reported on neuroblastoma cells (Grinvald et al., 1983). In other experiments by Loew's group, however, di-4-ANEPPS has shown good sensitivity across several widely different preparations (Gross et al., 1986).

A.4 PROPERTIES OF STYRYL DYES

Since the dyes used in this thesis were all styryls, it is worth describing at some length their membrane-binding, spectroscopic, and voltage-sensing properties. These biophysical properties have been characterized by Leslie Loew's group (Loew et al., 1979; Loew and Simpson, 1981; Fluhler et al., 1985; Loew et al., 1985), from whose papers the parameters quoted here have been taken. Many different styryls have been synthesized, both by Loew's group (Hassner et al., 1984; Fluhler et al., 1985) and by Amiram Grinvald's group (Grinvald et al., 1982, Grinvald et al., 1983; Grinvald et al., 1987).

Fig A.3 shows the structures of RH421, RH423, di-4-ANEPPS, and di-6-ASPPS. The first three have all been tested for the experiments described here (see Chapter 4); RH423 was chosen and used for most of the experiments. RH421 and di-4-ANEPPS have given large signals on other preparations (see section 2.3.3), and Loew's group has studied the properties and potentiometric mechanisms of di-4-ANEPPS and di-6-
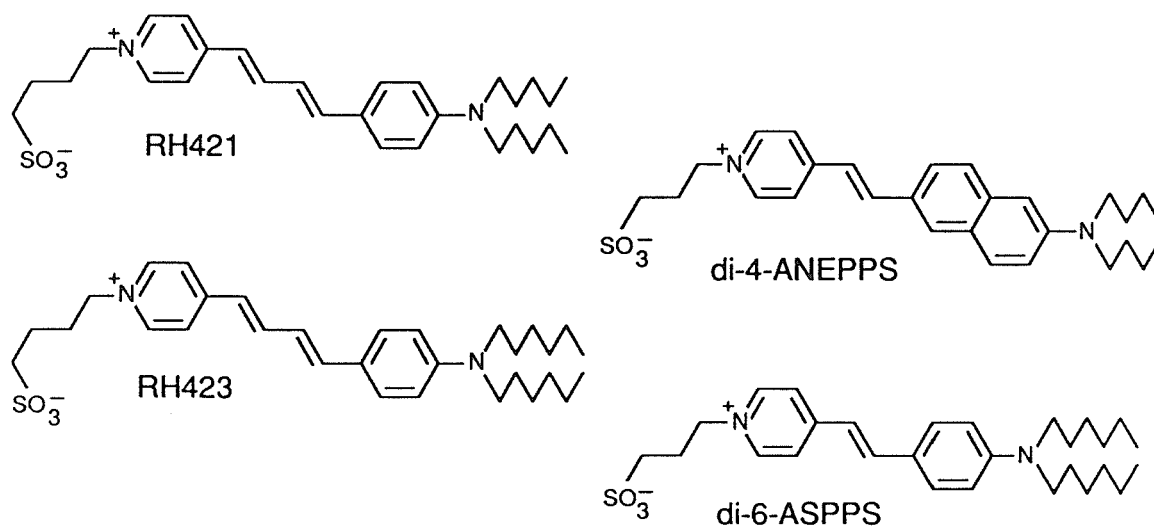
Figure A.3 Structures for four styryl dyes. RH421 and RH423 were synthesized by Rina Hildesheim in Amiram Grinvald's laboratory; di-6-ASPPS and di-4-ANEPPS were synthesized in Leslie Loew's laboratory. Sources for structures: RH421 (Grinvald et al., 1983); RH423 (A. Grinvald, personal communication); di-4-ANEPPS and di-6-ASPPS (Fluhler et al., 1985).

ASPPS. In the following discussion, di-6-ASPPS is taken as a surrogate for RH421 and RH423, since its structure is quite similar to theirs, and many of its properties have been well characterized where theirs have not.

A.4.1 Membrane binding

Styryl dyes all have the same general structure: a pyridine ring linked by a conjugated carbon chain to a phenyl ring (replaced by a naphthalene for di-4-ANEPPS), which has an amino group with two alkyl tails. In addition, the styryls that have proven useful as voltage-sensitive dyes all have a charged anchoring group that prevents them from passing through the membrane (for all of the dyes shown, this is a sulfate group on a short linker). This structure is amphipathic: when the dye molecule is bound to a membrane, the highly hydrophobic tails will presumably be in the interior, while the charged sulfate is outside the membrane where it can be efficiently solvated. Because of this structure, these dyes bind strongly to the membrane, but remain well-oriented (sulfate out), and do not easily pass through.

Fluhler *et al.* (1985) measured dye binding by titrating solutions of dye with vesicles made from phosphatidylcholine vesicles, and found that it took .03 mg/ml of vesicles to bind half the dye in a 1 μM solution of di-4-ANEPPS. The concentration of phosphatidylcholine may be estimated by assuming an average molecular weight of 700: .03 mg/ml=43 μM. Since the vesicles bound half the dye, there were 86 phospholipid molecules per dye molecule (a very high molar fraction of dye!). This should be considered a lower limit, since these dyes do not cross membranes well. The inner leaflets of the membrane were presumably unstained, and these suspensions (prepared by simple sonication) were most likely a heterogeneous assortment of unilamellar and multilamellar vesicles; the inner layers of multilamellar vesicles were presumably unstained. The corresponding numbers for di-6-ASPPS were .015 mg/ml of vesicles, or 1 dye molecule for every 42 phospholipids.

Since the structures of RH421 and RH423 are very similar to that of di-6-ASPPS, their membrane binding is presumably similar as well. (Real membranes should be roughly similar to phosphatidylcholine vesicles.) In the typical staining protocol used in this thesis (see Chapter 6), a culture is exposed for 5-10 minutes to a dye concentration of 2 μM. The cells' fluorescence increases continually over this time, so the staining does not reach equilibrium, but it seems quite likely that the final molar fraction of dye in the membrane is a few percent. This concentration is quite high, and one should be wary of the dye's pharmacological effects.

A.4.2 Chromophore

The styryls have a linear chromophore, as do most voltage-sensitive dyes; theirs comprises a conjugated carbon chain with rings at either end. On the basis of both molecular orbital calculations (Loew et al., 1978) and experimental evidence (Loew et al., 1979), Loew's group has proposed that the chromophore acts as follows.
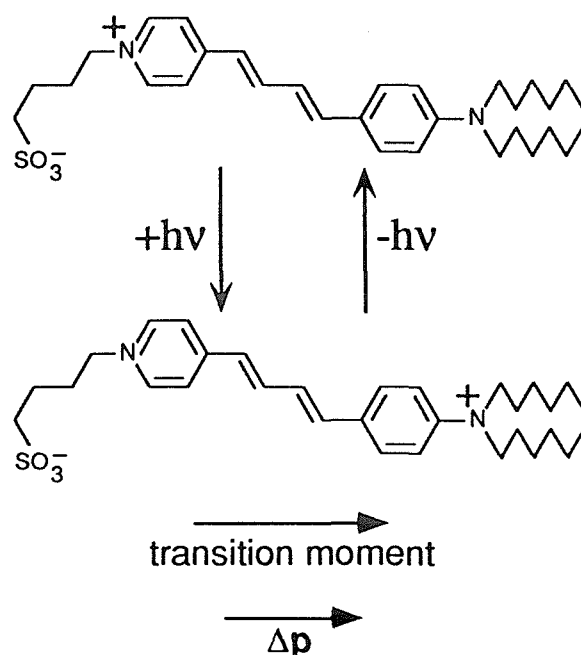
Figure A.4 Proposed ground state (*top*) and excited state (*bottom*) for RH423. The *plus signs* represent the delocalized charge of the molecule, which shifts when a photon is absorbed or emitted.

In the ground state at neutral pH, there is a partially delocalized positive charge centered on the pyridinium nitrogen, as shown in Fig A.4 for the example of RH423. When the molecule absorbs a photon, this charge shifts along the chromophore, to the amino nitrogen. The resulting absorption transition moment is oriented parallel to the length of the molecule; the emission transition moment is presumably antiparallel to the absorption moment. Thus, the dye molecule acts as an electric dipole, preferentially absorbing light polarized along its long axis, as well as emitting light polarized along this axis. The change in dipole moment between ground and excited states, Δp, is also parallel to the length of the molecule. If the dye molecule is strongly oriented in the membrane, it will preferentially absorb light that is polarized perpendicular to the plane of the membrane.

A.4.3 Spectroscopic properties

Fluhler *et al.* (1985) showed that styryls absorb light efficiently, with extinction coefficients of 10^4 to 4×10^4 $M^{-1}cm^{-1}$ when bound to lipid vesicles. They also showed that the quantum yield for styryls increases about a hundredfold when the dye binds to lipid vesicles. (This increase is convenient for experiments, since it means that the fluorescence of unbound aqueous dye can usually be neglected.) For di-6-ASPPS, they measured $\varepsilon = 3 \times 10^4$ $M^{-1}cm^{-1}$, and found that q increased from .002 when the dye was in aqueous solution to .3 when the dye was bound to lipid vesicles.

It is difficult to know what ε and q should be in the case of RH423 bound to a neuron, both because the dyes differ slightly from di-6-ASPPS, and because the neuronal membrane is not a phosphatidylcholine vesicle. Nor is it possible to measure these values experimentally. A very rough comparison with experimental values can be made, however, by assuming that RH423 has the same binding properties and spectroscopic properties as di-6-ASPPS, and predicting the fluorescence expected from a typical neuron illuminated under typical conditions.

A.4.4 Staining model

Model the typical neuron as a smooth sphere 30 μm in diameter. Assume that it is stained with a 2% molar fraction of RH423 (1 dye molecule for every 50 phospholipids in the outer leaflet of the membrane), and that RH423 when bound to the membrane has $\epsilon=3\times10^4$ $M^{-1}cm^{-1}=5.0\times10^{-3}$ nm^2, and $q=.3$. The surface area of the cell is 1.1×10^{10} nm^2; each phospholipid takes up an area of about 0.7 nm^2 (see Cornell et al., 1980), giving 1.6×10^{10} phospholipids, and 3.2×10^8 dye molecules. For the apparatus in this thesis (see Chapter 3), the pixels are 45 μm squares. The optical density averaged over this pixel is $\epsilon cl=(5.0\times10^{-3}$ $nm^2)$ (3.2×10^8) $/(45$ μm$)^2 = 7.9\times10^{-4}$. Multiplying by (ln 10) gives the fraction of incident light absorbed: 1.8×10^{-3}.

To find the fluorescence of the cell, this fraction must be multiplied by the illuminating intensity and the quantum yield of the dye. Taking an incident intensity of 10 W/cm^2 at a wavelength of 546 nm, 5.6×10^{14} photons/s are incident on the pixel; 1.0×10^{12} photons/s of these are absorbed. With a quantum yield of .3, the fluorescence of the cell will be 3.1×10^{11} photons/s. The objective normally used to collect this fluorescence has a numerical aperture of .75, and so should have a collection efficiency of .087 (see section B.3). Assuming that the photodiode detector has a quantum efficiency of .85, the detected photocurrent should be 3.6 nA.

In the present apparatus, typical rat SCG neurons stained with RH423 give detected photocurrents of about 1 nA. This is remarkably close to the above estimate, considering the crudity of the calculation: many factors such as light losses in the detection system have been ignored, and the staining estimate was somewhat arbitrary. Still, this rough agreement gives one confidence that the properties of RH423 are indeed similar to those of better-studied styryls, and that the staining estimate of a 2% molar fraction of dye is within the right order of magnitude.
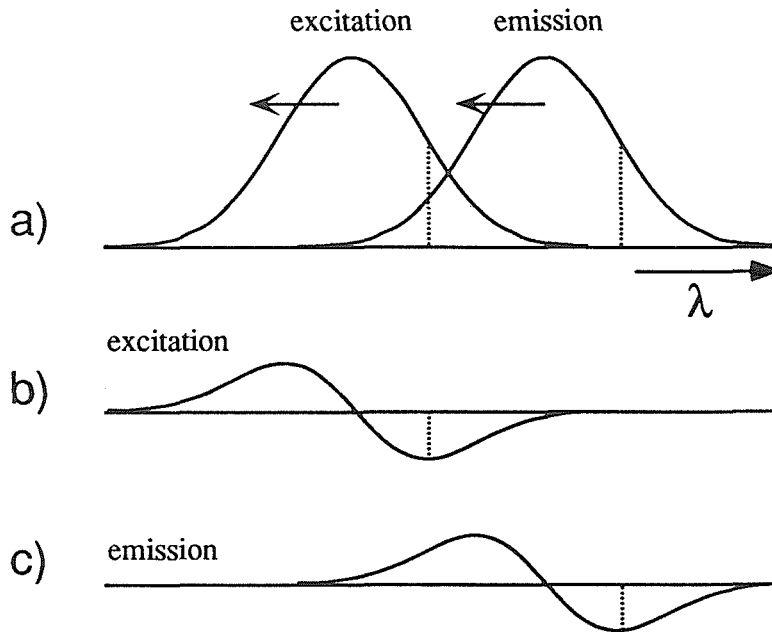
Figure A.5 Action spectra for an electrochromic dye. *a)* Depolarization will blue-shift the dye's excitation and emission spectra. *b)* The action spectrum for excitation. *c)* The action spectrum for emission. *Dashed lines* indicate optimal wavelengths for excitation and emission.

A.4.5 Electrochromic action spectra

If the styryls indeed operate by an electrochromic mechanism, a change in membrane potential will simply shift the absorption and emission spectra in the same direction. The sign of this shift can be predicted as follows. The delocalized positive charge is deeper inside the membrane in the excited state than in the ground state. Therefore, a depolarization of the cell—raising the potential inside—will raise the energy of the excited state more than that of the ground state. This depolarization thus leads to a blue shift in both the excitation and emission spectra, as illustrated in Fig A.5a.

This simple spectral shift leads to biphasic action spectra, which are just derivatives of the excitation and emission spectra. Fig A.5b shows the excitation action spectrum, which would be measured by illuminating with monochromatic light while monitoring at a single wavelength, at the peak of the emission spectrum (the crossover point for the

212

emission action spectrum). The emission action spectrum, shown in Fig A.5c, would be measured by the converse experiment.

If dye-recording experiments were done with monochromatic light, it would be best to pick an excitation wavelength on the red or blue shoulder of the absorption spectrum, where the spectrum's slope is highest. Similarly, the best emission wavelength to monitor would be on a shoulder of the emission spectrum. Of course, the same shoulder should be picked in both cases, so that the signals reinforce; see Fig A.5.

In practice, extreme monochromaticity is not advisable. Extremely narrowband illumination would be undesirably dim (if it were made by filtering a broadband light source). Narrowband detection is even less desirable, because of phototoxicity. A phototoxic cost has been paid for every fluoresced photon; one does not casually throw them away with an overly narrow emission filter. Fig A.6 shows a reasonable compromise: excitation with a bandpass filter, and detection with a long-pass filter. With the excitation and emission wavelengths both on the red shoulders of their respective spectra, as shown, the fluorescence should decrease in response to depolarization; this agrees with the polarity observed on SCG neurons (*e.g.*, Fig 2.3). For reasonable signal sizes, the only requirements are that the filters both be on the same side of their peaks, and that the filters be reasonably sharp, with cutoffs narrower than the widths of the dye's spectra.
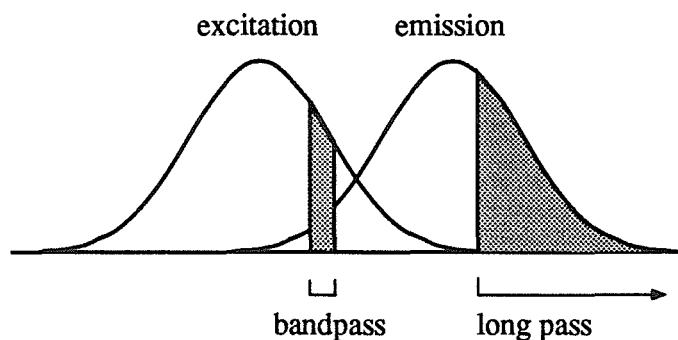
Figure A.6 A typical filter set for recording fluorescence signals from an electrochromic dye.

APPENDIX A REFERENCES

L. B. Cohen, B. M. Salzberg, H. V. Davila, W. N. Ross, D. Landowne, A. S. Waggoner, and C. H. Wang (1974) Changes in axon fluorescence during activity: molecular probes of membrane potential. *J. Membr. Biol.* **19**:1-36.

B. A. Cornell, J. Middlehurst, and F. Separovic (1980) The molecular packing and stability within highly curved phospholipid bilayers. *Biochim. Biophys. Acta* **598**:405-410.

P. R. Dragsten and W. W. Webb (1978) Mechanism of the membrane potential sensitivity of the fluorescent membrane probe merocyanine 540. *Biochemistry* **17**:5228-5240.

B. Ehrenberg, D. L. Farkas, E. N. Fluhler, Z. Lojewska, and L. M. Loew (1987) Membrane potential induced by external electric field pulses can be followed with a potentiometric dye. *Biophys. J.* **51**:833-837.

E. Fluhler, V. G. Burnham, and L. M. Loew (1985) Spectra, membrane binding, and potentiometric responses of new charge shift probes. *Biochemistry* **24**:5749-5755.

E. B. George, P. Nyirjesy, M. Basson, L. A. Ernst, P. R. Pratap, J. C. Freedman, and A. S. Waggoner (1988a) Impermeant potential-sensitive oxonol dyes: I. Evidence for an "on-off" mechanism. *J. Membr. Biol.* **103**:245-353.

E. B. George, P. Nyirjesy, P. R. Pratap, J. C. Freedman, and A. S. Waggoner (1988b) Impermeant potential-sensitive oxonol dyes: III. The dependence of the absorption signal on membrane potential. *J. Membr. Biol.* **105**:55-64.

A. Grinvald, R. Hildesheim, I. C. Farber, and L. Anglister (1982) Improved fluorescent probes for the measurement of rapid changes in membrane potential. *Biophys. J.* **39**:301-308.

A. Grinvald, A. Fine, I. C. Farber, and R. Hildesheim (1983) Fluorescence monitoring of electrical responses from small neurons and their processes. *Biophys. J.* **42**:195-198.

A. Grinvald, B. M. Salzberg, V. Lev-Ram, and R. Hildesheim (1987) Optical recording of synaptic potentials from processes of single neurons using intracellular potentiometric dyes. *Biophys. J.* **51**:643-651.

D. Gross, L. M. Loew, and W. W. Webb (1986) Optical imaging of cell membrane potential changes induced by applied electric fields. *Biophys. J.* **50**:339-348.

A. Hassner, D. Birnbaum, and L. M. Loew (1984) Charge shift probes of membrane potential. Synthesis. *J. Org. Chem.* **49**:2546-2550.

L. M. Loew, G. W. Bonneville, and J. Surow (1978) Charge shift optical probes of membrane potential. Theory. *Biochemistry* **17**:4065-4071.

L. M. Loew, S. Scully, L. Simpson, and A. S. Waggoner (1979) Evidence for a charge-shift electrochromic mechanism in a probe of membrane potential. *Nature* **281**:497-499.

L. M. Loew and L. L. Simpson (1981) Charge-shift probes of membrane potential: a probable electrochromic mechanism for p-aminostyrylpyridinium probes on a hemispherical lipid bilayer. *Biophys. J.* 34:353-365.

L. M. Loew, L. B. Cohen, B. M. Salzberg, A. L. Obaid, and F. Bezanilla. (1985) Charge-shift probes of membrane potential: Characterization of aminostyrylpyridinium dyes on the squid giant axon. *Biophys. J.* 47:71-77.

L. M. Loew (1988a) Introduction to fluorescence and its application to membrane structure and dynamics. In *Spectroscopic Membrane Probes,* vol. I, ed. L. M. Loew. CRC Press, Boca Raton, FL. pp. 1-11.

L. M. Loew (1988b) How to choose a potentiometric membrane probe. In *Spectroscopic Membrane Probes,* vol. II, ed. L. M. Loew. CRC Press, Boca Raton, FL. pp. 140-151.

P. Nyirjesy, E. B. George, R. K. Gupta, M. Basson, P. R. Pratap, J. C. Freedman, K. Raman, and A. S. Waggoner (1988) Impermeant potential-sensitive oxonol dyes: II. The dependence of the absorption signal on the length of alkyl substituents attached to the dye. *J. Membr. Biol.* 105:45-53.

J. A. F. Op den Kamp (1979) Lipid asymmetry in membranes. *Ann. Rev. Biochem.* 48:47-71.

W. N. Ross and L. F. Reichardt (1979) Species-specific effects on the optical signals of voltage-sensitive dyes. *J. Membrane Biol.* 48:343-356.

D. L. Taylor and E. D. Salmon (1989) Basic fluorescence microscopy. *Meth. Cell Biol.* 29:207-237.

A. S. Waggoner and A. Grinvald (1977) Mechanisms of rapid optical changes of potential sensitive dyes. *Ann. N. Y. Acad. Sci.* 303:217-242.

A. S. Waggoner, C. H. Wang, and R. L. Tolles (1977) Mechanism of potential-dependent light absorption changes of lipid bilayer membranes in the presence of cyanine and oxonol dyes. *J. Membr. Biol.* 33:109-140.

A. S. Waggoner (1979) Dye indicators of membrane potential. *Ann. Rev. Biophys. Bioeng.* 8:47-68.

B. E. Wolf and A. S. Waggoner (1986) Optical studies of the mechanism of membrane potential sensitivity of merocyanine 540. In *Optical Methods in Cell Physiology,* eds. P. DeWeer and B. M. Salzberg. Wiley (Interscience), New York, NY. pp. 101-113.

Appendix B
Fluorescence *vs.* Absorption

B.1 INTRODUCTION

This appendix analyzes the choice between fluorescence and absorption for voltage-sensitive dye recording. For some preparations, this choice may be predetermined by mechanical or optical considerations: for instance, when recording from vertebrate cortex, absorption measurements are impossible (intact vertebrate brains are quite thick and opaque!), so fluorescence must be used. However, for many preparations both modes are possible. The neuronal cultures used here are flat, transparent, and easily accessible, so that fluorescence and absorption can be used with equal ease. In such a case, one chooses the mode with the higher signal-to-noise ratio.

The relative S/N ratios for absorption and fluorescence depend on the optical system and optical detector, which are easy to analyze, and on the staining of the specimen and the properties of the dye, which are not. It would be quite interesting to understand the relative advantages of absorption and fluorescence for the preparations in which dye recording has already been used; however, this would require numbers lacking in the literature. It has been standard practice to cite fractional changes in intensity ($\Delta F/F$, ΔA, or sometimes $\Delta A/A$) without citing the illumination intensity, the resting transmission of the stained preparation, or its resting fluorescence. Another problem is the paucity of preparations in which fluorescence and absorption have both been tried. The exception is the squid giant axon, where dyes were screened for signals in both modes, and where some of the relevant light levels have been measured (Ross *et al.*, 1977; Gupta *et al.*, 1981). Despite this lack of information about other preparations, it's possible to derive a

general formula that compares the two modes, and then to decide which is best for the rat SCG culture system, with the help of some simple estimates.

Section B.2 presents a model comparing absorption with fluorescence in the case where shot noise is limiting; section B.3 discusses the effects of dark noise and illumination noise. Section B.4 gives some typical numbers for cultured SCG neurons. For a comparison of absorption and fluorescence in general, see Hirschfeld (1977). Waggoner and Grinvald (1977) and Cohen and Lesher (1986) address many of the same issues discussed here; see also Grinvald *et al.* (1988) for a further comparison. The present model strips the comparison to its bare essentials, and analyzes it quantitatively.

B.2 SHOT-NOISE ANALYSIS

The simple model presented here compares the S/N ratios for absorption and fluorescence in the shot-noise limit, given a preparation stained with a dye that gives signals in both modes[1]. The model makes the following assumptions:

1) It assumes that the same illumination system can be used for both modes, so that their illumination intensities are equal; one can think of the two measurements being made simultaneously. Equal intensities with the same dye will give the same level of photodamage for both modes, so it is fair to compare them on the basis of S/N alone[2].

2) It takes account of the differences in collection efficiency (the fraction of emitted photons that reaches the detector) between the two modes, but for convenience assumes that photons are *detected* perfectly in both modes (*i.e.*, every photon that reaches the detector is counted). Alternately, one

---

[1]In practice, the dyes that give the largest absorbance signals are not those that give the largest fluorescence signals, but the extrapolation from this model to a comparison of two different dyes is straightforward.

[2]For a two-dye model, differing phototoxicities will have to be taken into account. If dye A has a slightly lower S/N than dye B at a given illumination intensity, but is much less phototoxic, then dye A is preferable since it will give a greater S/N at an equivalent level of phototoxicity.

can think of the differences in detection efficiency as being lumped in with collection efficiency.

3) It treats background staining in a simple way, by assuming that background dye has the same spectral properties as dye bound to the cell of interest.

4) It assumes that the optical density of the stained preparation is small, so that the fraction of light absorbed may be treated as linear in the number of dye molecules. (In the general form of de Beer's law, the fraction absorbed is exponential in the number of molecules.) Put another way, it's assumed that the stained preparation does not screen itself.

This little model is not meant to be universal, but rather to illustrate the main differences between absorption and fluorescence. Assumptions 1 and 2 are for simplicity, and could be removed with simple extensions of the model. Assumption 3 is simple-minded, but not unrealistic; again, it would be relatively simple to extend the model by adding parameters to describe the spectral properties of background dye. Finally, assumption 4 is perfectly justified, since even such a large preparation as the squid giant axon only absorbs 25% more when stained (Ross *et al.*, 1977).

The parameters of the model are listed in Table B.1. The S/N ratios of the two modes depend directly on experimental values: the resting intensities and voltage-dependent changes in intensity. These experimental values depend in turn on more basic parameters: the intrinsic properties of the dye, the staining of the preparation, and the collection efficiencies of the optics. The derivation below first relates the experimentally-measured values (measured intensities and voltage-dependent signals) to the basic parameters (collection efficiencies, staining properties, and intrinsic dye properties), and then derives an equation relating the S/N ratios to the basic parameters.

For notational simplicity, all intensities are quoted in units of photons per unit time per pixel. I_0 is the intensity used to illuminate the specimen. As usual, T and F denote the detected intensities of transmitted and fluorescent light, and ΔT and ΔF denote the changes in these intensities due to a shift in membrane potential; again for simplicity, all changes are

resting intensities
I_0 intensity incident on specimen
T transmitted intensity
I_0-T intensity absorbed
F fluorescent intensity

voltage-dependent changes
ΔT voltage-dependent change in T
ΔF voltage-dependent change in F

collection efficiencies
1   collection efficiency for transmitted light
c collection efficiency for fluorescent light

staining properties
$a = \dfrac{I_0-T}{I_0}$ fraction of incident light absorbed
b fraction of dye bound to cell
$1-b$ fraction of dye due to background staining

intrinsic dye properties
q fluorescent quantum yield
$s_F = \dfrac{\Delta F}{bF}$ fluorescent sensitivity
$s_A = \dfrac{\Delta T}{b(I_0-T)}$ absorptive sensitivity

Table B.1. Parameters of the model.

normalized to a 100 mV potential shift. It's assumed that the transmitted light is collected with perfect efficiency[3]; therefore, I_0-T is the intensity absorbed by the stained specimen. It's convenient to characterize the degree of staining of the preparation by the fraction a of light absorbed, defined by $a=(I_0-T)/I_0$.

The detected fluorescence intensity F depends on the amount of light absorbed, the quantum yield of the dye, and the collection efficiency of the optics. Using q for the quantum yield, the total fluorescence emitted by the specimen will be $q(I_0-T)$. Letting c be

[3]This requires only that the numerical aperture of the objective match or exceed the NA of the condenser; see Appendix A.

the collection efficiency (the fraction of the fluorescence that is collected by the optics), the detected fluorescent intensity is given by

$$F = qc(I_0 - T) = qcaI_0 \quad . \tag{B.1}$$

Background staining is treated by assuming that there is some fraction b of dye that is bound to the cell(s) of interest, with a fraction $1-b$ that is due to background. It's assumed that the background dye has the same quantum yield and emission spectrum as dye bound to the cells. This is a quite reasonable assumption for the styryl dyes that I have used, since unbound dye is washed away and most of the background staining seems to be from other cells, neurites, and membrane debris. One expects such background dye and cell-bound dye to be in similar environments (both are in membranes), and thus to have similar spectral properties. More generally, background staining may represent unbound dye in solution, or dye bound to other cells, membranous debris, or nonmembranous debris.

We wish to compare the relative signal-to-noise ratios obtained in fluorescence and in absorption. These depend on the intrinsic voltage sensitivity of the dye in each of the two modes, s_F and s_A, which are related to experimental values by

$$\begin{cases} s_F = \dfrac{\Delta F}{bF} \\[2ex] s_A = \dfrac{\Delta T}{b(I_0 - T)} \end{cases} \tag{B.2}$$

Assuming a straightforward voltage-sensing mechanism where dye molecules act independently, s_F and s_A are the average fractional changes in fluorescence and absorption of a single dye molecule. As discussed in section 2.2, these changes should be characteristic of the dye and (in a simple model) independent of illumination intensity and dye concentration. In the special case where the emission properties of the dye are *not* voltage-sensitive, changes in fluorescence will be due solely to changes in the number of photons absorbed, so that $s_F = s_A$. More generally, the emission properties *will* be voltage-

sensitive, but the change in emission may reduce or reinforce the change in absorption, depending on the emission and excitation wavelengths used. s_F and s_A should usually be of the same order of magnitude, and it should usually be possible to pick filters so that $s_F > s_A$.

Having defined this plethora of parameters, it is now straightforward to derive expressions for the S/N ratios for absorption and fluorescence. In the shot-noise limit, the noise in a measured intensity I is proportional to $\sqrt{I}$, with a constant of proportionality that depends only on the frequency bandwidth used for measurement (see section 3.2). Thus, the two S/N ratios are given by

$$
\begin{cases}
(S/N)_F = k\dfrac{\Delta F}{\sqrt{F}} \\[2mm]
(S/N)_A = k\dfrac{\Delta T}{\sqrt{T}}
\end{cases}
\tag{B.3}
$$

where the constant k is the same in both expressions.

Substitution into (B.3) with (B.1), (B.2) and the definition of a gives

$$
\begin{cases}
(S/N)_F = s_F\sqrt{qca}\left(kb\sqrt{I_0}\right) \\[2mm]
(S/N)_A = s_A\dfrac{a}{\sqrt{1-a}}\left(kb\sqrt{I_0}\right)
\end{cases}
$$

which can be divided through to obtain F/A, the ratio of the S/N ratios for fluorescence and absorption:

$$
\begin{aligned}
F/A &\equiv \frac{(S/N)_F}{(S/N)_A} \\[3mm]
&= \frac{s_F}{s_A}\sqrt{qc\left(\frac{1}{a}-1\right)}
\end{aligned}
\tag{B.4}
$$

If F/A is greater than 1, fluorescence gives the higher S/N ratio; if it's less, absorption does. The terms in this expression can be interpreted as follows:

- The s_F/s_A factor is expected: if the dye has a higher intrinsic sensitivity in one mode, that mode will be favored.

- Since q and c are always less than 1, the factor of qc favors absorption. Fluorescence is at a disadvantage because fewer dye molecules emit photons than absorb photons, and because the emitted photons go off in all directions, and only a fraction can be collected.

- Since a is usually much less than 1, the factor of $(1/a-1)$ favors fluorescence. Absorption is at a disadvantage because the transmitted light (much greater than the absorbed light) adds shot noise without contributing to the signal; in fluorescence, all of the emitted light (except for background fluorescence) contributes to ΔF .

Clearly, increased background staining should favor absorption, since it will increase the noise for fluorescence, but slightly *decrease* the noise for absorption. b does not appear explicitly in (B.4), however. The ratio F/A depends only on the total staining, and cares not what part of the staining is from cells and what part is from background. (Of course, the absolute values of $(S/N)_F$ and $(S/N)_A$ depend on b, but their ratio is independent of b.) Thus, the effects of background staining only appear implicitly, by affecting a. For example, assume the usual case of $a<<1$, so that $(1/a-1)\cong 1/a$. F/A is then inversely proportional to the square root of the total staining: if one were to take a given preparation and add enough background staining to quadruple a, F/A would be halved.

Increasing the empty space in a pixel, on the other hand, decreases a and favors fluorescence. The intensities and other parameters used here refer to a single pixel—the area of the specimen imaged by a single photodetector. (This may be either a lone photodetector, or one of an array of photodetectors.) In absorption, if the cell being observed does not fill the pixel, transmitted light that goes past the cell will never get a chance to contribute to the absorption signal, but will add to the noise. In contrast, in fluorescence the empty space around the cell does not emit any light (unless there is background staining), and so does not affect the S/N ratio. Thus, in absorption mode it is especially important to have pixels as small as or smaller than the cells; pixel size is not as critical in fluorescence unless there is bright background.

The case for fluorescence *vs.* absorption can be summarized quite simply. Fluorescence is put at an initial disadvantage by the quantum efficiency of the dye and the collection efficiency of the optics: both are less than 1, and F/A is proportional to the square root of qc. This disadvantage may be partially or completely overcome if the specimen is lightly stained, in which case the transmitted light adds a lot of absorption noise, without affecting the fluorescence noise. F/A is inversely proportional to a (assuming that $a<<1$), so fluorescence is better for small or thin structures, while absorption is better for large cells with a large area of membrane, or preparations that have many layers. Fluorescence is quite sensitive to background staining, while absorption is relatively insensitive. For absorption, the pixel should be filled by the specimen, while for fluorescence pixel size is not crucial. Finally, all of these general considerations will be modified by the phototoxicity of the dye and its voltage-sensitivity in the mode being considered.

B.3 EFFECTS OF OTHER NOISE

Absorption and fluorescence are affected differently by forms of noise besides shot noise. This is due to differences in detected intensities and fractional signals. The detected intensities in fluorescence are much lower: F is typically several orders of magnitude smaller than T (see the next section for an example). On the other hand, the fractional signals for fluorescence are much larger: with today's best dyes, $\Delta F/F$ is usually in the range 10^{-2} to 10^{-1} per 100 mV, while for $\Delta T/T$ this range is 10^{-4} to 10^{-3} per 100 mV.

Dark noise, or noise due to the optical detector and amplifiers, is independent of the detected intensity. Illumination noise, due to fluctuations in the light source or motion in the light path, is proportional to the detected intensity. (See section 3.2 for a discussion of dark, shot, and illumination noise.) Dark noise dominates the total noise at low intensities, illumination noise dominates at high intensities, and (most desirably) shot noise dominates in between. In order to escape the dark-noise-dominated regime, the detected intensity (F

or T) must be high enough that its shot noise masks the dark noise. To escape illumination noise, the fractional signal size ($\Delta F/F$ or $\Delta T/T$) must be larger than the fractional fluctuations in illumination.

In fluorescence, dark noise threatens, since the intensity is low; illumination noise is unimportant because of the large fractional signal. The light source need not be extraordinarily stable, but the detection system must have very low dark noise (the amplifiers must be very, very quiet).

In absorption, on the other hand, dark noise is swamped because of the high intensity, but illumination noise threatens because of the small fractional signal. Amplifiers needn't be particularly quiet, but stability of the light source is particularly important.

B.4 A QUANTITATIVE EXAMPLE

When starting our experiments with rat SCG cultures, it seemed clear that fluorescence was the mode of choice, considering both the general considerations mentioned above and the dyes available. The cells are relatively small (so that a is likely to be small), and Amiram Grinvald's group had developed styryl dyes that gave very large signals on cultured mouse neuroblastoma cells (Grinvald *et al.*, 1983), which could plausibly be expected to give good signals for SCG neurons. The following calculations evaluate this choice in retrospect. The experimental values given are typical for a 30 μm-diameter rat SCG neuron that has been stained for 5 minutes with a 1 μM solution of the styryl dye RH423.

Though the quantum yield of RH423 when bound to these cells is not known, Loew's group has measured the quantum yields of related styryl dyes. Di-4-ABPPS and di-6-ASPPS are quite similar in structure to RH423, and both have quantum yields of .3 when bound to lipid vesicles (Fluhler *et al.*, 1985). It is thus reasonable to take $q=.3$ for RH423.

The collection efficiency of the microscope system can be calculated from the numerical aperture of the objective lens. The objective usually used for dye-recording experiments was a dry 20x objective with NA 0.75 (see section 4.1.3). The cells are immersed in an aqueous medium ($n = 1.33$), so the cone of collected rays has a half-angle of $\sin^{-1}(.75/1.33)=34.3°$, and covers a solid angle of $4\pi(.087)$ steradians. Making the approximation that the fluorescence is isotropic, the collection efficiency can thus be estimated by $c=.087$.

The fraction of light absorbed by the stained specimen is difficult to measure, since a is much less than 1. However, it can be estimated using (B.1): $a=F/(qcI_0)$. Using a mercury arc lamp and the usual filters, the illumination intensity for a 45x45 μm pixel is about 6×10^{14} photons/s, and the fluorescence detected from a 30 μm cell in the pixel is typically 7×10^9 photons/s. Assuming that $q=.3$ and $c=.087$, this gives an estimate for a of about 4.5×10^{-4}.

Putting these estimates for q, c, and a into (B.4) gives $F/A=7.6s_F/s_A$, so fluorescence will give the greater S/N unless $s_F/s_A<0.13$. Unfortunately, s_F/s_A can only be estimated indirectly: many fluorescence measurements have been made from SCG neurons with RH423, so observed values of $\Delta F/F$ place a limit on s_F, but no absorption measurements have ever been made. $\Delta F/F$ from RH423 on these cells is typically about 1%/100 mV, and occasionally as high as 7%/100 mV (see Chapter 6). Assuming that s_F does not vary between cells, and that variations in $\Delta F/F$ are due to variations in b, s_F must be at least as large as the largest $\Delta F/F$ seen: $s_F>7\%/100$ mV. Indirect information about s_A comes from experiments with different emission filters (Chapter 6), in which the fluorescence signal $\Delta F/F$ showed no dependence on emission wavelength. These results make it unlikely that s_A is much larger than s_F, since this would require a large voltage-dependent change in quantum efficiency, opposite in sign to the voltage-dependent absorption changes, which cancelled most of s_A. Another argument in favor of fluorescence is that $s_F/s_A=0.13$ would require s_A of about 50%/100 mV, which is

improbably high: it would mean that a 100 mV change in membrane potential stopped half the dye molecules from absorbing light. Though a definitive answer would direct absorption measurements, it seems quite certain that for RH423 on SCG neurons, fluorescence is the mode of choice.

This raises the question of whether absorption might be preferable for a different dye; after all, the styryls have only been used in fluorescence. For absorption measurements to be preferable, either s_A would have to reach the improbable value of 50%/100 mV, or the dye would have to stain more heavily and give a higher value of a. An increase in a would require either an increase in the extinction coefficient, or an increase in the concentration of dye in the cell membrane. The extinction coefficient of styryls is already quite high (*e.g.*, $3 \times 10^4 M^{-1} cm^{-1}$ for di-6-ASPPS; see section A.4.3), and the cells are already very heavily stained: there is approximately one dye molecule per 50 phospholipids in the stained membrane (section A.4.4). It seems very likely that fluorescence will always be the mode of choice for cells of this size.

The above arguments were made on the basis of shot noise alone; dark and illumination noise must also be considered. For fluorescence, illumination noise is not critical, but dark noise is. The fluorescence level of 7×10^9 photons/s quoted above corresponds to a photocurrent of about 1 nA; assuming a 400 Hz noise bandwidth, the shot noise in this current is 360 fA rms. For the apparatus used here, this level of shot noise far exceeds the mean amplifier dark noise of 78 fA (see subsection 5.1.5), so fluorescence measurements are indeed shot-noise limited. For absorption, dark noise is unimportant, but illumination noise must be checked. Since a is very small, $T \cong I_0$, and we may approximate $\Delta T/T = a(bs_A)$. The illumination noise from even a well-regulated mercury arc lamp is of the order of 1 part in 10^4 (see section 4.2); in order for $\Delta T/T$ to exceed this level with $a = 4.5 \times 10^{-4}$, bs_A would need to be at least 20%/100 mV. Since $bs_F = \Delta F/F$ is usually about 1%/100 mV, this would require s_A to be twentyfold higher than s_F, which is unlikely for the reasons discussed above. (Illumination noise could be

reduced by using an incandescent lamp, as is usual for absorption experiments; however, the lower intensity of an incandescent lamp would increase the fractional shot noise.) For RH423 on these cells with a mercury-arc light source, fluorescence measurements are shot-noise limited, whereas absorption measurements would quite likely be limited by illumination noise; this is another reason for using fluorescence.

APPENDIX B REFERENCES

L. B. Cohen and S. Lesher (1986) Optical monitoring of membrane potential: Methods of multisite optical measurement. In *Optical Methods in Cell Physiology*, eds. P. DeWeer and B. M. Salzberg. Wiley (Interscience), New York, NY. pp. 71-99.

E. Fluhler, V. G. Burnham, and L. M. Loew (1985) Spectra, membrane binding, and potentiometric responses of new charge shift probes. *Biochemistry* 24:5749-5755.

A. Grinvald, A. Fine, I. C. Farber, and R. Hildesheim (1983) Fluorescence monitoring of electrical responses from small neurons and their processes. *Biophys. J.* 42:195-198.

A. Grinvald, R. D. Frostig, E. Lieke, R. Hildesheim (1988) Optical imaging of neuronal activity. *Physiol. Rev.* 68:1285-1366.

R. K. Gupta, B. M. Salzberg, A. Grinvald, L. B. Cohen, K. Kamino, S. Lesher, M. B. Boyle, A. S. Waggoner, and C. H. Wang (1981) Improvements in optical methods for measuring rapid changes in membrane potential. *J. Membr. Biol.* 58:123-137.

T. Hirschfeld (1977) The choice between absorption and fluorescent techniques. *Appl. Spectrosc.* 31:245.

W. N. Ross, B. M. Salzberg, L. B. Cohen, A. Grinvald, H. V. Davila, A. S. Waggoner, and C. H. Wang (1977) Changes in absorption, fluorescence, dichroism, and birefringence in stained giant axons: optical measurement of membrane potential. *J. Membr. Biol.* 33:141-183.

A. S. Waggoner and A. Grinvald (1977) Mechanisms of rapid optical changes of potential sensitive dyes. *Ann. N. Y. Acad. Sci.* 303:217-242.

Appendix C
Theoretical Microscopy

C.1 INTRODUCTION

This appendix discusses the optical efficiency of the microscope, a subject that has not been dealt with extensively in the dye-recording literature. The first two sections cover some basic background: section C.2 defines the crucial concept of numerical aperture (NA), and section C.3 describes Kohler illumination, the most common arrangement for illumination with a small nonuniform light source. For optical efficiency, the microscope must get light both in and out: section C.4 discusses illumination intensity, and section C.5 discusses collection efficiency. Both illumination intensity and collection efficiency depend critically on the NA of the lenses used. Throughout, theoretical results are compared with experimental measurements from the apparatus used in this thesis (see Chapter 4 for a full description of the microscope). Section C.6 summarizes the results.

For an excellent discussion of basic and not-so-basic microscopy, see the pamphlet by Bradbury (1984); for a dictionary of terms, see the pamphlet by Bradbury *et al.* (1989). Efficient design of optical systems for dye recording has been previously discussed in the literature, particularly by Grinvald and coworkers (Grinvald *et al.*, 1983), who gave a quantitative treatment of a epifluorescence system for fluorescence dye recording. Their formulae for illumination intensity and collection efficiency are only approximate; see the results of sections C.4 and C.5.
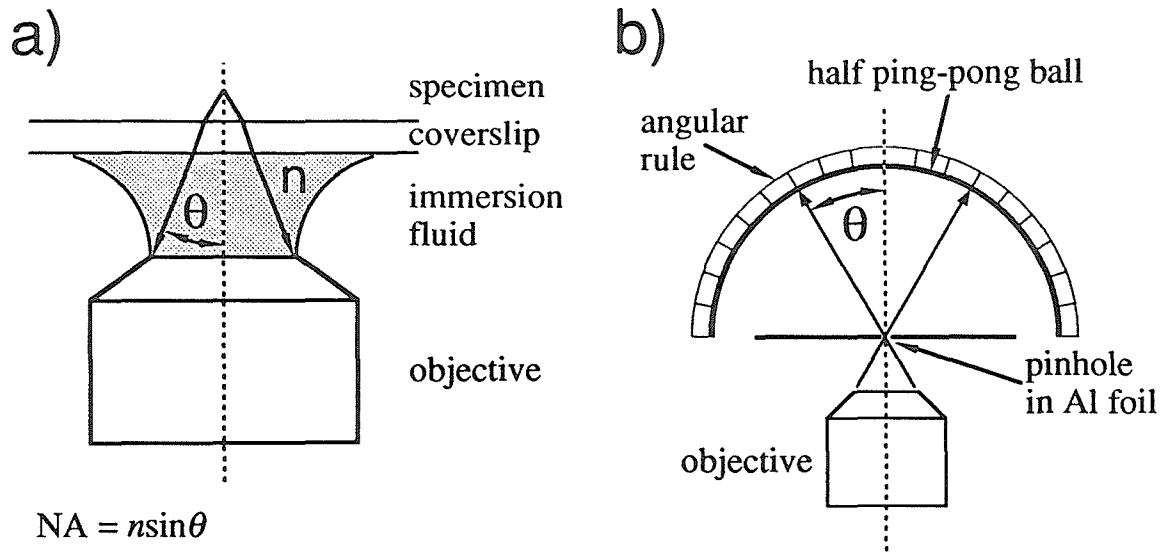
Figure C.1. a) Definition of numerical aperture. *n* is the index of refraction of the immersion fluid; *θ* is the half-angle of rays collected by the objective from a single point in the specimen. b) An apparatus for measuring the NA of a dry objective, shown in cross-section. The lens is used to illuminate a pinhole in a sheet of aluminum foil. The light that passes through this pinhole is then projected on a hemispherical screen (a ping-pong ball cut in half), which has angular divisions marked on the outside. The screen shows the angular distribution of illuminating light.

C.2 NUMERICAL APERTURE

The numerical aperture of a microscope objective is nearly as important as its magnification. Whereas the magnification (M) determines the size of the microscope's field of view, the numerical aperture (NA) determines the size of the cone of rays collected from each point in the field of view.

Fig C.1*a* illustrates the definition of the numerical aperture. Using θ for the half-angle of the cone of rays once it reaches the immersion fluid of the lens, and n for the index of refraction of the immersion fluid, the NA is defined by

$$NA = n \sin\theta \ .$$

Since $n \sin\theta$ is conserved along any given ray (by Snell's law), the numerical aperture is independent of the index of refraction of the coverslip and the specimen, and depends only on the properties of the objective and its immersion fluid.

Obviously, the NA can't be larger than n. Dry (air-immersion) lenses have NA less than 1, and even lenses that use oil immersion ($n=1.5$) have a maximum NA of about 1.3. For conventional biological microscopes, high-NA objective lenses must be very close to the specimen in order to capture a large solid angle, and so have short working distances and large magnifications.

The NA of a lens determines not only the cone of rays that it can collect from a specimen, but also the cone with which it can illuminate the specimen. Fig C.1*b* shows a simple apparatus that measures the numerical aperture of a dry microscope objective by measuring this cone of illumination. The objective is focussed on a pinhole to provide a point source of light and illuminate the inside of a hemispherical screen. The maximum half-angle of illumination θ is read off by means of a protractor attached to the outside of the screen, and the NA is given simply by NA=$\sin\theta$, since $n=1$ for a dry objective.

objective	M	NA	$\sin^{-1}$NA	θ_{exp}
Olympus SPlan 4PL	4x	.13	7.5°	9°
Olympus SPlan 10PL	10x	.30	17.5°	21°
Olympus LWD CDPlan 20PL	20x	.40	23.6°	25°
Nikon Fluor 20 Ph3DL	20x	.75	48.6°	49°
Olympus LWD CDPlan 40PL	40x	.60	36.9°	37°
Nikon Fluor 40 Ph3DL	40x	.85	58.2°	57°

Table C.1. Measurement of numerical aperture for six different air objectives. The first three columns list the objective's manufacturer and name, its magnification, and its specified NA. The last two columns show the predicted and measured half-angles of illumination, in degrees.

Table C.1 shows measurements made in this way for six objectives that were used for the work in this thesis. The agreement of measured θ values with those predicted by

$\sin^{-1}(NA)$ is excellent, and well within the limits of the crude measurements. This ping-pong meter is also useful for looking at the angular distribution of incident illumination (see section C.4).

As well as being important for illumination intensity and collection efficiency, the NA of a lens determines its resolving power and depth of focus: a higher numerical aperture gives finer resolution and a shallower depth of field. These properties are not critical for dye-recording applications, however, and will not be discussed further.

C.3 KOHLER ILLUMINATION

Kohler illumination is widely used as a method for uniformly illuminating a specimen while using a light source that is nonuniform. Fig C.2 shows ray diagrams for Kohler illumination, for both a transmitted-light microscope and an epifluorescence microscope[1]. Epiillumination is more complex than transillumination, but the essential feature of Kohler illumination is the same for both: the plane of the light source is conjugate to the plane of the aperture iris, which is in turn conjugate to the back focal plane of the condenser (BFPC)[2]. That is to say, a real image of the light source is formed in the BFPC. Since the light source is very much out of focus at the specimen plane, the specimen is illuminated uniformly, despite the nonuniformity of the source.

Nonuniformity has not been completely banished; instead, it has been hidden in angles. In Kohler illumination, the bundle of rays emitted from a particular point in the light source becomes a bundle of parallel rays at the specimen: each *position* in the light source is mapped into a *direction* at the specimen. The original *spatial* nonuniformity of the

---

[1]These diagrams are in fact the correct ones for the Olympus IMT-2 microscope that I have used. Fig C.2*a* is the arrangement for phase-contrast illumination, and *b*, for epifluorescence illumination.

[2]In transillumination (Fig C.2*a*), the plane of the aperture iris is in fact *identical* to the back focal plane of the condenser.

light source is thus transmuted into *angular* nonuniformity at the specimen. For most purposes this doesn't matter; all that matters is that each position in the specimen receives the same total light intensity, regardless of the directions from which the light comes.
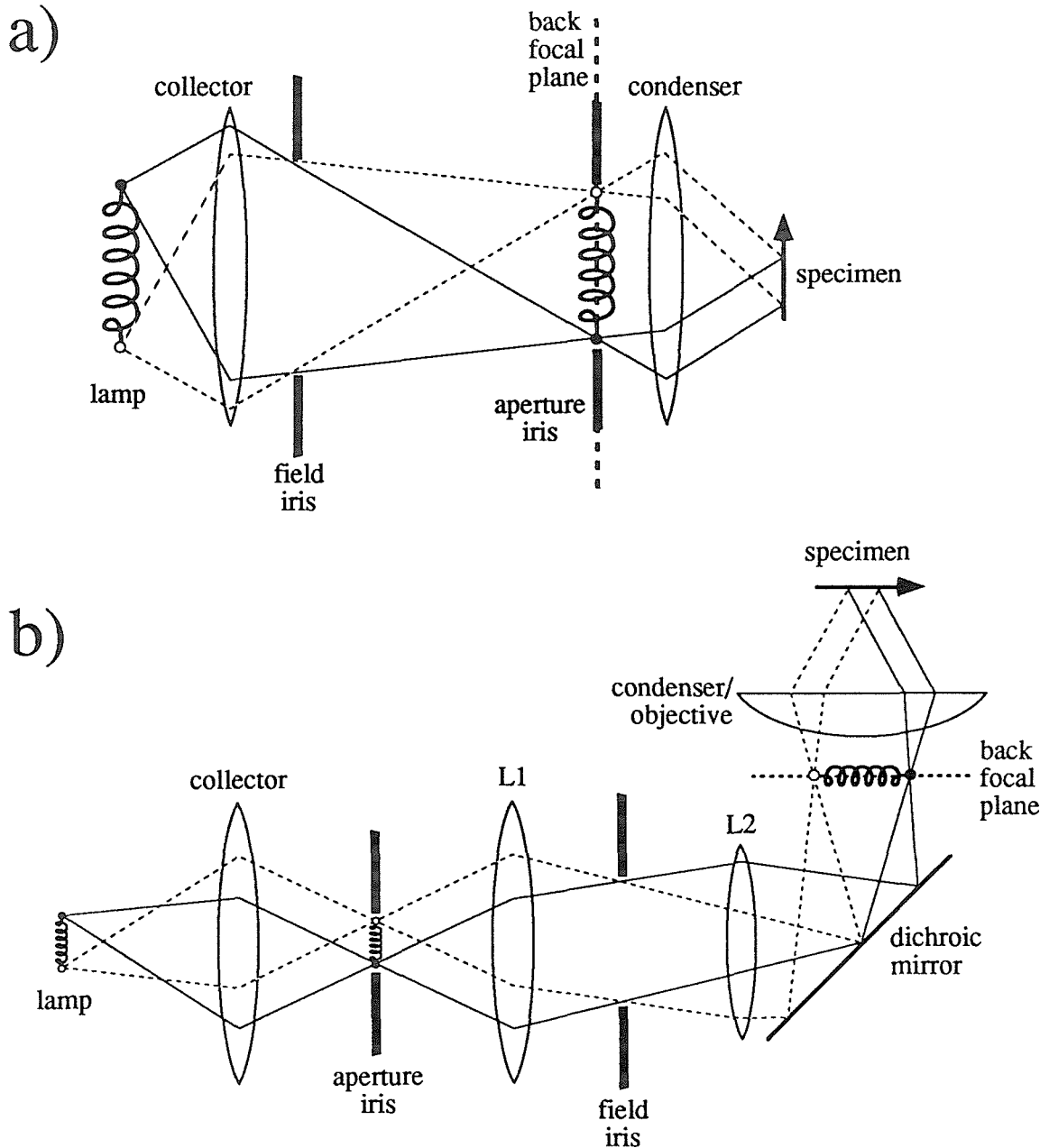
Figure C.2. Kohler illumination. a) A ray diagram of Kohler illumination for a transmitted-light microscope. The objective, not shown, is off to the right. b) Kohler illumination for an epifluorescence microscope, where the objective lens does double duty as the condenser. Lenses L1 and L2 are relay lenses. The outgoing light path (not shown) descends through the dichroic mirror. [Both *a* and *b* are adapted from Bradbury (Bradbury, 1984, figures 14 and 15).]

In order to maximize illumination intensity, it is important to match the illumination optics (by which I mean the collector lens, the relay lenses, and the field and aperture irises) to the condenser lens. In particular, the lamp's image at the BFPC should just fill the entrance pupil of the condenser. The illumination optics and the size of the lamp set the size of the lamp's image at the BFPC; the diameter of the condenser's entrance pupil is roughly proportional to NA_{cond}/M_{cond} (the quotient of its numerical aperture and its magnification).

C.4 ILLUMINATION INTENSITY

With this explanation of Kohler illumination in mind, consider the optimization of the illumination intensity. Take the ideal case of a microscope with no absorptive or reflective losses. The illumination intensity I at the specimen is determined by three components: the light source, the illumination optics, and the condenser lens. The task of the illumination optics and condenser is to collect the light put out by the light source, and focus it on the specimen, with the aim of maximizing I. In this task they are restricted by two fundamental physical laws: conservation of energy, and conservation of phase space density (Liouville's theorem).

C.4.1 Phase-space incompressibility

Consider a small bundle of rays with power dP_1 emitted from a small area dA_1 of the light source into a small cone of solid angle $d\Omega_1$, and follow its progress through the optical system (Fig C.3). When this bundle reaches the specimen, it has power dP_s, area dA_s, and solid angle $d\Omega_s$. Since we are ignoring absorptive and reflective losses, conservation of energy requires that

$$dP_s = dP_1 \ .$$
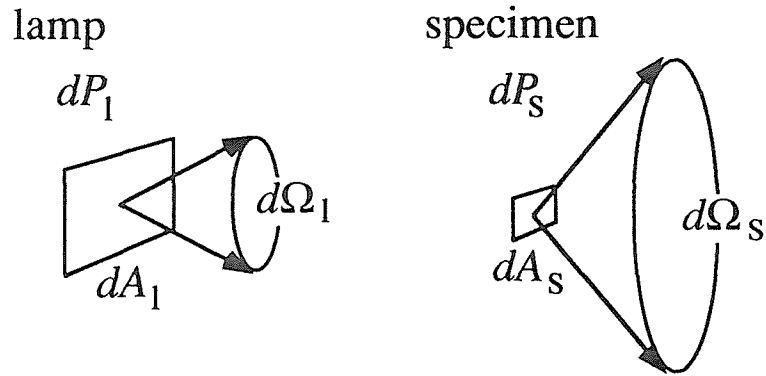
lamp   specimen

Figure C.3. Definition of *dA*, *d*Ω, and *dP*. *dP* is the power in a bundle of rays passing through an area *dA*, and subtending a solid angle *d*Ω. The subscripts *l* and *s* denote "lamp" and "specimen," respectively. If *dA* for the ray bundle decreases, Liouville's theorem requires that *d*Ω must increase (see text).

Further, in the geometric-optics approximation the photons that make up the bundle are noninteracting particles, so Liouville's theorem requires that the phase-space density $dP/dAd\Omega$ be conserved as the bundle propagates:

$$\frac{dP_s}{dA_s d\Omega_s} = \frac{dP_l}{dA_l d\Omega_l} \quad .$$

Conservation of energy and of phase-space density combine to give a statement of phase-space "incompressibility":

$$dA_s \, d\Omega_s = dA_l \, d\Omega_l \quad ,$$

i.e., the phase-space volume taken up by the bundle is constant along its path.

C.4.2 Dependence of I on NA_{cond}

With the principle of phase-space incompressibility in mind, consider how to get the brightest possible illumination. *I* is maximized by starting with a light source of high luminance $dP_l/dA_l d\Omega_l$, then using the illumination optics and condenser lens to maximize dP_s/dA_s by manipulating the illuminating ray bundles.

Choosing a bright light source is simple: there are two light sources commonly used for dye-recording, mercury arcs and tungsten-halogen lamps, and the luminance of mercury arcs exceeds that of tungsten-halogen lamps by about an order of magnitude. (Tungsten-halogen lamps are used for applications where lamp stability is more important than brightness.) Design of the illumination system is more complex, since it depends on intimate details of microscope engineering. Because of this complexity, and because commercial biological microscopes come with a fixed illumination system which cannot be adjusted anyway, I will not attempt to analyze the properties of the illumination system. In the following discussion, I treat the illumination system as a black box that provides a real image of the light source at the back focal plane of the condenser, and consider the effects of the condenser lens.

Maximization of the illumination intensity dP_S/dA_S from a ray bundle requires that dA_S be minimized; because of phase-space incompressibility, this requires that $d\Omega_S$ be maximized. Therefore, the numerical aperture of the condenser, NA_{cond}, must be as large as possible. A large NA_{cond} allows the solid angle of the bundle to be expanded, in order to compress its area.

Next consider the quantitative dependence of the illumination intensity on NA_{cond}. The illumination intensity I received by a particular point in the specimen (not to be confused with the photocurrent I used elsewhere) is found by integrating over incoming directions:

$$I = \int \frac{dP_S}{dA_S \, d\Omega_S} \cos\theta \, d\Omega_S \quad ,$$

where θ is the angle between each incoming ray bundle and the normal to the specimen (assuming a flat specimen). This integral is quite difficult to evaluate, since the illumination is not in general isotropic. If we make the simplifying assumption that the illumination is

both isotropic and uniform, we may define the lamp source luminance $L \equiv dP/dAd\Omega$, which is independent both of position and incoming direction. The integral then evaluates simply:

$$
\begin{aligned}
I &= \int_0^{\theta_{cond}} L \cos\theta (2\pi \sin\theta) d\theta \\
&= L\pi \sin^2 \theta_{cond} \\
&= \frac{L\pi}{n^2} (NA_{cond})^2
\end{aligned}
\tag{C.1}
$$

where n is the index of refraction of the condenser's immersion fluid, and $NA_{cond}=n\sin\theta_{cond}$. This formula assumes that the illumination is isotropic out to an angle θ_{cond} set by the condenser. For Kohler illumination, this is equivalent to assuming that the intensity of the light source is spatially uniform, and that its image at the BFPC fills the condenser's entrance pupil.

Now it is clear why it is important to match the illumination system to the condenser. If the lamp's image at the BFPC overflows the condenser's entrance pupil, light is wasted. If the lamp's image is smaller than the entrance pupil, the integral in (C.1) will stop short of θ_{cond}, and I will be less than the value given there. (Remember that L depends only on the light source, not the illumination optics.)

Note that (C.1) does not depend explicitly on the magnification of the condenser M_{cond}; this is perhaps counterintuitive. It would seem that increasing M_{cond} while keeping NA_{cond} constant—i.e., changing to a higher-magnification condenser with the same numerical aperture—would increase I by squeezing the same light into a smaller area. However, this higher-magnification condenser would have a smaller entrance pupil. If the lamp's image filled the original entrance pupil, some of it would fall outside the smaller pupil of the high-magnification lens, excluding enough light that I would be unchanged. (This is Liouville's theorem at work.) Thus, though the magnification of the condenser does not appear explicitly in (C.1), it appears implicitly by affecting the assumption that the lamp image just fills the condenser's entrance pupil.

C.4.3 Empirical measurements of I

The result (C.1), that illumination intensity is proportional to the square of the numerical aperture, has been stated by Grinvald *et al.* (1983). Unfortunately, this simple formula is not correct in practice. Fig C.4 shows empirical data for the dependence of illumination intensity on NA. This data was taken on an Olympus IMT-2 microscope, using the six objectives listed in Table C.1 as epifluorescence condensers (*i.e.,* illuminating as shown in Fig C.2*b*). The deviation from a simple quadratic relation is obvious.

There are two major reasons for this deviation: spatial nonuniformity of the lamp, and the size of its image at the BFPC. The derivation of (C.1) assumed that the illumination of the specimen was isotropic. Kohler illumination is uniform, but not isotropic (see section C.2); the anisotropy is due to the nonuniform light source, in this case a mercury arc lamp. This anisotropy can be seen directly using the ping-pong ball meter of Fig C.1: the image of the mercury arc is not a uniform circle, but a horizontal band, brightest in the center. A condenser with a small entrance pupil uses light only from the bright core of the arc's image, whereas a condenser with a large entrance pupil includes the dim fringes of the image. Thus, increasing the NA at a given magnification yields diminishing returns. This can be seen by comparing the two 20x lenses (CDPlan 20PL and Fluor 20 Ph3DL) or the two 40x lenses (CDPlan 40PL and Fluor 40 Ph3DL) in Fig C.4.

The second reason is the match between the size of the lamp's image at the BFPC and the entrance pupil of the condenser. Ideally, this image should just fill the entrance pupil of the condenser, as shown in Fig C.2, so that the illuminating rays use the full NA. However, the size of this image is fixed by the illuminating optics, while the size of the entrance pupil varies with the lens's NA and magnification. The ping-pong ball meter can be used to see how well the size of the image of the light source matches the entrance pupil of the condenser. For instance, this match is quite poor for the Fluor 20 Ph3DL objective:
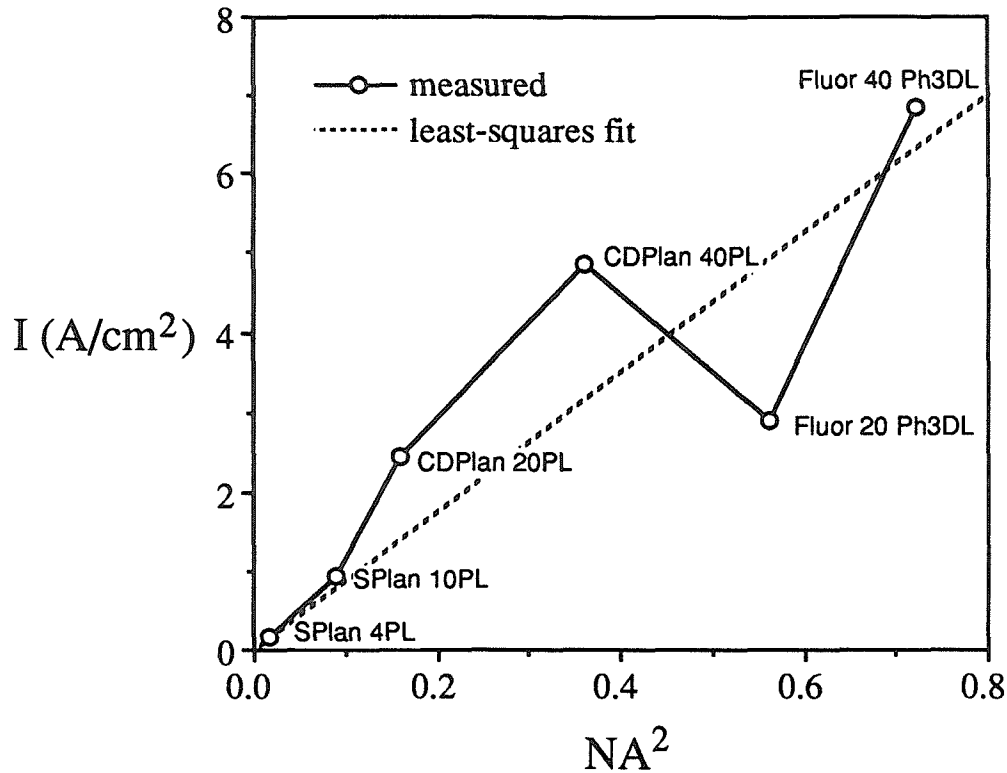
Figure C.4. Dependence of illumination intensity on numerical aperture. Six different objectives were used to epiilluminate a 100 μm-diameter photodiode detector placed on the stage of an Olympus IMT-2 microscope. The light source was the standard 100W mercury arc lamp (see section 4.2). The graph shows the resulting photocurrent (normalized to amperes per square centimeter) plotted against the square of the NA; the dashed line shows the result of a least-squares fit. The lenses are listed in Table C.1.

the image of the arc is quite small, and a large area of the entrance pupil is unilluminated. The full NA is not used, Liouville's theorem intercedes, and the illuminating intensity with this lens is quite low (see the figure).

Several other minor effects also cause deviations from (C.1) for epifluorescence illumination. 1) The high-NA objectives designed for epifluorescence usually have a phase annulus in the back focal plane, which allows viewing in phase contrast as well as fluorescence. This annulus blocks some of the illumination. 2) There is some reflection by the coverslip. The coefficient of reflection depends on θ, and so introduces an extra θ-dependent factor into the integral of (C.1). 3) A dye-stained cell is not a flat specimen, so

the factor of $\cos\theta$ in (C.1) must be modified. In fact, a spherical cell should absorb isotropically, so the $\cos\theta$ factor should be omitted altogether. These effects are quite complex, and no attempt is made to quantitate them here.

For the above reasons, both major and minor, the illumination intensity does not exactly follow a simple quadratic dependence on NA_{cond}. Despite this, two simple qualitative statements can be made: NA_{cond} should be as large as possible, and the illumination system should be matched to the condenser so that the image of the light source just fills the condenser's back focal plane.

C.5 COLLECTION EFFICIENCY

The last section dealt with the efficiency of getting light in to the specimen. For an efficient microscope, it's just as important to get light out. Again, numerical aperture plays a starring role.

The numerical aperture of the objective determines the cone of rays that can be collected from a given point on the specimen. In order to understand the effect of the objective's NA, it's necessary to know the angular distribution of outgoing rays. This distribution is illustrated by Fig C.5. When viewing in transmission, the outgoing cone is limited by the NA_{cond}; thus, collection efficiency is maximal as long as NA_{obj} equals or exceeds NA_{cond}, a criterion that is easily met. Letting c be the collection efficiency of the microscope (the fraction of emitted light captured by the objective), $c=1$ if this criterion is met and absorptive and reflective losses can be ignored. The case of epifluorescence is considerably more complicated, and takes up the rest of this section.

In epifluorescence, the same lens serves both as condenser and as objective, and its NA limits the cone of illumination. Unlike transmission, where the outgoing light is limited to a cone, the fluorescent light spreads out in all directions. In order to maximize collection efficiency, the NA must be as large as possible. The exact expression for
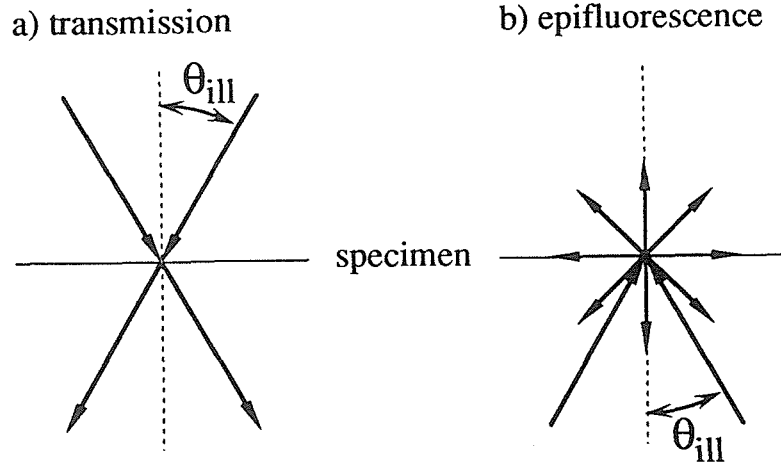
Figure C.5. Distribution of outgoing rays from a given point on the specimen. In both *a* and *b*, θ_{ill} is determined by the numerical aperture of the illuminating lens. a) In transmission, the half-angle of the cone of outgoing rays is equal to θ_{ill}. b) In epifluorescence, the outgoing rays go in all directions.

collection efficiency depends on the angular distribution of the emitted light. Let $f(\theta, \phi)$ be the angular distribution function. Then the collection efficiency c is given by

$$c = \int_0^{\theta_{obj}} f(\theta,\phi) 2\pi \sin\theta \, d\theta \quad,$$

where θ_{obj} is the maximum angle collected by the objective. If θ_{obj} is small, or if $f(\theta,\phi)$ can be approximated by $\cos\theta$, then

$$c \propto NA^2_{obj}, \qquad\qquad (C.2)$$

where NA_{obj} is the NA of the objective. This is the formula given by Grinvald *et al.* (1983).

Again, a simple quadratic dependence on NA is not generally correct. The angular distribution $f(\theta, \phi)$ can be quite complicated for fluorescence. Modelling the dye molecules as electric dipoles, their absorption and fluorescence are both highly anisotropic: a dipole preferentially absorbs and emits photons whose polarizations are parallel to its dipole

moment, and so prefers to absorb or emit photons propagating in the plane perpendicular to its dipole moment. Because of this anisotropic behavior of dye molecules, $f(\theta, \phi)$ depends on the exact angular distribution of illumination. The illumination, which is mostly from one direction (along the optical axis of the microscope), preferentially excites molecules that lie in the plane perpendicular to the optical axis. The combined fluorescence of these molecules is then maximal along the optical axis, so that as NA_{obj} is increased, c rises more slowly than $(NA_{obj})^2$.

Fig C.6 shows an empirical determination of the dependence of c on NA_{obj}. Four different objectives were used to measure epifluorescence from freshly-plated SCG neurons (which do not have neurites to speak of), stained for 10 minutes with 5 μM RH423. The illumination intensity I of each objective was first measured using a photodiode detector with a 100 μm circular aperture, as for Fig C.4. For each cell ($n=5$),
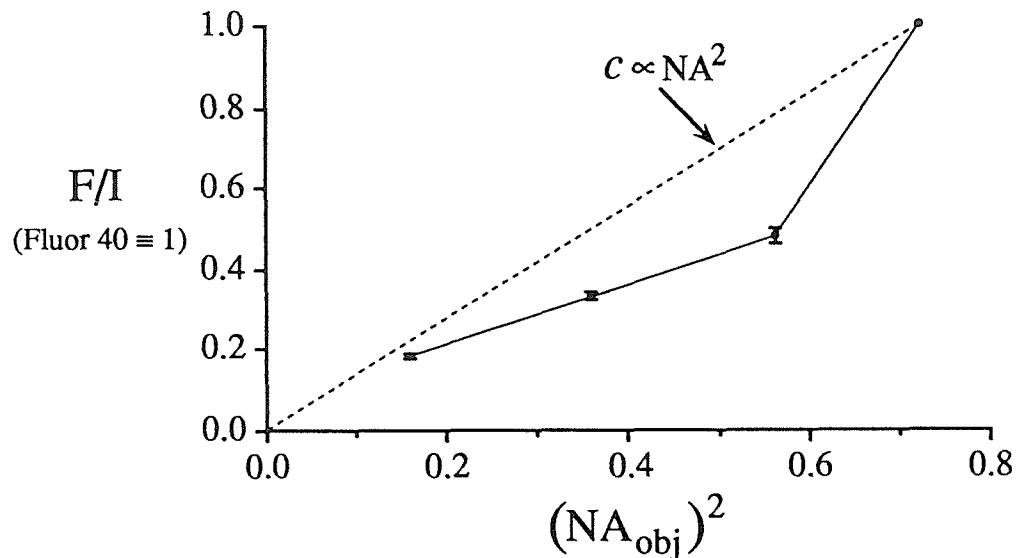
Figure C.6. Dependence of collection efficiency on numerical aperture. F/I was measured for five cells with each of four objectives: (from left to right) CDPlan 20PL, CDPlan 40PL, Fluor 20 Ph3DL, and Fluor 40 Ph3DL. After correcting for background, the values were normalized to the value for the Fluor 40 objective. Bleaching during the measurement was insignificant. The *curve* and *bars* show the mean and s.e.m. for each objective; the *dashed line* shows the theoretical curve $c \propto NA^2$.

the fluorescent intensity F was measured with all four objectives and then corrected for background fluorescence. The fluorescent intensity was then divided through by the illumination intensity to find F/I, an estimate of the relative collection efficiency for fluorescence. These F/I values, normalized by the value for the Fluor 40 Ph3DL objective, should be proportional to c, and thus (by C.2) to $(NA_{obj})^2$.

The figure shows that F/I does not follow $(NA_{obj})^2$ very well, and in fact rises *faster* than $(NA_{obj})^2$. One can imagine various explanations for this behavior, but it's perhaps best to conclude that collection efficiency does not depend in a simple way on the numerical aperture, though it certainly increases with increasing NA. A safe rule is that the NA should be maximized in order to maximize collection efficiency.

C.6 SUMMARY

Incandescent filaments and arc lamps, the most commonly-used light sources for microscopes, are nonuniform, so that Kohler illumination must be used in order to illuminate the specimen uniformly. In a simplified model, the illumination intensity should be proportional to $(NA_{cond})^2$, but this simple relation is not borne out in practice. In order to maximize illumination intensity, the NA of the condenser should be as large as possible, and the Kohler illumination should be adjusted so that the image of the light source just fills the entrance pupil of the condenser.

For transmitted-light microscopy, maximum collection efficiency of transmitted light is obtained if NA_{obj} meets or exceeds NA_{cond}. For fluorescence microscopy, the emitted light spreads in all directions, and NA_{obj} must be as large as possible. In a crude model the collection efficiency will be proportional to $(NA_{obj})^2$; again, this is not followed very well in practice.

The guidelines for maximizing optical efficiency, then, are best stated separately for transmitted-light and fluorescence microscopy. For transmitted light, NA_{cond} should be as

large as possible, and NA_{obj} must equal or exceed it. For fluorescence, NA_{cond} and NA_{obj} must both be as large as possible.

APPENDIX C REFERENCES

S. Bradbury (1984) *An introduction to the optical microscope.* Royal Microscopical Society Microscopy Handbooks, Oxford University Press, New York.

S. Bradbury, P. J. Evennett, H. Haselmann, and H. Piller. (1989) *Dictionary of Light Microscopy,* Oxford University Press, New York.

A. Grinvald, A. Fine, I. C. Farber, and R. Hildesheim (1983) Fluorescence monitoring of electrical responses from small neurons and their processes. *Biophys. J.* **42**:195-198.

Appendix D
A Low-Noise Preamplifier

D.1 INTRODUCTION

This appendix describes the low-noise preamplifier circuit for the optical detector of section 5.1, concentrating especially on its noise design and noise performance. As described in that section, the main design goal for the preamplifier is that its noise should be less than shot noise for photocurrents as low as 200 pA. Ordinary operational amplifiers are not quiet enough for this task, and so this preamplifier supplements a conventional OP-27 op-amp with a low-noise input stage built from discrete JFETs (junction field-effect transistors). The preamplifier circuit diagram is shown below as Fig D.3 (Fig 5.5a shows the same circuit).

In the discussion below, section D.2 first defines some basic terms: Johnson and shot noise, voltage and current noise, and spectral density, and section D.3 describes the basic operation of the JFET input stage. With these two sections as background, section D.4 describes the noise design of the amplifier, and section D.5, its actual noise performance.

For an elementary discussion of noise in electronic circuits, see Horowitz and Hill (Horowitz and Hill, 1980, chapter 7). For a noise analysis of a very similar transimpedance amplifier used for patch-clamping, see Sigworth (1983).

D.2 NOISE THEORY

Before discussing the design of this particular low-noise amplifier, some basic theory and terminology are in order. First, some typographical conventions for voltages

and currents: in this appendix, *capital* letters signify DC values: I_d, V_{bb}; while *lowercase*

letters specify root-mean-square (rms) noises, spectral densities, or noise densities: i_{sh}, v_J,

S_{total}.

It is convenient to lump the intrinsic noise sources of any amplifier into two parts:

the current noise i_n, and the voltage noise v_n. These are illustrated in Fig D.1a for the

present case of a transimpedance amplifier. Current noise is equivalent to a current source

in *parallel* with the input signal, while voltage noise is equivalent to a voltage source in

series with the input. The relative contributions of i_n and v_n depend on the impedance at

the input Z_{in}, with the total equivalent input current noise given by

$$(i_{total})^2 = (i_n)^2 + (v_n/Z_{in})^2 .$$

Noise can arise from a variety of physical mechanisms, but only two are easy to

analyze: Johnson noise and shot noise. Fortunately, these two are the most important for

this discussion. Johnson noise is the inherent thermal noise present in any resistor R; it

may be represented as a voltage noise v_J in series with the resistor, or equivalently as a
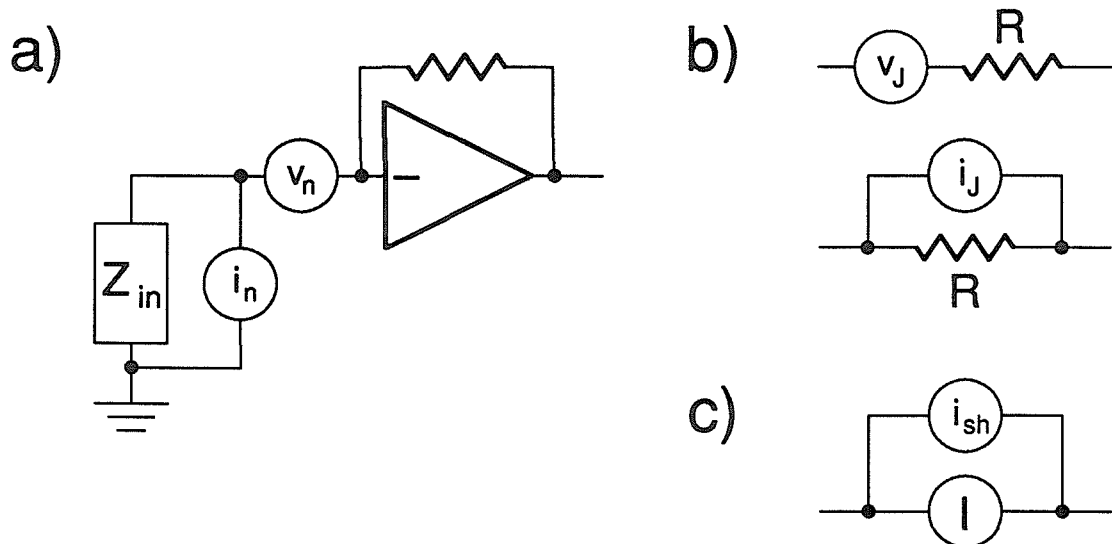
Figure D.1 Basic noise concepts. *a)* Equivalent input voltage and current noise, shown for the case of a transimpedance amplifier. *b)* Johnson noise, which can be treated either as a voltage noise or a current noise. *c)* Shot noise.

current noise i_J in parallel with the resistor (Fig D.1b). The amplitude of Johnson noise is given by

$$v_J = \sqrt{4kTRB}$$

$$\text{or} \quad i_J = \sqrt{4kTB/R} \quad ,$$

where B is the bandwidth with which the noises are measured, k is Boltzmann's constant, and T is the resistor's temperature (at 300°K, $\sqrt{4kT}$ =1.29x10^{-10} V/$\sqrt{\Omega\text{-Hz}}$). Shot noise is statistical noise, due to the quantization of the charge carriers that make up a current. For a given current I, the shot noise may be represented as a parallel current source i_{sh} (Fig D.1c), whose amplitude is given by

$$i_{sh} = \sqrt{2qIB} \quad ,$$

where q is the electronic charge ($\sqrt{2q}$ =5.66x10^{-10}/$\sqrt{\text{A-Hz}}$).

In the formulae above, Johnson noise and shot noise take very similar forms; this is because they are both examples of *white* noise. A white noise source has a flat frequency spectrum, meaning that if it is viewed through a perfect bandpass filter of width B, centered at a frequency f, the rms amplitude depends only on B, not f. The rms amplitude is in fact proportional to $\sqrt{B}$, a dependence that can be understood as follows. (1) Noises at different frequencies are necessarily uncorrelated. (2) When uncorrelated noise sources are combined, their amplitudes add in quadrature. Equivalently, their powers—proportional to the squares of their amplitudes—add linearly. (3) Therefore, the power of a white noise source viewed with a bandpass filter must be proportional to B, and thus, its rms amplitude must be proportional to $\sqrt{B}$.

More general types of noise sources may not be white, and so it is useful to define the *spectral density* of a noise source, which is proportional to its noise power per unit frequency. For a current noise, for instance, the spectral density $s_i(f)$ at a frequency f is defined by $s_i(f)df = (i_{rms})^2$, where i_{rms} is the rms amplitude of the noise measured through

a bandpass filter at f with width df. Since the spectral density is proportional to noise power, spectral densities at different frequencies sum linearly. Therefore, the rms amplitude i_{rms} measured from a noise source with spectral density $s_i(f)$ through a filter whose transfer function is $T(f)$ is given by

$$(i_{rms})^2 = \int s_i(f) \, |T(f)|^2 \, df \quad .$$

Using this concept, white noise can be defined precisely as noise whose spectral density is constant with frequency. The rms amplitude of a white noise source viewed through a filter $T(f)$ is given by

$$(i_{rms})^2 = s_i \int |T(f)|^2 \, df \quad .$$

Bringing the discussion full circle, the formulae for Johnson and shot noise can be cast in this white-noise form by defining $s_{i,Johnson} = 4kT/R$ and $s_{i,shot} = 2qI$, and using a precise definition of bandwidth:

$$B = \int |T(f)|^2 \, df \quad .$$

The spectral density of a signal is intimately related to its Fourier transform. For a signal with Fourier transform $F(f)$, the spectral density $s(f)$ is proportional to $|F(f)|^2$ (the constant of proportionality depends on the normalization convention). The power spectrum—another name for the spectral density distribution—is also equal to the Fourier transform of the autocorrelation function. In section D.5, the power spectrum is used as a way of testing a measured amplifier noise signal against predictions. This comparison is especially useful because it does not make any *a priori* assumptions about the amplifiers' frequency response.

When specifying noise characteristics of an amplifier, it is common to quote the *noise density*, which is equal to the square root of the spectral density and has units such as

$nV/\sqrt{Hz}$ or $pA/\sqrt{Hz}$. Noise densities are often more convenient than spectral densities because they are proportional to noise amplitudes rather than squared amplitudes, and because their values can be written without large negative exponents. They add in quadrature, just as noise amplitudes do. The noise sources in section D.4 are quantified as noise densities.

D.3 JFET INPUT STAGE

The job of the JFET input stage is to have very low noise itself, and provide a moderate amplification of the signal so that noise in the second stage of the preamplifier will be unimportant. The OP27 in the second stage then provides the advantages of a good commercial operational amplifier: moderately low noise and very high gain. JFETs are used because they have extremely low input leakage current (less than 1 pA). The input
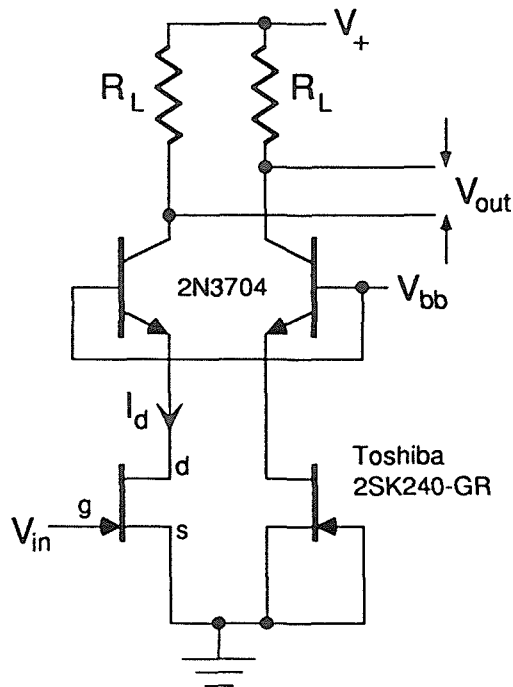
$$V_+ = 12V$$
$$V_{bb} = 5V$$

$$R_L = 499 \ \Omega \ (1\%)$$

FET characteristics

$$g_m \geq 15 \ mS$$
$$I_{DSS} = 2.6 - 6.5 \ mA$$
$$I_g < 1 \ pA \ for \ V_{ds} < 8V$$

Figure D.2 The FET input stage of the preamplifier. This stage amplifies the input voltage V_{in}, producing the output voltage difference V_{out}. Various parameters are labelled and their values indicated. The letters d, g, and s indicate the FET drain, gate, and source, respectively.

current may be as low as 200 pA, and the leakage current needs to be held well below this level, since its shot noise adds directly to the shot noise of the input current. The basic design of the input stage is described here; its noise design is described in the next section.

The input stage is shown in Fig D.2, with the most important circuit parameters labelled and values for them indicated. The FET is held in saturation, where it is a good transconductance device: for small changes ΔV_{in} in the input voltage, the change in drain current ΔI_d is given by $\Delta I_d = g_m(\Delta V_{in})$, where g_m is the FET's transconductance. (In the context of the complete amplifier circuit, the gate is held near ground by negative feedback, so ΔV_{in} is always infinitesimal.) This change in I_d then changes the voltage drop across the load resistor, leading to a change in output voltage of $\Delta V_{out} = g_m R_L (\Delta V_{in})$. The overall gain of the input stage is thus $g_m R_L$.

The discussion above applies to the left-hand FET, which does all the work. In order that it may work properly, its environment is set up by the bipolar transistors and the right-hand FET (the other half of a matched pair). The matched FET pair is a simple way to set the DC offset of V_{out} near zero, since the drain current of the right FET is nearly equal to I_d of the left FET. A small mismatch in I_{DSS} (the value of I_d with the gate voltage $V_{gs}=0$) will merely cause a small input voltage offset, as the feedback network changes V_{in} in order to match drain currents exactly. The bipolar transistors serve two purposes. First, they set the drain-source voltage V_{ds} at one diode drop below a chosen voltage V_{bb}: V_{ds} is set high enough that the FET is kept in saturation, but low enough that the input leakage current I_g is kept small. Second, they prevent noise in the load resistors and V_+ from coupling back to the input through the FET's capacitance (see the next section).

The bipolar transistors are not critical; they need only be reasonably quiet and have a fairly large current gain. The supply voltages and load resistors were chosen as follows.

a) $V_+=12$ V is simply the largest voltage that was convenient to generate with an on-card voltage regulator.

b) R_L should be as large as possible, in order to maximize the gain of the input stage. On the other hand, there must be room between V_+ and V_{bb} for the voltage drop across R_L. For these 2SK240-GR FETs, the specified range for I_{DSS} is 2.6 mA to 6.5 mA, giving voltage drops across 499 Ω of 1.3 V to 3.25 V. With $V_+=12$ V, these drops leave plenty of leeway for V_{bb}, and in fact R_L could be somewhat larger. Multiplying 499 Ω by 15 mS (the minimum specified transconductance for these FETs) gives a minimum input-stage gain of 7.5. This gain is high enough that noise sources after the input stage are insignificant compared to the FET's input voltage noise (see below).

c) V_{ds} must be less than about 8 V in order to keep I_g below 1 pA, and greater than about 4 V in order to keep the FETs in saturation. $V_{bb}=5$ V was chosen to give V_{ds} slightly greater than 4 V.

D.4 NOISE DESIGN

A noise analysis of this amplifier design is but a catalog of noise sources and their amplitudes. The noise sources fall in two classes: those equivalent to an input current, and those equivalent to an input voltage. The amplitudes of all the noise sources are calculated below and summarized in Table D.1. During these calculations, it may be convenient to refer to Fig D.3, which shows the preamplifier circuit diagram, including two capacitances that are important for noise: the input capacitance C_{in} and the FET's gate-drain capacitance (reverse transfer capacitance) C_{gd}.

D.4.1 Equivalent current noises

Input current noise comes from the components connected to the input of the preamplifier: the feedback resistor, photodiode, and FET. There is also a contribution from voltage noises later in the circuit, which couple to the input through C_{gd}.
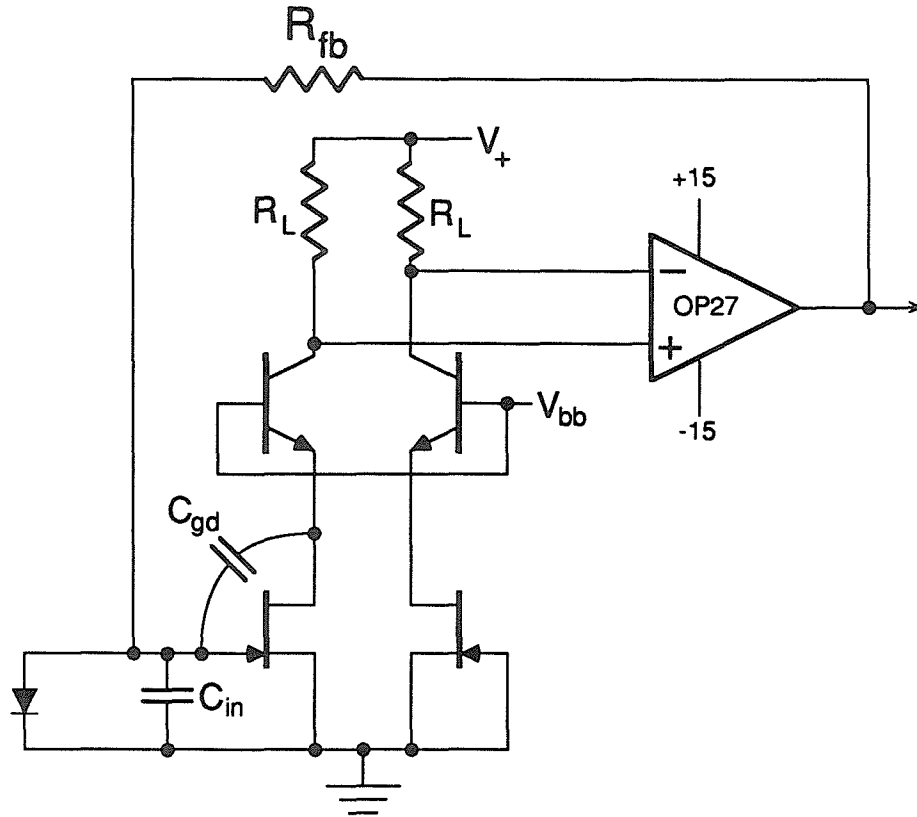
Figure D.3 The preamplifier circuit, showing the input capacitance and FET reverse transfer capacitance.

current noises	
Johnson noise from R_{fb}	1.7 fA/$\sqrt{Hz}$
photodiode noise	0.32 fA/$\sqrt{Hz}$
shot noise in I_g	<0.57 fA/$\sqrt{Hz}$
noise in V_{bb} (noise density v_{bb})	$2\pi f C_{gd} v_{bb}$
	(<1 fA/$\sqrt{Hz}$)
voltage noises	
FET input voltage noise	1.3 nV/$\sqrt{Hz}$
Johnson noise in R_L	0.54 nV/$\sqrt{Hz}$
OP27 input voltage noise	0.57 nV/$\sqrt{Hz}$
OP27 input current noise	0.09 nV/$\sqrt{Hz}$
noise in V_+	insignificant

Table D.1. Equivalent input noise sources and their amplitudes.

Johnson noise from feedback resistor. The Johnson noise in R_{fb} is always present, since the feedback resistor is essential to the circuit, and so is a useful standard against which other current noises may be compared. If R_{fb}=6 GΩ, its Johnson noise is 1.7 fA/√Hz; for reference, this noise density is equal to the shot noise in a current of 9 pA.

Photodiode noise. The Hamamatsu S1087-01 photodiode is specified to have a noise-equivalent-power of 0.8 fW/√Hz; multiplying by the peak radiant sensitivity of 0.4 A/W gives a noise current density of 0.32 fA/√Hz.

Shot noise in FET gate current. With V_{ds}=4 V, I_g is specified to be less than 1 pA for these FETs. Thus, its shot noise is less than 0.57 fA/√Hz.

Noise in V_{bb}. The noise density v_{bb} of the noise in V_{bb} is not possible to calculate here, since it depends on voltage regulators outside the preamplifier circuit. However, the effect of v_{bb} may be understood: it talks back to the amplifier input through C_{gd}, creating an input noise current density of $2\pi f C_{gd} v_{bb}$. For the FETs used here, the typical C_{gd} is nominally 6 pF, but was experimentally determined to be 10 pF. The effect of this capacitance depends on frequency; a typical amplifier's response starts to roll off at about 400 Hz, so this is a reasonable guess for the highest frequency that will be important. Taking 10 pF at a frequency of 400 Hz, v_{bb} would need to be 40 nV/√Hz to give an effective input current noise of 1 fA/√Hz. Since V_{bb} has very little load and may be filtered heavily, it is easy to keep v_{bb} below this level and thus insignificant compared to the Johnson noise in the feedback resistor.

Other coupling through C_{gd}. The effect of noise in V_{bb} shows why the cascode configuration—the bipolar transistors atop the dual JFET—is so important. Without the bipolar transistors, noise in V_{ds}—from the Johnson noise of R_L or noise in the OP27— would couple to the input via C_{gd}. The bipolar transistors regulate V_{ds} and eliminate this coupling. As an aside, the cascode configuration also eliminates the Miller effect, which would add an effective capacitance of $(1+ g_m R_L)C_{gd}$ to C_{in}. A full explanation of this effect may be found elsewhere (Horowitz and Hill, 1980, chapter 2).

D.4.2 Equivalent voltage noises

Equivalent voltage noise sources include the JFET's voltage noise (due to thermal fluctuations in its channel), and all noise sources beyond the JFET. In the calculations below, voltage noises at the load resistors are converted to equivalent input noises by dividing by the minimum input stage gain, $g_m R_L$=7.5. Some noises are multiplied by a factor of $\sqrt{2}$, since they occur in both the left and right halves of the input stage.

FET voltage noise. These FETs have a specified voltage noise density of 0.95 nV/$\sqrt{Hz}$ over the frequencies of interest here. This noise must be multiplied by $\sqrt{2}$ because of the dual-FET circuit, giving a noise density of 1.3 nV/$\sqrt{Hz}$.

Johnson noise in load resistor. The Johnson noise of R_L=499 Ω must be multiplied by $\sqrt{2}$, then divided by 7.5 in order to find its equivalent input noise density, 0.54 nV/$\sqrt{Hz}$.

OP27 voltage noise. The typical input voltage noise of the OP27 is specified to be 3 nV/$\sqrt{Hz}$. After multiplying by $\sqrt{2}$ and dividing by 7.5, the equivalent input noise is 0.57 nV/$\sqrt{Hz}$.

OP27 current noise. The typical input current noise of the OP27 is specified to be 1 pA/$\sqrt{Hz}$. Multiplying by $\sqrt{2}$ and dividing by 15 mS (the minimum specification for g_m), the equivalent input voltage noise is .09 nV/$\sqrt{Hz}$.

Noise in V_+. As with V_{bb}, this noise source depends on the power supply and filters, not on amplifier parameters, but it is clear that is unimportant. The cascode configuration prevents small changes in V_+ from affecting I_d; therefore, such changes simply show up as a common-mode signal at the OP27 inputs. The common-mode rejection ratio of the OP27 is nominally 120 dB; this makes any conceivable noise in V_{bb} completely unimportant.

D.4.3 Summary

The above noise discussion may be summarized very simply: the Johnson noise of R_{fb} dominates the equivalent input current noise, while the FET input noise dominates the equivalent input voltage noise, with noise densities of 1.7 fA/$\sqrt{Hz}$ and 1.3 nV/$\sqrt{Hz}$, respectively. The relative importance of these two noise sources depends on the input load, which is just the input capacitance C_{in} (the photodiode's parallel resistance is greater than 20 GΩ, and may be ignored). Three capacitances contribute to C_{in}: the photodiode capacitance, the capacitance of the coaxial cable, and the FET input capacitance C_{gs}. The nominal photodiode capacitance, experimentally confirmed, is 200 pF. The RG174/U coaxial cable's capacitance is specified as 100 pF/m; the lengths used here add about 60 pF. Finally, the typical input capacitance for these FETs is specified as 30 pF. The total input capacitance C_{in} is therefore about 300 pF. The effects of voltage and current noise will be equal when the input impedance is 1.3 nV/1.7 fA=0.76 MΩ; for a 300 pF input load, this corresponds to a frequency of 700 Hz. Most of the preamplifiers roll off below this frequency. Thus, over this preamplifier circuit's entire frequency range, its noise should be well approximated by the Johnson noise of its feedback resistor.

D.5 NOISE PERFORMANCE

The above predictions for the noise performance of this preamplifier circuit were tested twice, first for a prototype amplifier built on a hand-printed circuit board, then for the full production run of sixteen amplifier cards with sixteen amplifiers each. For the prototype amplifier, the total rms noise amplitude was indeed quite close to the expected Johnson noise of the feedback resistor. For the final amplifier cards, two kinds of measurements were made. First, the total rms noise was measured for all 256 amplifiers; second, a particularly quiet and a particularly noisy channel were picked out for more detailed study, and their power spectra measured.
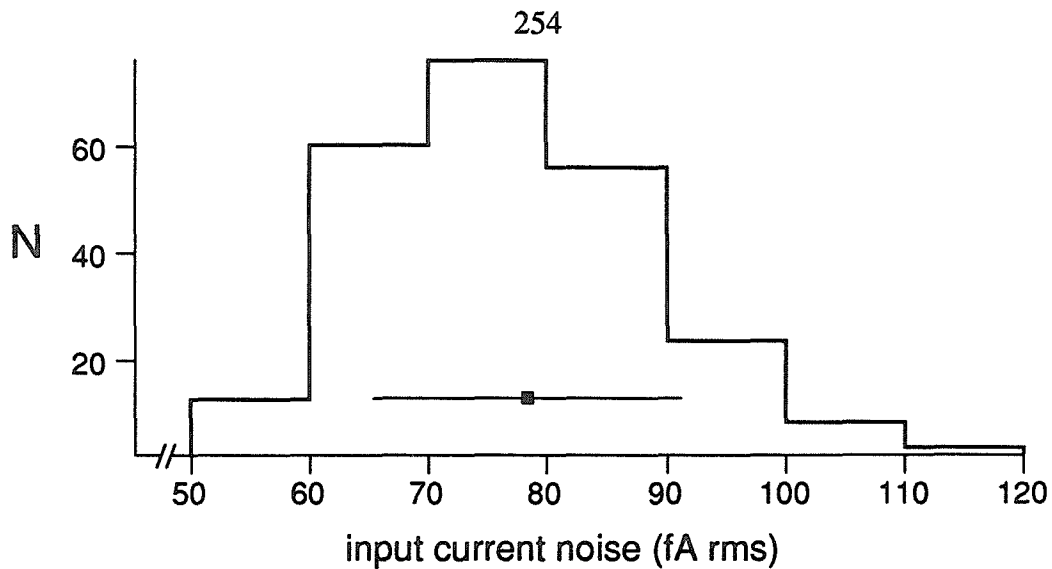
Figure D.4 Distribution of amplifier dark noises, showing equivalent input current noises measured from 240 preamplifiers. The *square* and *line* indicate the mean ± s.d.

The distribution of total amplifier noise is shown in Fig D.4, in terms of equivalent rms input current noise[1]. The range of noises is 54-117 fA rms, with a mean and standard deviation of 78 ± 13 fA. This is somewhat larger than expected: assuming a feedback resistance of 6 GΩ and a bandwidth of 400 Hz, the Johnson noise should be 33 fA rms. On the other hand, these amplifier noises more than satisfy the design goal of being below the shot noise from 200 pA. Again assuming a bandwidth of 400 Hz, the shot noise in a photocurrent of 200 pA would be 160 fA, which would be dominant for even the noisiest amplifier (117 fA).

These amplifier noises are thus quite low enough for the task. In order to understand them somewhat better, however, power spectra were measured from one of the quietest amplifiers, amplifier 9-15, and one of the noisiest, 4-3. Fig D.5 shows the dark noise density of these two amplifiers, with a predicted Johnson noise line for comparison. Not surprisingly, both spectra show significant peaks at the line frequency and harmonics

---

[1]This histogram includes the 240 amplifiers on cards 2-15 and 17. The other card that is usually used, card 16, has auxiliary inputs spliced in (see section 5.1.4), and is excluded because its amplifiers pick up large line-frequency components from the auxiliary inputs.
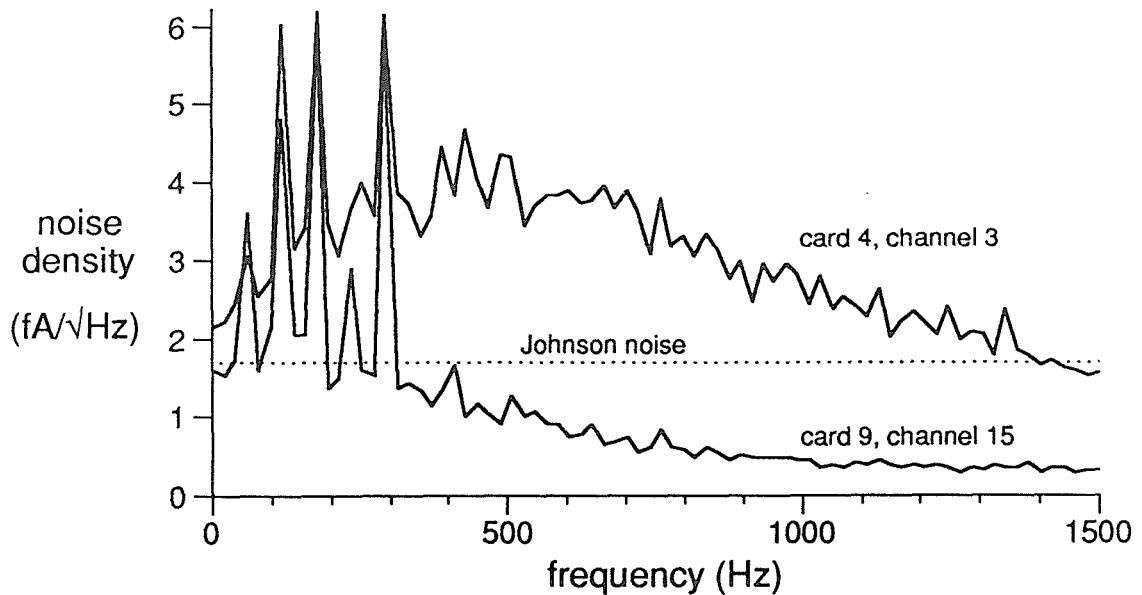
Figure D.5 Noise density spectra for dark noise from amplifiers 4-3 and 9-15. The *dotted line* shows the Johnson noise expected from a 6 GΩ resistor. The feedback resistances for amplifiers 4-3 and 9-15 are 6.2 GΩ and 5.8 GΩ, respectively.

thereof. Apart from these line-frequency components however, the noise from amplifier 9-15 agrees quite well with the Johnson noise prediction at low frequencies, and starts rolling off at about 400 Hz. In contrast, the noise from amplifier 4-3 is well above Johnson noise, and does not start rolling off until about 1000 Hz. At low frequencies, amplifier 4-3's noise density seems to increase with frequency, suggesting that there is a contribution from input voltage noise sources. Thus, there seem to be three reasons that the amplifiers' noise exceeds the 33 fA Johnson noise calculated above: a) both 9-15 and 4-3 have line-frequency pickup; b) 4-3 has a larger noise bandwidth than the 400 Hz used to calculate the 33 fA figure; c) 4-3 seems to have excess voltage noise. There are many possible causes for this voltage noise, but it was not investigated further.

Finally, power spectra were measured from amplifier 9-15 while it was illuminated with an LED, in order to test the shot-noise predictions. Fig D.6 shows the noise density from this amplifier with three different light levels: no light, 0.36 nA photocurrent, and
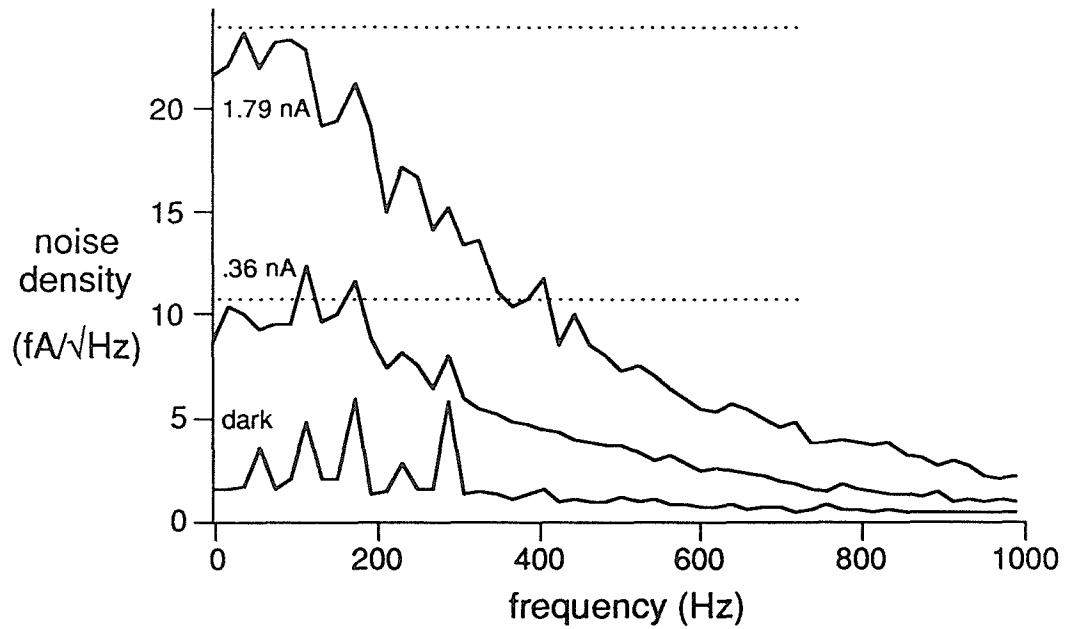
Figure D.6 Noise density spectra for amplifier 9-15, illuminated with an LED. The curves show spectra for no illumination, 0.36 nA photocurrent, and 1.79 nA photocurrent; the dotted lines show the expected shot noise for the two illuminated conditions.

1.79 nA photocurrent. The dotted lines show the noise densities predicted from shot noise, which agree quite well with the measured values.

APPENDIX D REFERENCES

P. Horowitz and W. Hill (1980) *The Art of Electronics*, 1st ed. Cambridge University Press, New York.

F. J. Sigworth (1983) Electronic design of the patch clamp. In *Single-Channel Recording*, eds. B. Sakmann and E. Neher. Plenum, New York. pp. 3-35.